An Investigation of the Role of Poly(ADP-Ribosyl)ation in *Arabidopsis thaliana* Stress Responses

Mai-Britt Vadekrog Jensen

Thesis submitted for the degree of Doctor of Philosophy

Institute of Molecular, Cell and Systems Biology
College of Medical, Veterinary and Life Sciences
University of Glasgow

September 2011

Abstract

Post-translational modifications (PTMs) are receiving more and more attention, since it has been found that the majority of the proteome is altered in some way. The best known PTMs are phosporylation, which activates or deactivates several important enzyme pathways, ubiqiutination, which targets proteins for degradation and glycosylation, which is a requirement of plasma membrane and secretory proteins for localisation. One of the lesser known protein modifications is poly(ADP-ribosyl)ation, which is the attachment of polymers of ADP-ribose moieties onto glutamate residues of target proteins. The reaction is catalysed by poly(ADP-ribose) polymerase (PARP), which uses NAD^+ as a substrate. The removal of the polymer is catalysed by poly(ADP-ribose) glycohydrolase (PARG). There are many PARPs in every organism, but only one gene encoding for PARG. The main functions of poly(ADP-ribosyl)ation are thought to be in DNA repair, cell division and genome maintenance.

While this PTM is well characterized in mammals, there is limited information on its role in plants. Plants contain 3 PARPs. So far AtPARP1 and AtPARP2 transcripts have been demonstrated to increase after exposure to DNA damaging stress, and links to a response to abiotic stress have been made, while there is virtually no information available about AtPARP3. One of the only organisms found to contain two PARGs is *Arabidopsis thaliana*. The discovery of a mutant of AtPARG1 highlighted a possible connection to circadian rhythm.

This study aimed to expand the current knowledge of poly(ADP-ribosyl)ation in plants. Insertional mutant lines were obtained for each of the plant family members, and characterisation of these revealed a hypersentivity of *parg1* to DNA damaging agents, as well as hypersensitivity of both *parg1* and *parg2* to salt. The expression of recombinant AtPARGs, revealed that AtPARG1 had significantly higher activity than AtPARG2. Site directed mutagenesis of highly conserved residues confirmed their importance in plant PARGs. In addition, this study provided a comprehensive comparison of transcript levels of all the plant poly(ADP-ribosyl)ation family members, and thereby provided novel information on the regulation of the two virtually uncharacterised genes, AtPARP3 and AtPARG2.

Table of Contents

List of Figures

List of Tables

Acknowledgements

I would like to start by thanking my supervisor, Dr Susan Rosser for taking me on as her PhD student and for her guidance and patience and the BBSRC for funding. So many people have helped me over the years with various experimental advice: Dr Christopher Grefen for his help with the yeast two-hybrid system, Dr Catherine Cloix for her help with plant protein expression, Dr John Christie for help using the insect cell expression system, and members of the Blatt group for help with confocal microscopy in particular Cornelia Eisenach and Dr Annegret Honsbein. Mads Sønderkær was a great help in analysing the SAGE data and a very welcoming host at Aalborg University. Elizabeth O'Donnell provided invaluable technical support during the latter stages of my studies. I would also like to thank past and present residents of the Bower building in general for helpful guidance in experimental work. I have found it an utter pleasure to work among you all and I have made some great friends while being here. Glasgow Handball Club provided me with plenty of social "distractions" as well as a forum for venting frustrations, and I would like to thank in particular Dr Cecilia Simonsen for her constant encouragement. Lynsey McLeay for movie nights, shapes and desk chair karaoke. I would like to thank my parents for providing a much needed break every Christmas holiday. Finally, I'd like to thank my lab "husband" and fellow "master procrastinator" Scott Ramsay, who has been an immense support over the past four years.

Author's declaration

I hereby declare that all the work presented here as part of this thesis is my own, except where explicitly stated otherwise.

Mai-Britt Vadekrog Jensen

26th of September 2011

List of abbreviations

3-AB	3-aminobenzamide
AAA-ATPase	ATPases associated with various cellular activities
ABA	Abscisic acid
AD	Activation domain
ADP	Adenosine diphosphate
AIF	Apoptosis inducing factor
APP	*Arabidopsis thaliana* homologue of PARP (AtPARP2)
ATP	Adenosine triphosphate
AtPARG1	At2g31870
AtPARG2	At2g31865
AtPARP1	At2g31320
AtPARP2	At4g02390
AtPARP3	At5g22470
BD	DNA binding domain
BER	Base excision repair
BRCT	Breast cancer 1 protein (BRCA1) C-terminus
cADPr	Cyclic adenosine diphosphate ribose
CaMV	Cauliflower mosaic virus
cDNA	Complementary DNA
Col-0	Colombia 0 ecotype
DEPC	Diethyl dicarbonate
dNTP	deoxynucleotide triphosphate
EDTA	Ethylenediaminetetraacetic acid
ER	Endoplasmic reticulum
gDNA	Genomic DNA
GFP	Green fluorescent protein
HA	Haemaglutinin of influenza virus
HR	Homologous recombination
HRP	Horseradish peroxidase
IPTG	Isopropyl ß-D-1-thiogalatopyranoside
LB	Luria Bertani broth medium
LiAc	Lithium acetate
MEF	Mouse embryonic fibroblasts

MES	2-(*N*-morpholino)ethanesulfonic acid
MMS	Methyl methane suphonate
MNNG	*N*-methyl-*N'*-nitro-*N*-nitrosoguanidine
MNU	*N*-methyl-*N*-nitrosourea
MSMO	Murashige and Skoog with minimal organics
NAD^+	Nicotinamide adenine dinucleotide
$NADP^+$	Nicotinamide adenine dinucleotide phosphate
NAP	Non-classical PARP (maize PARP2)
NER	Nucleotide excision repair
NES	Nuclear exclusion signal
NHEJ	Non-homologous end joining
NLS	Nuclear localisation signal
NoLS	Nucleolar localisation signal
PAGE	Polyacrylamide gel electrophoresis
PAR	Poly(ADP-ribose)
PARylation	Poly(ADP-ribos)ylation
PARG	Poly(ADP-ribose) glycohydrolase
PARP	Poly(ADP-ribose) polymerase
PCR	Polymerase chain reaction
RFP	Red fluorescent protein
RNAi	RNA interference
ROS	Reactive oxygen species
SAGE	Serial analysis of gene expression
SQRT-PCR	Semi-quantitative reverse transcriptional PCR
T-DNA	Transfer DNA
TE	Tris EDTA
TEMED	N,N,N',*N'*- tetramethyl-ethane-1,2-diamine
WT	Wild type
XRCC1	X-ray repair cross-complementing 1
ZAP	Zn-finger PARP (maize PARP1)

1 Introduction

1.1 Discovery of poly(ADP-ribosyl)ation

There are many types of post translational protein modifications, which all involve the attachment of smaller chemical groups or moieties. The most well known types of modification include phosphorylation, which is involved in the activation or deactivation of enzymes, glycosylation, a requirement of plasma membrane and secretory proteins for localisation, and ubiquitination, which targets proteins for degradation. One modification that has received less attention until recent years is poly(ADP-ribosyl)ation (PARylation), which is the attachment of polymers of ADP-ribose moieties onto glutamate residues of target proteins. This transient post-translational modification was discovered nearly 50 years ago when nuclear enzymatic activity in hen liver extracts incorporating nicotinamide adenine dinucleotide (NAD^+), resulted in synthesis of an adenine containing RNA-like polymer (Chambon *et al.*, 1963). Later, several separate groups identified the polymer, named poly(ADP-ribose), as being composed of an adenine, two ribose moieties, and two phosphates per unit polymer (Nishizuka *et al.*, 1967; Sugimura *et al.*, 1967) and that the formation of the polymer was inhibited by nicotinamide and its derivatives (Nishizuka *et al.*, 1967; Sugimura *et al.*, 1967). The protein responsible for the synthesis and attachment of the polymer is poly(ADP-ribose) polymerase (PARP) (also referred to as poly(ADP-ribose) synthetase (PARS) or transferase (pADPRT)). During initial characterisation of purified PARP protein, the enzyme activity was found to be dependent on the presence of DNA (Yamada *et al.*, 1971; Okayama *et al.*, 1977). Later, an increase in cellular poly(ADP-ribose) was shown to occur in response to DNA damaging agents (Juarez-Salinas *et al.*, 1979; Benjamin and Gill, 1980a) while the inhibition of PARP activity resulted in an increase of unrepaired single strand breaks after exposure to DNA damaging agents (Durkacz *et al.*, 1980), thus implicating PARylation as having a role in DNA repair. An enzymatic activity responsible for the breakdown of the polymer was first discovered, when calf thymus nuclear extract was added to poly(ADP-ribose) and cleavage of the ribose-ribose bonds was observed (Miwa and Sugimura, 1971) although the enzyme catalysing this reaction, poly(ADP-ribose) glycohydrolase (PARG), was not isolated until a couple of years later (Miwa *et al.*, 1974).

1.2 Polymer formation

PARylation is a post translational modification, where polymers of poly ADP-ribose (PAR) are covalently attached to target proteins. The polymers are synthesized using the oxidised form of nicotinamide adenine dinucleotide (NAD^+) as a substrate and produce nicotinamide as a bi-product. The polymers are linear or branched repeats of ADP ribose units linked by glycosidic ribose-ribose bonds The process of PARylation consists of four steps as illustrated in figure 1.1.

1) PARylation is initiated through the covalent attachment of the proximal mono ADP-ribose unit via the formation of an ester bond between glutamate residues on target proteins and the ADP-ribose moiety.

2) Polymer elongation using the initial mono(ADP-ribose) as a starting point occurs by glycolysis of the ribose – ribose (1''➔2') bond.

3) Branching of the polymer occurs every 20-50 units, through (1'''➔2") glycosidic ribose –ribose bonds.

4) Degradation of the heterogenous polymer is catalysed by PARG through hydrolysis of glycosidic linkages, and this enzyme has both endo and exoglycosidic activity.

The basal level of polymer within unstimulated cells is usually very low, but is increased by 10-500 fold (Alvarez-Gonzalez and Althaus, 1989) proportional to the amount of single and double DNA strand breaks in genomic DNA (Althaus and Richter, 1987; Benjamin and Gill, 1980b).

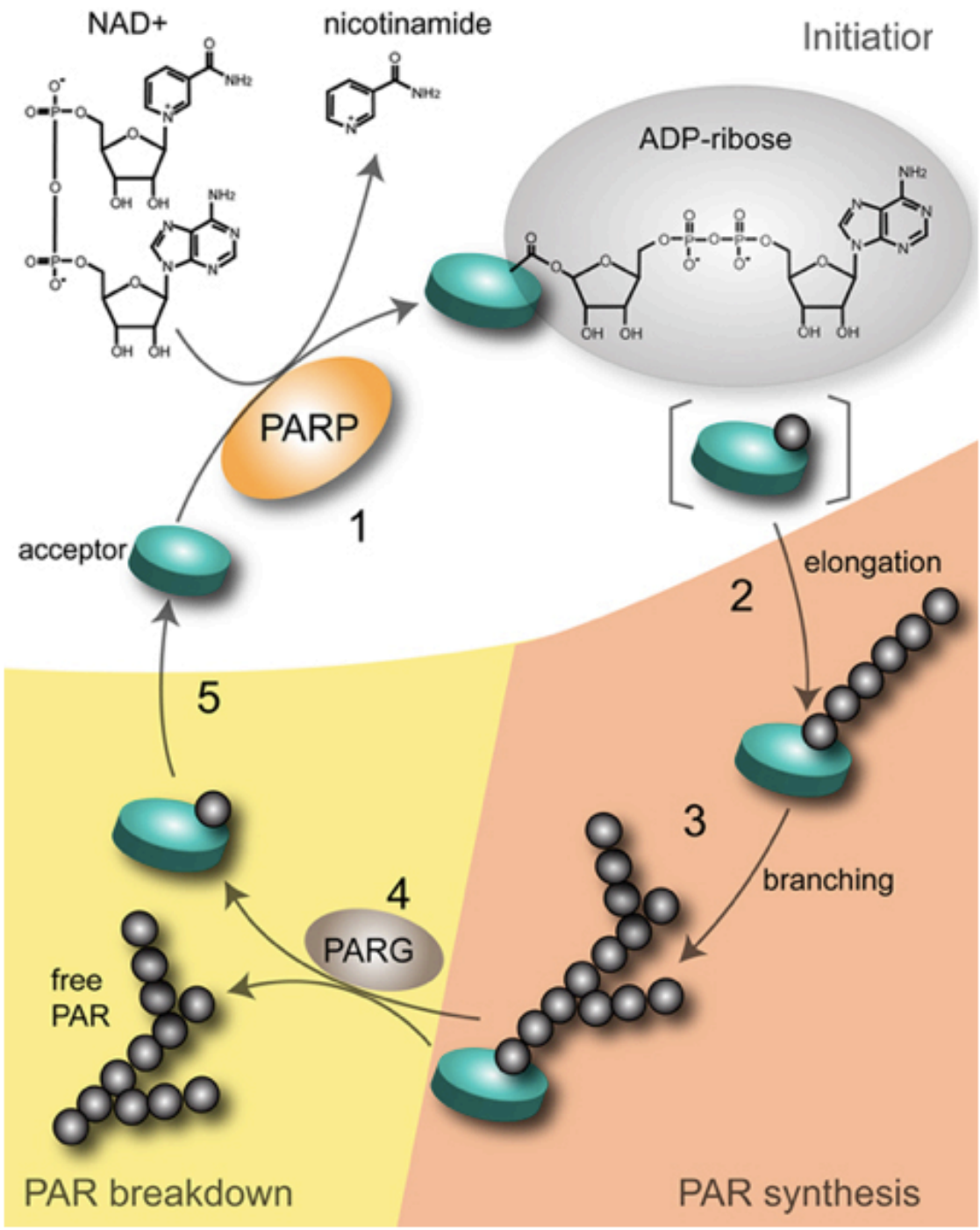

Figure 1.1 Mechanism of PAR polymer build-up and break-down
(1) Poly(ADP-ribose) polymerase (PARP) initiates poly(ADP-ribosyl)ation by cleaving the glycosidic bond between the nicotinamide and ribose moieties of NAD^+. The nicotinamide moiety is released and the ADP-ribose unit is covalently attached to glutamate residues of acceptor proteins. (2) Linear polymer elongation occurs through liking of glycosidic ribose - ribose bonds. (3) Branching, which is also catalysed by PARP, occurs every 20-50 ADP-ribose units through ribose - ribose linkages. (4) Breakdown of PAR is catalysed by PARG, which has both exoglycosidic and endoglycosidic activity. (5) Removal of the final proximal ADP-ribose moiety from the acceptor protein is catalysed by ADP-ribosyl protein lyase. Taken from (David *et al.*, 2009).

1.3 Cellular regulation of NAD^+ by poly(ADP-ribosyl)ation

The role of NAD^+ in the cell is mainly as a co-factor in many metabolic processes In its role in cellular redox reactions NAD^+ acts as both an oxidising and a reducing agent and thus shuttles between oxidised (NAD^+) and reduced (NADH) states. These reactions do not alter the nucleotide structure and thus do not affecting the net cellular concentration of NAD^+ and derivatives. NAD^+, along with ATP, is the most important cellular energy transducer through its roles as hydrogen donor and acceptor. There are two main pools of NAD^+ in the cell; the cytoplasmic and the mitochondrial pools. The ratios of NAD^+/NADH are 100-fold higher in the cytoplasmic pool (Williamson *et al.*, 1967; Stubbs *et al.*, 1972; Veech *et al.*, 1969).

It is through its role as a substrate that the cellular concentration of NAD^+ is altered. The PARylation mechanism is the main cataboliser of NAD+ in mammals (D'Amours *et al.*, 1999). It is dependent on the concentration of cellular NAD^+ (Durkacz *et al.*, 1980; Mendoza-Alvarez and Alvarez-Gonzales, 1993). The cellular NAD^+ levels can undergo rapid decreases after exposure to DNA damaging agents; within 5-10 minutes the levels can be decreased to as little as 10-20% of the normal levels after high doses of MNU (N-Nitroso-N-methylurea) and γ-irradiation (Skidmore *et al.*, 1979), which coincides with an increase in the appearance of poly(ADP-ribose) polymers (Benjamin and Gill., 1980b). To replenish the cellular pool of NAD^+, it has to be synthesized either through the *de novo* pathway, or the salvage pathway, which uses five and three molecules of ATP, respectively, per molecule of NAD^+ (DeBlock *et al.*, 2005). Excess consumption of NAD+ would therefore lead to a disruption in cellular energy homeostasis and could lead to necrotic cell death.

1.4 Poly(ADP-ribose) structure

The PAR polymers are heterogenous structures have been shown to reach up to 400 units both *in* vitro and in *vivo* (Hassa *et al.*, 2006). Branching of poly(ADP-ribose) occurs both *in vitro* (Miwa *et al.*, 1979) and *in vivo* (Juarez-Salinas *et al.*, 1982). PARs are highly negatively charged large polymers (two charges per monomer), which implies that addition of this polymer to target proteins or DNA could prevent them from interacting with other proteins or anionic molecules through charge repulsion or through steric hindrance due to the bulk of the attached polymer (figure 1.2). The type of polymer produced is dependent on the conditions of growth of the cells. Under conditions in which no external DNA damage is present, the majority of polymer is found as metabolically stable mono or oligo ADP-ribose units on target proteins, compared to much longer and more complicated structures when production is stimulated by x-ray or endonuclease induced DNA breaks (Benjamin and Gill, 1980a). The half-life of the polymers produced in unstimulated cells also differs greatly from those produced under DNA damaging conditions cells: from 7.7 hours to less than a minute (Wielckens *et al.*, 1983; Alvarez-Gonzalez and Althaus, 1989).

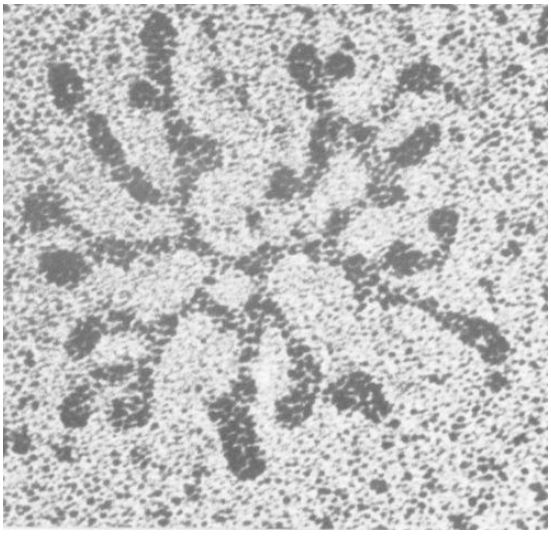

Figure 1.2. Structure of poly(ADP-ribose) polymer
Electron micrograph of the ADP-ribose polymer purified from automodified PARP enzyme from calf thymus. The polymer is 100-120 nm in diameter. Figure taken from (De Murcia *et al.*, 1983).

1.5 Poly(ADP-ribose) polymerase

PARylation is found in all eukaryotes except yeast. It has been mostly studied in humans, which contain 17 PARPs (reviewed in Hassa and Hottiger, 2008; Amé, Spenlehauer and de Murcia, 2004; Schreiber *et al.*, 2006). Other organisms, such as mouse, fruit fly, nematode and plants, also contain several PARP or PARP-like genes (reviewed in Otto *et al.*, 2005; Citarelli *et al.*, 2010). However, it still has not been determined whether all the members of the mammalian PARP family are able to effectively synthesize PAR and under which conditions, as only PARPs 1 to 6 have been extensively studied, and several of the proteins found to contain a PARP signature are missing residues found to be critical for activity (Citarelli *et al.*, 2010). This will be discussed further in section 1.5.1.3.

1.5.1 Structure of PARP1-type PARPs

The general structure of DNA –damage-dependent PARPs is in three domains: a DNA binding domain at the N-terminal containing zinc fingers, an automodification domain and a catalytic domain responsible for the activities for NAD+ binding, ADP-ribosyl transfer and branching reactions. The PARP family of proteins have very varied N-terminal domain compositions (figure 1.3), but most members share conservation in the PARP signature in the catalytic domain, though not all have PARP activity (Citarelli *et al.*, 2010). The functions of all the members of the family are not known. The different properties of the structural domains, based on those of the 113 KDa mammalian PARP1, the founding and best characterized member of the PARP family, are discussed in the following sections.

1.5.1.1 DNA binding domain

The N-terminal region of PARP1 contains a DNA binding domain (DBD) consisting of two zinc fingers necessary for recognition and binding to DNA single and double strand breaks (Gradwohl *et al.*, 1990) but also recognizes other altered DNA structures such as hairpins, cruciforms, and loops (Lonskaya *et al.*, 2005), rather than a particular sequence. The two zinc fingers have distinct functions; the first zinc finger is required for DNA dependent automodification activity as

the base stacking loop found in zinc finger 1, when bound to DNA, positions certain residues in contact with other domains of PARP1, and contribute to activity. These residues are not conserved in zinc finger 2 (Langelier *et al.*, 2011). The second zinc finger is necessary for DNA binding (Gradwohl *et al.*, 1990) and in fact has 100-fold higher affinity for DNA than zinc finger 1 on its own (Langelier *et al.*, 2011). However, the second zinc finger is dispensable for DNA dependent activation both *in vitro* and *in vivo* (Langelier *et al.*, 2011). Recently a third zinc-binding domain was identified in the C-terminal region of the DNA binding domain after the nuclear localisation signal (NLS) (Langelier *et al*, 2008). This motif is conserved in other mammals, as well as *Xenopus laevis*, *Drosophila melanogaster*, and *Arabidopsis thaliana*, and is distinct in structure and function from zinc finger 1 and 2, but does not share any sequence homology to any known structural motifs (Langelier *et al*, 2008). This zinc-binding domain was shown to be involved in interdomain interactions necessary for DNA-dependent automodification (Langelier *et al*, 2008; Schreiber *et al.*, 1995). The region also contains a bipartite nuclear localisation signal (NLS) and a caspase cleavage site (Germain *et al.*, 1999). PARP1 is constitutively expressed, but activity is induced by the binding of the zinc fingers in the DBD to DNA single and double strand breaks after DNA damage (Juarez-Salinas *et al.*, 1979; Benjamin and Gill, 1980a).

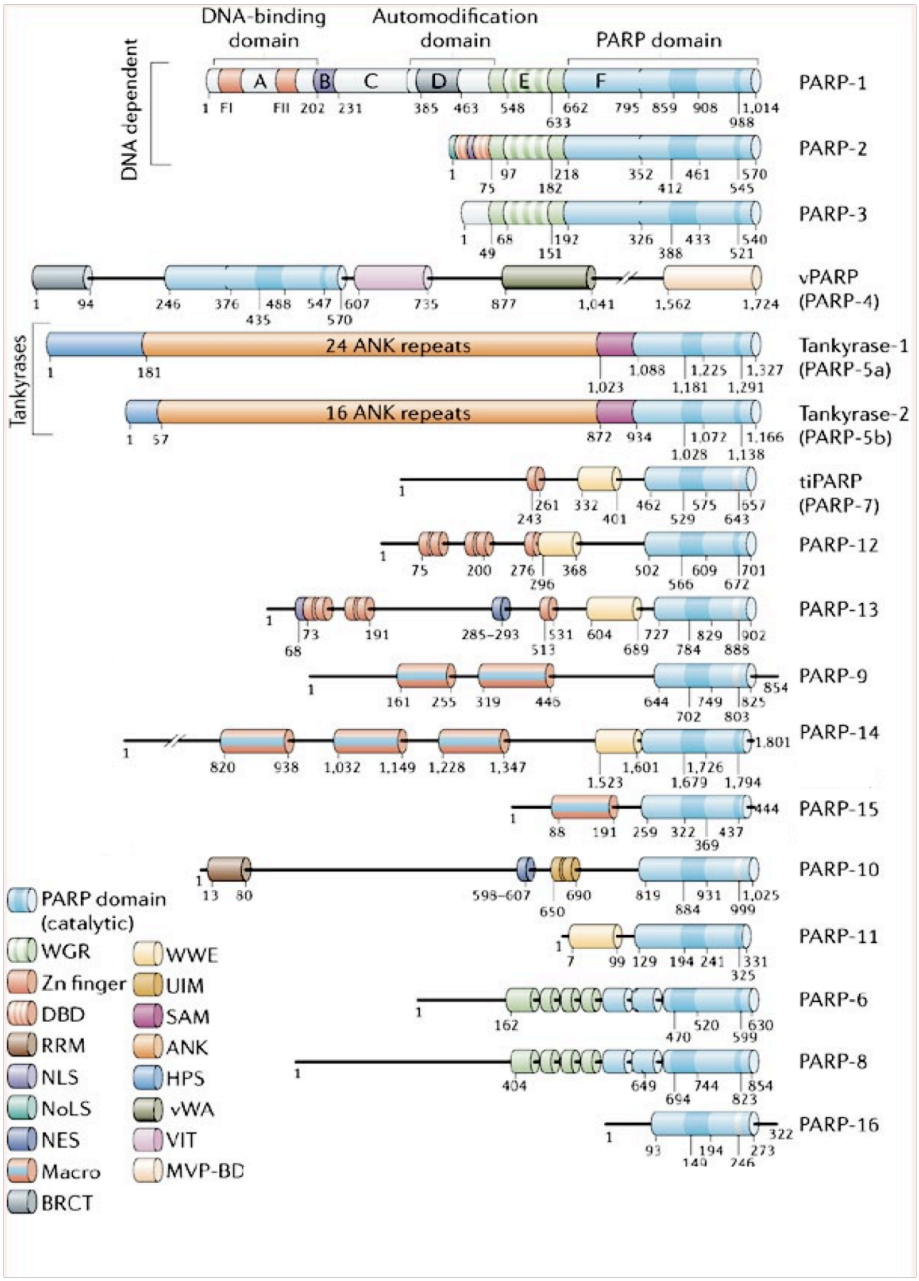

Figure 1.3. The mammalian PARP superfamily
An overview of the different types of 17 PARPs that have so far been found in mammals and their diverse domain architechture. Within the PARP domains, the regions homologous to the PARP signature are darkened. WGR represents a domain with conserved Trp, Gly, and Arg residues, but of unknown function. Zn fingers are DNA or RNA binding. DBD are DNA binding domains. RRM are RNA binding domains. NLS are nuclear localisation signals. NoLS are nucleolar localisation signals. NES are nuclear exclusion signals. Macro domains are ADP, ADP-ribose, or poly(ADP-ribose) binding domains. BRCT (BRCA1 C terminus) and WWE domains are protein-protein interaction domain. UIM are ubiquitin interacting domains. SAM (sterile α-motif) and ANK (ankyrin) are protein-protein interaction domains. HPS contains a homopolymeric run of His, Pro, and Ser residues and its function is unknown. vWA domain (von Willebrand factor type A) is thought to be a metal-ion-dependent site for binding proteins. The function of VIT domain (vault inter-α-trypsin) is not known. MVP-BD is a binding site for major vault protein (MVP). Numbers represent amino acid positions. Taken from (Schreiber *et al.*, 2006).

1.5.1.2 Automodification domain

PARP1 performs auto-ADP-ribosylation, and was in fact shown to be the major acceptor of PAR *in vivo* (Ogata *et al.*, 1981). This action in time forces the PARP1 to dissociate from the site of DNA damage to which it was bound due to charge repulsion (Zahradka and Ebisuzaki, 1982). The automodification domain of PARP1 has not been extensively characterized. It contains 15 glutamic acid residues, which are the targets for automodification (Cherney *et al.*, 1987; Kawaichi *et al.*, 1981). The automodification domain provides a mechanism of negative feedback, as when polymers are attached to the 15 glutamate residues in the domain, the modified PARP1 is inactive (Kawaichi *et al.*, 1981), and it is also thought that the charge of the highly negative polymer will repel the PARP1 from its site of DNA binding thus releasing it from its bound state and leaving it free to be activated again. The automodification domain also contains a breast cancer 1 protein (BRCA1) C-terminus (BRCT) motif, which was originally identified by comparing regions of the BRCA1 to protein sequence databases (Koonin *et al.*, 1996). This motif is found in many proteins involved in DNA damage repair and cell-cycle checkpoints, such as XRCC1, DNA ligase III and IV, and p53 (Bork *et al.*, 1997; Huyton *et al.*, 2000). The main role of BRCT domains are as protein-protein interaction modules (Rodriguez and Songyang, 2008; Watts and Brissett, 2010). This is also the role this domain plays in PARP1, which will be discussed in detail later in section 1.6.2.3. In addition to the BRCT motif, a leucine zipper was also found in the N-terminal of the automodification domain. This domain is highly conserved even in lower eukaryotes and is thought to be responsible for homo and hetero dimerization (Uchida *et al.*, 1993). The auto-PARylation reaction was found to be an intermolecular event as second order kinetics showed PARP to be acting as a catalytic dimer (Mendoza-Alvarez and Alvarez-Gonzales, 1993). This central part of the protein also contains a WGR domain named after its most conserved central motif of tryptophan (W), glycine (G), and arginine (R) residues. This domain has been thought to represent a nucleic acid binding domain (Citarelli *et al.*, 2010), and recent studies have indicated that it is involved in RNA-dependent activation of PARP1 (Huambachano *et al.*, 2011).

1.5.1.3 Catalytic domain

The PARP catalytic region is found at the C-terminal of the protein. The crystal structure of the catalytic fragment of PARP1 was resolved in 1996 (Ruf *et al.*, 1996) and showed similar structural features to the active site of bacterial (ADP-ribosyl)ating toxins such as Diphtheria and Pertussis toxins, and the sites for NAD+ binding were identified. The crystal structure of the catalytic domain of the chicken PARP (Ruf *et al.*, 1998) and murine PARP2 (Oliver *et al.*, 2004) revealed an active site containing a β-α-loop-β-α structural motif responsible for NAD^+ binding and resembling that of mono(ADP-ribose) transferases (Ruf *et al.*, 1998). While the activity of this catalytic fragment alone is not induced by DNA strand breaks, it is still able form polymers at a level comparable to that of the full length PARP1 in *in vitro* assays with no DNA present (Simonin *et al.*, 1993). PARPs from most organisms share a high conservation in the 50 amino acid stretch from residue 859 – 908 considered the "PARP signature" (de Murcia and Menissier de Murcia, 1994). The histidine and tyrosine residues at positions 862 and 896, respectively, are important for NAD^+ binding (Otto *et al.*, 2005), while the lysine at position K^{893} is required for acitivity (Simonin *et al.*, 1990; Simonin *et al.*, 1993)(figure 1.3 B). Several residues outside this motif are also important for true PARP activity. The glutamic acid residue at position E^{988} in human PARP1 has been shown to be highly important for activity and is conserved across all organisms (Citarelli *et al.*, 2010). Site directed mutagenesis of this residue resulted in a reduction of polymer elongation of more than 2000-fold (Marsischky *et al*, 1995). The aspartate residue at position D^{993} has also been determined as crucial for activity, as non-conservative site directed mutagenesis of this residue resulted in complete loss of activity (Simonin *et al.*, 1993).

A

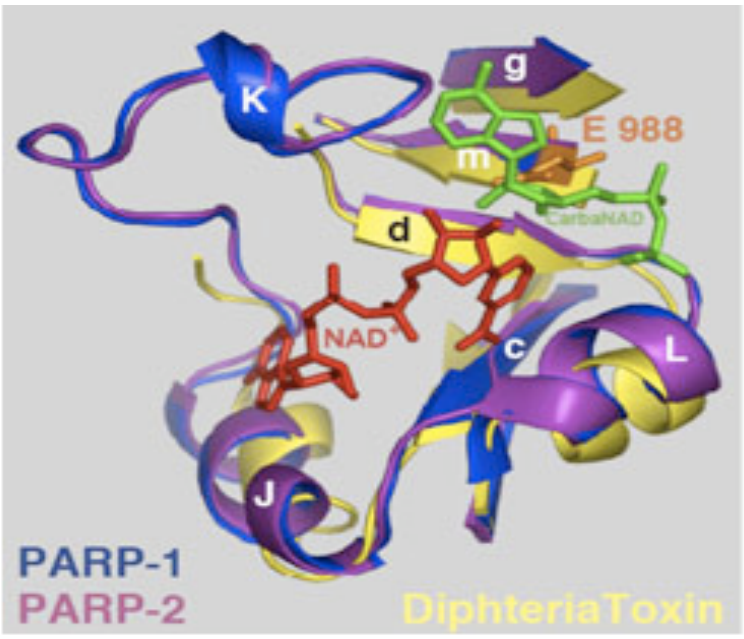

B

huPARP1	859	LLWHGSRTTNFAGILSQGLRIAPPEAPVTGYMFGKGIYFADMVSKSANYC	908
boPARP1	861	LLWHGSRTTNFAGILSQGLRIAPPEAPVTGYMFGKGIYFADMVSKSANYC	910
moPARP1	859	LLWHGSRTTNFAGILSQGLRIAPPEAPVTGYMFGKGIYFADMVSKSANYC	908
xePARP1	855	LLWHGSRTTNFAGILSQGLRIAPPEAPVTGYMFGKGIYFADMVSKSANYC	904
daPARP	858	LLWHGSRTTNYAGILSQGLRIAPPEAPVTGYMFGKGVYFADMVSKSANYC	907
drPARP1	841	LLWHGSRLTNFVGILSHGLRIAPPEAPPTGYMFGKGIYFADMVSKSANYC	890
cePme1	785	LLWHGSGKMNFAGILGQGLRIAPPEAPVSGYMFGKGVYFADMFSKSFFYC	834
AtPARP1	830	LLWHGSRLTNFVGILNQGLRIAPPEAPATGYMFGKGIYFADLVSKSAQYC	879
ZAP	827	LLWHGSRLTNFVGILSQGLRIAPPEAPVTGYMFGKGLYFADLVSKSAQYC	876
		****** * *** ********** ******* **** *** **	

Figure 1.4 The structure of PARP
A) Superimposition of the 3D structures of the catalytic domains of chicken PARP1 (blue), murine PARP2 (purple), Diphtheria toxin (yellow),PARP1 inhibitor CarbaNAD (green). Taken from (Oliver *et al.*, 2004; Yelamos *et al.*, 2008).
B) The 50 amino acid PARP signature is highly conserved across species. Alignment of human, bovine, mouse, xenopus, zebrafish, fruitfly, nematode, *Arabidopsis* and maize PARP signatures, respectively. Conserved residues are indicated by an asterisk.

1.5.2 Other characterised PARPs

1.5.2.1 PARP2

PARP1 was long thought to be the only protein responsible for PARylation in mammals. A second enzyme with PARP activity was found when residual PAR synthesis was detected in PARP1 deficient mouse embryonic fibroblast (MEF) cells in response to DNA damage (Shieh *et al.*, 1998) and polymer formation in the PARP1-deficient cells was suppressed by the addition of the PARP inhibitor 3 amino benzamide (3-AB). Murine and human PARP2 were identified and cloned based on sequences of shorter plant PARPs with different structure to PARP1 (Amé *et al.*, 1999). These displayed some organisational homology with PARP1 in that they also contained an N-terminal regulatory domain and a C-terminal catalytic domain. The catalytic domain of human PARP2 shares 69% similarity to PARP1 and 47% identity to the plant APP, however the N-terminal part of the protein shows no sequence homology to any of the other PARPs. It contains an NLS, a nucleolar localisation signal (NoLS) (Yelamos *et al.*, 2008), and shows some homology to the SAF A/B, Acinus and PIAS (SAP) domain (Aravind and Koonin, 2000) found in other nuclear proteins such as AP-endonucleases and Ku70 that also play a role in DNA repair and chromosomal maintenance (Amé *et al.*, 2004). The crystal structure the catalytic domain of murine PARP2 was found to be very similar to that of PARP1 (figure 1.4A). The abundance of PARP2 protein in the mammalian cell lines 3T3 and HeLa was determined to be comparable to that of PARP1, but when comparing amount of PAR in wild type cells stimulated by Dnase I treated DNA, PARP1 deficient cells were only able to produce 5-20% of polymer seen in wild type cells (Amé et al., 1999; Schreiber *et al.*, 2002). PARP2 deficient mice display no phenotypic abnormalities under control conditions, but are hypersensitive to γ-irradiation and the alkylating agent MNU (Menissier de Murcia *et al.*, 2003).

1.5.2.2 Tankyrases

Another distinct type of PARP are the two tankyrases (TRF1-interacting, Ankyrin-related ADP-ribose polymerase), which share 85% amino acid identity (Smith *et al.*, 1998; Monz *et al.*, 2001). Like PARP2, they have a highly conserved PARP catalytic region, and are also susceptible to the PARP inhibitor 3-AB (Seimiya *et*

al., 2005; Smith *et al.*, 1998). Tankyrases contain no DNA binding motif, and are not activated by DNA damaging agents, rather are activated by phosphorylation by MAP kinase (Chi and Lodish, 2000;), but do contain 24 ankyrin repeats, a motif spread widely in the genome, and which functions solely to mediate protein-protein interactions (Li *et al.*, 2006). Tankyrase 1 was discovered in a yeast two hybrid screen using telomeric repeat binding factor (TRF) 1 as bait (Smith *et al.*, 1998), while Tankyrase 2 was initially found as a tumour antigen (Monz *et al.*, 2001) and in a similar TRF1 yeast two hybrid screen (Kaminker *et al.*, 2001). TRF1 is a negative regulator of telomere length by telomerase in *cis* by inhibiting the action of telomerase at the ends of telomeres (Van Steensel and de Lange, 1997). The tankyrases interact with each other and both target TRF1 as well as poly(ADP-ribosyl)ate it, thus releasing TRF1 from telomeres (Sbodio *et al.*, 2002). Single knock-out mice for either tankyrase are viable, develop normally, and display no telomere length maintenance defects while double knock-outs are embryonic lethal, thus indicating redundancy between the two tankyrases, and a requirement for tankyrase function for normal embryonic development (Chiang *et al.*, 2008). Tankyrase has also been found in *Drosophila melanogaster* (Smith *et al.*, 1998) and *Caenorhabditis elegans* (Gravel *et al.*, 2004).

PARPs 1 and 2 are expressed constitutively and ubiquitously in all human tissues, although not at the same level (Johansson, 1999) thus indicating regulation at the protein level. PARP1 exists at a very high abundance in the cell. Concentrations have been measured in mammalian cells at (0.2 -2) x 10^6 molecules per cell (Yamanaka *et al.*, 1988; Ludwig *et al.*, 1988). In spite of there being a high similarity in the C-terminal region of the different PARPs, their N-terminal domains are very varied (for review see Hassa and Hottiger, 2008; Otto *et al.*, 2005), and while the activity of PARP1 and PARP2 are regulated by the presence of DNA strand breaks (Schreiber *et al.*, 2002), it is not understood what mechanism regulates the other PARPs present in mammalian cells.

1.5.2.3 PARP inhibitors

Since the crystal structure of the catalytic domain of PARP1 was resolved (Ruf *et al.*, 1998), inhibitors have been designed to imitate the substrate-enzyme interaction of NAD^+ with PARP1, thus acting as competitive inhibitors and

blocking the NAD^+ binding site, due to their structural resemblance to the substrate (figure 1.4A). Many studies employ the use of PARP inhibitors, but no isoform specificity currently exist, as the target NAD+ binding site is highly conserved among the PARPs, thus making it hard to attribute particular functional changes after application of inhibitors to any one PARP. However, with the crystal structures of PARP2 and PARP3 resolved and distinct unique loops discovered in the regions surrounding the catalytic domain, this information could be used to design inhibitors specific for these PARP isoforms (Oliver *et al.*, 2004; Lehtiö *et al.*, 2009)

1.6 PolyADP-ribose glycohydrolase

1.6.1 Stucture and function of PARG

PARG is the main enzyme known to perform the converse action of PARP i.e. the removal of polyADP-ribose, through the cleavage of the ribose–ribose bond. It was first discovered by Miwa and Sugimura (1971) when addition of calf thymus nuclear fraction to poly(ADP-ribose) resulted in splitting of the ribose-ribose bond indicating the presence of an enzyme capable of polymer hydrolysis. In this way PARG removes the PAR on inactive automodified PARP1, which has dissociated from DNA and thus returns it to the active form (Zahradka and Ebisuzaki, 1982). In contrast to the many polymerases, only a single gene for PARG has been found in mammals (Meyer *et al.*, 2003) and flies (Hanai *et al.*, 2004), while the only organisms known to contain two genes coding for PARGs are nematodes (St-Laurent *et al.*, 2007) and *Arabidopsis* (Panda *et al.*, 2002). The PARG protein contains a catalytic domain, an NLS (Lin *et al.*, 1997), a nuclear export signal (NES) (Shimokawa *et al.*, 1999) and a caspase-3 cleavage site (Affar *et al.*, 2001) in the N-terminal regulatory domain. PARG has both endo and exoglycosidic activity (Brochu *et al.*, 1994) and degrades long linear polymers much faster than shorter branched polymers under the same conditions, suggested by the fact that the K_m value for PARG for small polymers is higher by 2 orders of magnitude than for large polymers (Hakateyama *et al.*, 1986). Protein free and protein bound polymer were degraded at the same rate (Hatakeyama *et al.*, 1986). The half life of ADP-ribose polymers is lowered significantly upon the introduction of DNA damage; from more than 7 hrs to less

than a minute when exposed to *N*-methyl-*N*'-nitro-*N*-nitrosoguanidine (MNNG) (Alvarez-Gonzalez and Althaus, 1989) and UV irradiation (Jacobson *et al.*, 1983), suggesting very tight control of the metabolism of poly(ADP-ribose). Contrary to the very high abundance of PARP1 protein in mammalian cells (Yamanaka *et al.*, 1988; Ludwig *et al.*, 1988), PARG abundance is 100 to 1000-fold less at 2000 molecules per cell (Hakateyama *et al.*, 1986). Although only one gene coding for PARG has been found, it has been shown that this gene results in several protein isoforms that localize to different subcellular compartments (figure 1.5A) (Amé *et al.*, 1999); the full length nuclear 110 KDa protein, the cytoplasmic 102 KDa protein lacking exon 1, the cytoplasmic 99 KDa protein lacking exon 1 and 2 (Meyer-Ficca *et al.*, 2004), the cytoplasmic and mitochondrial 60 KDa protein and the mitochondrial 55 KDa protein (Meyer *et al.*, 2007; Whatcott *et al.*, 2009). Mitochondrial localisation of the smaller isoforms originating from alternative translational start codons in exon 4, was found to be due to a regulatory segment also in the 4th exon containing a mitochondrial targeting sequence (MTS) (Niere *et al.*, 2008). The 102 KDa cytoplasmic isoform is the most abundant in Hela cells (Meyer-Ficca *et al.*, 2004) and the majority of glycohydrolase activity was found in to be in the cytoplasmic fraction of HEK293 cells (80%) and the activity in the cytoplasm was increased after exposure to MNNG (90%) (Meyer-Ficca *et al.*, 2004). However, after the discovery of additional shorter cytoplasmic isoforms (Meyer *et al.*, 2007), the total cytoplasmic activity can no longer be attributed solely to the 102 KDa isoform. The distribution of these isoforms is not permanent, but is regulated spatio-temporally in response to DNA damage, as it was shown that the cytoplasmic 103 KDa isoform relocalizes to the nucleus, while the 110 KDa nuclear isoform moves to the cytoplasm upon exposure to γ-irradiation (Haince *et al.*, 2006).

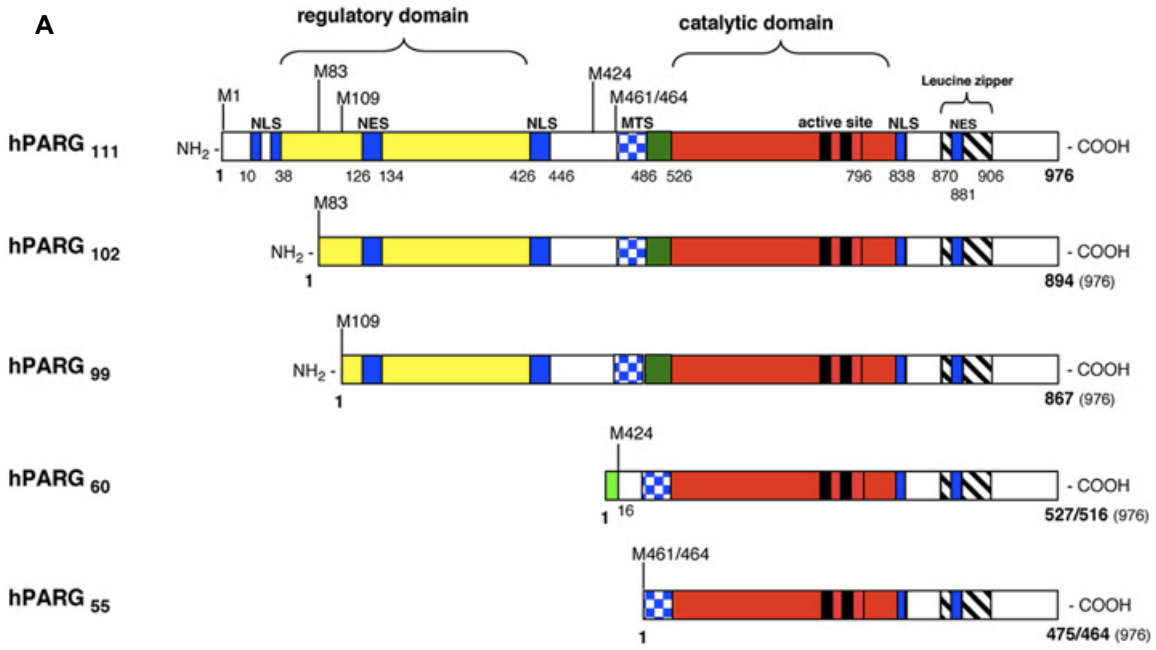

B

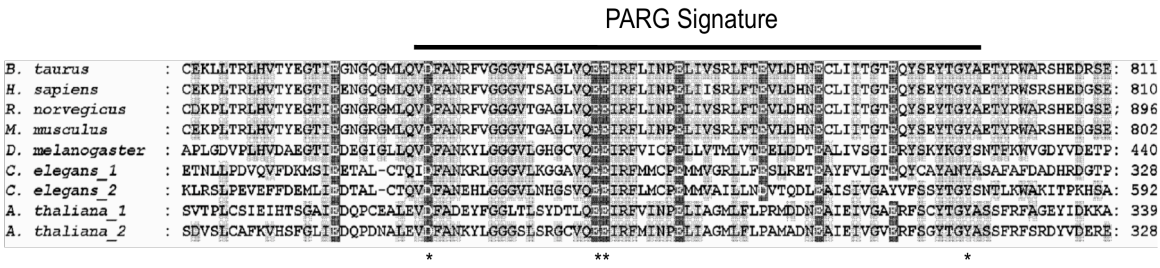

Figure 1.5. Structure of mammalian PARG

A) The domain architecture of the five human isoforms of human PARG. NLS: nuclear localisation signal, NES: nuclear export signal, MTS: mitochondrial targeting sequence. hPARG60 contains an alternative 16 amino acid N-terminal sequence not found in any of the isoforms indicated in light green. Numbers represent amino acid positions. Taken from (Hassa and Hottiger, 2008).

B) Alignment of the PARG signatures from model organisms. Residues conserved across all species are highlighted in dark grey, residues found in most species are highlighted in light grey, and non-conserved residues in white. Asterisks indicate residues found to be important for activity through mutagenesis in bovine and nematode PARGs. Figure taken from (Patel *et al.*, 2005).

1.6.2 Mammalian PARG deficiency studies

The full length PARG has been notoriously hard to purify due to the low cellular abundance and instability during purification (Haketeyama *et al.*, 1986; Lin *et al.*, 1997). So far it has only been possible to fully purify the catalytic region of PARG, which has so far been done for bovine, rat, and more recently human PARG (Lin *et al.*, 1997; Shimokawa *et al.*, 1999; Okita *et al.*, 2010). Due to the lack of potent and selective inhibitors for use *in vivo* (Falsig *et al.*, 2004), the role of PARG has mostly been investigated through knock out or knock-down/RNAi techniques. A disruption in exon 4 (PARG-Δ4), resulting in total loss of PARG activity lead to embryonic lethality in homozygous mutant mice (Koh *et al.*, 2004). A partial knock out was made in mice where exons 2 and 3 were left out (PARG-Δ2-3) resulting in complete depletion of the nuclear localized 110 KDa isoform of PARG (Cortes *et al.*, 2004). This mutant cell mouse line showed hypersensitivity to the DNA damaging agent MNU and ionizing radiation (Cortes *et al.*, 2004). While PARG activity in the nuclei of the mutant cells were reduced to 28% of wild type, they showed a 3-fold increase in PARG activity in the mitochondria. It was suggested that the loss of the nuclear $PARG^{110}$ isoform upregulates the $PARG^{60}$ isoform in mitochondria as compensation (Cortes *et al.*, 2004). The $PARG^{60}$ isoform, present in PARG-Δ2-3 cells, was later shown to have prolonged activity after DNA damage. This higher activity resulted in a decrease in automodified PARP, which in turn lead to a higher level of activity of PARP, resulting in increased NAD consumption when exposed to the alkylating agent MNNG (Gao *et al.*, 2007). The increased period of PARG activity was proposed to be due to the lack of the N-terminal regulatory domain. However, as the full-length protein has yet to be purified due to the reasons listed earlier, this hypothesis is yet to be explored.

An *in vitro* screen of conserved acidic residues of the catalytic region of bovine PARG in the region of an inhibitor binding Tyr^{796} residue (figure 1.5) (Koh *et al.*, 2003) investigated their importance in PARG activity (Patel *et al.*, 2005). Mutation of the three acidic residues Asp^{738}, Glu^{756}, and Glu^{757} into a polar asparagine residue lowered PARG activity to below a detectable level. The MTS found in exon 4 (Niere *et al.*, 2008; Whatcott *et al.*, 2009) was later shown to

contain residues required for activity of the smaller mitochondrial PARG, as well as the full-length nuclear PARG (Botta and Jacobson, 2010).

While PARG is responsible for the majority of the breakdown of PAR, the final proximal ADP-ribose moiety is removed from target proteins by the actions of ADP-ribosyl protein lyase (Oka *et al.*, 1984) and the resulting enzymatic product was a dehydrated form of ADP-ribose, thus indicating a differential activity to PARG (Oka *et al.*, 1984). However, any further involvement of this protein in the PARylation process has not been extensively studied.

1.6.2.1 PARGs in invertebrates

The fruit fly, *Drosophila melanogaster* also contains only one PARG gene. The *Drosophila* PARP and PARG were found to localise to different nuclear compartments; PARP associated mainly with chromosomes and nucleoli, while PARG was found in the nucleoplasm (Tulin *et al.*, 2006). A loss of function mutation in the single PARG gene results in lethality at the larval stage at 25°C, but flies are able to progress to adulthood at 29°C (Hanai et al., 2004). However, these adult mutant flies showed accumulation of PAR in neuronal cells, and advanced neurodegeneration as well as reduced lifespan, thus indicating a specific role for PARG in *Drosophila* neuronal development, as well as in general development. Overexpression of PARG resulted in the same phenotype as observed in PARP defective mutants as they were sensitive to heat shock and became contaminated with intracellular bacteria (Tulin and Spradling, 2003; Tulin *et al.*, 2006). These mutant phenotypes demonstrate the need for strict regulation of PARylation.

In the worm, *Caenorhabditis elegans*, two PARGs have been found: poly(ADP-ribose) metabolism enzyme 3 (PME-3) which is the main PARG in worm neuronal cells, and exists in two isoforms, PME-3L (89 KDa) and PME-3S (87 KDa), both of which are expressed throughout the life cycle of the worm. However, the function of each isoform remains to be determined. The smaller poly(ADP-ribose) metabolism enzyme 4 (PME-4) is 58 KDa. The *C. elegans* PME-3 and PME-4 only share 18 and 22% identity with the human PARG, respectively (St-Laurent *et al.*, 2007). Both proteins showed glychydrolase activity, and the same residues within the PARG signature identified as important in bovine PARG (Koh *et al.*,

2003; Patel *et al.*, 2005), were shown to be required for activity in the *C. elegans* proteins (St-Laurent *et al.*, 2007). Gamma irradiation was shown to reduce survival rates in RNAi treated (knock down) worms, although no major differences were observed between single and double knock-down lines (St. Laurent *et al.*, 2007). Null worms for each of the PARG proteins would help determine their roles in *C. elegans* PARylation and whether any functional redundancy exists between them.

1.6.3 ADP-ribosylhydrolase 3

A second enzyme capable of hydrolysing ADP-linkages has been discovered (Oka *et al.*, 2006). This protein shares very little sequence homology with the PARG catalytic domain (19%), but is still able to remove ADP-ribose units from PARylated proteins, although only at 10% of the activity of the 111 KDa PARG (Oka *et al.*, 2006), and due to the embryonic lethal phenotype of PARG deficient mice (Koh *et al.*, 2004), the glycohydrolase activity provided by ARH3 is not sufficient for survival. The hydrolysis reaction of *O*-acetyl-ADP-ribose was significantly faster than its cleavage of poly ADP-ribose (Ono *et al.*, 2006), which indicates a substrate preference of ARH3 for *O*-acetyl-ADP-ribose, rather than poly(ADP-ribose).

1.7 Poly(ADP-ribosyl)ation functions

1.7.1 Roles of PARP in maintenance of genome stability

While the embryonic lethal phenotype of PARG deficient mice limits further investigation of the biological functions of PARG (Koh *et al.*, 2004), mouse lines lacking the 110 KDa nuclear isoform of PARG have been used to investigate the role of PARG in DNA damage response, and showed increased lethality after exposure to genotoxic agents (Cortes *et al.*, 2004; Gao *et al.*, 2007). When exposed to an alkylating agent PARP1 deficient mice displayed 2 to 3-fold higher rate of sister-chromatid exchange (SCE) compared to wild type mice (Menissier de Murcia *et al.*, 1997), as well as an increase of chromosome end to end fusions and aneuploid cells (d'Adda di Fagagna *et al.*, 1999). The inverse phenotype was observed, when inducible overexpression of PARP1 was shown to decrease

genomic instability as indicated by suppression of alkylation induced SCEs in stably transformed hamster cells compared to control cells (Meyer *et al.*, 2000). Over expression of the DNA-binding domain of PARP1 blocked DNA damage repair (Molinete *et al.*, 1993; Schreiber *et al.*, 1995) and also increased both spontaneous and alkylation induced SCEs (Schreiber *et al.*, 1995). PARylation of histones serve to decondensate the chromatin (Realini and Althaus, 1992) and allow access of the DNA damage repair enzymes as well as transcription machinery to the DNA. PARP1 preferentially targets histone H1 while PARP2 targets histone H2B (Poirier *et al.*, 1982). In *Drosophila melanogaster*, due to the nature of its polytene chromosomes in the salivary glands, transcriptional activity can be seen as "puffs" on these, showing areas of decondensed chromatin. Tulin and Spradling (2003) used this feature to determine localisation of PARP1 protein and PAR during *Drosophila* development. After heat-shocking the flies, PAR transiently accumulates at puff loci known to contain stress response genes. Hypomorphic mutant larvae showed a three-fold reduction in puff sizes, and puffs were not seen in wild type larvae, which were fed the PARP inhibitor 3-aminobenzamide (3-AB). PARG Δ2-3 cells (described in section 1.6.2) showed an increase in SCEs compared with wild type cells, both with and without the presence of DNA damaging agents, as well as a higher number of chromosome aberrations after treatment with genotoxic agents (Min *et al.*, 2010). Taken together these results indicate that PARP1 acts as a negative regulator of DNA-damage induced genomic instability and PARG-mediated homeostasis of PARylation is important for stabilisation of the genome.

1.7.2 Roles of PARP in DNA damage repair

The most lethal form of DNA damage is double strand breaks (DSBs). They can be the result of exposure to genotoxic stress, such as ionising radiation or radiomimetics, or endogenous sources such as replication fork collapse during DNA replication or repair events. Failure to repair DSBs before DNA replication or mitosis can result in cell cycle arrest and apoptosis, while incorrect repair can lead to genomic instability in the form of chromosomal aberrations that could lead to cancer. PARP was implicated as being involved in DNA strand break repair very early after its discovery, as several groups showed an increase in cellular poly(ADP-ribose) polymers shortly after addition of DNA damaging agents

(Juarez-Salinas *et al.*, 1979; Benjamin and Gill, 1980a). Further evidence towards the involvement of PARPs in DNA repair came, when PARP1 (Menissier de Murcia *et al.*, 1997) and PARP2 (Menissier de Murcia *et al.*, 2003) deficient mice as well as cells treated with PARP inhibitors (Durkacz *et al.*, 1980) showed hypersensitivity to genotoxic agents. MEFs deficient of the 110 KDa PARG isoform show delays in DNA repair after both DSBs and SSBs as the repair efficiency in the mutant cells was 30% less than the wild type cells at any given time point post damage during a 24-hour period (Min *et al.*, 2010). Mammalian cells have two major pathways for repairing DSBs: Non-homologus end joining (NHEJ) and homologous recombination (HR). NHEJ is the major type of DSB repair in G0/G1 cells, while HR predominates during S and G2 phases of the cell cycle. Single strand breaks are predominant and endogenous alkylation of bases occurs. The repair mechanisms include base excision repair (BER). The involvement of PARylation in these repair mechanism is discussed in the following sections and hypotheses of repair progression are shown in figure 1.6, and 1.7.

1.7.2.1 Non-homologous end joining

The key proteins in the repair machinery responsible for NHEJ are Ku70/80, DNA-dependent protein kinase catalytic subunit (DNA-PKcs), X-ray repair cross-complementing 4 (XRCC4) and DNA ligase IV. In brief, the mechanism of NHEJ proceeds as follows: DSBs are introduced through endogenous or exogenous genotoxic stress. Heterodimers of Ku70/80 bind to the double stranded DNA ends, after which DNA-PKcs is recruited to the site of damage and binds to each of the Ku heterodimer-DNA end complexes. The DNA is then held together as the ligation is subsequently carried out by the XRCC4/DNA ligase IV complex. Finally, the NHEJ machinery is released (figure 1.6A).

PARP1 has been shown to interact with the Ku heterodimer and DNA-PK (Galande and Kohwi-Shigematsu, 1999). Additionally it was recently shown that using just the BRCT domain of PARP1 as bait in a pull down assay, the whole DNA-PK/Ku heterotrimeric complex was co-immunoprecipitated (Paddock *et al.*, 2011). PARP1 has been shown to PARylate DNA-PKcs *in vitro* which increased the kinase activity of DNA-PK (Ruscetti *et al*, 1998). DNA-PK phosphorylates PARP1 in the presence of dsDNA and this modification in turn decreases PARP1 automodification (Ariumi *et al.*, 1999). This reciprocal regulation was further

confirmed as it was found that inactive PARP1 inhibits the activity of DNA-PK and vice versa *in vitro* (Veuger *et al.*, 2004). One model of the role of PARP1 in NHEJ was proposed by Ariumi *et al.* (1999). PARP1 has been shown to locate to sites of DSB DNA damage and bind to the DNA. As the DNA-PK/Ku complex arrives at the site, DNA-PK is modified by PARP1, which elevates its activity. The automodificaton of PARP1 is inhibited by phosphorylation by DNA-PK, and PARP1 is then displaced from the DNA by the stronger affinity of dsDNA for Ku (Aruimi *et al.*, 1999), and repair through NHEJ can be completed. Another hypothesis for the role of PARP1 in repair through NHEJ is that it acts as a chromatin decondenser, thereby allowing access of large multisubunit protein complexes to the site of DNA damage, that might not otherwise be reached due to steric hindrance by highly condensed chromatin (D'Amours *et al.*, 1999).

1.7.2.2 Homologous recombination

The key proteins responsible for DNA damage repair through HR are BRCA1, the protein kinases Ataxia-telangiectasia mutated (ATM) and ATM-related (ATR), Rad51 and Rad52. In brief, the mechanism of HR involves the physical replacement of sequence information lost due to DNA damage on one double stranded DNA molecule with a segment from an intact homologous DNA molecule. ATM and ATR phosphorylate BRCA1 and along with Rad51, are re-localized to the site of damage. Here Rad52 binds to the DNA ends, and Rad51 forms a filament that allows DNA strand invasion. The bound 3' end invades a homologous DNA duplex and is extended by DNA polymerase (figure 1.6B).

ATM deficient mouse lines exhibit high genomic instability and defective response to DSBs (Barlow *et al.*, 1996). The embryonic lethality of PARP1/ATM (Menissier de Murcia *et al.*, 2001) and PARP2/ATM (Huber *et al.*, 2004) double mutants implies that these proteins are required for repair of endogenous DNA damage of highly proliferating embryonic cells. PARP1 was further implicated in HR when mutants deficient for proteins required for HR (BRCA1, BRCA2, XRCC2, or XRCC3) were found to be sensitive to PARP inhibition (Bryant *et al.*, 2005; Farmer *et al.*, 2005). In addition, a recent study showed the prolonged persistence of Rad51 foci after DNA damage in PARG Δ2.3 cells compared with wild type, indicating that more time is required for HR complexes to repair damaged replication forks in the mutant cells (Min *et al.*, 2010). It was proposed

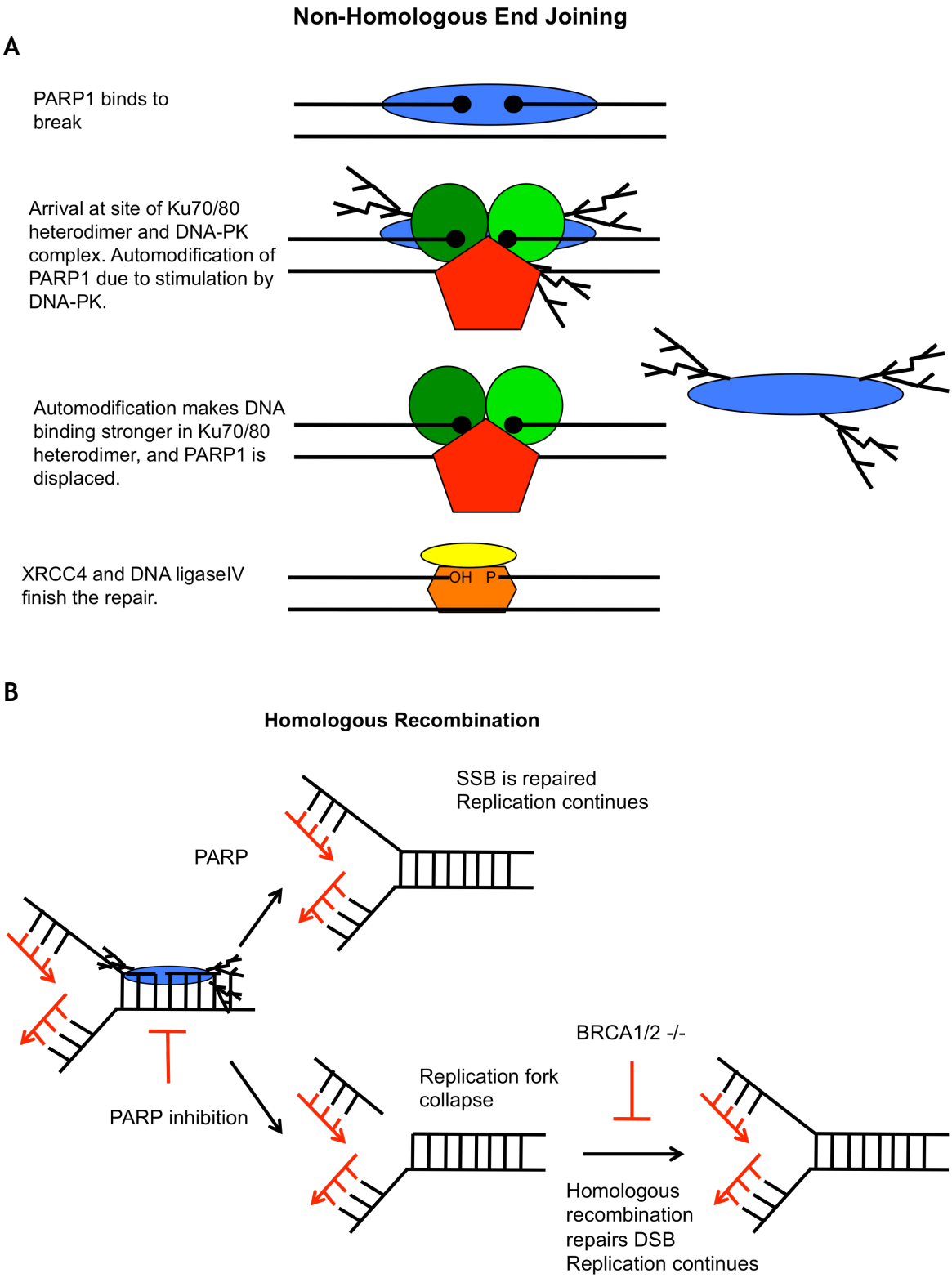

Figure 1.6. Double strand break repair
A) The proposed mechanism for the involvement of PARP1 in NHEJ. PARP1 binds to DNA breaks initially, and is then replaced by the stronger affinity for DNA of the Ku70/80 heterodimer. DNA-PK binds to the Ku heterodimer and stimulates the activity of PARP1, which then automodifies and leaves the DNA. XRCC4 and DNA ligase IV then catalyse the ligation of the gap.
B) The proposed mechanism for involvement of PARP1 in HR. PARP1 is involved in the repair of single strand breaks. If PARP1 is inhibited, the break persists and the replication fork collapses into a one-ended double strand break. In cells deficient in BRCA1 or BRCA2 the collapsed replication forks are repaired by error-prone repair pathways, leading to further genetic instability or are directly lethal to cells.

that if PARP1 is inhibited and thus not able to repair SSBs through BER (as described earlier), these breaks result in DSBs at the replication fork, which is repaired by HR using error free sister chromatid recombination repair. In cells also deficient for HR, this repair pathway can no longer be used, and the DSB at the replication fork will be repaired by error-prone NHEJ or single strand annealing which can result in further genetic instability in the form of chromatid rearrangements and be potentially lethal (Farmer *et al.*, 2005; Helleday *et al.*, 2005).

1.7.2.3 Base excision repair

Most of the work to date implicating PARP in DNA damage repair has been done on the base excision repair (BER) pathway (figure 1.7). The proposed mechanism of BER starts with detection of the break by PARP1 followed by automodification. This action then recruits the scaffold protein X-ray repair cross-complementing 1 (XRCC1) and DNA ligase III to the site of damage through an unknown mechanism. DNA polymerase ß and polynucleotide kinase (PNK) are then recruited to the complex, where the former fills the gap. PNK processes the ends, and the gap is finally closed by DNA ligase III (figure 1.7).

A role for PARP1 in BER was initially proposed, when overexpression of the DNA-binding domain blocked repair of single stranded breaks caused by alkylating agents (Molinete *et al.*, 1993). The interaction of PARP1 with XRCC1 was found to occur through the BRCT domain and zinc fingers of PARP1 (Masson *et al.*, 1998). XRCC1 contains three BRCT motifs and interacts with the PARP1 through the central one of these (Masson *et al.*, 1998). The other BRCT domains bind to DNA ligase III (Caldecott *et al.*, 1995), and DNA polymerase ß (Kubota *et al.*, 1995), which are also part of the BER complex. Both DNA Polymerase ß and DNA ligase III interact directly with PARP1 (Dantzer *et al.*, 2000; Leppard *et al.*, 2003) and the same three proteins have also been shown to interact with PARP2 (Schreiber *et al.*, 2002). PARG has been shown to interact with XRCC1 (Keil *et al.*, 2006) and the PARG-Δ2-3 cell line, in which only the smaller 60 KDa PARG isoform lacking the N-terminal regulatory domain,is present in the nucleus, shows deficiency in the formation of XRCC1 foci and are hypersensitive to alkylating agents (Gao *et al.*, 2007) implicating PARylation and the precise regulation thereof further in direct participation in the BER pathway. XRCC1

lowers the catalytic activity of PARP1 and PARP2 in a dose dependent manner (Masson *et al.*, 1998; Schreiber *et al.*, 2002). PARP1 and PARP2 have been shown to homo- and heterodimerise, and are able to modify each other (Schreiber *et al.*, 2002). The kinetics for recruitment at the site of damage differs for the two PARPs. While PARP1 appears rapidly and transiently, PARP2 showed a delayed and persistent accumulation at damage sites, indicating a role for PARP2 at a later stage in the repair process (Mortusewicz *et al.*, 2007).

Following DNA damage a cell will follow one of two fates, depending on the extent of the damage; if the amount of DNA damage is limited, PARP activity is induced and recruits the cellular DNA repair machinery to the site of injury, the DNA is repaired and the cell survives. If the DNA damage is too extensive, PARP1 and PARP2 are activated by DNA strand breaks, too much polymer is produced, depleting the cell of NAD^+, and thus ATP, and the cell undergoes necrosis or apoptosis (figure 1.8). The involvement of PAR in these two types of cell death will be discussed later in section 1.7.4. Experiments using alkylating agents and ionising radiation showed single PARP1 and PARP2 single knockout mice were viable and fertile and showed no obvious phenotype, but are hypersensitive to DNA damage (de Murcia *et al.*, 1997; Schreiber *et al.*, 2002). Double PARP1 and PARP2 knockout mouse lines are embryonic lethal, thus demonstrating that the remaining PARP enzymes in the cell exhibit partial functional redundancy and that DNA-dependent PARylation is required for embryogenesis (Menissier de Murcia *et al.*, 2003). The phenotypes observed in the experiments using knockout mouse lines as well as the evidence presented in the previous sections above, all point to a role for PARylation in several DNA repair pathways.

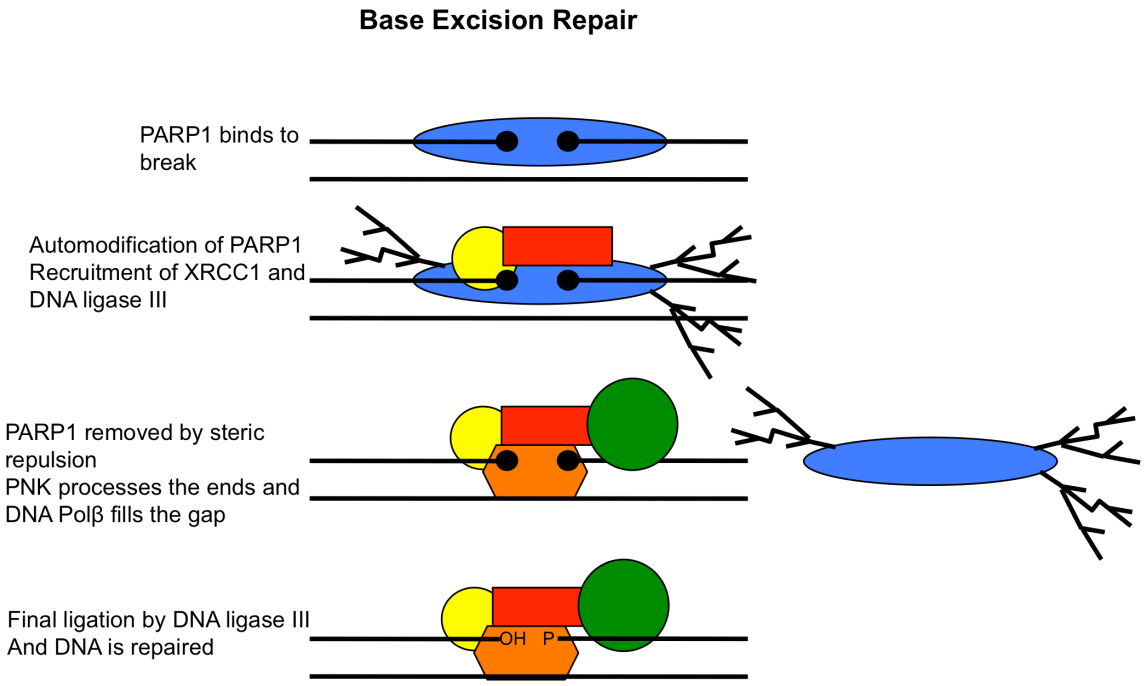

Figure 1.7. Base Excision Repair
The proposed mechanism for the involvement of PARP1 in the BER pathway. Upon DNA damage , the break is detected by PARP1, which binds to the site of damage. This stimulates automodification, which in turn recruits the scaffolding protein X-ray repair cross-complementing 1 (XRCC1) and DNA ligase III to the site of damage through an unknown mechanism. DNA polymerase ß and polynucleotide kinase (PNK) are then recruited to the complex, where the former fills the gap. PNK processes the ends, and the gap is finally closed by DNA ligase III.

1.7.3 Cell cycle progression

PARylation has been shown to be involved in the G_1 and G_2 cell cycle check points where G_1 arrest was suppressed by the inclusion of PARP inhibitors after exposure to γ-irradiation (Matsutani *et al.*, 1995) and while G_2 arrest was enhanced following treatment with PARP inhibitors and MNNG (Jacobson *et al.*, 1996). There is also a requirement for PARylation to induce the G_0 to G_1 transition in resting cells (Carbone *et al.*, 2008). Pleschke *et al* (2000) discovered a 20-amino acid consensus PAR-binding motif, consisting of a cluster rich in basic residues and a pattern of hydrophobic amino acids interspersed with basic residues. This motif has been shown to be present in several DNA damage checkpoint proteins, shown to interact with PARP or to be PARyated, such as p53 and p21 (Pleschke *et al.*, 2000). The tumour suppressor p53, a transcription factor, which is known for its involvement in DNA damage and cell cycle checkpoint progression as well as being one of the most frequently mutated proteins in cancers, is a target for PARylation (Malanga *et al.*, 1998; Kumari, Mendoza-Alvarez and Alvarez-Gonzalez, 1998). The attachment of the PAR to p53 was shown *in vitro* through electrophoretic mobility shift assays where the binding of p53 to its DNA consensus sequences was prevented, and thus demonstrating that PARP acts as a transcriptional repressor of p53 activated genes (Mendoza-Alvarez and Alvarez-Gonzalez, 2001). Differences in chain length and branching could also provide an additional source of regulation as it was shown that p53 has higher affinity for chains of PAR of over 39 units (Fahrer *et al.*, 2007). The p53 sequence contains three PAR-binding motifs: two in the DNA binding region and one in the domain responsible for oligomerisation (Pleschke *et al.*, 2000). The affinity for longer polymers would therefore be likely to disrupt the oligomerisation of p53 and therefore result in the decreased binding to consensus DNA sequences mentioned above.

1.7.3.1 Mitotic apparatus

PARylation plays a role in the progression of mitotic cell division. Both PARP1 and PARP2 localize to mitotic centromeres during prometa and metaphase (Earle *et al.*, 2000; Saxena *et al.*, 2002b). The key structural centromeric proteins Cenpa, Cenpb as well as the mitotic spindle checkpoint protein Bub3 interact

both with PARP1 and PARP2 (Saxena *et al.*, 2002a; Saxena *et al.*, 2002b) and are also PARylated (Saxena *et al.*, 2002a). PARP2 deficient cells display kinetochore defects resulting from mis-segregation (Menissier de Murcia *et al.*, 2003). PARP1 localises to centrosomes throughout the cell cycle (Kanai *et al.*, 2000) where it is involved in the regulation of centrosomal function, as PARP1 deficient cells displayed aneuploidy, which is known to be caused by hyperamplifiction of centrosomes (Kanai *et al.*, 2003). Aside from its role as a cell cycle checkpoint protein (for review see Ko and Prives, 1996), p53 is also involved in the control of centrosome duplication through physical interactions with centrosomes (Tarapore *et al.*, 2001). PARP1 was shown to also PARylate p53 at the centrosome, and this modification of p53 could be part of the regulation of p53 in its role of controlling the centrosome duplication cycle (Kanai *et al.*, 2003). Both PARG and PAR were shown to localize to spindle poles and addition of excess PARG or anti-PAR antibody resulted in rapid breakdown of spindle structure (Chang *et al.*, 2004). The telomeric tankyrase1 is also involved in spindle assembly, but localises to spindle poles (Smith and de Lange, 1999), and has been shown to interact with and PARylate the spindle protein nuclear mitotic apparatus protein (NuMa) (Chang *et al.*, 2005) As it is unlikely that PAR binds microtubules directly, due to the negative charge of both polymers, it was proposed that the interaction between NuMa and tankyrase 1 and the PARylation of the former might help form clusters of microtubule minus ends and create two discrete poles (Chang *et al.*, 2009).

1.7.3.2 Telomere maintenance

PARP2 has been shown to interact with and PARylate TRF 2 (Dantzer *et al.*, 2004), while tankyrase 1 and 2 PARylate TRF1 (Sbodio *et al.*, 2002), which is a negative regulator of telomere extension by telomerase (van Steensel and de Lange, 1997). Tankyrase-1 has been shown to positively regulate telomere length and thus providing stability of chromosome ends by inhibiting the binding of TRF-1 to telomeric repeats through ADP-ribosylation, allowing access of telomerase to the telomeric complex (Smith and de Lange, 2000). A role for PARP1 in telomere maintenance was also suggested, when PARP1 deficient mice displayed extensive telomere shortening compared to wild type animals, in spite of no alteration of telomerase activity (d'Adda di Fagagna *et al.*, 1999), although this could be a side effect of inefficient DNA repair.

1.7.4 PARP in cell death

When the level of DNA damage in the cell gets too high this results in cell death through necrosis due to hypersynthesis of PAR and thus depletion of cellular NAD^+ (figure 1.8). To restore cellular NAD^+ levels, its re-synthesis requires consumption of 2-4 molecules of ATP to one NAD^+, leading to a depletion of ATP and cellular energy failure, finally resulting in necrotic cell death (Ha and Snyder, 1999; Filipovic *et al.*, 1999). However, it has also been shown that PARP1 activity and the overproduction of polymer is part of a caspase-independent apoptotic pathway (Figure 1.8). Yu *et al.* (2002) compared the effect of alkylating agents on wild type and PARP1 deficient MEFs as well as simultaneous blocking of caspase activity using broad spectrum caspase inhibitors. The latter could not prevent PARP1 cell death, but the application of a PARP1 inhibitor brought the survival rate of wild type cells up to the same level as in the PARP1 knockouts. The pro-apoptotic flavoprotein apoptosis inducing factor (AIF), which is localized to the mitochondria, has been shown to induce caspase-independent cell death (Cregan, Dawson and Slack, 2004). In this study they observed the translocation of AIF from the mitochondria to the nucleus upon MNNG or H_2O_2 exposure in wild type cells, but adding a PARP1 inhibitor prevented this event. The release of cytochrome-c from mitochondria happens after the activation of PARP1 and the translocation of AIF. This process is caspase-independent, as studies using a broad range caspase-inhibitor still exhibit apoptotic symptoms after exposure to DNA damaging agents. Later it was proposed that the PAR polymer itself is toxic. When *in vitro* synthesized PAR was introduced into PARP1 knockout mouse cortical neurons, it resulted in high rates of cell death, which was prevented by the pre-treatment of PAR polymers with PARG. The PAR induced cell death rate was also seen to increase with polymer length and complexity. The finding that introduction of PAR into PARP1 knockout cells induces the release of AIF helped to confirm the theory of PARP1 mediated cell death. Upon extensive DNA damage PARP1 synthesizes excessive amounts of PAR, which in turn moves from the nucleus to the mitochondria where it, through an unknown mechanism triggers the release of AIF. AIF then translocates to the nucleus, where it induces DNA fragmentation, possibly through the recruitment of nucleases (Andrabi *et al.*, 2006; Yu *et al.*, 2006). A recent study showed the effects of silencing PARP1, PARP2, both PARPs, and PARG in HeLa

cells using RNAi. Only silencing of PARP1 had any cytoprotective effect, and these cells were also the only ones in which AIF release was blocked. Staining with markers for apoptotic and necrotic death has shown the majority of cell death after exposure to alkylating agents is apoptotic (Cohausz *et al*. 2008). All these results could suggest that interference with PAR rather than PARP-1 could be an alternative therapy approach, as it would not compromise the DNA repair properties of PARP1 (Andrabi *et al*., 2006). There are currently no known inhibitors of AIF to investigate this further. The exact nature of the mechanisms by which levels of PARP and PAR are involved in inducing cell death through the release of AIF, are still unknown. PARP1 is inactivated during apoptosis (Soldani and Scovassi, 2002) and cleaved by caspase 3 and 7 into a short N-terminal fragment containing the DNA-binding domain and a larger C- terminal fragment which no longer has DNA damage activated activity (Kaufmann *et al*, 1993).

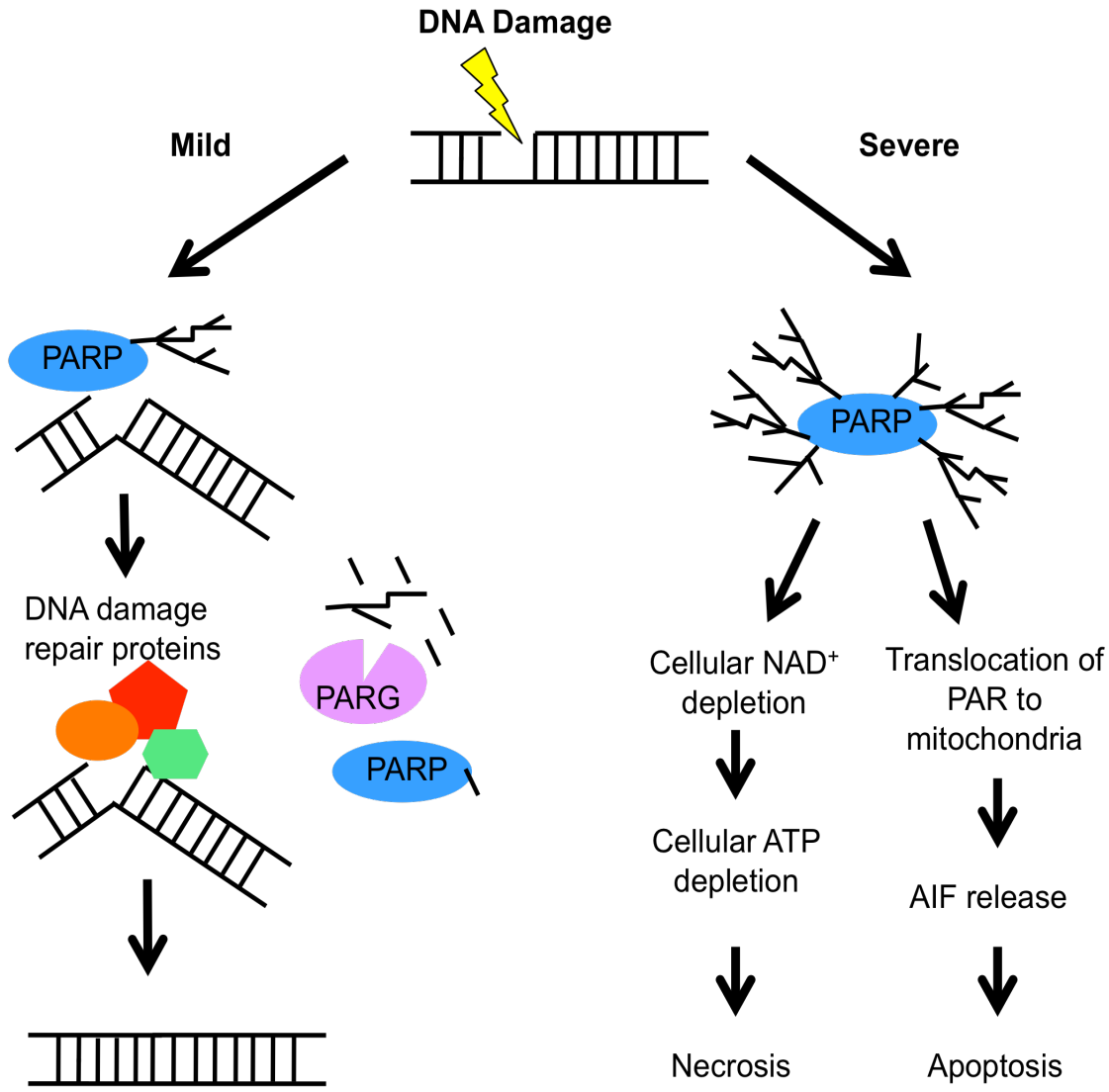

Figure 1.8. Poly(ADP-ribosyl)ation in response to DNA damaging stress
Poly(ADP-ribosyl)ation can result in different fates for the cell, depending on the severity of damage. Following mild DNA damage, PARP will bind to the site of damage through its DNA binding domain, automodify itself and decondensate the chromatin. DNA repair machinery is then recruited to the site, while PARP is removed and PAR polymers processed by PARG. Finally, the DNA repaired and the cell survives. If the DNA damage is severe, the overproduction of PAR polymer by PARP will either use up the cellular NAD^+, thus using up the cellular energy store and ultimately resulting in necrotic death. Alternatively the excess PAR polymer is translocated to the mitochondria, where it triggers the release of AIF. This molecule then shuttles to the nucleus and triggers apoptosis.

1.7.5 Poly(ADP-ribosyl)ation in mitochondria

Apart from the movement of PAR into mitochondria upon overactivation of PARP1 in response to lethal levels of DNA damage described in previous sections, several studies confirm the involvement of PARylation in the maintenance of mitochondrial DNA. PARylation was observed in mitochondria relatively early in PARP research (Kun *et al.*, 1975). The depletion of PARP1 was shown to inhibit repair of mitochondrial DNA in response to alkylating agents (Druzhyna *et al.*, 2000), although the impact of PARP1 on repair of mitochondrial DNA could be through epigenetic regulation of nuclear encoded mitochondrial proteins (Lapucci *et al.*, 2011). Research into the role of PARylation in mitochondria has since then been somewhat abandoned until recently with the discovery of mitochondrially localized PARG isoforms (Meyer *et al.*, 2007). Mitochondria contain a significant proportion of the cellular NAD^+ pool, about 10-fold of what was seen in the cytoplasm (Tischler *et al.*, 1977). There is debate about the existence of mitochondrial PARylation, as several groups have found conflicting results regarding the presence of PARP1 in mitochondria (Du *et al*, 2003; Rossi *et al.*, 2009), although when cells transformed with a truncated catalytically active PARP1 with an artificial mitochondrial targeting sequence, endogenous PAR-degrading activity could be observed in the mitochondria (Niere *et al.*, 2008). PARP1 was shown to interact with mitofilin (Rossi *et al.*, 2009), a mitochondrial protein involved in control of mitochondrial christae morphology (John *et al.*, 2005) and a mechanism of mitochondrial import (Xie *et al.*, 2007), and that the localization of PARP1 to mitochondria was dependent on the presence of mitofilin (Rossi *et al.*, 2009).

1.8 Poly (ADP-ribosyl)ation in plants

While PARylation is well characterised in mammals, comparatively little is known about its role in plants. PARP activity was first observed in plants in 1976, when poly(ADP-ribose) was detected cytologically in nuclei of germinating onion seeds and meristematic tissue through incorporation of radio labelled NAD^+ (Payne and Bol, 1976). Poly(ADP-ribose) was later found in chromatin preparations from ungerminated wheat seeds as well as wheat seedling root tip nuclei, and that the appearance of the this polymer could be inhibited by addition of the PARP

inhibitor 3-AB (Whitby and Whish, 1977). The association of poly(ADP-ribose) with chromatin in plants was confirmed when Willmitzer (1979) showed covalent attachment of PAR to histones H1, H2A, and H2B in nuclei from *Nicotiana tobaccum* cultures, as well, further likening the process of PARylation in plants to what had been established in mammals. Initial experiments recorded the average PAR polymer chain length to be between 2.5 and 8.2 units (Whitby *et al.*, 1979; Willmitzer, 1979), while examination of polymer chain length in maize was later shown to reach up to 45 units (Chen *et al.*, 1994; Mahajan and Zuo, 1998). While this was considerably less than seen in mammalian cells, the plant tissue used for determination of polymer length had not been exposed to DNA damaging agents.

When examining the PARylation activity of isolated nuclei in higher plant seedlings, the activity of NAD^+ incorporation was found to be 3-fold higher in maize than in pea and wheat, with Km for NAD^+ comparable to that of PARPs in mammalian cells (Chen *et al.*, 1994). Use of antibodies to the mammalian PARP1 did not react to any proteins in the maize nuclear extracts, but a PARP of similar size (114 KDa) to the mammalian PARP1, was identified by its automodification activity (Chen *et al.*, 1994), and was later cloned and partially purified (Mahajan and Zuo, 1998). This enzyme was found to share sequence conservation in both the zinc finger domains and the catalytic domain and had an overall amino acid identity of 40-42% and 50% similarity to the mammalian PARP1 (Mahajan and Zuo, 1998). This maize enzyme showed sensitivity to different mammalian PARP inhibitors (Chen *et al.*, 1994; Mahajan and Zuo, 1998), while they were not affected by an inhibitor specific for mono(ADP)-ribosyltransferases (Mahajan and Zuo, 1998). A yeast screen searching for Arabidopsis genes allowing yeast to grow under various types of stress, found a shorter cDNA homologous to mammalian PARP. This was used to clone APP (AtPARP2/At4g02390) from *A. thaliana* (Lepiniec *et al*, 1995) and a homologue (NAP) was also found in maize (Babiychuk *et al.*, 1998). The AtPARP2 sequence showed high similarity to the PARP catalytic domain, and contained a glutamate rich region for automodification, but showed no similarity to the N-terminal zinc finger domain (Lepiniec *et al.*, 1995). Further analysis of the N-terminal sequence of AtPARP2, like the mammalian PARP2, showed homology to the SAF-A domain (Babiychuk *et al.*, 2001). A longer homologue of PARP1 with high similarity to maize ZAP (74%

similarity) was found in *Arabidopsis* (AtPARP1/At2g31320) and was shown to contain two zinc finger domains and an NLS (Doucet-Chabeaud *et al*., 2001). The DNA-binding activity of AtPARP1 and AtPARP2 (Doucet-Chabeaud *et al*., 2001; Babiychuk *et al*., 2001) and the DNA-dependency for activity of AtPARP2 (Babiychuk *et al*., 1998), as well as the nuclear localisation of both AtPARP2 and ZAP (Babiychuk *et al*., 2001) further likened the plant PARPs to their mammalian homologues. Later a third PARP (AtPARP3/At5g22470) was found through sequence homology with the PARP signature (Hunt *et al*., 2004). A comparison of the structures of AtPARPs compared to other higher plant and mammalian PARPS is shown in figure 1.9. Although papers have recently been published describing *Arabidopsis* genes (RCD1, SRO1) other than the above-mentioned AtPARPs as having both an N-terminal WWE domain as well as the PARP signature (Ahlfors *et al*., 2004; Citarelli *et al*., 2010), neither contain all the conserved catalytic residues within the signature domain required for activity (Jaspers *et al*., 2010).

Like *C. elegans*, *Arabidopsis* has two genes that encode PARGs. Unlike the AtPARPs, which are spread out across the *A. thaliana* genome, the two AtPARGs are located next to each other on chromosome 2 and are thus very likely to represent a gene duplication (Hunt *et al*., 2004). The two AtPARG genes are very similar in their primary sequence with 51.5% identity and 66.9% similarity. However, neither have any similarity to the N-terminal part of the longer isoforms of mammalian PARG.

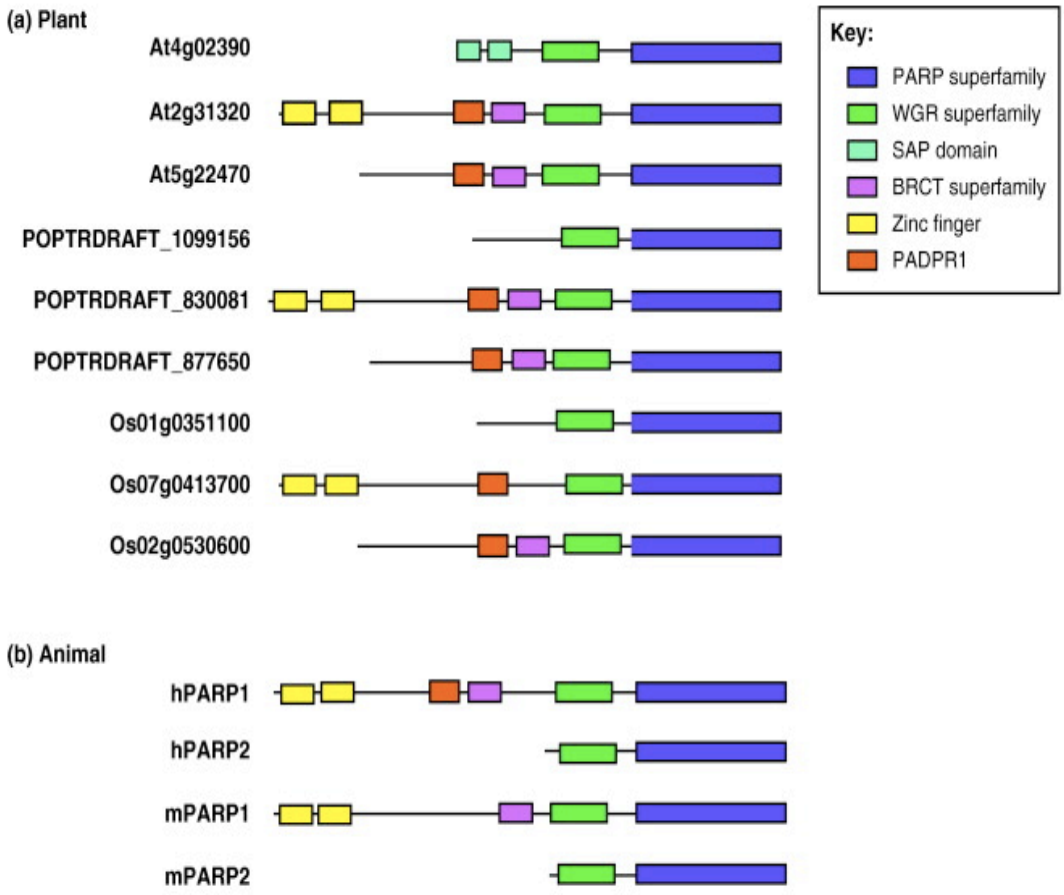

Figure 1.9. Comparison of conserved protein domains in plant and animal PARPs
Sequences from *Arabidopsis* (At), poplar (POPTRDRAFT), rice (Os), human (h), and mouse (m) were analysed for structural similarity. Figure taken from (Briggs and Bent, 2011).

1.8.1 Role of poly(ADP-ribosyl)ation in plants

1.8.1.1 Genome maintenance

Like their mammalian homologues, PARPs in plants are also likely to play a role in genome maintenance, as they were found to associate with mitotic chromosomes in dividing cells (Babiychuk *et al*, 2001). Higher levels of AtPARP2 transcript were seen in *A. thaliana* suspension cultures, compared to whole plant levels (Lepiniec *et al.*, 1995), and PARP activity increased during times of high cell cycle activity (Pellny *et al.*, 2009). In addition, the differentiation of tracheary elements in pea and artichoke was inhibited by the inhibitor 3-AB (Phillips and Hawkins, 1985). The addition of PARP inhibitor 3-methoxybenzamide (3-MB) to the medium of both *Arabidopsis* and tobacco seedlings and mature plants showed an increase in intrachromosomal homologous recombination events (Puchta *et al.*, 1995). Growth of seedlings in liquid media supplemented with the PARP inhibitor 3-AB significantly reduced

seedling fresh weight (Adams-Phillips *et al.*, 2008). Taken together, these results indicate the possible involvement of PARylation in cell division and differentiation.

1.8.1.2 Genotoxic stress

Unlike their mammalian counterparts, which are regulated at the protein level, so far evidence points to the plant PARPs being under transcriptional control. This is demonstrated by the fact that AtPARP2 shows strong dose-dependent expression in response to the radiomimetic zeocin (De Schutter *et al.*, 2007) and the massive upregulation of AtPARP1 and AtPARP2 transcripts in response to γ-irradiation and treatment with the radiomimetic bleomycin and the DNA crosslinker mitomycin C (Doucet-Chabeaud *et al.*, 2001; Garcia *et al.*, 2003; Chen *et al.*, 2003; Culligan *et al.*, 2006). The number of *Arabidopsis* PARP inhibitor treated seedlings surviving doses of the alkylating agent methyl methanesulphonate (MMS), that were sub-lethal to control seedlings, were decreased (Puchta *et al.*, 1995). AtPARP1 and AtPARP2 are regulated by the protein kinase ataxia telangiectasia mutated (ATM) (Garcia *et al.*, 2003; Culligan *et al.*, 2006). In wild type plants the increase of AtPARP1 and AtPARP2 transcripts in response to γ-irradiation was confirmed, while in irradiated ATM deficient mutants transcript levels were no different to those observed in control conditions (Garcia *et al.*, 2003). Another potential regulator is Sta1 (starik1), a mitochondrial ABC transporter, as it was demonstrated that in *sta1* plants both AtPARP1 and AtPARP2 transcript levels, along with the DNA repair protein AtRAD51, were constitutively upregulated compared to the levels observed in the wild type plants (Kushnir *et al.*, 2001). The same phenotype could be seen in mutants of brushy1, a gene thought to be involved in epigenetic maintenance (Takeda *et al.*, 2004).

1.8.1.3 Oxidative stress

Both AtPARP1 and AtPARP2 transcript levels rise after the exposure to H_2O_2 (Doucet-Chabeaud *et al.*, 2001). The effect of oxidative stress was examined using the PARP inhibitors 3-AB and nicotinamide, as well as overexpression and silencing of AtPARP2 on soybean cell cultures (Amor *et al.*, 1998). At lower concentrations of H_2O_2, PARP inhibitor and AtPARP2 overexpressing lines show

lower amounts of cell death, compared to control and AtPARP2 silenced lines. At higher concentrations the AtPARP2 overexpressing lines showed increased amount of cell death compared to control and AtPARP2 silenced lines (Amor *et al.*, 1998). This indicates a mechanism of cell death regulation similar to that proposed for mammalian cells, that when the level of DNA-damage is too high, the cells die due to overconsumption of NAD^+. Oxidative stress in the form of H_2O_2 produced by methyl viologen (MV) induced poly(ADP-ribose) levels (Ishikawa *et al.*, 2009; Ogawa *et al.*, 2009). The amount of seedlings surviving the combination of PARP inhibitor and MV treatment was significantly lower than the amount of seedlings surviving either treatment with either chemical separately (Ishikawa *et al.*, 2009). Seeds from an AtPARG1 deficient mutant displayed a decreased germination rate, as well as reduced expression of oxidative stress-related genes, compared to wild type seeds when exposed to MV (Li *et al.*, 2010). Oxidative stress treatment using MV of AtPARP1 or AtPARP2 silenced lines showed higher chlorophyll content than the wild type plants (De Block *et al.*, 2005), while AtPARG1 deficiency had the opposite effect (Li *et al.*, 2010).

1.8.1.4 Abiotic stress

Several groups have shown an involvement of PARylation in response to abiotic stress. While AtPARP1 and AtPARP2 transcript levels were upregulated in response to drought (Doucet-Chabeaud *et al.*, 2001), down-regulation of AtPARP1 or AtPARP2 in *Arabidopsis* or in *Brassica napus* enhanced their tolerance to heat, drought and high light (De Block *et al.*, 2005). A drought sensitive phenotype was observed in plants deficient of AtPARG1 (Li *et al.*, 2010). The AtPARP1 and AtPARP2 down-regulated lines were found to have higher concentrations of NAD^+ and a decrease in radical oxygen species production post-stress, resulting in higher energy use efficiency (De Block *et al.*, 2005). A microarray comparing the AtPARP2 down-regulated lines with wild type under high light stress, showed a high proportion of genes involved in response to ABA, dehydration, and cold to be highly upregulated, compared to the wild type, while genes responsive to oxidative stress were induced in the wild type, but were delayed or absent in the AtPARP2 down-regulated lines (Vanderauwera *et al.*, 2007). The down-regulation of AtPARPs did not affect the growth, development, or fertility of the silenced lines. In addition, the DNA-repair mechanisms of these lines did not appear to be deficient, as no higher mutation

frequency could be observed with application of an alkylating agent, than could be seen in the controls (De Block *et al.*, 2005). Interestingly, while a slight increase in AtPARP2 transcript was seen in response to treatment with MV and salinity, a massive increase in the transcript levels of AtPARP3 could be seen in response to MV, drought, salinity and high light (Ogawa *et al.*, 2008). AtPARP3 is virtually uncharacterized, and has so far only been implicated in seed development, during which it is highly expressed (Hunt *et al.*, 2007).

1.8.1.5 Alternative roles for poly(ADP-ribosyl)ation in plants

Most of the work exploring the role of PARylation in plants, have focused on their implication in DNA-repair, based on the knowledge gained from studies on the mammalian PARPs. AtPARG1 was shown to be involved in circadian rhythm. A single basepair mutant at the third glycine in the triplet in the highly conserved catalytic PARG signature domain showed alteration in phasing (Panda *et al.*, 2002). This resulted in an early flowering phenotype and also an increase in total cellular PAR content (Panda *et al.*, 2002). A link to circadian rhythm in mammals was discoved recently,as circadian regulation of PARP1 activity was shown, as well as PARylation of CLOCK, one of the main regulators of circadian rhythm in mammals (Asher *et al.*, 2010). Studies have also demonstrated an involvement in pathogen defence of AtPARGs (Adams-Phillips *et al.*, 2008, Adams-Phillips *et al.*, 2010). AtPARG2 transcript was increased by several *R-avr* interactions and flg22 treatment (Adams-Phillips *et al.*, 2008). Use of PARP inhibitors blocked the deposition of callose, normally observed in the basal immune response to the microbe-associated molecular patterns (MAMPs) flg22 and elf18 (Adams-Phillips *et al.*, 2008). Levels of PAR polymer were significantly increased during bacterial and fungal infection (Adams-Phillips *et al.*, 2010). Plant defence against pathogens include an oxidative burst involving H_2O_2, a known inducer of PARylation in both animals and plants (Blenn *et al.*, 2007; Amor *et al.*, 1998). In addition, the application of salicylic acid, known to be produced in response to pathogens, to onion bulb root cells showed a dose dependent relationship to DNA damage (Tuteja *et al.*, 2008), which could provide the signal for AtPARG upregulation in response to pathogens.

1.9 Study objectives

The existing knowledge of PARylation is mainly based on studies on mammals. There is very limited information available on this mechanism in plants, but there have been implications of the involvement of PARPs in functions other than DNA damage such as abiotic stress and circadian rhythm.

This study aims to characterize the genes involved in PARylation in *A. thaliana* through reverse genetics. Phenotypes of insertional mutant lines in genes responsible for the PARylation mechanism were examined under genotoxic, abiotic and oxidative stress. The generation of GFP fusion constructs allowed us to observe subcellular localisation of the AtPARGs.

Putative interactors of AtPARG1 were identified through a yeast two hybrid screen carried out by Dual Systems (Switzerland) with AtPARG1 as bait against an *Arabidopsis thaliana* cDNA library. Interaction partners would then help identify any potential roles outside of DNA damage repair, and be examined *in planta*. The well-characterised interaction between PARP1 and PARP2 with XRCC1 was also examined using their respective plant homologues.

A comprehensive *in silico* investigation into the transcriptome of the AtPARGs and AtPARPs was undertaken using microarray results available through online data sets. The role of AtPARG1 was also examined through transcriptional analysis using SAGE of wild type and an AtPARG1 T-DNA insertion lines under normal conditions and in response to genotoxic stress.

2 Methods

2.1 Materials

2.1.1 Chemicals

All chemicals used in this study were provided by Sigma-Aldrich (Poole, UK) or Fischer-Scietific UK (Southampton, UK).

2.1.2 Materials for DNA and RNA manipulation

Kod Hotstart Polymerase (Merck/Novagen), Phusion polymerase (Finnzymes), Reddymix (AB Gene), restriction endonucleases, Reverse transcriptase, dNTPs, (Promega), DNase (Ambion), QiaPrep plasmid miniprep kit, QiaQuick gel extraction kit, and QiaQuick PCR purification kit (Qiagen, Crawley, UK), T4 DNA ligase (New England Bioscience), TRIzol (Invitrogen, Paisley, UK)

2.1.3 Materials for protein manipulation

Broad protein marker (New England Biosciences), Coomassie, Ponceau, Bradford reagent (Sigma-Aldrich, Poole, UK), protease inhibitor tablets (Roche, Mannheim, Germany), Acrylamide, PVDF and nitrocellulose membranes (Bio-Rad), HRP substrate (Pierce), X-ray films (Kodak)

2.1.4 Antibiotics

Antibiotics were made up as described in table 2.1, filter sterilised using a Sartorious Minisart disc filter (0.2 μm), and stored at -20°C.

Antibiotic	Solvent	Stock concentration	Working concentration	Supplier
Kanamycin	H_2O	50 mg/ml	50 μg/ml	Melford
Gentamycin	H_2O	30 mg/ml	30 μg/ml	Melford
Hygromycin B	PBS	50 mg/ml	50 μg/ml	Roche
Spectinomycin	H_2O	100 mg/ml	100 μg/ml	Sigma
Carbenicillin	60% EtOH	50 mg/ml	50 μg/ml	Fischer Scientific
Chloramphenicol	100 % EtOH	80 mg/ml	80 μg/ml	
Rifampicin	DMSO	50 mg/ml	50 μg/ml	Sigma

Table 2.1. Antibiotics used for plasmid and bacterial selection.

2.1.5 Strains

Strain		Purpose
E. coli	Top10	Cloning/ amplification
E. coli	Rosetta-Gami 2 pLysS	Protein expression in *E. coli*
Agrobacterium tumefasciens	GV3101	Transient expression in tobacco Transient expression in *A. thaliana* Floral dip of *A. thaliana*
Saccharomyces cerevisiae	PJ69-4a Pj69-4α	Yeast-two-hybrid protein interaction studies

Table 2.2. Strains of bacteria and yeast used in this study.

2.1.6 Antibodies

All antibodies used in this study (table 2.3 and 2.4) were diluted using TBST (10mM Tris-HCl pH 8, 150 mM NaCl, 0.1% (v/v) Tween 20) with 5% milk powder (Marvel, UK)

Antibody	Source	Dilution	Supplier
Anti-cMyc	Mouse monoclonal	1:3000	Sigma-Aldrich
Anti-HA	Mouse monoclonal	1:3000	Sigma-Aldrich
Anti-His	Mouse	1:10000	Sigma-Aldrich
Anti-RFP	Mouse	1:1000	ABgene
Anti-GFP	Mouse monoclonal	1:5000	Clontech
Anti-PAR	Rabbit polyclonal	1:15000	Calbiochem

Table 2.3. Primary antibodies used for western blots in this study.

Antibody	Dilution	Feature	Supplier
Anti-mouse	1:5-15000	HRP-conjugated	Sigma-Aldrich
Anti-rabbit	1:5-20000	HRP-conjugated	Sigma-Aldrich

Table 2.4. Secondary antibodies used for western blots in this study.

2.1.7 *Arabidopsis thaliana* T-DNA insertion plant lines

Arabidopsis T-DNA insertion lines were obtained from the Nottingham Arabidopsis Stock Centre (NASC) and GABI-Kat (Cologne, Germany) as described in table 2.5. All T-DNA insertions were in a Columbia (Col-0) background.

Gene name and number	Insertion line	Company developed
AtPARP1 /At2g31320	GK 380 E06 (*parp1-1*)	GabiKat
AtPARP2 /At4g02390	GK 420 G03 (*parp2-1*)	GabiKat
AtPARP3 /At5g22470	SALK 108092 (*parp3-1*)	SALK
AtPARG1/At2g31870	SALK 147805 (*parg1-1)*	SALK
AtPARG1 /At2g31870	SALK 116088 (*parg1-2*)	SALK
AtPARG2 /At2g31865	GK 072 B04 (*parg2-1*)	GabiKat

Table 2.5. *A. thaliana* T-DNA insertion lines used in this study.

2.1.8 Plasmid vectors

Plasmid vector	Description	Source
pCRTopo 4.0	Subcloning	Invitrogen
pENTR-D-TOPO	Gateway entry cloning	Invitrogen
pDONR 207	Gateway entry cloning	Invitrogen
pDEST17	Gateway expression in *E. coli* N-term His tag	Invitrogen
pB7WGR2	Gateway N-term RFP tag binary vector	Karimi *et al*, 2007
pB7RWG2	Gateway C-term RFP tag binary vector	Karimi *et al*, 2007
pH7WGF2	Gateway N-term GFP tag	Karimi *et al*, 2007
pH7FWG2	Gateway C-term GFP tag	Karimi *et al*, 2007
pGWB6	Gateway N-term GFP tag	Nakagawa *et al*., 2007
pEARLEY 201	Gateway N-term HA-tag	Earley *et al*., 2005
pAcHLTA	Baculovirus transfer N-term His tag	BD Biosciences
pGADT7-dest	Gateway Y2H activation domain	Dr C. Grefen
pGBKT7-dest	Gateway Y2H binding domain	Dr C. Grefen

Table 2.6. Plasmid DNA vectors used in this study.

2.2 Plant Methods

2.2.1 Surface Sterilisation of Seeds

One chlorine tablet (Covchlor) was dissolved in 35 ml dH2O with one drop of Tween 20. Once fully dissolved, 5 ml of this was added to 45 ml ethanol, mixed gently by inversion and left at room temperature for 5 min. White precipitate

was pelleted by centrifugation at 2000 rpm for 5 min (Sorvall Legend RT) and the supernatant was used as bleach solution. Under sterile conditions in a flow hood, seeds to be sterilised were transferred to an eppendorf tube and soaked in 70% ethanol for 2 min. The ethanol was removed by pipetting and seeds were soaked in 1 ml bleach solution for 8 min, mixing occasionally by inversion. The bleach solution was removed by pipetting and the seeds were then washed twice in 70% ethanol, followed by two washes with 100% ethanol. The seeds were then left to air dry, and once all traces of ethanol were removed the seeds were washed 5 times in sterile dH2O. Seeds were then either stored at 4°C for two days or distributed on ½ MSMSO agar plates and stored for two days at 4°C to stratify.

2.2.2 Growth of *Arabidopsis thaliana* on agar plates

For selection of transgenic plants, germination assays etc., surface sterilised seeds were sown onto 0.8% agar plates containing 5 g/l sucrose and 2.2 g/l Murashige and Skoog with minimal organics (MSMO) basal salts (Sigma-Aldrich) with appropriate antibiotics if applicable. Plates were stratified for 2 days at 4°C and grown under 24 hour light.

2.2.3 Growth of *Arabidopsis* on soil

Seeds were spread onto soil (Levington F2) soaked in the insecticide intercept (Scotts, UK) and vernalised at 4°C for 2 days in the dark. Plants were grown in light conditions as described below with regular watering until seeds were harvested.

Long day: 16 hour photoperiod, light intensity approx. 100-150 µmoles m^{-2} s^{-1}, 22 ºC/18 ºC day/night temperature and 60 %/70 % day/night relative humidity

Short day: 9 hour photoperiod, light intensity approx. 100-150 µmoles m^{-2} s^{-1}, 22 ºC/18 ºC day/night temperature and 60 %/70 % day/night relative humidity

2.2.4 Stress treatment for *A. thaliana* Col-0 RT-PCR

Seeds were surface sterilised and then 20 seeds were added to 24 well plates with each well containing 1ml of ½ MS media before stratification in the dark

and cold for 2 days. The plates were uncovered and placed in 24 hour light on a shaker set at 40rpm for 7 days when another 1ml of MS media was added. The seedlings were grown for another 4 days for 12 days total. In the sterile hood all media was removed from the plates and a fresh 1 ml MS media added to ensure the same quantity. The plates were returned to the growth room for another 2 hours after which time the control samples were taken and the stress chemicals added (see table 2.7). Seedlings were removed from the wells and gently dried on tissue paper before freezing at –80C at time points 0, 2, 4, 8, 24 and 48 hours.

Stress chemical	Final concentration	Stock dissolved in
Mannitol	2.5 M	½ MS Media
NaCl	200 mM	½ MS Media
Abscisic Acid	50 µM	1% Methanol
Jasmonic Acid	50 µM	Ethanol
LPS	1 µg/ml	
NAA	5 µM	1M NaOH
ACC	200 µM	Water
Salicylic Acid	10 µM	Water
MMS	1.2mM	Water
Bleomycin	0.5µg/ml	Water
UV-B	Plates grown in 3µE	
Wounding	Seedling crushed twice with forceps	

Table 2.7. Concentrations for stress conditions for *A. thaliana* seedlings

2.2.5 Stress treatments of T-DNA insertion lines

Seeds were surface sterilised and spread onto agar plates as described in sections 2.2.1 and 2.2.2 above. After 7 days in continuous light, 7 seedlings of the same size were transferred from the agar plates to each well of 12-well plates containing 2 ml ½ MSMO with sucrose as well as increasing concentrations of stress chemical. The plates were then sealed and placed back in continuous light for a further one to two weeks until a phenotype was visible.

2.2.6 UV-B treatment of soil grown T-DNA insertion lines

Seeds were spread onto soil (Levington F2) soaked in the insecticide intercept (Scotts, UK) and vernalised at 4°C for 2 days in the dark. Plants were grown in constant light of approx 100 μM m^{-2} s^{-1} for 12 days. The control group was left in constant light and the rest exposed to constant light supplemented with UV-B at 5 μmol m^{-2} s^{-1} for 48 hours. The experimental group was returned to constant light for a 5-day recovery period. The plants were then photographed.

2.2.7 Chlorophyll content

To determine chlorophyll *a* and *b* content, fresh weights of 15-day old seedlings grown on ½ MSMO agar plates in long day conditions were measured before chlorophyll from individual genotypes was extracted in 10 ml methanol by leaving the plant tissue in methanol solution at 60°C for one hour. Chlorophyll *a* and *b* levels were determined spectroscopically, and total chlorophyll content was calculated using the formula below (Hipkins and Baker, 1986)

Total chlorophyll content = [(25.8 x *A*650 + 4 x *A*665)]x 10/mg tissue

2.2.8 Cross-pollination of *Arabidopsis*

To make genetic crosses, parent lines of *Arabidopsis* were grown in long day conditions for 3-4 weeks until the plants started to flower. Fine forceps were used to remove open or budding flowers that were not selected for crossing. Unopened buds of the female parent plants selected for crossing were emasculated using fine forceps under a stereo microscope, and all organs except the stigma and ovary were removed. The female parents were fertilized with pollen from an open male flower and returned to long day growth conditions until F1 seeds from successful crosses were ready for harvesting.

2.3 Molecular methods

2.3.1 Primers

Primers were designed *de novo* using Primer 3 (Rozen and Skaletsky, 2000) or netprimer software as appropriate. Primers were typically 18-25 bp in length, with a melting temperature (T_m) of 60°C and a GC content of ≥ 40%. Primers were synthesized by MWG Eurofins or Invitrogen and supplied as lyophilised powder and diluted to 100 μM stocks with sterile dH_2O. Primers used in this study are listed in tables 2.8 to 2.12.

Primer name	Primer sequence
M1LP390_G03	TCTGCTCCTCTGCGAGGTAT
M1RP390_G03	CAACATCCCCTGCAAAAGTT
LP320_E06	TTTGCACTTCATTGCTTGATG
RP320_E06	CCACATCAAAAAGCATCTTC
LP865_B04	AATTTCCAGAGAAGAGTCGGC
RP865_B04	TCATAACTCAGAGTAAGGCCTCC
LP870_086	AATCCTGATTGAGGCATGTTG
PARG KO R	TGTTCCACAGATCTCCAACAGT
LP470_092	AAGAAGGCAAAGCCTGAAAAC
RP470_092	GAATTCCTTTCCCTTCCACTG
GK8409	ATATTGACCATCATACTCATTGC
LBb1	GCGTGGACCGCTTGCTGCAACT

Table 2.8. Primers used for genotyping *A. thaliana* T-DNA insertion lines.

Primer name	Primer sequence
Actin 2a	CTTACAATTTCCCGCTCTGC
Actin 2s	GTTGGGATGAACCAGAAGGA
31320L2	CAAATTCAAGAGCAGGCACA
RP320_E06	CCACATCAAAAAGCATCTTC
02390L1	ATTGTGGTTTGACGCCAGTAG
02390R2	ACTGGTTTGCCAAGTGGAACAAC
LP470_092	AAGAAGGCAAAGCCTGAAAAC
PARP3 KOR	TCTTTCCTCCTCTCTCCTGAA
LP865_B04	AATTTCCAGAGAAGAGTCGGC
RP865_B04	TCATAACTCAGAGTAAGGCCTCC
31870_1_for	TGATTGGAGCTCTTCTTGCAT
PARG KO R	TGTTCCACAGATCTCCAACAGT

Table 2.9 Primers used for genotyping RT-PCR

Primer name	Primer sequence
02390_DONR_for	**GGGGACAAGTTTGTACAAAAAAGCAGGCT**TAATGGCGAACAAGCTCAAAGT
02390_DONR_rev	**GGGGACCACTTTGTACAAGAAAGCTGGGT**TTAGTGCTTGTAGTTGAATTTGAC
For320GW	**CACC**ATGGCAAGCCCACATAAG
Rev320GW	TCATCTCTTGTGCTTAAACCTT
For865GW	**CACC**ATGGAACTGAGGGCAGATC
Rev865GW	CTAGGTAGACAGTGAGGTCATGA
For870GW	**CACC**ATGGAGAATCGCGAAGATC
Rev870GW	TCAAGGCGGCTGGATAGCTTTGT
865cDNAinsect_f	CCATGGATGGAACTGAGGGCAGATC
865cDNAinsect_r	CTGCAGTGCTAGGTAGACAGTGAGGTCATGA
870cDNAinsect_f	CCATGGATGGAGATTCGCGAAGATC
870cDNAinsect_r	CTGCAGTGTCAAGGCGGCTGGATAGCTTTGT
attBatKu_for	**GGGGACAAGTTTGTACAAAAAAGCAGGCT**TAATGGAATTGGACCCAGATGATG
attBatKu_rev	**GGGGACCACTTTGTACAAGAAAGCTGGGT**TTATTTACCAATGTGAGTCAGAATCC
attB08530_for	**GGGGACAAGTTTGTACAAAAAAGCAGGCT**TAATGGCACCCGTGAGGGGGATTCTT
attB08530_rev	**GGGGACCACTTTGTACAAGAAAGCTGGGT**TTAAGCAGCCTGTAGCAACTCCCTTTC A
attB09840_for	**GGGGACAAGTTTGTACAAAAAAGCAGGCT**TAATGTCTACCCCAGCTGAATCTTCAG
attB09840_rev	**GGGGACCACTTTGTACAAGAAAGCTGGGT**CTAATTGTAGAGATCATCATCGTCCCC AC

Table 2.10. Primers used for cloning *A. thaliana* genes. AttB sequences highlighted in bold.

Primer name	Primer sequences
E960A320SDM_for	CTTATGTACAATGCATATATCGTCTACG
E960A320SDM_rev	CGATATATGCATTGTACATAAGCTCAG
865SDM L275G_f	GAGTATTTTGGAGGCGGTACTCT
865SDM L275G_r	CATACCTCAGAGTACCGCCTCC
870SDM_D255N_for	GCTCTCGAAGTGAACTTTGCAAAC
870SDM_D255N_rev	CCGAGATACTTGTTTGCAAAGTTCAC
870SDM_E274N_for	GTGCAGGAAAACATACGCTTCATG
870SDM_E274N_rev	GGTTAATCATGAAGCGTATGTTTTCCTGC
870SDM_E273N_for	GGGTGCGTGCAGAATGAGATAC
870SDM_E273N_rev	CATGAAGCGTATCTCATTCTGCACGC
870tejSDM_for	TATCTCGAAGGTGGTTCCCTAAG
870tejSDM_rev	TCTACTTAGGGAACCACCTTCG

Table 2.11. Primers used for site directed mutagenesis.

Primer name	Cycle number	Primer sequence
Actin 2a	25	CTTACAATTTCCCGCTCTGC
Actin 2s		GTTGGGATGAACCAGAAGGA
AtPARP1 for	32	ACCTCCAGAAGCTCCTGCTAC
AtPARP1 rev		GTTTTCCACAGGGAACAGTCA
AtPARP2 for	25	ATTGTGGTTTGACGCCAGTAG
AtPARP2 rev		GAGGAGCTATTCGCAGACCTT
AtPARP3 for	38	CGAGGAGACACACTCGATGAT
AtPARP3 rev		AACCAACCGTCCACAAGGAACTTT
AtPARG2 for	32	CGTTTCCGTATATGCGTCACT
AtPARG2 rev		CATCCATACGAGGCAAAAAGA
AtPARG1 for	31	TTGATTGGAGCTCTTCTTGCATGC
AtPARG1 rev		AAACGAAGATGCATACCCTGTGTA

Table 2.12. Primers used for RT-PCR for determination of expression levels

2.3.2 Extraction of plant genomic DNA

Plant tissue was homogenised in 400 μl extraction buffer (200 mM Tris, pH 7.5, 250 mM NaCl, 25 mM EDTA, 0.5% SDS (w/v)) and vortexed for 10 secs , followed by centrifugation at 10,000 x *g* for 1 minute. The supernatant was transferred to a fresh 1.5 ml eppendorf tube, mixed with 300 μl isoproanol and left at room temperature for 5 minutes. The sample was then centrifuged for 5 minutes at

10,000 x *g* and the supernatant removed. The remaining pellet was washed in 500 μl 90% ethanol, followed by centrifugation for 5 minutes at 10,000 x *g*. All ethanol was removed, and the pellet was left to dry at 37-50°C for 20 minutes. The pellets were then resuspended in 1x TE by gentle flicking and stored at -20°C.

2.3.3 Amplification of DNA by polymerase chain reaction

Polymerase chain reactions (PCR) were performed using a MJ Research DNA Engine PTC-200 Peltier Thermal Cycler (Genetic Research Instrumentation, Essex, UK) Typical PCR reactions were completed in a final volume of 20 μl. Template DNA (0.1 – 0.2 ng) was added to 1x Reddy Mix (Thermo Scientific) (0.5 units Thermoprime Plus DNA Polymerase, 30 mM Tris-HCl (pH 8.8), 8 mM $(NH_4)_2SO_4$, 0.6 mM $MgCl_2$, 0.004% Tween® 20, 80 μM each of dATP, dCTP, dTTP and dGTP and a precipitant and red dye for electrophoresis) along with 0.5 μM forward and reverse primer. Amplification of genes for cloning applications was completed using the proofreading DNA polymerases Kod (Novagen) or Phusion (Finnzymes) according to the manufacturers instructions.

A typical PCR reaction would have an initial denaturing step at 95°C for 2 mins, followed by a suitable number of cycles of denaturing at 95°C for 30 secs, annealing at 55-60°C for 30 secs, and extension 72°C for 1 min per Kb of product amplicon size, followed by a final 5 minute extension step at 72°C.

2.3.4 Transformation of chemically competent *E. coli* cells

Plasmid DNA was added to a 50 μl aliquot of chemically competent TOP10 *E. coli* cells (Invitrogen, Paisley, UK) thawed on ice. This was briefly mixed by flicking and immediately placed back on ice for 5 to 30 minutes. The cells and DNA were heat-shocked in a waterbath at 42°C for 30 seconds and returned to ice immediately. After two mins the mixture had 250 μl LB broth added and was then incubated at 37°C with gentle shaking for one hour, before plating out onto solid LB agar containing appropriate antibiotics for plasmid selection and incubated at 37°C overnight.

2.3.5 Gateway recombination based cloning

2.3.5.1 pENTR-D-TOPO based cloning

Primers for use in the Gateway based cloning vector pENTR D-TOPO had CACC added to the 5' end of the forward primer and genes were amplified using proof-reading KOD Hotstart DNA polymerase. A Topo reaction was then set up with PCR product, salt solution supplied with the kit, and pENTR D-TOPO vector mix containing topoisomerase. Reaction was mixed by flicking, and left at room temperature for 5-10 minutes before 2 μl was used to transform chemically competent *E.coli*. Positive transformants were selected on LB agar plates containing kanamycin and analysed by miniprep, restriction digestion, and sequencing.

2.3.5.2 Gateway® BP recombination based cloning

Primers for use with the Gateway based cloning vector pDONR207 had attB recombination sites added to the 5' end of both forward and reverse primers. Genes were then amplified using proof-reading KOD Hotstart DNA polymerase using a two-step PCR protocol. BP recombination reactions were set up to contain X μl attB PCR product, 0.5 μl pDONR207, 2 μl TE buffer and 1 μl BP clonase enzyme mix (Invitrogen). Reactions were incubated for minimum one hour at room temperature, followed by inactivation by adding 1 unit Proteinase K (Invitrogen) and incubating at 37°C for 10 minutes. Recombination reactions were then used to transform chemically competent *E. coli* cells (section 2.3.4). Positive transformants were selected on LB agar plates containing gentamycin and analysed by miniprep, restriction digestion, and sequencing.

2.3.5.3 Gateway® LR recombination reaction

DNA fragments were cloned into pENTR D-TOPO or pDONR207 to allow for recombination based cloning into various destination vectors, which would facilitate expression of the gene. Recombination reactions were set up to contain 1.5 μl of entry clone, 0.5 μl of destination vector, 2 μl of TE buffer and 1 μl of LR clonase enzyme mix (Invitrogen). Reactions were incubated for minimum one hour at room temperature, followed by inactivation by adding 1

unit of Proteinase K and incubating at 37°C for 10 minutes. Recombination reactions (2 μl) were then used to transform chemically competent *E. coli* cells (section 2.3.4). Positive transformants were analysed by miniprep and restriction digestion.

2.3.6 Agarose Gel Electrophoresis of DNA

DNA agarose gels contained 1% agarose (w/v) melted in 1x TAE buffer (40 mM Tris-acetate, 1 mM EDTA). SYBR Safe (Invitrogen, Paisley, UK) was added to the agarose solution at a 1:10,000 dilution for DNA labelling. DNA samples were loaded alongside a 1 Kb DNA ladder (Promega, Southampton, UK) and separated by gel electrophoresis in 1x TAE buffer at 50-100 V and visualized under UV light.

2.3.7 Restriction digestion

Plasmid DNA was digested using restriction enzymes from either Promega or Roche. In a 1.5 ml eppendorf tube, 2-4 μl miniprepped plasmid DNA was mixed with 2 μl 10x buffer,(2 μl 10x BSA for Promega reactions), 1 μl enzyme and sterile dH_2O to 20 μl. The reaction was incubated at 37°C for one hour and then run out on 1% agarose gels to determine fragment sizes.

2.3.8 Isolation of DNA fragments from agarose gel

DNA bands were separated by agarose gel electrophoresis (section 2.3.6) and the DNA fragment of interest was excised using a razor blade on a UV illuminator and transferred to an eppendorf tube. DNA was purified using the Qiaquick Gel Extraction Kit (Crawley, UK) in accordance with the manufacturers instructions. Purified DNA was eluted in 30 μl sterile dH_2O.

2.3.9 Plasmid DNA isolation

A single colony from a selective LB agar plate was used to inoculate 5 ml of LB broth containing the appropriate antibiotic. The culture was placed in a 37°C incubator shaking at 200 rpm overnight. The culture was pelleted by centrifugation of 4 ml culture at 10,000 x *g* for 1 minute and supernatant

removed. The plasmid DNA was extracted from the pellet using the QiaPrep Spin Miniprep kit (Qiagen, Crawley, UK) according to the manufacturers instructions. Purified plasmid DNA was eluted in 30-40 μl sterile dH_2O and stored at -20°C.

2.3.10 DNA ligation

DNA obtained from PCR amplification or restriction digest were ligated into plasmid vectors in a 10 μl reaction volume. Insert and plasmid vector fragments were typically mixed at a 5:1 ratio with 1x ligation buffer (New England Biosciences), 1 unit T4 DNA ligase (New England Biosciences) and sterile dH2O to a final volume of 10 μl. The ligation mix was incubated at room temperature for 1-4 hours or overnight at 4°C. Typically, 4 μl of the reaction were used to transform chemically competent *E. coli*.

2.3.11 Site-directed mutagenesis of plasmid DNA

Site-directed mutagenesis was performed using specific primers carrying a mutagenic codon. PCR was performed using the proofreading KOD Hotstart polymerase using the appropriate DNA template and mutagenic primers. Primers used for site-directed mutagenesis are listed in table z. Following PCR, the methylated plasmid DNA template DNA was removed by restriction digest with DpnI (10 units) for one hour at 37°C. Following incubation, 2 μl of undigested mutant plasmid was used to transform chemically competent *E. coli* TOP 10 cells (section 2.3.4). Positive transformants were selected on LB agar containing the appropriate antibiotic. Resultant clones were then sequenced to confirm presence of mutation as well as sequence integrity.

2.3.12 Plant RNA extraction

Plant tissue was ground in liquid nitrogen using a mortar and pestle and then transferred to eppendorf tubes. To the ground plant powder, 1.2 ml TRIzol reagent (Invitrogen) was added and mixed by inversion. This was followed by centrifugation at 12,000 x *g* for 10 minutes at 4°C, after which the supernatant was transferred to a fresh 1.5 ml eppendorf tube and 0.2 ml chloroform added. This mixture was then vortexed for 30 seconds, followed by centrifugation at

12,000 x *g* for 10 minutes at 4°C, producing two phases. From the colourless upper aqueous layer, containing the RNA, 600 μl was transferred to a fresh 1.5 ml eppendorf tube, mixed with an equal amount of isopropanol by inversion and left at room temperature for 10 minutes for RNA to precipitate. This was followed by centrifugation at 12,000 x *g* for 10 minutes at 4°C. The supernatant was carefully removed after which the pellet was washed twice using 75% ethanol followed by centrifugation at 12,000 x *g* for 5 minutes at 4°C. The pellet was air-dried for 10 minutes, removing any remaining ethanol, and then resuspended in 50-100 μl DEPC-teated H_2O.

2.3.13 DNAse treatment of RNA

To remove any genomic DNA contamination, extracted RNA (section 2.3.12) was treated with the DNAFree kit (Ambion) in accordance with the manufacturers instructions. RNA extracts were incubated with 0.1x volume 10x DNase I buffer (100 mM Tris-HCl pH 7.5, 25 mM $MgCl_2$, 5mM $CaCl_2$) and 2 units of rDNase I for 25 minutes at 37°C. The rDNase I was inactivated by adding 0.1x volume DNase Inactivation Reagent, mixed and incubated for 2 minutes at room temperature. Treated RNA extracts were centrifuged at 10000x g for 1.5 minutes and supernatant was transferred to a fresh eppendorf tube.

2.3.14 cDNA Synthesis

The DNase treated RNA sample (1.5 to 2.5 μg) was mixed with 0.5 μM oligodT for 10 minutes at 70°C and cooled at 4°C. After this, a reaction mixture containing 1x AMV reverse transciptase buffer (Promega UK Ltd., Southampton, UK), 1 mM dNTPs (Promega UK Ltd., Southampton, UK), 1 U/ μl RNase inhibitor (Promega UK Ltd., Southampton, UK), and 0.4 U/ μl AMV reverse transcriptase (Promega UK Ltd., Southampton, UK), was added to the RNA and the reverse transcription reaction was carried out at 48°C for 45 minutes, followed by inactivation of the enzymes at 95°C for 5 minutes.

2.3.15 Quantification of DNA and RNA

Purified plasmid DNA concentration, as well as the concentration of RNA extracted from plants were assessed by measuring absorbance at 260 and 280 nm using a spectrophotometer (GeneQuant). DNA or RNA samples were diluted 40 fold in sterile H_2O (2 μl in 80 μl), transferred to a quartz cuvette and absorbance at 260 and 280 nm were measured against a blank sterile H_2O sample. Plasmid DNA or RNA concentrations in μg/μl were calculated using the following formula:

DNA (μg/μl) = (OD_{260} x 50) x Dilution Factor

RNA (μg/μl) = (OD_{260} x 40) x Dilution Factor

The purity of the sample is indicated by the ratio of 260/280 nm absorbance values, with optimal purity being 1.8 for DNA and 2.0 for RNA.

2.3.16 Sequencing

Sequencing was carried out by MWG Eurofins or Dundee Sequencing Service (University of Dundee) according to their instructions. Sequencing was carried out on all initial plasmid clones to verify sequence integrity of the insert.

2.4 Yeast Two Hybrid

2.4.1 Dualsystems yeast two-hybrid screen

The yeast two-hybrid screen using AtPARG1 bait was carried out by Dualsystems Biotech AG, Zurich, Switzerland. The bait construct for yeast two-hybrid screening was made by subcloning a cDNA encoding amino acids 1 to 548 of AtPARG1 into the vector pLexA-DIR (Dualsystems Biotech AG, Zurich, Switzerland). The bait construct was transformed into the strain NMY32 (MATa his3Δ200 trp1-901 leu2-3, 112 $(lexAop)_8$-ADE2 LYS2::$(lexAop)_4$-HIS3 URA3:$(lexAop)_8$-lacZ GAL4) using standard procedures (Gietz and Woods, 2001). Correct expression of the bait was verified by western blotting of cell extracts using a mouse monoclonal antibody directed against the LexA domain

(Dualsystems Biotech, Switzerland). The absence of self-activation was verified by co-transformation of the bait together with a control prey and selection on minimal medium lacking the amino acids tryptophan, leucine and histidine (selective medium). For the yeast two-hybrid screen, the bait was co-transformed together with an *Arabidopsis thaliana* cDNA library into NMY32. 4.2 x 10^7 transformants were screened yielding 50 transformants that grew on selective medium. Positive transformants were tested for ß-galactosidase activity using a PXG ß-galactosidase assay (Dualsystems Biotech). 48 of the 50 initial positives showed ß-galactosidase acitivity and were considered to be true positives. Library plasmids were isolated from positive clones. The identity of positive interactors was determined by sequencing.

2.4.2 Transformation of Yeast

Single colonies of the PJ69-4A/α yeast strain on YPD plates were picked using a sterile loop and used to inoculate 5 ml of YPD. Cultures were grown in a shaking incubator 28-30°C overnight. The pre-culture was used to inoculate 45 ml YPD in conical flasks and incubated shaking for 3-6 hours until OD_{600} reaches 0.5-0.8. Cells were harvested by centrifugation for10 minutes at 2000 x *g* (Sorvall Legend RT) and supernatant discarded. The pellet was washed with 20 ml sterile dH_2O and centrifuged again. The supernatant was discarded and cell pellet was resuspended in 1 ml of filtersterilised 0.1 M LiAc and transferred to a 2 ml eppendorf tube. This was then centrifuged at 1500 x *g* for 5 minutes, supernatant removed, filtersterilised 0.1 M LiAc added to a final OD_{600} of 10-20 and suspension was incubated for 30 minutes at room temperature. Mastermix was prepared by mixing 70 μl of filtersterilsed 50% PEG 3550, 10.5 μl of 1 M LiAc, 1.5 μl of boiled ssDNA and 18 μl of competent yeast for each transformation and mixed thoroughly by vortexing. Sterile PCR tube strips (Fischer Scientific) with 10 μl of boiled ssDNA and 2.5 μl of AD and BD plasmid per transformation had 100 μl of mastermix added and was mixed by pipetting. The mixture was incubated at 30°C for 30 minutes, mixing by pipetting after 20 minutes, followed by heat shock at 43°C for 15 minutes. Cells were then spun down at 1000 x *g* for 5 minutes and supernatant was removed by pipetting. Cells were washed with 100 μl sterile dH_2O, spun down again and supernatant removed by pipetting. Finally cells were resuspended in 80 μl of sterile dH_2O and plated out on solid SC

drop out medium (-TRP, -LEU, Clontech), and incubated at 28-30°C for 48-72 hours to ensure selection of plasmid uptake.

2.4.3 Yeast interactions

Colonies were picked from initial transformation plates (section 2.4.2) and grown in 5 ml liquid SD broth (-L, -W) shaking at 28°C overnight. Once cells reached an OD_{600} of 0.8-2.5, cells were pelleted at 1,500 x *g* for 5 minutes. Supernatant was discarded and pellets were resuspended in sterile dH_2O to an OD_{600} of 1.0 and a further 10-fold dilution was made and 5 μl of each of these were spotted onto control plates (-L, -W) to verify the presence of both plasmids and selective plates (-L, -W, -A, -H) to test for interaction.

2.4.4 Protein extraction from yeast

Colonies were picked from plasmid selective plates and grown up in liquid SD broth (-Leu, -Trp) shaking at 28°C overnight. Cells were pelleted at 10,000 x *g* for 5 minutes and supernatant removed. The pellet was then resuspended in "lyse & load" buffer (50 mM Tris-HCl (pH 6.8), 4% SDS, 8 M urea, 30% glycerol, 0.1 M DTT, 0.005% bromophenol blue) to an OD_{600} of 100 and heated at 65°C for 5 minutes, before samples were resolved using SDS-PAGE.

2.5 Protein Methods

2.5.1 Protein expression in *E.coli*

Expression of AtPARG fusion proteins with an N-terminal 6xHis tag was carried out using Rosetta-Gami *E. coli* cells (Novagen). DNA fragments were cloned by Gateway recombination from pENTR-D-TOPO entry clones to the pDEST17 destination vector and transformed into Rosetta-Gami *E. coli* for expression studies. Bacterial cells from a single colony were used to inoculate 5 ml LB overnight initial culture, which was grown at 37°C in a shaking incubator at 200 rpm. A 45 ml expression culture was inoculated using the 5 ml initial culture and was grown at 37°C until an OD_{600} of 0.6 was reached. Recombinant protein expression was induced by the addition of isopropyl ß-D-galactopyranoside

(IPTG) to a final concentration of 1 mM. Following induction expression cultures were grown at 37 °C for 4 hours. Culture samples were taken prior to and 4 hours after induction of recombinant protein expression analysis.

2.5.2 Protein expression in *S. frugiperda*

Spodoptera frugiperda (*Sf*9 cells, Invitrogen) were used to express AtPARG proteins. Recombinant baculovirus carrying N-terminal histidine tagged AtPARG fusion proteins were generated using the BaculoGold™ Transfection kit (BD Biosciences) according to the manufacturers instructions.

2.5.3 Protein extraction from *S. frugiperda*

Cells were washed of the bottom of culture flasks using a pipette and transferred to polypropylene tubes followed by centrifugation at 1000x *g* for 3 minutes. The majority of the supernatant was discarded and the cell pellet was resuspended in the remaining ~ 0.5 ml supernatant, transferred to a 1.5 ml eppendorf and centrifuged at 1000x *g* for 1 minute. All supernatant was removed using a pipette, the cell pellet resuspended in PBS followed by lysis by sonication. The cell suspension was then placed on ice for 2 minutes and centrifuged at 14,000x g for 10 minutes at 4°C. The supernatant, containing the crude soluble protein fraction was transferred to a fresh 1.5 ml eppendorf and the pellet, containing the insoluble fraction, had 100 μl PBS added and was then briefly sonicated to aid resuspension. Fractions were stored on ice or at -20°C before further use.

2.5.4 Quantification of protein concentration

Protein content of samples was determined using Bradford reagent (Sigma, Poole, UK). A standard curve was set up using bovine serum albumin concentrations of 0.25, 0.5, 0.75, 1.0, and 1.4 mg/ml. 33 μl of each of these concentrations was added to 1 ml of Bradford reagent in an eppendorf tube and mixed by pipetting. This mixture was left at room temperature for 5 minutes, after which it was transferred to a 1 ml cuvette and the absorbance at 595 nm measured against a blank of 33 μl sterile water in 1 ml Bradford reagent. A 33-

fold dilution was used for protein of unknown concentration and the absorbance at 595 nm was used to calculate their concentration from a standard curve.

2.5.5 SDS-PAGE under denaturing conditions

The protean mini gel kit from BioRad (Hercules, USA) was used for running the gels and was assembled according to the manufacturers instructions. Resolving gels was made to 7.5-15% acrylamide (30:2) (0.375 M Tris HCl pH 8.8, 0.1% SDS, 0.1% $(NH_4)_2S_2O_8$ and 0.1% TEMED) and immediately poured into casts adding 60μl isopropanol per gel to remove any bubbles and flatten the top surface. Once the resolving gel had set a stacking gel made up to 5.7% acrylamide (0.125 M Tris HCl pH 6.8, 0.1% SDS, 0.1% $(NH_4)_2S_2O_8$ and 0.1% TEMED) was poured on top and a plastic comb inserted to create wells. After the stacking gel had set, the plastic comb was removed and the wells washed out with water, prior to assembling the gel running kit, after which enough 1x running buffer (20 mM Tris base, 0.195 M glycine, 0.1% SDS, pH 8.3) was added to the protein tank to cover both electrodes. Equal amounts of protein were added to each well and a broad range pre-stained protein marker was run alongside samples. The acrylamide gel was electrophoresed at 65 V until the proteins reached the end of the stacking gel, after which the voltage was increased to 135 V until the end of the gel was reached. The glass plates containing the gel were disassembled and the the gel was used for westen blotting (see below) or stained in Coomassie blue stain (45% methanol, 10% acetic acid, 0.5g Coomassie blue) for 30 minutes to 1 hour followed by de-staining (10% methanol, 5% acetic acid) overnight.

2.5.6 Electrophoretic transfer of proteins to membrane

To transfer proteins from an acrylamide gel to a polyvinylidene diflouride (PVDF) or nitrocellulose membrane, the gels were resolved as described in section 2.5.5, and the glass plates disassembled but the gel was not stained. PVDF/nitrocellulose membrane was cut to the same dimensions as the gel and soaked first in methanol for five minutes then in 1x transfer buffer (25 mM Tris, 195 mM Glycine, 20% methanol, pH 8.3) to equilibrate (nitrocellulose membranes do not require this step). After electrophoresis the gel and filter paper was soaked in 1x transfer buffer, before being assembled in a transfer cassette,

along with the equilibrated PVDF/nitrocellulose membrane, according to the manufacturers instructions. This along with a cooling block was then placed in a transfer tank and filled with 1x transfer buffer, and run at 25 V in a cold room (-4°C) overnight while gently stirring or at 100 V for 1 hour on ice.

2.5.7 Western blot

After electrophoretic transfer (section 2.5.6) the transfer cassette was disassembled, rinsed twice in dH_2O, soaked in methanol, and dried. The membrane was then briefly rehydrated in methanol, rinsed for five minutes in dH_2O followed by five minutes in 1x TBST (10mM Tris-HCl pH 8, 150 mM NaCl, 0.1% (v/v) Tween 20), before blocking the membrane in 1x TBST with 5% milk powder with gentle agitation for 30 minutes. The membranes were then incubated with primary antibody diluted in 1x TBST with 5% dried milk for one hour with gentle agitation. The membrane was then rinsed twice for 10 minutes in 1x TBST, followed by incubation with secondary horseradish-peroxidase conjugated antibody diluted in 1x TBST with 5% dried milk for one hour with gentle agitation. After this incubation, the membrane was washed twice for 10 minutes in 1x TBST and rinsed briefly in dH_2O, before the chemiluminescent substrate (ECL, Pierce), consisting of luminol reagent and peroxide reagent at a 1:1 ratio, was added and left for 1 minute. All excess substrate was removed and the membrane was placed protein side up in between two acetate sheets. In the dark the sheets were placed within an X-ray film casstte (Kodak, UK) and X-ray film (Kodak, UK) was placed over the membrane and the cassette closed for exposure. The exposure time varied with each western blot and the film was developed using an X-omat developing system.

2.5.8 Protein purification

2.5.8.1 Preparation of resin

Purification of protein under native conditions was always tried first, however if insufficient protein was in the soluble fraction then all the protein was denatured before being bound to the nickel resin. The protein was then refolded on the resin and eluted. Nickel resin was resuspended and 1.5 ml was transferred to a 15 ml falcon tube. The resin was pelleted by low speed

centrifugation at 800x *g* for 1 min and the supernatant gently removed. The resin was the resuspended in 6 ml sterile dH_2O. The resin was pelleted by centrifugation at 800 x *g* for 1 min and the supernatant removed.

2.5.8.2 Native purification

Cells were pelleted by centrifugation at 2500 x *g* for 15 mins and resuspended in 8 ml native binding buffer (50 mM NaH_2PO_4, 0.5 M NaCl, 10 mM imidazole, pH 8.0) with 8 mg of lysozyme (Sigma-Aldrich) and incubated on ice for 30 mins. Lysates were then sonicated on ice with six 10 sec bursts at high intensity with 10 sec cooling period between bursts, followed by centrifugation at 3000 x *g* at 4°C for 15 mins. Nickel resin was prepared as described in section and washed twice in 6 ml native binding buffer followed by centrifugation at 800 x *g* for 1 min. The supernatant was removed and the nickel resin resuspended in 8 ml of bacterial lysate. This solution was incubated on a rotor at 4°C for 1 hour, followed by centrifugation at 800 x *g* for 1 min. The supernatant was saved for SDS-PAGE analysis, and the resin was washed four times with 8 ml native wash buffer (50 mM NaH_2PO_4, 0.5 M NaCl, 20 mM imidazole, pH 8.0), with each wash being followed by centrifugation at 800 x *g* for 1 min. All wash supernatants were saved for SDS-PAGE analysis. After the final wash, the resin was resuspended in 8 ml cold native elution buffer (50 mM NaH_2PO_4, 0.5 M NaCl, 250 mM imidazole, pH 8.0). A 10 ml syringe had a small ball of glass wool pushed in the end, and a thin piece of tubing with a clamp was attached. The syringe was held in a vertical position and the resin resuspended in the elution buffer was transferred to the syringe. The clamp was opened slightly and the protein elutes collected in 1 ml fractions and analysed by SDS-PAGE.

2.5.8.3 Hybrid purification

Cells were pelleted by centrifugation at 2500 x *g* for 15 mins and resuspended in guanidinium lysis buffer (200 mM sodium phosphate, 0.5 M NaCl, 6 M guanidine HCl, pH 7.8) and rocked at room temperature for 10 mins. Lysates were then sonicated on ice with three 5 second bursts at high intensity, followed by centrifugation at 3000 x *g* for 15 mins. Nickel resin was prepared as described in section and washed twice in 6 ml denaturing binding buffer (20 mM sodium phosphate, 0.5 M NaCl, 8 M urea, pH 7.8) followed by centrifugation at 800 x *g*

for 1 min. The supernatant was removed and the resin was resuspended in 8 ml of bacterial lysate. This solution was incubated on a rotor at room temperature for 30 mins, followed by centrifugation at 800 x *g* for 1 min. The supernatant was saved for SDS-PAGE analysis, and the resin was washed twice in 4 ml denaturing binding buffer, followed by two washes with denaturing wash buffer (20 mM sodium phosphate, 0.5 M NaCl, 8 M urea, pH 6.0). The resin was then washed four times in native wash buffer. Each wash was followed by centrifugation at 800 x *g* for 1 min and all supernatants were collected and saved for SDS-PAGE analysis. A 10 ml syringe had a small ball of glass wool pushed in the end, and a thin piece of tubing with a clamp was attached. The syringe was held in a vertical position and the resin resuspended in the elution buffer was transferred to the syringe. The clamp was opened slightly and the protein elutes collected in 1 ml fractions and analysed by SDS-PAGE.

2.5.9 Protein purification 6xHis purification kit

Column purification protocol (BD biosciences kit) was performed according to manufacturers instructions. Briefly, cells were infected with the appropriate virus stock as described in the manufacturers instructions and were harvested after 4 days at 27°C. Cells were spun down at 2.500 x *g* for 5 mins and resuspended in cold Insect Cell Lysis Buffer with Protease Inhibitor Cocktail (supplied with kit). The cells were then lysed on ice for 45 mins followed by centrifugation at 40.000 x *g* for 45 mins. The Ni-NTA agarose was prepared by resuspending the 50% slurry and transferring 600 μl to a column and allowing it to drain. The resin was then washed with 4 volumes of 6xHis Wash Buffer (supplied with kit) and the column drained again. The harvested insect cell lysate was applied to the column and the flow rate was reduced. the flow-through was collected and saved for SDS-PAGE analysis. The column was washed 5 times with 6xHis Wash Buffer and 5 times with 6xHis Wash Buffer containing 20 mM imidazole and all wash fractions were collected and pooled for SDS-PAGE analysis. Proteins were eluted in using 6xHis Elution Buffer containing 0.4 M imidazole and collected in 300 μl fractions and analysed by SDS-PAGE.

2.6 Generation of stable *A. thaliana* transgenic lines

2.6.1 Preparation of Electrocompetent *Agrobacterium tumefasciens*

An aliquot of the *Agrobacterium* strain GV3101 was used to inoculate 5 ml LB broth containing 25 μg/ml gentamycin and placed in a 28°C shaker incubator overnight. The following morning, the 5 ml culture was used to inoculate 500 ml LB broth containing 25 μg/ml gentamycin. This was then placed in a 28°C shaker incubator until the cell density reached OD_{600} of 0.5 to 0.8, after which the cultures were centrifuged at 4000 rpm for 5 minutes (Sorvall Legend RT). The supernatant was removed and the cell pellet resuspended in 30 ml chilled sterile dH_2O and then transferred to a sterile 50 ml falcon tube. The sterile cold dH_2O wash was repeated three times, centrifuging 4000 rpm for 5 minutes between each. After the final wash the cells were resuspended in 1 to 5 ml sterile 10% (v/v) Glycerol and 100 μl aliquots were placed on dry ice before storing at -80°C.

2.6.2 Transformation of *Agrobacterium tumefasciens* with plasmid DNA

Plasmid DNA was extracted from *E. coli* using the method described in section 2.3.9 and 2 μl added to a 50 μl aliquot of electrocompetent *A. tumefasciens* GV3101 thawed on ice. The cells were then transferred to an electroporation cuvette and pulsed at 2500 V. The cells were then transferred to a 15 ml falcon tube, 1 ml of LB broth added and the suspension placed in a 28°C shaker incubator for three hours. Finally the cells were plated out on LB agar containing rifampicin to select for *Agrobacterium*, gentamycin (to select for the TI-plasmid) and the appropriate antibiotic to which the plasmid construct carries resistance and placed in a 28°C static incubator for two days.

2.6.3 Stable transformation of *A. thaliana*

Stable transformation of *A. thaliana* was performed using the floral dip method (Clough and Bent, 1998). Pots containing six to eight evenly spaced *A. thaliana* Col-0 seeds were grown in long day conditions for five to six weeks, after which

any inflorescence stems were removed to encourage growth of secondary inflorescence. The plants were ready to transform five to ten days later, when roughly one fifth of the flowers had opened. A single colony of a confirmed positive *A. tumefasciens* transformant was used to inoculate 10 ml LB broth containing appropriate antibiotics for plasmid selection and grown in a 28°C shaker incubator for 8 hours. The cultures were then transferred to 500 ml LB broth with appropriate antibiotics and left to grow in a 28°C shaker incubator overnight. When cell density reached OD_{600} of 0.8 to 1.0, the cells were centrifuged at 4500 rpm for 10 minutes (Sorvall Legend RT) and supernatant removed. The cell pellet was resuspended in a 5% sucrose solutions containing 0.03% Silwet L-77, and the total volume made up to 500 ml. The cell suspension was then transferred to beakers approximately the diameter of the plant pots, and the *A. thaliana* Col-0 plants were upturned into the suspension for 1 min. Dipped plants were covered to increase humidity for 24 hours at room temperature, and finally returned to growth room and seeds collected as normal.

2.6.4 Screen for homozygous *Arabidopsis* lines.

T1 seeds were selected on 0.8% ½ x MSMO agar plates containing the appropriate antibiotics. Positive seeds were then transferred onto soil and grown up and T2 seeds collected as normal. T2 seeds were selected on 0.8% ½ x MSMO agar plates and lines displaying a 3:1 segregation were grown up and T3 seeds collected as normal. T3 seeds displaying 100% antibiotic resistance were selected and used for further study.

2.7 Transient expression of gene constructs in *Nicotiana* species

Constructs were transiently expressed in *N. benthamiana* using *Agrobacterium* mediated transformation. A single colony from a plate of *Agrobacterium* transformed with the construct was used to inoculate a 10 ml overnight culture of LB broth with gentamycin (30 μg/ml), rifampicin (50 μg/ml), and construct specific antibiotic, which was grown at 28°C shaking at 200 rpm. The next day the pre-cultures were used to inoculate 10 ml LB containing the appropriate

antibiotics and placed back in the 28°C shaking incubator. The cells were harvested by centrifugation at 4000 rpm for 15 minutes (Sorvall Legend RT), when they reached an OD_{600} of 0.5-1.5. Supernatant was removed and pellets were washed once in 10 mM $MgCl_2$, before being resuspended in 10 mM $MgCl_2$ to an OD_{600} of 0.3. Acetosyringone was then added to a final concentration of 200 μM, cultures inverted several times and left on ice for 30 minutes to one hour. A one ml blunt plastic syringe was then used to pressure infiltrate *Agrobacterium* cultures into the underside of leaves of *N. benthamiana* plants and were left in a warm room for 2-3 days to allow for gene expression before tissue was harvested or examined using confocal laser scanning microscopy (section 2.10).

2.8 Immunoprecipitation of tagged proteins from tobacco plant extract

Total protein was extracted from the plant samples as described in section 2.9.1. The protein samples were mixed with 50 μl anti-GFP beads (μMacs Miltenyi Biotec) and incubated on ice for 30 minutes. In the meantime μMacs columns were placed in the magnetic field of the μMacs separator and equilibrated using 200 μl lysis buffer (supplied with the kit). Following incubation the protein samples were applied to the columns, and flow through collected for SDS-PAGE analysis. The GFP-labelled proteins and their interaction partners should be retained on the column. The columns were then washed 4 times with lysis buffer and once with wash buffer 2 (supplied with the kit) to remove any non-specific interactions. To elute the proteins, the column was first incubated for 5 minutes with 20 μl triethylamine (pH 11.8) with 0.1% Triton X-100 (TET), and finally eluted by adding 50 μl TET, into 3 μl MES (pH 3.0) to neutralise. Input, flow through and elutes were analysed by SDS-PAGE.

2.9 Protein extraction from plants

2.9.1 Total protein extract

Plant tissue samples were frozen under liquid N_2 while grinding using a pestle and mortar. Ground tissue was transferred into eppendorf tubes and vortexed

with chilled protein extraction buffer (25 mM Tris-HCl, pH 7.5, 10% Glycerol (v/v), 1 mM EDTA, 150 mM NaCl, 0.1% Triton X-100 (v/v)) containing one protease inhibitor tablet. The homogenate was then centrifuged at 13,000 x *g* for 15 minutes at 4°C, and supernatant was transferred to new eppendorfs. The protein concentration was determined using the Bradford assay (section XX). The total protein fraction was then mixed with 1 x SDS loading buffer and boiled for 5 mins before separation by SDS-PAGE.

2.9.2 Nuclear fractionation

Plant material was ground in 1.5x volume of lysis buffer (20 mM Tris-HCl, pH 7.4, 25% glycerol, 20 mM KCl, 2 mM EDTA, 2.5 mM $MgCl_2$, 250 mM sucrose) with protease inhibitor tablets (Roche) at 4°C. The lysates were filtered twice through two layers of Miracloth (Calbiochem), and centrifuged at 1000x *g* for 10 minutes to pellet the nuclei. A sample of the supernatant was kept as the cytoplasmic fraction and the rest of the supernatant removed. The nuclear pellet was then washed three times in nuclei resuspension buffer (NRB) (20 mM Tris-HCl, pH 7.4, 25% glycerol, 2.5 mM $MgCl_2$, 0.5% (v/v) Triton X-100). The final nuclear pellet was resuspended in 30 – 50 μl NRB with no $MgCl_2$ and stored at 20°C.

2.10 Confocal microscopy

The subcellular localisation of YFP, GFP and RFP tagged proteins was visualised using a confocal laser scanning microscope (Zeiss LSM 510). GFP tags were excited using an argon laser at 488 nm. GFP emission was collected between 505-530 nm. RFP tags were excited using a laser at 543 nm. RFP emission was collected between 560-615 nm. YFP tags were excited using a laser at 514 nm. YFP emission was collected between 530-600 nm.

2.11 Poly(ADP-ribose) glycohydrolase (PARG) assay

The HT Colorimetric PARG Assay Kit from Trevigen (Gaithersburg, MD, USA) was used to investigate the activity of AtPARGs and single basepair mutants of these. In this assay histones attached to plate wells were initially poly(ADP-ribosyl)ated

by PARP using a biotinylated NAD substrate. The attached polymers were subsequently hydrolysed by the action of PARG in positive controls or experimental samples. Any remaining polymer was measured by incubation with Streptavidin-HRP and a colourimetric substrate for HRP. The extent of hydrolysis is reflected by the loss in absorbance at 450 nm compared to that obtained in the absence of PARG. Optical density measurements were made using a SpectraMax Plus spectrophotometer (Molecular Devices, Wokingham, UK). The assay was carried out in accordance with the manufacturers instructions.

2.12 Serial analysis of gene expression (SAGE)

Performed in collaboration with Dr Kåre Lehmann Nielsen and Mads Sønderkær at Aalborg University.

2.12.1 Sample preparation

RNA was extracted from plants as described in section 2.3.12 and the quality of the RNA was checked using an Agilent RNA BioAnalyzer 2100 (Austin, U.S.A.). In preparation for running on the sequencer, the samples were treated as desribed in Nielsen *et al*. (2008). Briefly, the RNA samples used for this experiment were initially attached to magnetic oligodT beads, cDNA was synthesized using the Invitrogen First Strand kit. This was followed by digestion of the bead-bound cDNA with NlaIII, which has the recognition site CATG. A biotinylated adapter molecule is then ligated onto the overhangs. Another enzyme MmeI recognizes a sequence in the adapter molecule immediately upstream of the NlaIII site and cuts the cDNA 18-20 bp downstream of this. The reaction is then transferred into new wells with magnetic Streptavidin beads, which binds the cDNA with the first adapter. A second adapter is then added to ligate to the MmeI overhangs. This second adapter molecule is unique to each sample and contains an identification key of 3 bp. The cDNA with adapters was then diluted and used as a template for PCR using primers for the known adapter tag sequences and run on a 15% polyacrylamide gel to estimate the quantity of product in each sample. Samples were then pooled by adding equal amounts of each sample replicate and run on a second 15% polyacrylamide gel to remove any contaminating linker dimers by gel extraction. The cDNA was then concentrated using phenol, chloroform

isoamyl precipitation. The sample concentrations were then determined, and equimolar amounts were mixed prior to sequencing.

2.12.2 Sequencing and data processing

The 2x8 DeepSAGE libraries were sequenced using a 26 cycle run on two lanes of a flow cell on a Illumina Genome Analyzer$_x$ sequencer. Clustering and sequencing were performed with reagents from version 2 cluster generation kits and version 3 sequencing kits (Illumina). Image analysis and base calling were performed using the Genome Analyzer pipeline v1.4 omitting chastity filtering otherwise standard settings. Using custom Perl scripts, 17 bp tag sequences were extracted from the output FASTQ files into separate files, sorting and counting unique tags. All samples were combined into one data matrix, and tags seen in less than 4 libraries were discarded. Sequence tags were annotated to the representative cDNA sequences of the TAIR10 (Dec 2010) release (ftp://ftp.arabidopsis.org/home/tair/Genes/TAIR10_genome_release/TAIR10_blastsets/TAIR10_cdna_20110103_representative_gene_model) by mapping the reads to the sequence flanking NlaIII restriction sites on both the coding and non-coding strands. Tags matching more than one gene region were discarded. Expression values for each gene were calculated by summing the count of all tags mapped to the same gene. Biological replicates were pooled, and the mean expression (exp) and standard deviation (std) were calculated using (1) and (2) respectively and subsequently normalized to counts per million (CPM). Pair-wise comparisons were performed using the z-test analysis (Kal et al. 1999). Genes were considered as differentially expressed with a Bonferoni adjusted p-value ≤ 0.01, and a foldchange ≥ 2.

$$(1)\ \exp = \frac{\sum_{i=1}^{N}(tag\ count_i)}{\sum_{i=1}^{N}(lib\ size_i)}$$

$$(2)\ std = \sqrt{\sum_{i=1}^{N}\left((tag\ count_i - \bar{x})^2 \cdot \frac{lib\ size_i}{\sum_{i=1}^{N}(lib\ size_i)}\right)}$$

2.13 Software

2.13.1 Sequence analysis

Protein sequence alignments for phylogenetic analysis were analysed using the ClustalW2 algorithm supplied by www.ebi.ac.uk/Tools/msa/clustalw2/ or the Emboss Needle pairwise sequence alignment supplied by www.ebi.ac.uk/Tools/psa/emboss_needle/. Both algorithms were used with all parameters set to default.

2.13.2 Densitometry

Density of spots in western dot blots and relative transcript levels in RT-PCR amplifications were analysed using Image J software.

2.13.3 Colocalisation

2.13.3.1 Pearson's correlation coefficient

The Pearson's correlation coefficient was used to determine colocalisation of GFP and RFP tagged proteins expressed transiently *in planta*. It was calculated using the Manders coefficient plugin for Image J software.

2.13.3.2 Fluorescence intensity profile

The fluorescence intensity profile determining signal intensity of each laser channel was used to determine areas of colocalisation of RFP and GFP signal, when these were expressed *in planta*. The profiles were generated using the Zeiss LSM software.

2.13.4 Promoter region analysis

The putative promoter regions of AtPARPs and AtPARGs (1 kb upstream of the start codon) were analysed using Athena software (O'Connor *et al.*, 2005).

2.13.5 Subcellular localisation

In silico subcellular localisation prediction was performed using TargetP, SUBA, NLSpredict online software.

2.13.6 Statistical analysis

All statistical analysis was carried out using Minitab 16 (Minitab Inc, U.S.A.). Significances were determined using analysis of variance (ANOVA) and Tukey's test at p-value set at 0.05.

3 Functional characterisation of *Arabidopsis* poly(ADP-ribosyl)ation mutants

3.1 Introduction

Poly(ADP-ribosyl)ation (PARylation) has been shown to be important for many cellular processes in mammals and *Drosophila*, such as chromatin structure, transcriptional regulation, and programmed cell death, but so far the main focus of PARP function has been through its involvement in the response to DNA damage, where it has been shown that PARP interacts with or modifies proteins involved in several of the major DNA repair pathways, such as NHEJ, BER and HR as described earlier. In plants, a link to abiotic stress has been suggested. *Arabidopsis* and *Brassica napus* were transformed with dsRNA hairpins containing the 5' end of AtPARP1 or AtPARP2 to generate transgenic RNAi knock-down plants. These transgenic plants were found to have enhanced tolerance to heat, drought and high light stress (DeBlock *et al.*, 2005). When the transcriptomes of the AtPARP1 knock-down plants were analysed after exposure to high light, they showed an increase in ABA-responsive genes (Vanderauwera *et al.*, 2007). However, neither of these studies directly showed the decrease of AtPARP1 at transcript or protein level (DeBlock *et al.*, 2005, Vanderauwera *et al.*, 2007). The transcripts of AtPARP1 and AtPARP2 were increased after exposure to drought (Doucet-Chabeaud *et al.*, 2001), while a T-DNA insertion line of AtPARG1 (*parg1-3*) displayed drought sensitivity (Li *et al.*, 2010).

While the functions, regulation and targets of PARylation are well characterized in mammals and the research into this modification continues to grow, there has so far been very little work on *Arabidopsis* PARPs and PARGs published. This chapter aims to make a thorough characterisation of AtPARPs and AtPARGs by analysing phenotypic differences in knock out plants based on response to various stresses and thus try and elucidate if the same functional redundancy observed in mammals exists between the known members of the family of *Arabidopsis* poly(ADP-ribosyl)ation enzymes.

3.2 Results

3.2.1 Arabidopsis PARPs

The generation of polymers of ADP-ribose as well as the attachment of these onto target proteins is performed through the activity of PARPs. These enzymes exist in all eukaryotic organisms, except yeast, and several different types have been discovered over the years, 18 in humans alone (Hassa and Hottiger, 2008). Although most of this superfamily of enzymes differ greatly in their N-terminal domains, they all share high conservation in their C-terminal catalytic regions. Most research so far has been on the founding member of the PARP family, PARP1, whose activity is induced by DNA damage (Juarez-Salinas *et al.*, 1979; Benjamin and Gill, 1980a). The general structure of PARPs includes an N-terminal DNA-binding domain, an automodification domain, and a C-terminal catalytic activity domain containing the "PARP signature" as described in detail earlier.

In *Arabidopsis* there are three PARPs which structurally only have the catalytic domain in common. A further two *Arabidopsis* genes (RCD1, SRO1) also contain the "PARP signature" (Ahlfors *et al.*, 2004; Citarelli *et al.*, 2010). However, neither contains all the conserved catalytic residues within the signature domain required for activity (Jaspers *et al.*, 2010). From sequence comparisons and alignments, it was found that AtPARP1, a 111 KDa protein, is structurally similar to the mammalian PARP1 containing two zinc fingers for DNA binding at the N-terminal part of the protein (Doucet-Chabeaud *et al.*, 2001) and in addition, contains the four cysteines shown to play an important part in a recently identified third zinc binding domain, involved in interdomain interaction (Langelier *et al.*, 2008) as well as an NLS (figure 3.1A). The structure of the N-terminal part of AtPARP2 (also known as APP), a shorter 72 KDa protein, resembles both mammalian PARP2 and maize PARP2 (NAP) (Lepiniec *et al.*, 1995; Amé *et al.*, 2004; Babiychuk *et al.*, 1998) and contains a DNA-binding domain with homology to the SAP domain (figure 3.1A), found in nuclear proteins involved in chromosomal organisation and DNA repair (Aravind and Koonin, 2000; Amé *et al.*, 2004). While both AtPARP1 and AtPARP2 have N-terminal DNA binding domains, the third *Arabidopsis* PARP, AtPARP3, a 91 KDa protein identified through a BLAST search of the *Arabidopsis* genome for the

PARP signature (Hunt *et al.*, 2004), contains no known DNA binding domains at its N-terminal (figure 3.1A). The central region of all three AtPARPs contains the WGR domain, the function of which is unknown. However, only AtPARP1 and AtPARP3 contain a BRCT domain (figure 3.1A), shown to be involved in interactions between several proteins including PARP1 and the BER proteins XRCC1 and DNA ligase III (Masson *et al.*, 1998; Leppard *et al.*, 2003). The PARP signature is well conserved in AtPARP1 and AtPARP2 with 88% and 92% identity to the mammalian PARP1, respectively (figure 3.1B). However, AtPARP3 only has 40% identity (58% similarity) to the mammalian PARP signature (figure 3.1B). Moreover, there seems to be differences at conserved residues shown to be important for NAD+ binding: histidine at position 862 (human PARP1 residue numbering used) is changed to a cysteine, while the tyrosine at position 896 is changed to a valine. AtPARP3 does however contain residues shown to be important for activity, such as the glutamate at position 988, the aspartate at position 993, and has an arginine instead of the usual lysine at position 893, but this latter conservative amino acid change has previously been shown not to significantly alter activity (Simonin *et al.*, 1993). The differences in the C-terminal sequences following the PARP signature are highlighted in figure 3.1B. Within vertebrates the percentage similarity between full-length PARP homologues is high, while when comparing with invertebrates and plants the overall similarity drops significantly (Table 3.1). To investigate the relationship between the *Arabidosis* AtPARPs, higher plant, and model organism homologues, the percentage identity and similarity values were calculated. These values were based on pairwise sequence alignments, performed using the Emboss-Needle method for global alignments (www.ebi.ac.uk), and are shown in table 3.1.

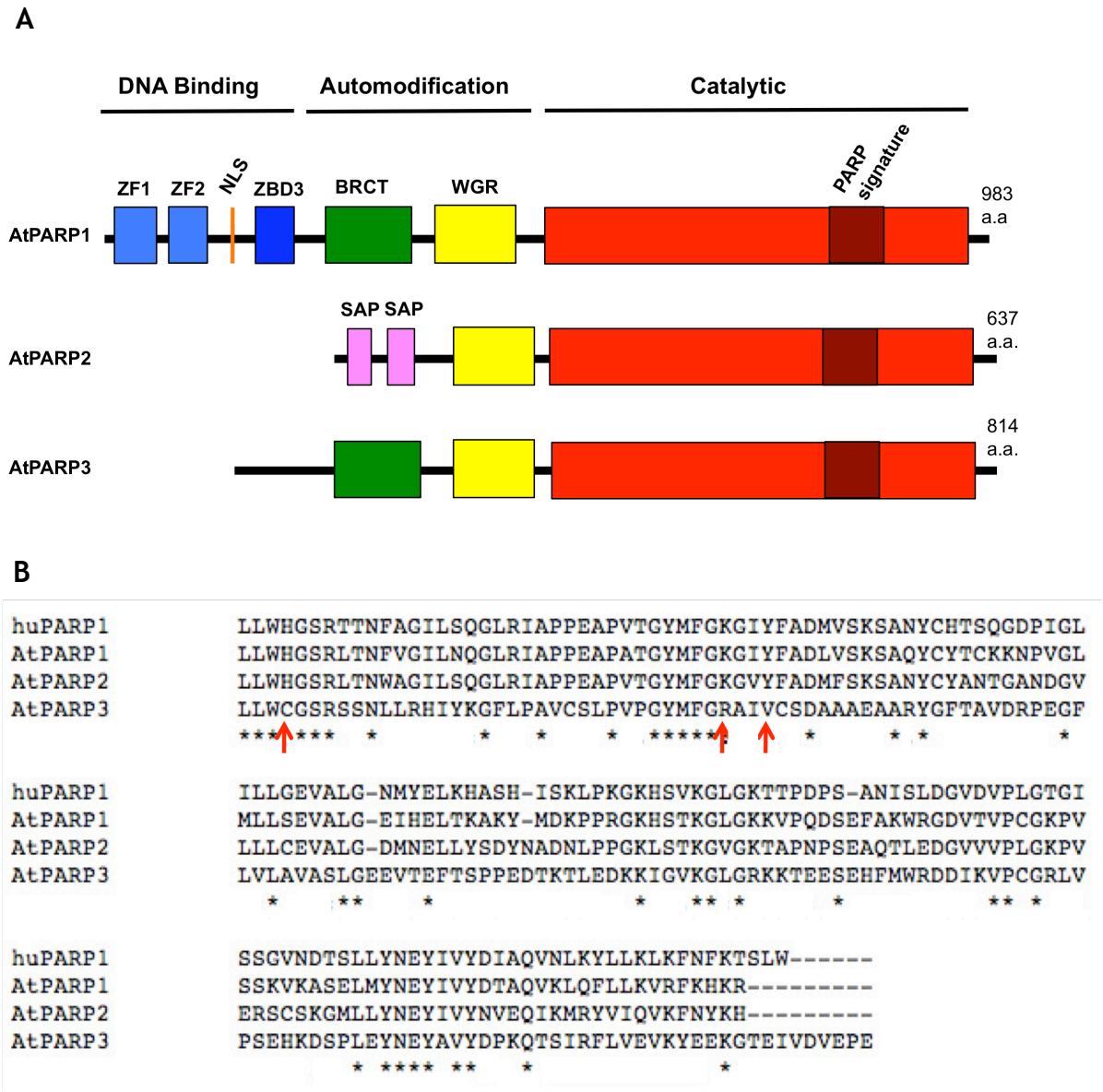

Figure 3.1. Structural features of *Arabidopsis* PARPs
A) Domain architecture of the AtPARPs. ZF denotes zinc finger domains, NLS is a nuclear localization signal, BRCT is the breast cancer 1 protein (BRCA1) C-terminus motif, WGR is involved in activation, SAP is a DNA-binding domain.
B) Alignment of the human PARP1 and AtPARP protein sequences from the PARP signature to the end using ClustalW2. Asterisks indicate residues conserved across all four sequences, and red arrows indicate residues described as important for activity, which are altered in AtPARP3.

% Identity

	AtPARP1	AtPARP2	AtPARP3	maPARP1	maPARP2	osPARP1	osPARP2	huPARP1	huPARP2	moPARP1	drPARP1	cePARP1
AtPARP1		19.6	24.3	59.7	21.7	62.2	21.1	38.0	22.3	38.0	33.5	31.1
AtPARP2	31.9		18.2	23.0	58.6	23.3	57.7	23.2	37.7	23.1	20.1	22.6
AtPARP3	39.0	32.3		23.6	20.1	24.4	19.7	21.9	18.3	21.2	20.0	17.9
maPARP1	73.8	35.2	40.8		25.3	79.0	24.7	37.5	22.7	37.3	33.7	29.8
maPARP2	34.4	72.5	35.5	36.7		24.6	78.7	23.6	38.6	23.1	20.6	33.9
osPARP1	75.7	35.2	41.4	87.8	36.1		23.7	38.4	22.8	37.8	33.0	31.6
osPARP2	33.1	72.5	35.1	36.7	86.4	36.1		24.5	38.0	22.8	20.5	23.9
huPARP1	55.0	34.0	36.2	55.7	35.6	55.6	35.3		22.7	92.0	40.5	32.2
huPARP2	34.6	52.3	32.3	33.8	52.8	34.2	53.0	33.3		22.0	20.9	19.7
moPARP1	55.8	34.1	36.3	54.6	35.7	54.8	34.0	96.0	32.0		40.4	31.8
drPARP1	52.3	30.8	35.7	51.7	32.4	51.9	30.9	58.8	31.8	58.4		29.0
cePARP1	47.3	35.6	28.2	45.4	22.2	48.7	37.1	49.6	30.1	49.3	47.1	

% Similarity

Table 3.1. Identities and similarities between PARPs from plants and other model organisms
Identity values are given in the top half of the table and similarity values in the bottom half. At Arabidopsis, ma Maize, os rice,hu human, mo mouse, dr fruit fly, ce nematode. Percentage identity and similarity were calculated using the Emboss global pairwise alignment algorithm.

3.2.2 Arabidopsis PARGs

The removal of poly (ADP-ribose) is catalysed by the enzyme poly(ADP-ribose) glycohydrolase. There is only one single PARG gene in most organisms and knocking out this gene results in embryonic lethality (Koh *et al.*, 2004). The mammalian PARG gene does however have several isoforms, which are found in different subcellular compartments (Meyer-Ficca *et al.*, 2004; Meyer *et al.*, 2007). *Arabidopsis* is the only organism, other than *C. elegans* found to date which also contains two PARGs: AtPARG1 (At2g31870) and AtPARG2 (At2g31865) which are situated next to each other on chromosome 2. A third PARG (At2g31860), next to the other two PARGs on chromosome 2, was found to have no ESTs or CDNAs associated with it and might therefore represent a pseudogene AtPARG 1 and AtPARG2 share 51.5% amino acid sequence identity and 66.9% similarity (table 3.2). Structurally, they only share homology to the mammalian PARG in the catalytically important "PARG signature", and the function of putative N-terminal regulatory domain remains unknown, as neither AtPARG was shown to contain any subcellular localisation signal when *in silico* analysis of the AtPARG protein amino acid sequences using the predictive localisation programs NLSPredict and LOCtree (http://www.predictprotein.org/) as well as TargetP (http://www.cbs.dtu.dk/services/TargetP/) was performed. The two AtPARGs are also smaller than their mammalian homologue. AtPARG1 and AtPARG2 are 62 KDa and 60 KDa, respectively, and are thus similar in size to the shorter cytoplasmic and mitochondrially localized isoforms of human PARG, which like the AtPARGs are missing the N-terminal regulatory domain (figure 3.2). To investigate the relationship between the *Arabidosis* AtPARGs, higher plant, and model organism homologues, the percentage identity and similarity values were calculated using the Emboss-Needle method for global alignments (www.ebi.ac.uk) (table 3.2). In this table, sequence comparisons to the AtPARGs were made using the full length mammalian PARG sequences, and therefore the identity and similarities were very low (below 16% and 25%, respectively). However, when the comparison is made across the catalytic PARG signature, the percentage identity to the human PARG increases to 54% and 48% for AtPARG1 and AtPARG2, respectively (St-Laurent *et al*, 2007). The presence of two PARGs in the genome is not conserved across all plants. While rice, poplar, tomato and maize were predicted to contain two PARGs, only one was predicted in peanut, sorghum and the castor oil plant (Briggs and Bent, 2011).

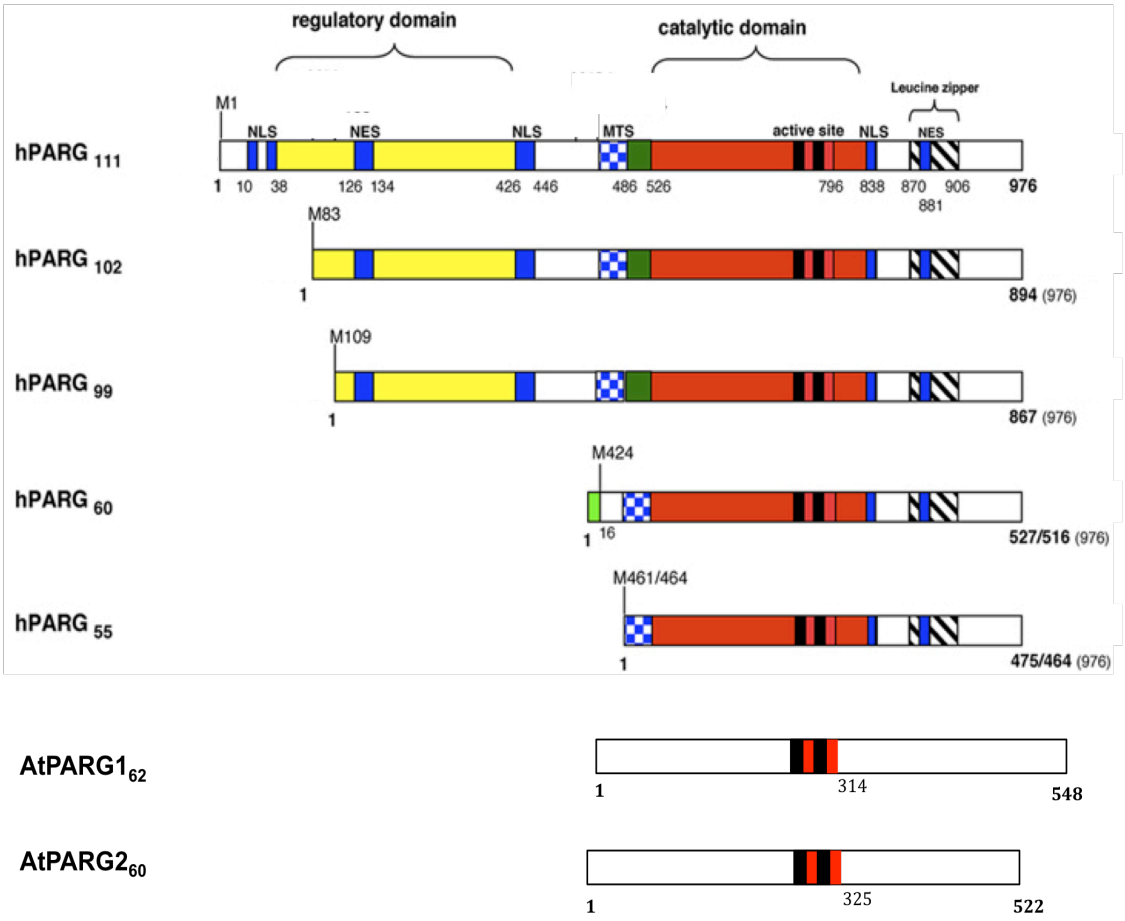

Figure 3.2. Structural features of PARGs
Domain architecture of human PARG isoforms and AtPARGs. Known regulatory elements are indicated by coloured boxes. NLS: nuclear localisation signal, NES: nuclear export signal, MTS mitochondrial targeting sequence. The size of each protein is given after the name (Kda) and at the end of each representative picture (amino acids). Figure adapted from (Hassa and Hottiger, 2008).

% Identity

	AtPARG1	AtPARG2	maPARG	osPARG	huPARG110	moPARG110	drPARG	cePARG1	cePARG2
AtPARG1		51.5	48.5	50.0	15.1	15.3	21.9	16.3	21.9
AtPARG2	66.9		47.3	47.3	14.4	14.5	18.1	16.9	22.7
maPARG	61.9	62.6		77.0	16.5	16.0	20.5	16.6	24.6
osPARG	64.3	63.7	83.8		15.5	15.6	20.8	16.2	25.3
huPARG	23.1	23.3	24.8	24.0		86.2	21.8	20.1	14.9
moPARG	21.9	23.4	24.3	28.8	91.0		21.7	19.1	14.2
drPARG	31.6	28.2	29.2	31.0	30.0	30.6		17.4	18.1
cePARG1	24.7	26.4	25.0	23.9	33.3	31.1	27.4		33.5
cePARG2	34.3	36.5	36.5	39.5	24.8	22.6	29.1	44.5	

% Similarity

Table 3.2 Identities and similarities between PARGs from plants and other model organisms
Identity values are given in the top half of the table and similarity values in the bottom half. At Arabidopsis, ma Maize, os rice,hu human, mo mouse, dr fruit fly, ce nematode. Percentage identity and similarity were calculated using the Emboss global pairwise alignment algorithm.

3.2.3 Isolation of homozygous T-DNA mutants through PCR genotyping

Stock centres contain many lines of *A. thaliana* seeds containing transfer DNA (T-DNA) within individual genes. The introduction of a 12 kb region of T-DNA into the coding region of a gene inactivates that gene as transcription is prevented. *Arabidopsis* T-DNA insertion lines corresponding to all PARP and PARG genes were obtained from either the European Arabidopsis Stock Centre (NASC – Nottingham, UK) or GABI-Kat (Cologne, Germany) repositories.

The seed line *parg1-1, parg1-2, parg2-1, parp1-1, and parp2-1* (table 2.5) were obtained from the stock centres were a segregating population of the T2 generation. In order to determine the zygosity of the plant lines, the T2 T-DNA insertion line seeds were grown on soil in long day conditions (section 2.2.3) and homozygous lines were identified by PCR amplification using genomic DNA as template and gene-specific primer pair and T-DNA left border specific primer (LBb1 or GK_8409) in combination with a gene specific primer (figures 3Aii, 3Bii, 4Aii, and 4Bii). In addition, RNA was extracted from plants and cDNA synthesized, and disruption of expression was confirmed by lack of transcript specific amplification using RT-PCR (figures 3Aiii, 3Biii, 4Aiii, and 4Biii). T-DNA insertion lines and primers used for genotyping them are listed in tables 2.5 and 2.8, respectively.

The *parg1-1* and *parg1-2* alleles contain a T-DNA insertion within the 9th and 8th intron, respectively (figure 4Ai), both of which are downstream of the PARG catalytic domain. The T-DNA insertion in the *parg2-1* allele sits in the 4th exon (figure 3Bi) and the insertion is located upstream of the PARG catalytic domain. The single allele mutants *parp1-1, parp2-1,* and contain T-DNA insertions in their 10th and 16th exon, respectively (figures 4Ai and 4Bi). The *parp1-1* insertion sits upstream of the PARP catalytic domain, while the *parp2-1* insertion sits downstream of the signature, but upstream of the catalytically important glutamic acid residue.

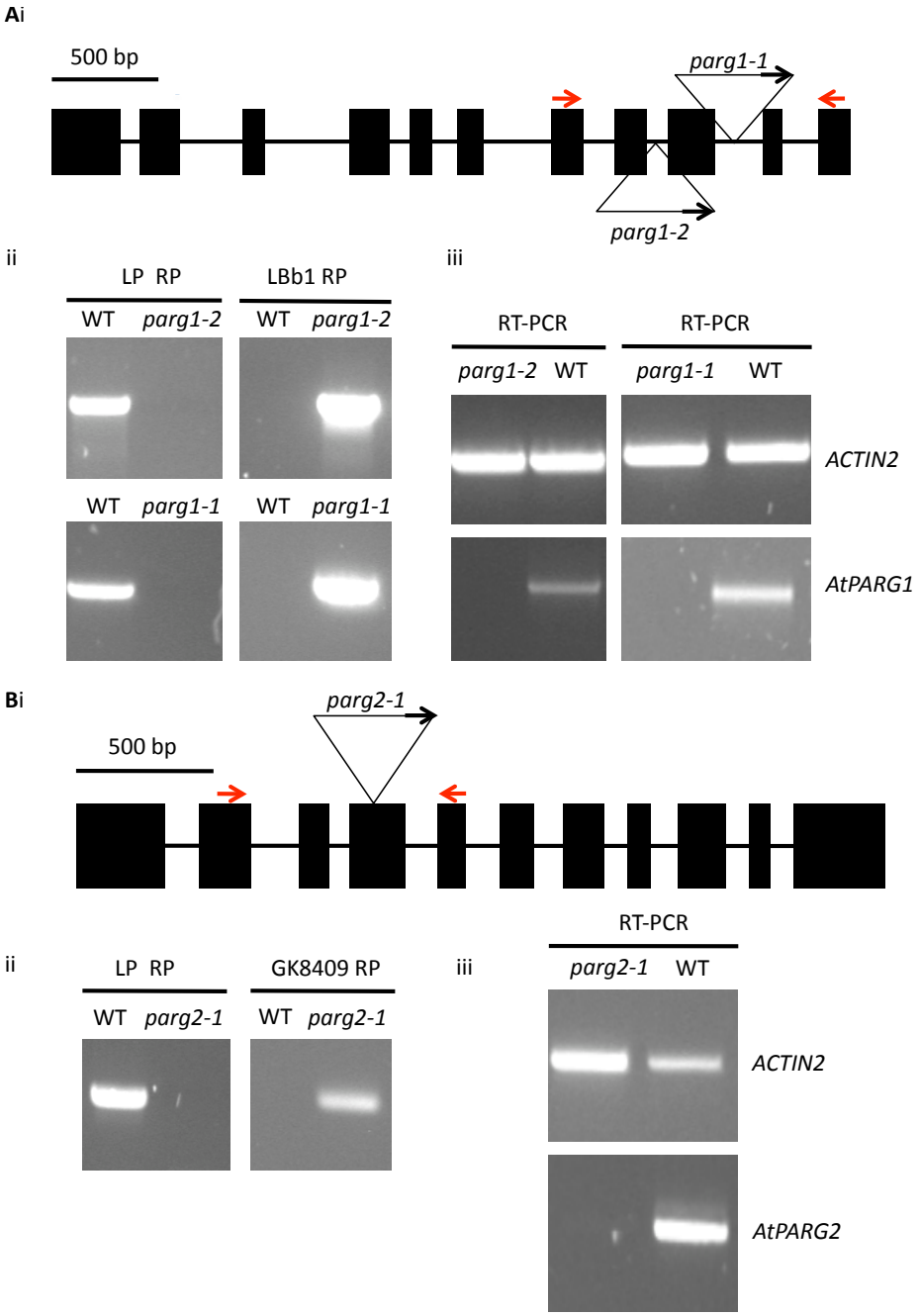

Figure 3.3. Isolation of *parg1-1, parg1-2,* and *parg2-1* homozygous plants
Ai) Gene structure of AtPARG1 where exons and introns are represented as black boxes and black lines, respectively. Location of *parg1-1* and *parg1-2* T-DNA insertions are indicated by triangles, wherein an arrow indicates the position of the T-DNA left border.
ii) PCR genotyping results for *parg1-1* and *parg1-2* alleles. PCR reactions were completed using Col-0 or *parp1-1* and *parg1-2* genomic DNA with primers for the regions flanking the inserts (LP RP) as well as for the T-DNA left border and genomic flanking regions (LBb1 RP, respectively).
iii) RT-PCR transcript analysis of *parg1-1* and *parg1-2*. PCR cycles were completed using Col-0 and *parp1-1* and *parg1-2* cDNA with primers for Actin2 (25 cycles) and *parg1-1* and *parg1-2* flanking regions indicated by red arrows (32 cycles).
Bi) Gene structure of AtPARG2 where exons and introns are represented as black boxes and black lines, respectively. Location of *parg2-1* T-DNA insertion is indicated by a triangle, wherein an arrow indicates the position of the T-DNA left border.
ii) PCR genotyping results for *parg2-1* allele. PCR reactions were completed using Col-0 or *parp2-1* genomic DNA with primers for the region flanking the insert (LP RP) as well as for the T-DNA left border and genomic flanking region (GK8409 RP, respectively).
iii) RT-PCR transcript analysis of *parg2-1*. PCR cycles were completed using Col-0 and *parp2-1* cDNA with primers for Actin2 (25 cycles) and *parg2-1* flanking region indicated by red arrows (31 cycles).

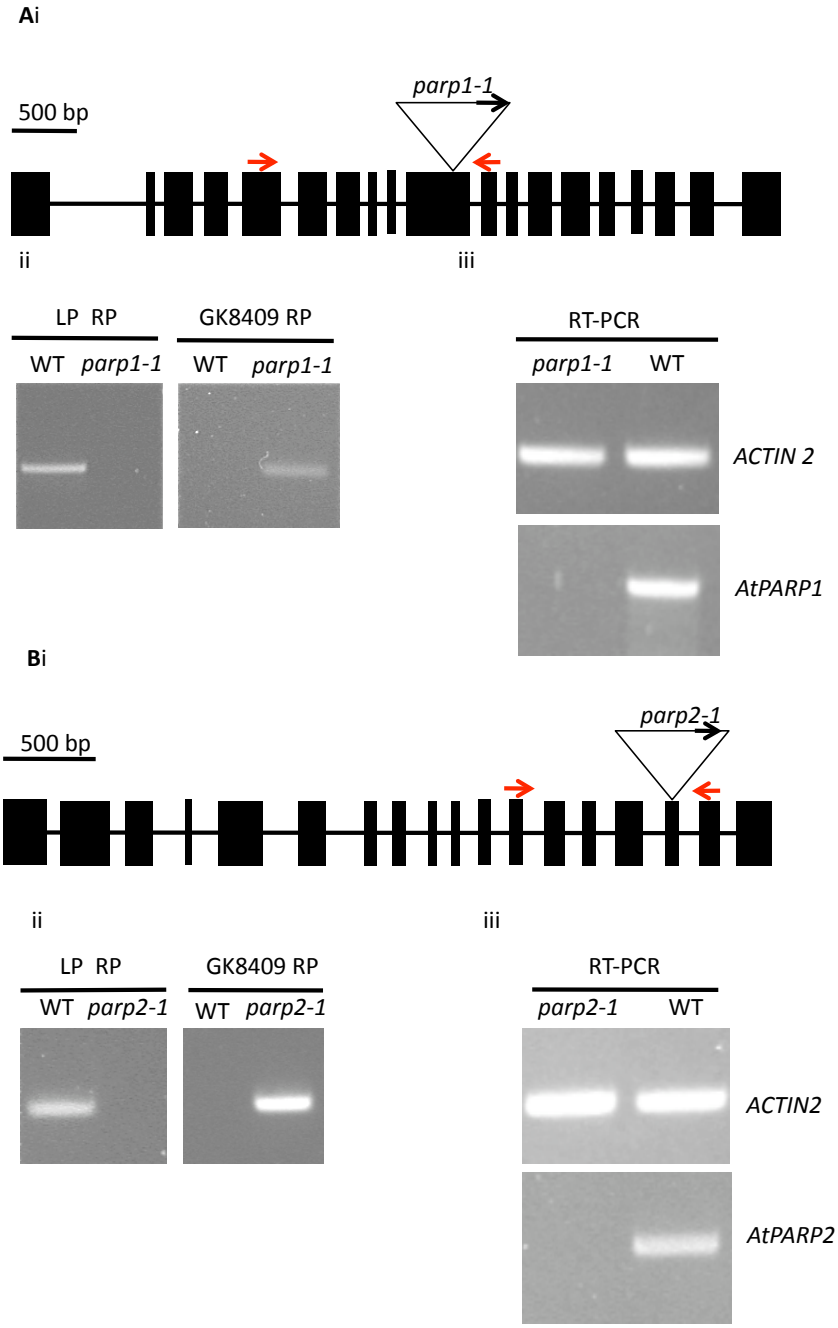

Figure 3.4. Isolation of *parp1-1* and *parp2-1* homozygous plants through genotyping
Ai) Gene structure of AtPARP1 where exons and introns are represented as black boxes and black lines, respectively. Location of *parp1-1* T-DNA insertion is indicated by a triangle, wherein an arrow indicates the position of the T-DNA left border.
ii) PCR genotyping results for *parp1-1* allele. PCR reactions were completed using Col-0 or *parp1-1* genomic DNA with primers for the region flanking the insert (LP RP) as well as for the T-DNA left border and genomic flanking region (GK8409 RP, respectively).
iii) RT-PCR transcript analysis of *parp1-1*. PCR cycles were completed using Col-0 and *parp1-1* cDNA with primers for Actin2 (25 cycles) and *parp1-1* flanking indicated by red arrows (37 cycles).
Bi) Gene structure of AtPARP2 where exons and introns are represented as black boxes and black lines, respectively. Location of *parp2-1* T-DNA insertion is indicated by a triangle, wherein an arrow indicates the position of the T-DNA left border.
ii) PCR genotyping results for *parp2-1* allele. PCR reactions were completed using Col-0 or *parp2-1* genomic DNA with primers for the region flanking the insert (LP RP) as well as for the T-DNA left border and genomic flanking region (GK8409 RP, respectively).
iii) RT-PCR transcript analysis of *parp2-1*. PCR cycles were completed using Col-0 and *parp2-1* cDNA with primers for Actin2 (25 cycles) and *parp2-1* flanking region indicated by red arrows (31 cycles).

The T-DNA insertion line for AtPARP3 (Salk line N653425) showed homozygosity when it was genotyped using PCR on genomic DNA, and initial RT-PCR on cDNA to check for lack of transcript. However, on further analysis the homozygous knockout line was found to accumulate transcript when exposed to ABA, and no further work was done using this T-DNA insertion line. An additional AtPARP3 T-DNA insertion line was recently acquired, in which the T-DNA insertion is in the second to last exon, placing it in the middle of the PARP signature. Homozygous mutants are currently being isolated and phenotyping of these will help elucidate the role of AtPARP3 in Arabidopsis.

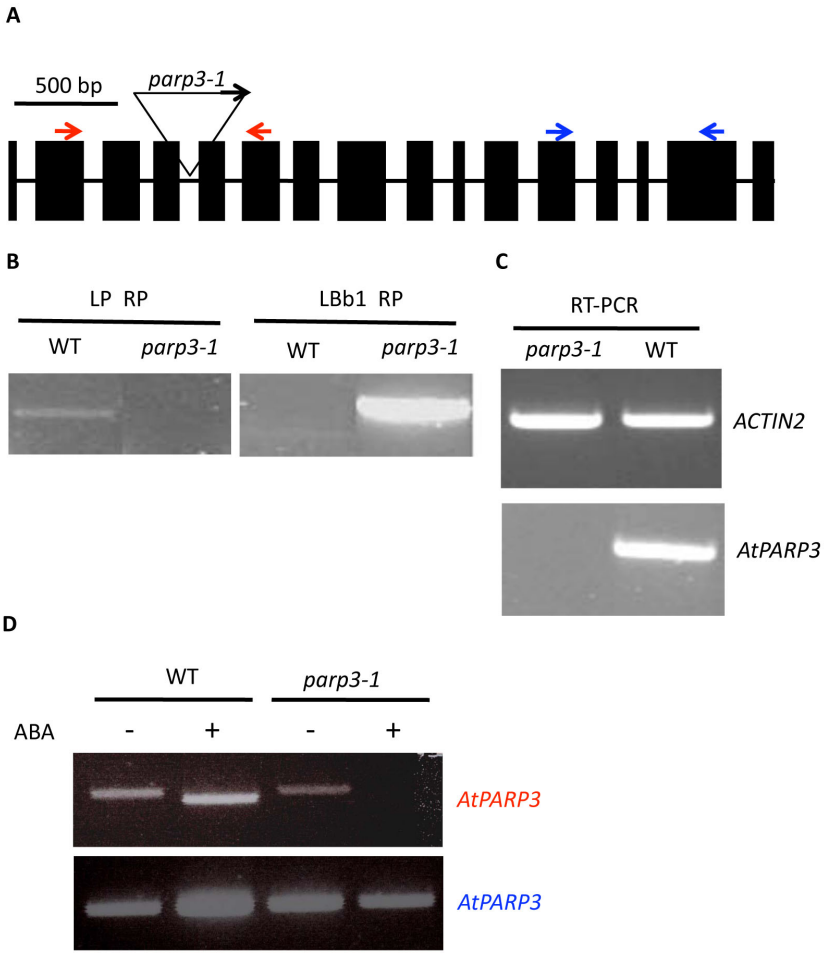

Figure 3.5. Isolation of *parp3-1* homozygous plants through genotyping
A) Gene structure of AtPARP3 where exons and introns are represented as black boxes and black lines, respectively. Location of *parp3-1* T-DNA insertion is indicated by a triangle, wherein an arrow indicates the position of the T-DNA left border.
B) PCR genotyping results for *parp3-1* allele. PCR reactions were completed using Col-0 or *parp3-1* genomic DNA with primers for the regions flanking the insert (LP RP) as well as for the T-DNA left border and genomic flanking region (LBb1 RP, respectively).
C) RT-PCR transcript analysis of*parp3-1*. PCR cycles were completed using Col-0 and *parp3-1* cDNA with primers for Actin2 (25 cycles) and *parp3-1* flanking region indicated by red arrows (45 cycles).
D) RT-PCR transcript analysis of *parp3-1* in response to ABA. PCR cycles were completed using primers for the T-DNA flanking region LP RP (red arrows) or for the C-terminal part of the gene (blue arrows) (40 cycles).

3.2.4 Overexpressor transgenic plants line isolation

To generate plant lines expressing AtPARG1 at increased levels, full-length AtPARG1 cDNA was PCR amplified from *A. thaliana* cDNA using Gateway® compatible primers and cloned into the Gateway® entry vector pENTR-D-TOPO (Invitrogen, Paisley, UK). Full-length cDNA from the entry vector was transferred to the pEarleyGate 201 (Earley *et al.*, 2006) binary destination vector (figure 3.6A) by Gateway® LR based recombination to generate N-terminally HA-tagged AtPARG1 under the control of the strong constitutive cauliflower mosaic virus (CaMV) 35S promoter. In addition, the T-DNA of this binary vector also carries the gene phosphinothricin-N-acetyltransferase, which confers resistance to the herbicide BASTA. Wild type Col-0 plants were transformed using the floral dip technique (Clough and Bent, 1998) and T1 transformants were selected for BASTA resistance and T2 seeds were collected from these. Any T2 seeds that showed a 3:1 segregation on BASTA agar plates were self-pollinated. T3 homozygotes were selected for on BASTA agar plates where lines that showed 100% survival rate were selected as homozygotes (figure 3.6B). Western blot analysis using anti-HA was performed on the T3 plants showing homozygous Basta resistance to ensure the overexpression was observed not only at the transcript level, but is carried over to the protein level (figure 3.6C). While there is currently no commercial antibody available for AtPARG1, the fact that bands are present at the right size in the anti-HA blot shows that this transgenic plant line will contain AtPARG1 protein in excess of wild type Col-0 plants.

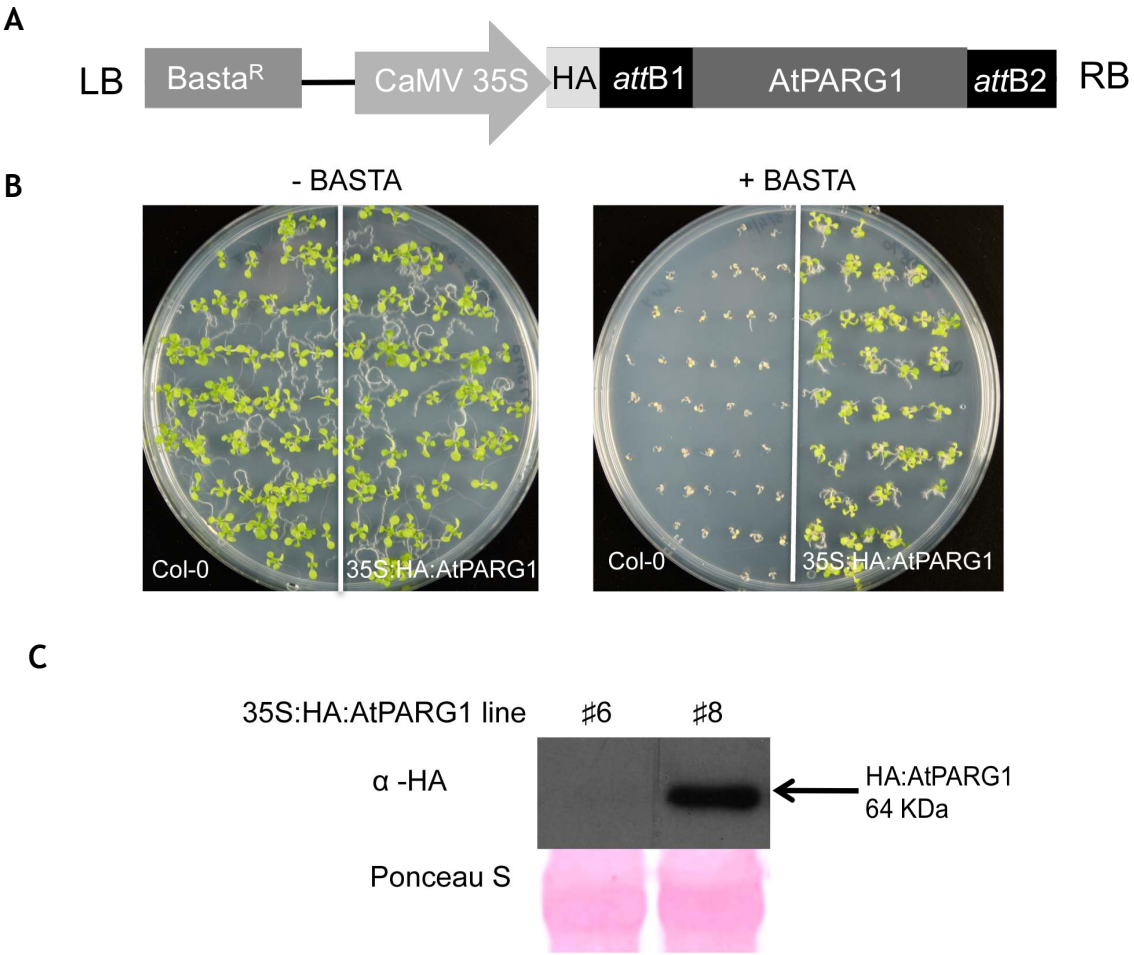

Figure 3.6. AtPARG1 overexpressor isolation
A) Features of the pEarleyGate 201 vector. The vector contains left border (LB) and right border (RB) sequences for *Agrobacterium* mediated transfer, resistance gene for the herbicide Basta to allow for selection of transgenic plants, and an N-terminal HA-tag.
B) Col-0 plants and T3 35S:HA:AtPARG1 plants on media without (left) and with (right) BASTA to select for homozygous insertion lines.
C) Western blot of the two homozygous overexpressing lines initially identified as homozygous through BASTA resistance. Ponceau S staining to represent equal loading.

3.2.5 Phenotypic differences during development

Any developmental differences were examined in wild type Col-0, T-DNA insertion lines and the 35S:HA:AtPARG1 lines on soil both in long and short day conditions (section 2.2.3). The number of rosette leaves as well as the width of the rosette across the widest part were recorded. Graphs comparing each genotype with wild type Col-0 plants in short and long day conditions can be seen in figures 3.7 and 3.8, respectively. The T-DNA insertion lines for each of the AtPARGs showed no developmental defects and were fertile. Although some significant diffences are apparent, no sensible trends were observed.

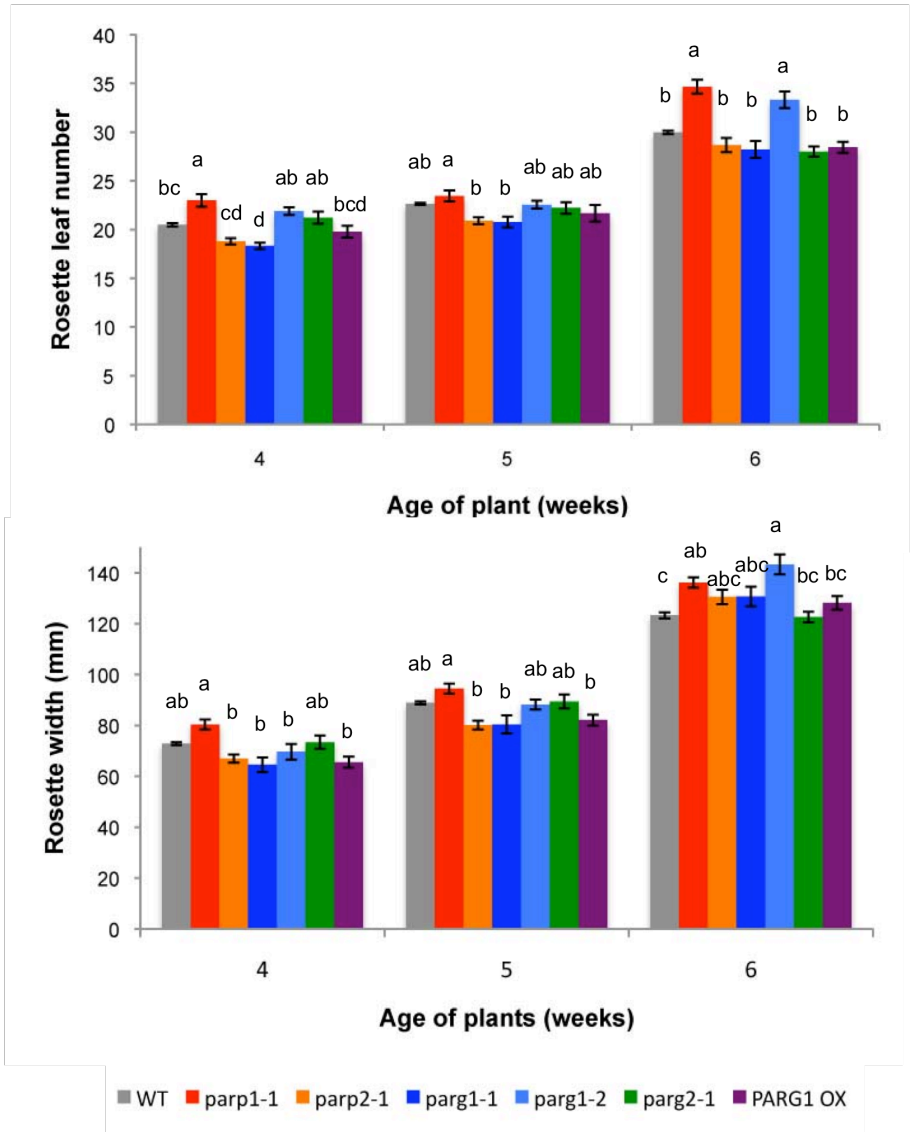

Figure 3.7. Development of T-DNA insertion lines, WT and 35s:HA:AtPARG1 (PARG OX) in short day conditions
Plants were grown in short day photoperiod (8 hours light/16 hours dark) until flowering. Rosette width (mm) and leaf numbers (excluding cotelydons) were recorded for several weeks. The legend is indicated at the bottom of the image (n=42 for WT and 9 for mutant lines). Error bars represent standard error. Different letters indicate between line statistical significance at each separate timepoint analysed by ANOVA ($p < 0.05$, Tukey's test).

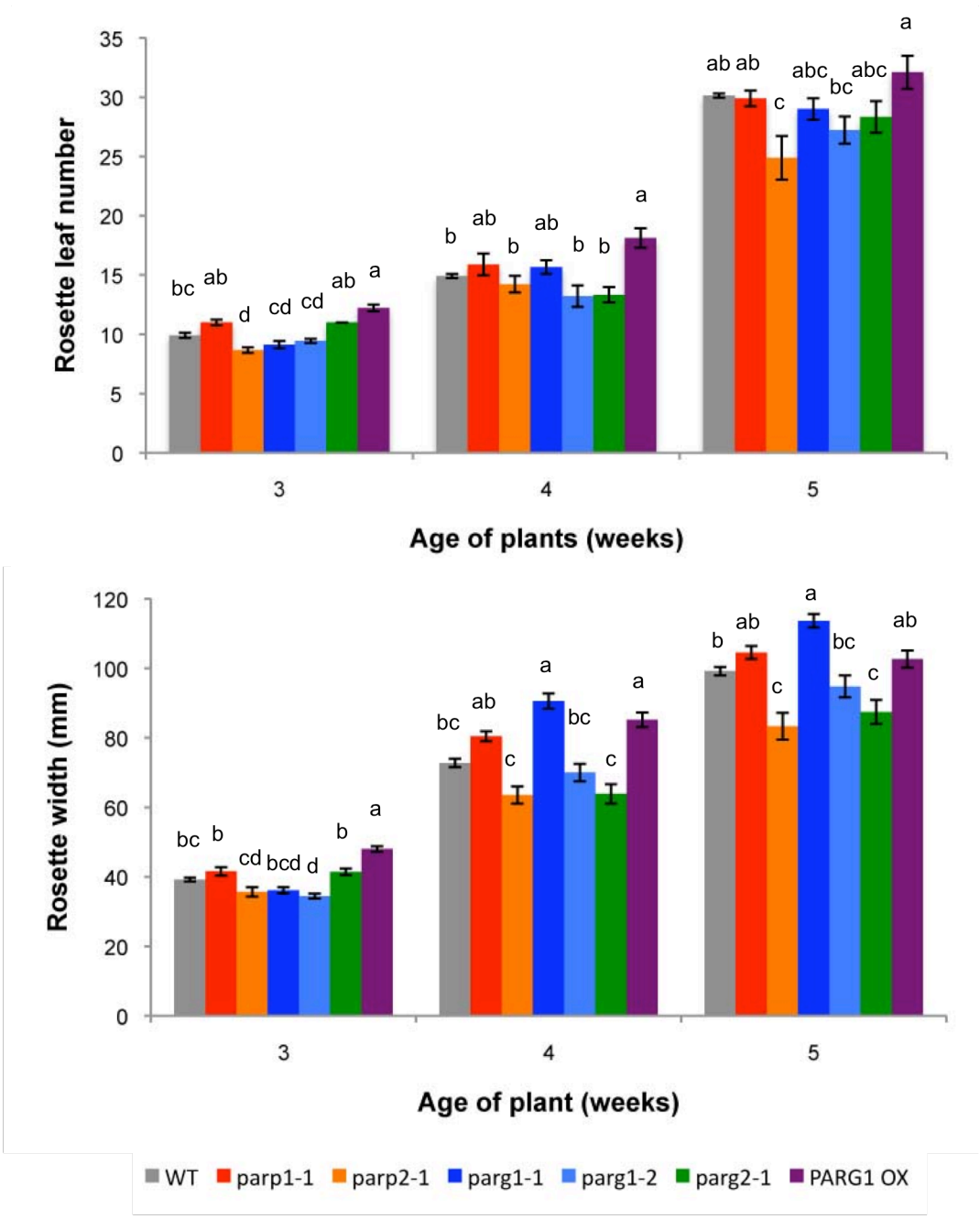

Figure 3.8. Development of T-DNA insertion lines, WT and 35s:HA:AtPARG1 (PARG OX) in long day conditions

Plants were grown in long day photoperiod (16 hours light/8 hours dark) until flowering. Rosette width (mm) and leaf numbers (excluding cotelydons) were recorded for several weeks. The legend is indicated at the bottom of the image (n=42 for WT and 9 for mutant lines). Error bars represent standard error. Different letters indicate between line statistical significance at each separate timepoint analysed by ANOVA ($p < 0.05$, Tukey's test).

3.2.5.1 Flowering time

To determine whether any of the T-DNA insertion lines would show alterations in flowering time, vegetative leaves were counted from plants that had visibly bolted, as judged by the appearance of the shoot apex at least one cm from the rosette. The *parg1-1* line had siginificantly ($p < 0.05$) fewer rosette leaves compared to wild type and *parg2-1* lines when bolted under long day conditions (figure 3.9A). However, this phenotype was not seen under short day conditions (figure 3.9B). On the contrary, both *parg1-1* and 35S:HA:AtPARG1 had significantly ($p < 0.05$) more leaves than wild type, *parg1-2,* and *parg2-1* plants (figure 3.9B). Wild type plants and *parp1-1* and *parp2-1* lines did not display any significant differences under long day conditions (figure 3.10A), while under short day conditions the *parp1-1* line had significantly more rosette leaves than wild type when bolting (figure 10B).

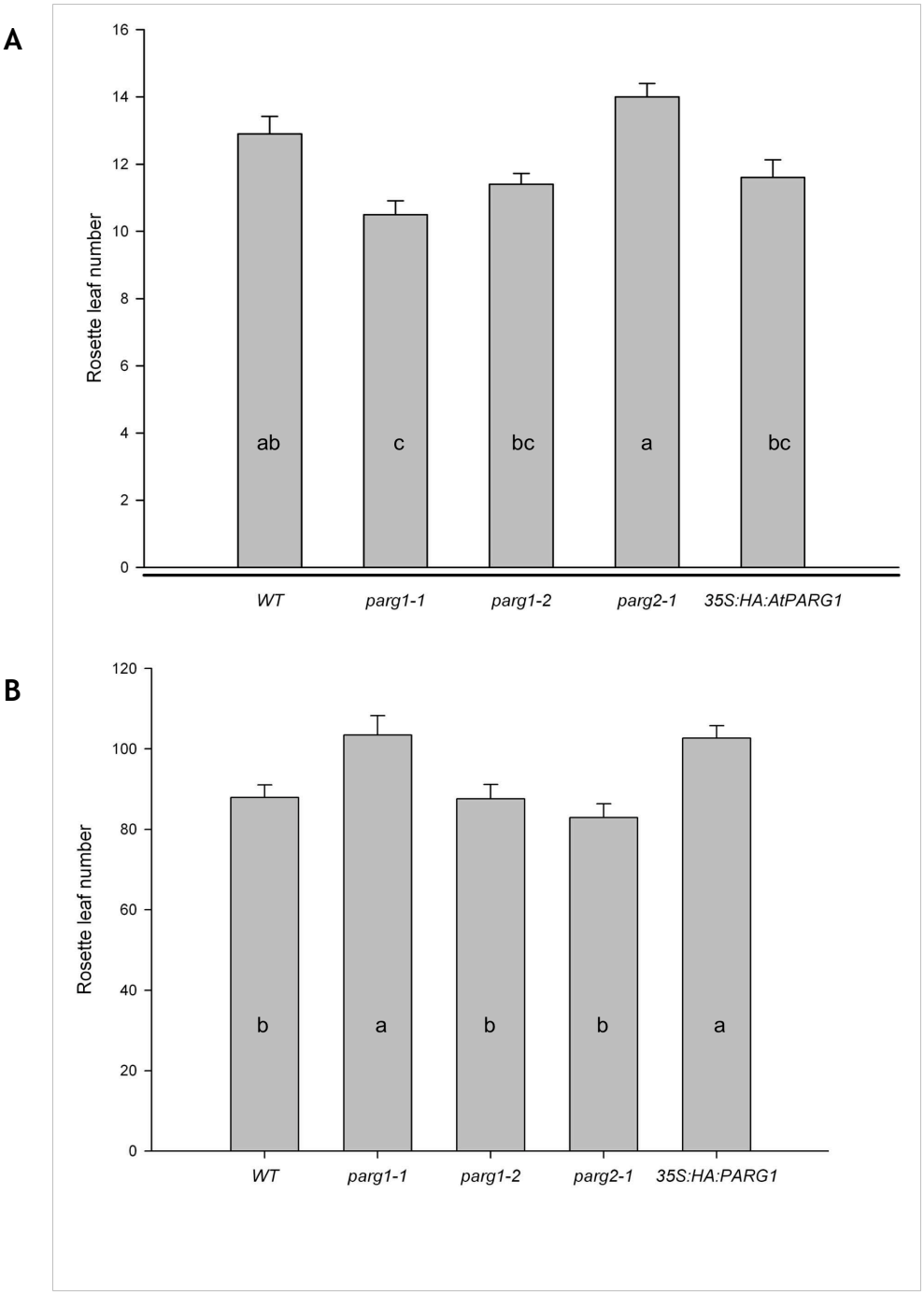

Figure 3.9. Bolting times of AtPARG mutants under long and short day conditions
A) Bolting times of Col-0, parg1-1, parg1-2, parg2-1 and a AtPARG1 overexpressing line under long days expressed as rosette leaf number after the stem has bolted approximately 1 cm. Plants were grown for approximately 4-6 weeks under a long day photoperiod (16 hours light/8 hours dark). Error bars represent standard error (n=10).
B) Bolting times of Col-0, parg1-1, parg1-2, parg2-1 and a AtPARG1 overexpressing line under short days expressed as rosette leaf number after the stem has bolted approximately 1 cm. Plants were grown for approximately 10-12 weeks under a short day photoperiod (8 hours light/16 hours dark). Error bars represent standard error (n=15).
Different letter codes indicate significant difference by ANOVA ($p < 0.05$, Tukey's test). See appendix A2.1 and A2.2 for tables.

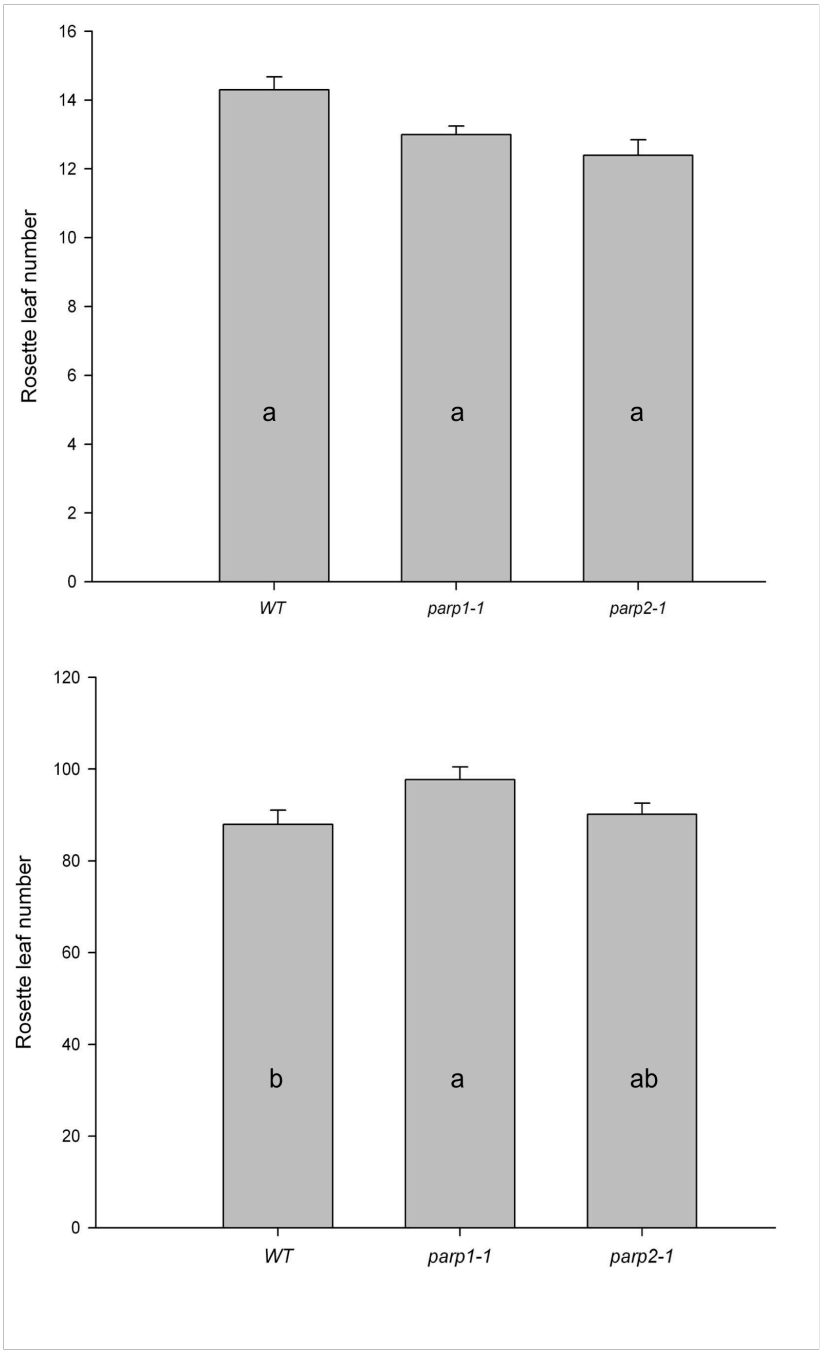

Figure 3.10. Bolting times of AtPARP mutants under long and short day conditions
A) Bolting times of Col-0, parp1-1, parp1-2 under long days expressed as rosette leaf number after the stem has bolted approximately 1 cm. Plants were grown for approximately 4-6 weeks under a long day photoperiod (16 hours light/8 hours dark). Error bars represent standard error (n=10).
B) Bolting times of Col-0, parp1-1, parp1-2 under short days expressed as rosette leaf number after the stem has bolted approximately 1 cm. Plants were grown for approximately 10-12 weeks under a short day photoperiod (8 hours light/16 hours dark). Error bars represent standard error (n=15).
Different letter codes indicate significant difference by ANOVA ($p < 0.05$, Tukey's test). See appendix A2.3 for table.

3.2.5.2 Germination

In order to investigate any differences in germination between mutant and WT plants, seeds were surface sterilised and put out on ½ MSMO agar plates with or without stress present, stratified for two days and then placed in 24 hour light for 5 days. The emergence of the radicle from the seed coat is generally regarded as the end of germination, and seeds on media plates were checked twice per day for radicle emergence until all seeds were germinated. As shown in figure 3.11A, none of the AtPARG T-DNA insertion lines showed significant difference to the wild type in germination rate. The *parp2-1* line germinated significantly faster ($p < 0.05$) at 36 and 47 hours after exposure to light, compared with wild type and the *parp1-1* line, which were no different to each other (figure 3.11B).

3.2.6 Genotoxic stress

Due to the DNA damage induction of PARP activity, the majority of studies to date have attempted to elucidate the role of PARylation in response to DNA damage. As mentioned earlier, PARP has been implicated as playing a role in several DNA repair pathways. In *Arabidopsis* a similar role for PARPs has been suggested. Several studies have shown an increase in transcript of both AtPARP1 and AtPARP2 in response to DNA damaging agents (Culligan *et al.*, 2006; Doucet-Chabeaud *et al.*, 2001; Chen *et al.*, 2003). Adding the PARP inhibitor 3-MB to growth medium was shown to increase the number of intrachromosomal recombination events in the absence of genotoxic stress (Puchta *et al.*, 1995). In addition both AtPARP1 and AtPARP2 have been found to associate with mitotic chromosomes (Babiychuk *et al.*, 2001), and PARP activity was shown to increase during the exponential growth phase of *Arabidopsis* cell culture (Pellny *et al.*, 2009). All the above findings point to AtPARPs having a similar role in DNA repair and genome maintenance to their mammalian homologues. Exposing plants lacking various members of the PARylation family to types of genotoxic stress could therefore help to confirm this hypothesis and elucidate more specifically their roles in efficient DNA repair in Arabidopsis.

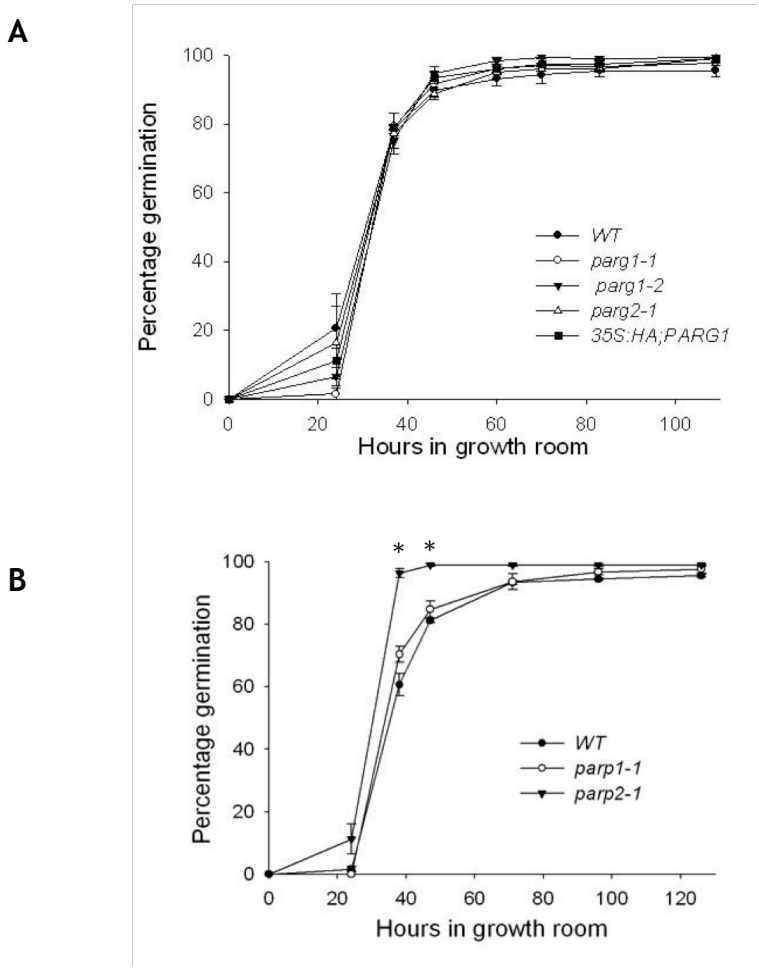

Figure 3.11. Germination rates of T-DNA insertion lines
Surface sterilised seeds of WT Col-0 and AtPARG (A) and AtPARP (B) T-DNA insertion mutants were plated out on ½ MSMO agar and the rates of germination measured by emergence of radicle. Each data point represents the average (± standard error) of three plates each containing approximately 50 seeds. Asterisks indicate statistically significant differences to the wild type at the indicated timepoints using ANOVA ($p < 0.05$, Tukey's test). See appendix A2.4 and A2.5 for tables.

3.2.6.1 Response to genotoxic stress in early development

To investigate the effect of genotoxins on early seedling development, the germination rate in the presence of the alkylating agent MMS was examined. Seeds were treated as described in section 3.2.6, with the inclusion of plates containing 0.0 mM, 0.5 mM and 1.0 mM MMS. On half strength MSMO agar with no MMS, germination rates, in all but the *parp2-1* line, were similar to that of wild type Col-0 seeds (figure 3.11). While no differences were observed between *parg2-1* and WT when the genotoxic agent MMS was included in the medium, both T-DNA insertion lines of AtPARG1 showed a significant delay in germination ($p < 0.05$) proportional to the amount of genotoxin in the medium (figure 3.12A and B). In addition the *parg1-1* and *parg1-2* lines were also much smaller when grown on MS agar plates containing 0.5 mM MMS was continued for two weeks (figure 3.13). While the majority of WT and *parg2-1* seeds germinated on 1.0 mM MMS were able to generate cotyledons, none of the *parg1-1* and *parg1-2* seeds were able to develop beyond radicle emergence (figure 3.13). The 35S:HA:AtPARG1 line showed no difference to wild type and *parg2-1* on 0.5 mM MMS, but a decrease in germination rate was observed on 1.0 mM MMS (figure 3.12B). Upon examination of PARP T-DNA insertion lines under the same conditions, *parp2-1* seeds displayed a similar phenotype to that observed under control conditions and germinated siginificantly faster ($p < 0.05$) than both the wild type and the *parp1-1* seeds at 0.5 mM MMS, but not at 1.0 mM MMS (figure 3.12C and D).

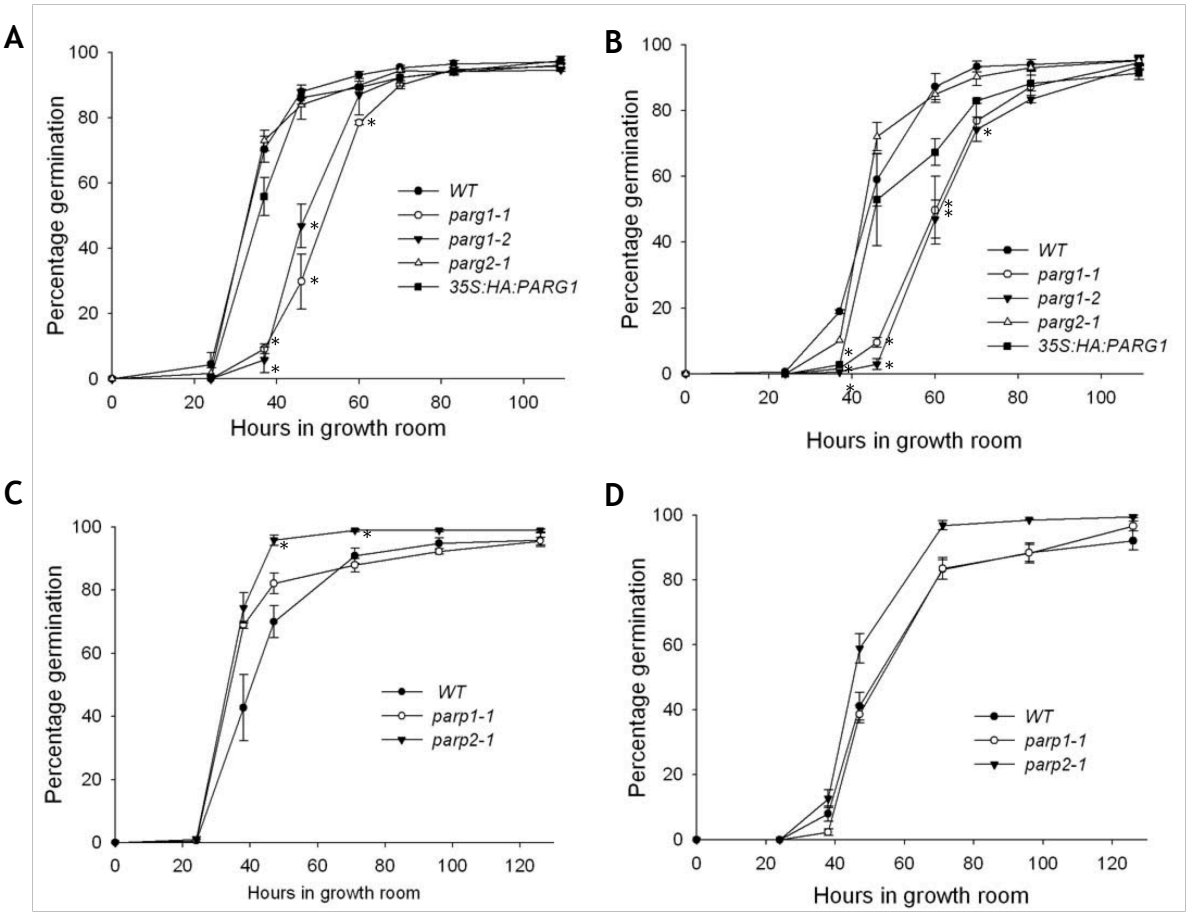

Figure 3.12. Germination assay on genotoxic stress
Sterilised seeds of Col-0, T-DNA insertion lines, and the 35S:HA:AtPARG1 line were plated out on ½ MSMO agar 0.5 mM MMS (A and C), or 1.0 mM MMS (B and D) and placed under constant light. The rates of germination were measured by emergence of the radicle. Each data point represents the average (± standard error) of three plates each containing approximately 50 seeds. Asterisks indicate statistically significant differences to the wild type at the indicated timepoints using ANOVA ($p < 0.05$, Tukey's test). See appendix A2.6 to A2.14 for tables.

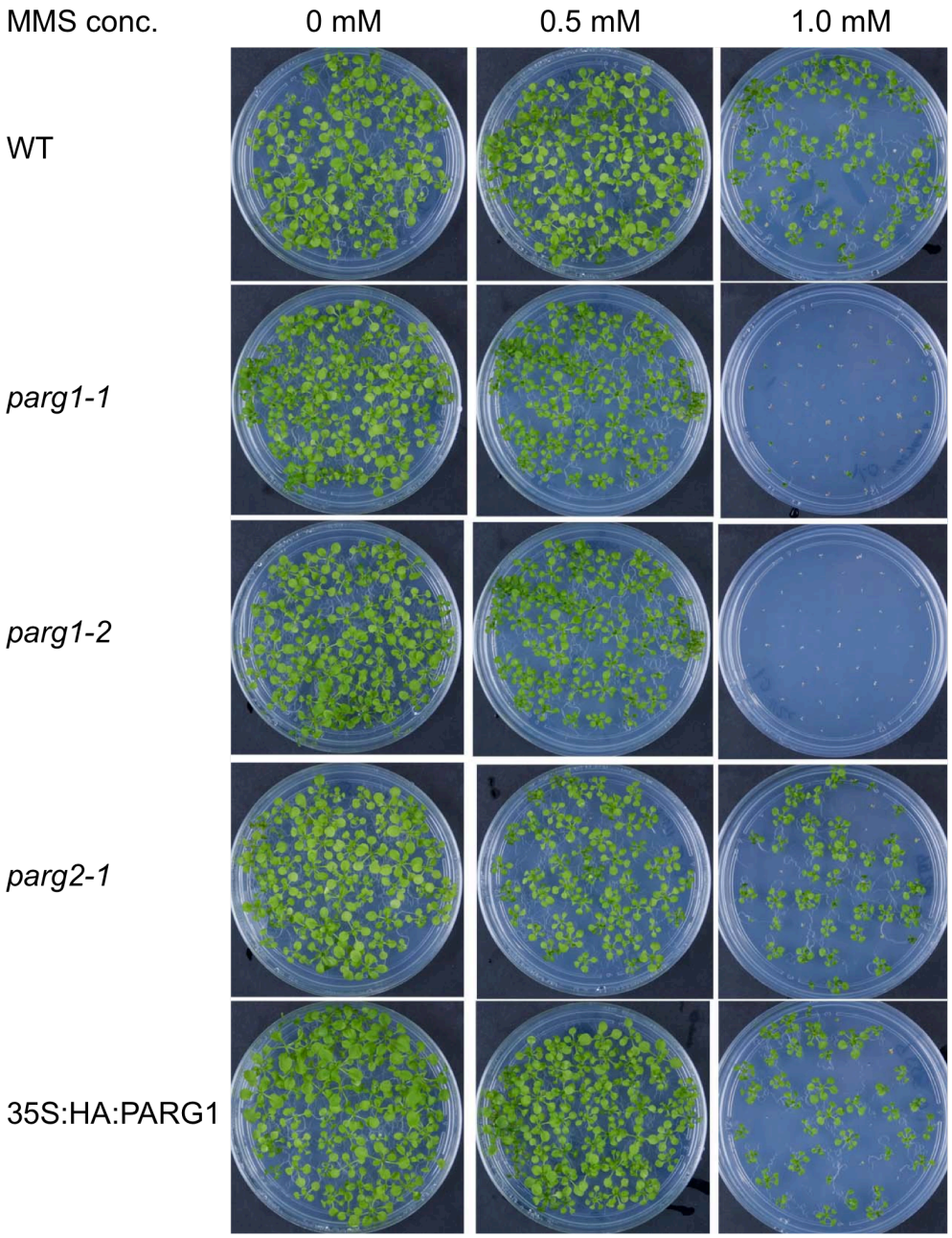

Figure 3.13. AtPARG deficient seedlings after two weeks growth on genotoxic stress
Seeds were treated as described in figures 3.10 and 3.11. The same plates were left in constant light for a further 2 weeks. Pictures are representative of triplicates.

3.2.6.2 Response to genotoxic stress in later development

WT and mutant seedlings were exposed to genotoxic stress by conditions that induce different DNA damage repair pathways in mammals to see if there is any functional redundancy between AtPARPs and AtPARGs. The radiomimetic bleomycin was used to induce double stranded breaks, and the alkylating agent MMS was used to induce single stranded breaks (although this has also been known to cause DSBs as well). Hypersensitive phenotypes have previously been observed in mutants of the *Arabidopsis* NHEJ homologues AtKu80 (Gallego *et al*, 2003; West *et al*., 2002) and AtKu70 (Bundock *et al*., 2002; Riha *et al*, 2002) when exposed to these DNA damaging agents.

3.2.6.3 AtPARG1 T-DNA insertion lines are hypersensitive to the alkylating agent MMS

Surface sterilised seeds were stratified on ½ MSMO agar plates for two days at 4°C before germination for 7 days in constant light. Seedlings were transferred into 12-well plates containing 2 ml ½ MSMO media + 0.5% sucrose supplemented with 0, 0.5, 1.0, and 1.5 mM MMS and placed back into constant light. Within a week, a hypersensitive phenotype was observed in AtPARG1 deficient seedlings. No differences were observed between wild type and *parg2-1* at any of the concentrations. At 1.0 mM and 1.5 mM of MMS *parg1-1* and *parg1-2* showed hypersensitivity (figure 3.14). None of the other mutant lines showed any noticeable differences to wild type seedlings.

3.2.6.4 AtPARG1 T-DNA insertion lines show hypersensitivity to the radio mimetic bleomycin

Surface sterilised seeds were stratified on ½ MSMO agar plates for two days at 4°C before germination for 7 days in constant light. Seedlings were transferred into 12-well plates containing 2 ml ½ MSMO media + 0.5% sucrose supplemented with 0, 1, 5, and 10 μg/ml bleomycin and placed back into constant light. A hypersensitive phenotype of both AtPARG1 mutant lines could be observed at 1.0 and 1.5 μg/ml, while none of the other mutant lines showed any noticeable difference in tolerance to wild type (figure 3.15).

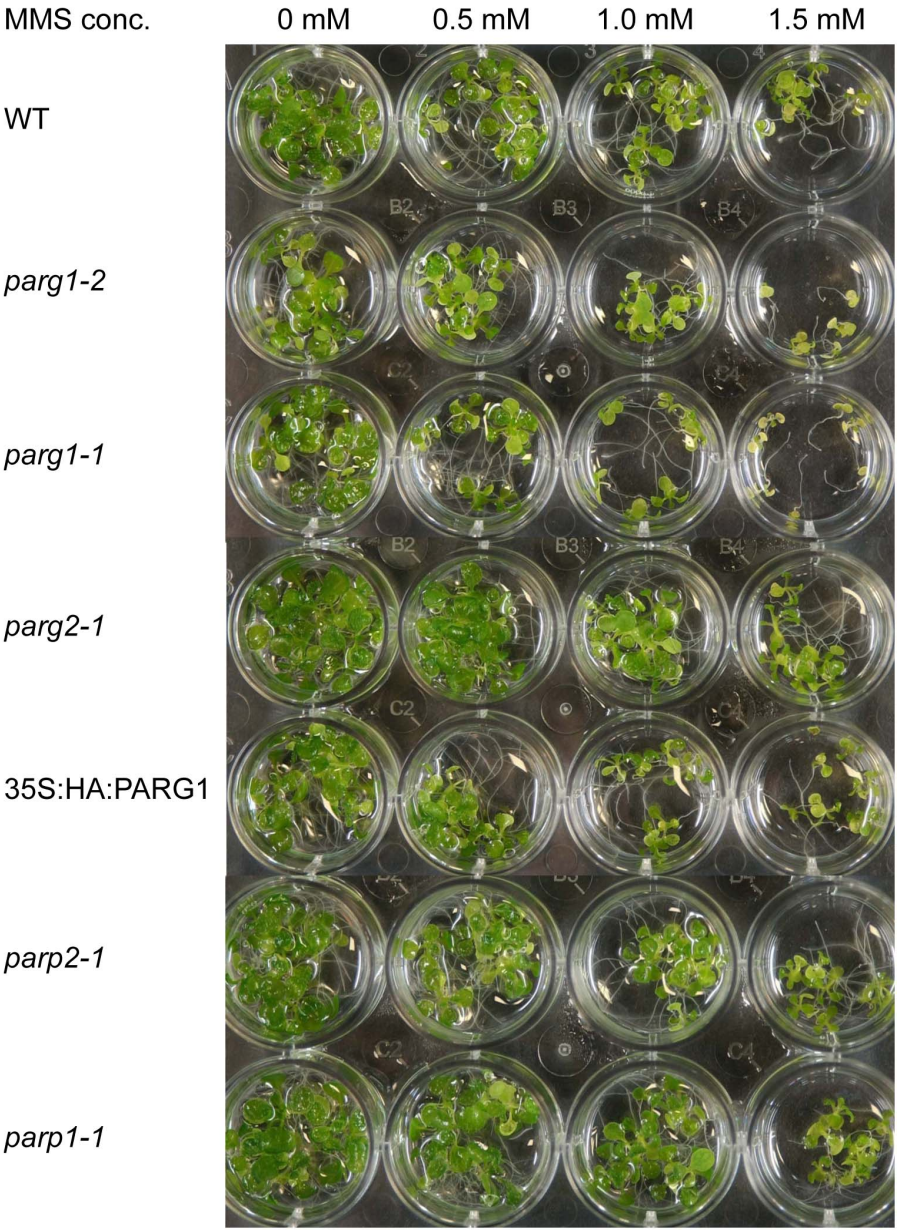

Figure 3.14. Phenotypes of wild type and mutant seedlings after transfer to MMS containing media
Seeds were germinated on ½ MSMO for one week before 5 seedlings were transferred to wells containing ½ MSMO and 0, 0.5, 1.0 and 1.5 mM of MMS. Pictures are representative of biological triplicates.

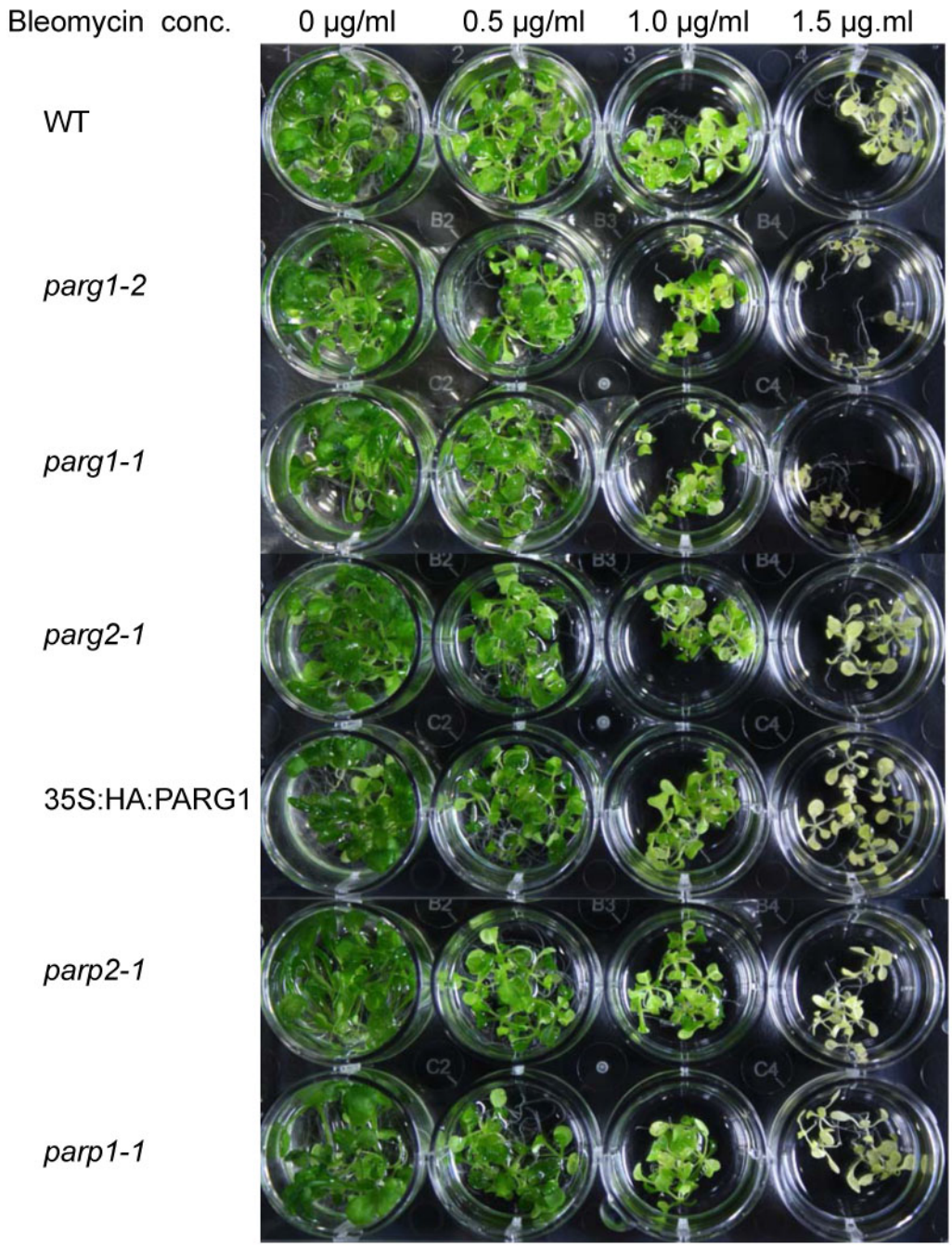

Figure 3.15. Phenotypes of wild type and mutant seedlings after transfer to bleomycin containing media

Seeds were germinated on ½ MSMO for one week before 5 seedlings were transferred to wells containing ½ MSMO and 0, 0.5, 1.0 and 1.5 µg/ml of bleomycin. Pictures are representative of biological triplicates.

3.2.6.5 Phenotypes of WT and homozygous T-DNA insertion lines exposed to UV-B

UV-B light (280-320 nm) induces the formation of bulky pyrimidine dimers in the DNA, which in plants manifests itself in desiccation and necrosis. While UV-B induced damage in mammals is mainly repaired by nucleotide excision repair (NER), high doses of UV-B induce homologous recombination in plants (Ries *et al.*, 2000a) and increased homologous recombination is proportional to the amount of pyrimidine dimers formed (Ries *et al.*, 2000b). However, another report published around the same time, suggested the repair of UV-B induced damage was repaired by proteins similar to those involved in mammalian NER (Liu *et al.*, 2000).

To examine the effects of UV-B exposure on the T-DNA insertion lines and the AtPARG1 overexpressing line, UV-B treatment was performed as described in Brown and Jenkins (2008). Briefly, seeds were sown on soil and grown in constant light for 12 days before they were exposed to 48 hours of supplemental UV-B light. The plants were then placed back into constant light for 5 days. Photographs were taken after the 5-day recovery period (figure 3.16). The *parg1-2* and 35S:PARG1 overexpressor plants were generally smaller than wild type after treatment, while the *parp1-1* and *parp2-1* plants were larger than wild type (figure 3.16).

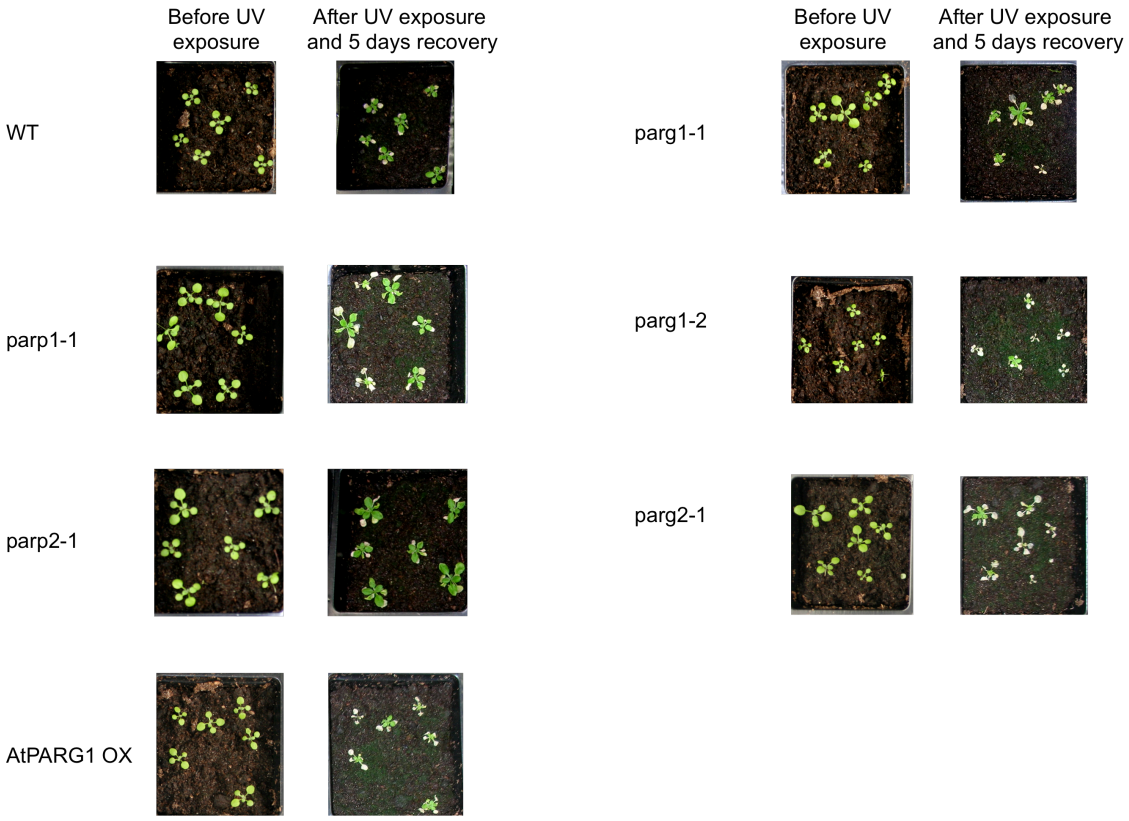

Figure 3.16 UV-B sensitivtity assay
Plants were grown on soil in constant light for 12 days before exposure to supplemental UVB (5 μmol m^{-2} s^{-1}) for 48 hours. The plants were then returned to constant light for a 5-day recovery period. Pictures were taken immediately prior to UVB treatment and after the 5-day recovery period.

3.2.7 Oxidative stress

Oxidative stress occurs when there is an imbalance in the generation of reactive oxygen species (ROS), with more ROS being produced than are metabolised by antioxidant enzymes or by reaction with antioxidant molecules. Normally used as a herbicide, methyl viologen (MV), also known as Paraquat, is an inducer of oxidative stress in photosynthetic plants. Briefly, it blocks photosynthesis by accepting electrons from photosystem I (PSI), and transfers them to molecular oxygen, thereby creating ROS, which can damage DNA. MV has been shown to induce the production of poly(ADP-ribose) in *Arabidopsis* (Ogawa *et al.*, 2009; Ishikawa *et al.*, 2009). As MV blocks photosynthesis, this will result in a reduction in chlorophyll production, and the chlorophyll content of the plant can thus be used as a measure of the plant response to oxidative stress.

To measure the chlorophyll content of the plant lines used in this study, seeds from all the genotypes were grown on ½ MSMO agar plates+sucrose for two weeks, before shoots were weighed and transferred to liquid ½ MSMO with or without 10 μM methyl viologen for 24 hours. The tissue was then harvested and the chlorophyll content of seedlings exposed to media with or without the oxidative agent was measured. The *parg1-2* line had significantly higher initial chlorophyll content than the wild type Col-0 seedlings ($p < 0.05$), while no differences were observed between the chlorophyll content of the wild type and the rest of the T-DNA insertion line seedlings (figure 3.17). However, when compared with the AtPARG1 overexpressing line, a significantly lower chlorophyll content was measured under control conditions ($p < 0.05$), and unlike the other genotypes, this did not change significantly after MV treatment (figure 3.17).

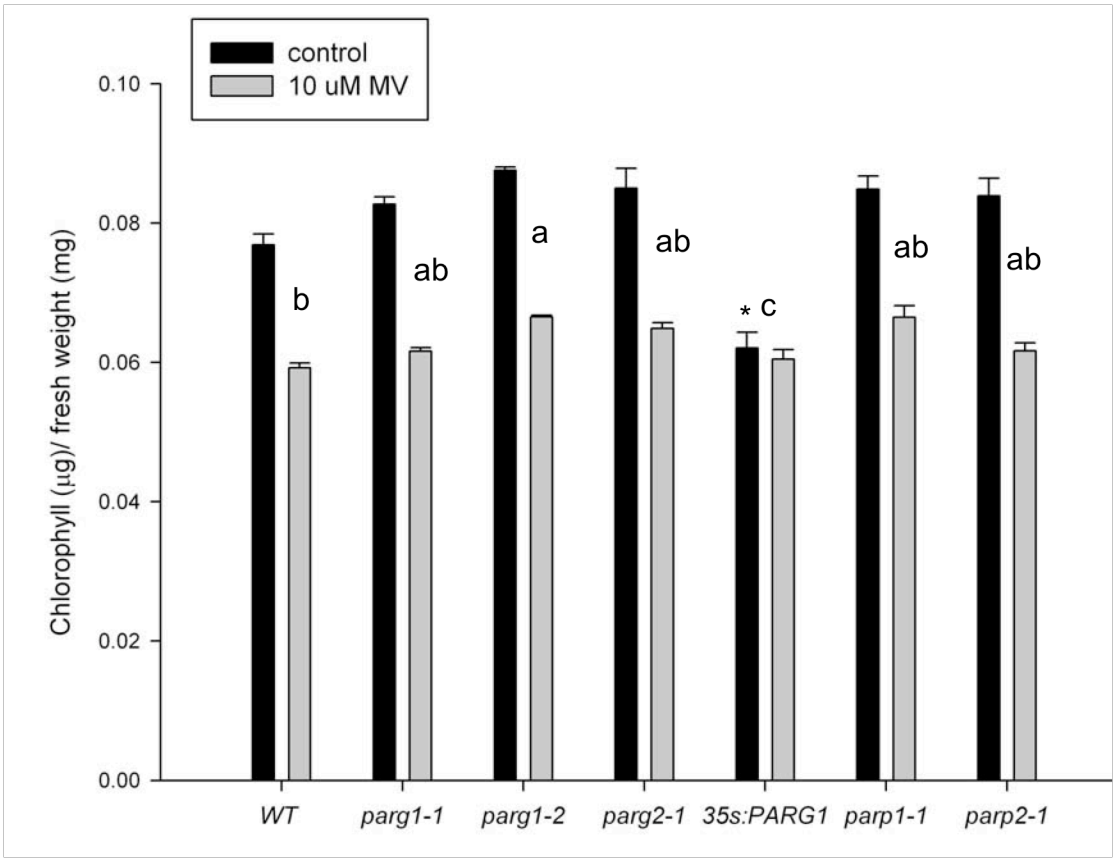

Figure 3.17. Chlorophyll content of AtPARP and AtPARG T-DNA insertion lines
Seedlings were grown on ½ MSMO agar plates for two weeks in long day conditions (16 hours light: 8 hours dark). Vegetative tissue was harvested and exposed to 10 μM methyl viologen (MV) in ½ MSMO for 24 hours. The fresh weight was measured and chlorophyll content determined spectrophotometrically. Error bars represent SE of three measurements. Asterisks indicate a significantly different interaction (effect of MV treatment; $p < 0.05$, Tukey's test). Different letter codes indicate significant between-line differences for control only (no MV) treatment using ANOVA ($p < 0.05$, Tukey's test). See appendix A2.15 for table.

3.2.8 ABA-regulated abiotic stress

The response to several abiotic stresses, such as drought, heat, cold, salt and osmotic stress, is mediated in part by the phytohormone ABA. It induces the closure of stomata to reduce transpirational water loss. During ABA responsive stress signalling, ROS is produced in the form of H_2O_2, which has been shown to act as a second messenger in ABA-induced stomatal closure (Kwak *et al.*, 2003). Since several papers have shown a link between ABA-induced abiotic stress responses and poly(ADP-ribosyl)ation (Doucet-Chabeaud *et al.*, 2001; DeBlock *et al.*, 2005; Vanderauwera *et al.*, 2007; Li *et al.*, 2010), and AtPARP1 and AtPARP2 are upregulated after the application of drought and H_2O_2 (Doucet-Chabeaud *et al.*, 2001; Amor *et al.*, 1998) the response of T-DNA insertion and the AtPARG1 overexpressing line were investigated using different stresses in the following sections.

3.2.8.1 Salt stress

Surface sterilised seeds were placed onto ½ MSMO + 0.5% sucrose vertical agar plates containing increasing amounts of NaCl (0, 50, 75, 100 mM), stratified for 2 days at 4°C and placed in constant light. After 15 days pictures were taken. On plates containing no salt and 50 mM salt, there were no observable differences between the different genotypes (figure 3.18). When the salt concentration was increased to 75 and 100 mM, the seedlings deficient of either of the two AtPARGs showed a decrease in size as well as appearing more chlorotic, compared with the wild type (figure 3.18). The 35S:HA:AtPARG1 line also displayed higher sensitivity on 100 mM NaCl (figure 3.18).

3.2.8.2 Osmotic stress

To investigate the effects of osmotic stress on the AtPARP/AtPARG T-DNA insertion lines, surface sterilised seeds were placed onto ½ MSMO + 0.5% sucrose vertical agar plates containing increasing amounts of mannitol (0, 100, 150, 200 mM), stratified for 2 days at 4°C and placed in constant light. After 14 days pictures were taken. Overall, most of the genotypes look similar across the concentrations of mannitol. Only *parg1-2* seedlings appear smaller on 150 and 200 mM mannitol (figure 3 19).

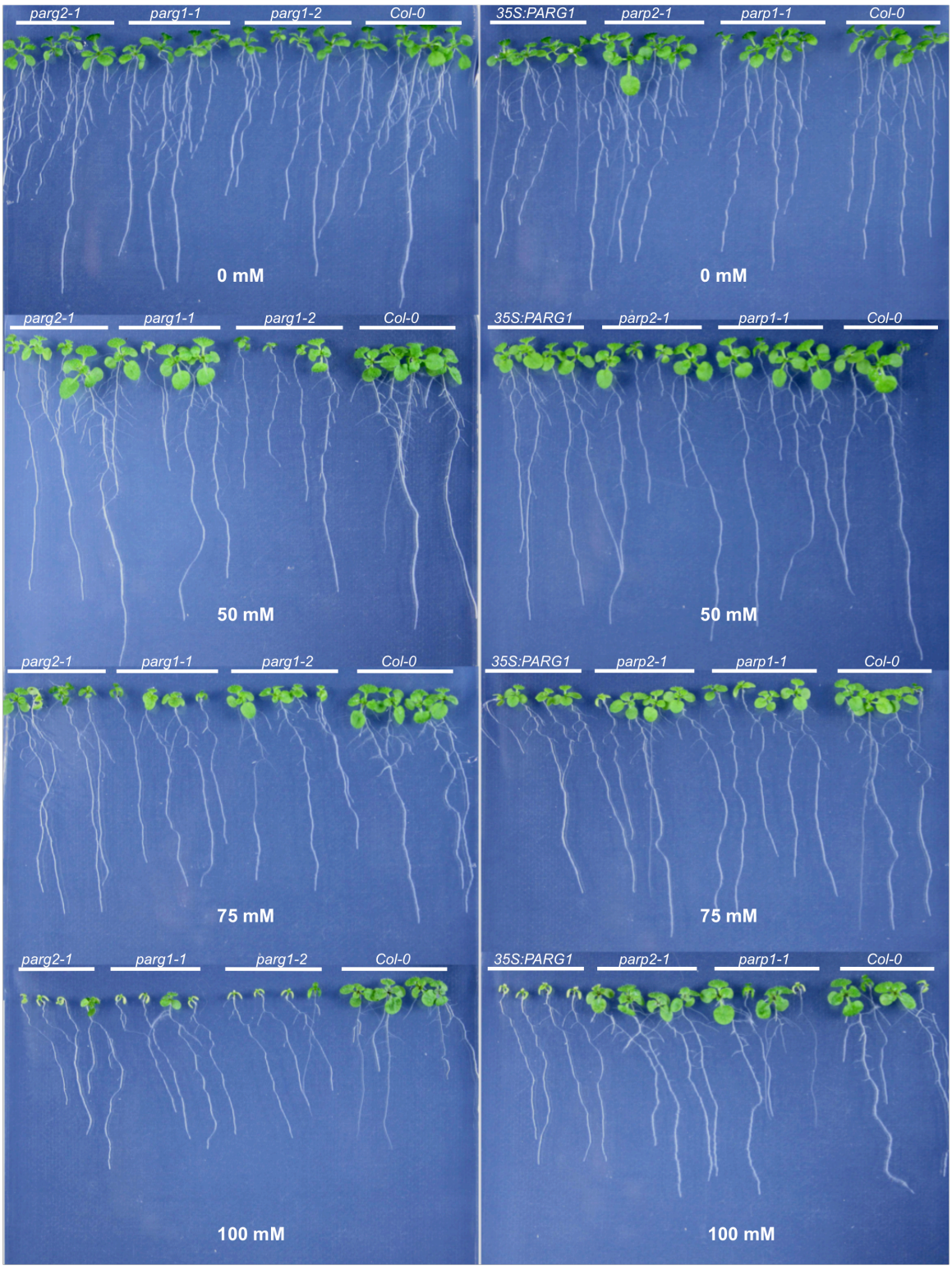

Figure 3.18 Exposure to salt stress
Seeds were sown onto vertical ½ MSMO agar with NaCl at 0, 50, 75 and 100 mM and left for 15 days under constant light conditions. Pictures are representative of triplicates.

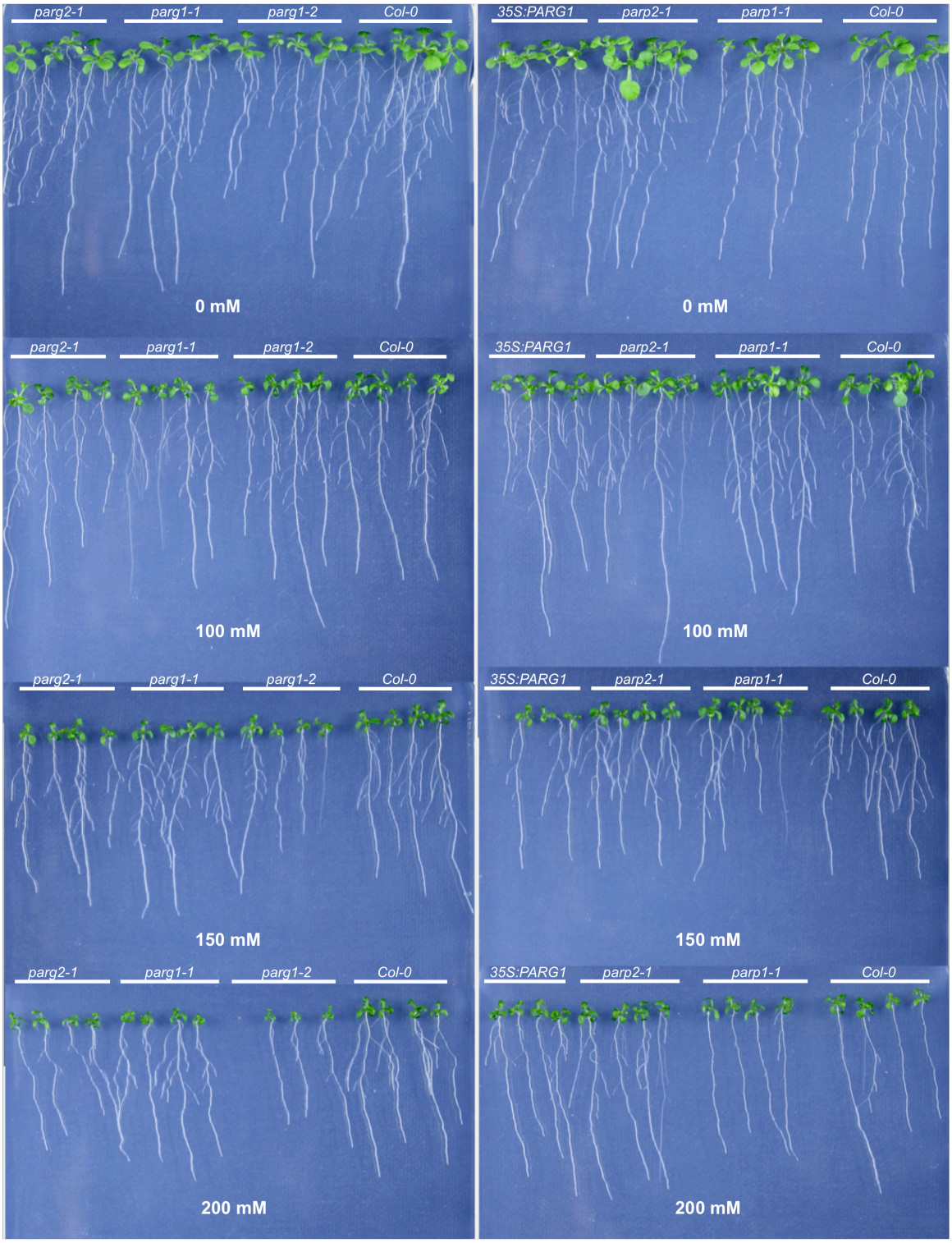

Figure 3.19 Exposure to osmotic stress
Seeds were sown onto vertical ½ MSMO agar with mannitol at 0, 100, 150 and 200 mM and left for 15 days under constant light conditions. Pictures are representative of triplicates.

3.2.8.3 Drought stress

To investigate the effects of drought on the AtPARP/AtPARG T-DNA insertion lines used in this study, seeds were placed on soil and grown in long day light conditions with regular watering for 2 or 3 weeks, after which watering was stopped. Pictures in figures 3.20A were taken after two weeks growth on the last day of watering (top panel). Below are the same plants 10 (middle panel) and 17 days (bottom panel) after watering stopped. Pictures in figure 3.20B were taken after three weeks growth on the last day of watering (top panel). Below are the same plants 10 days after watering stopped. No discernable differences could be seen between any of the genotypes examined in any of the two conditions.

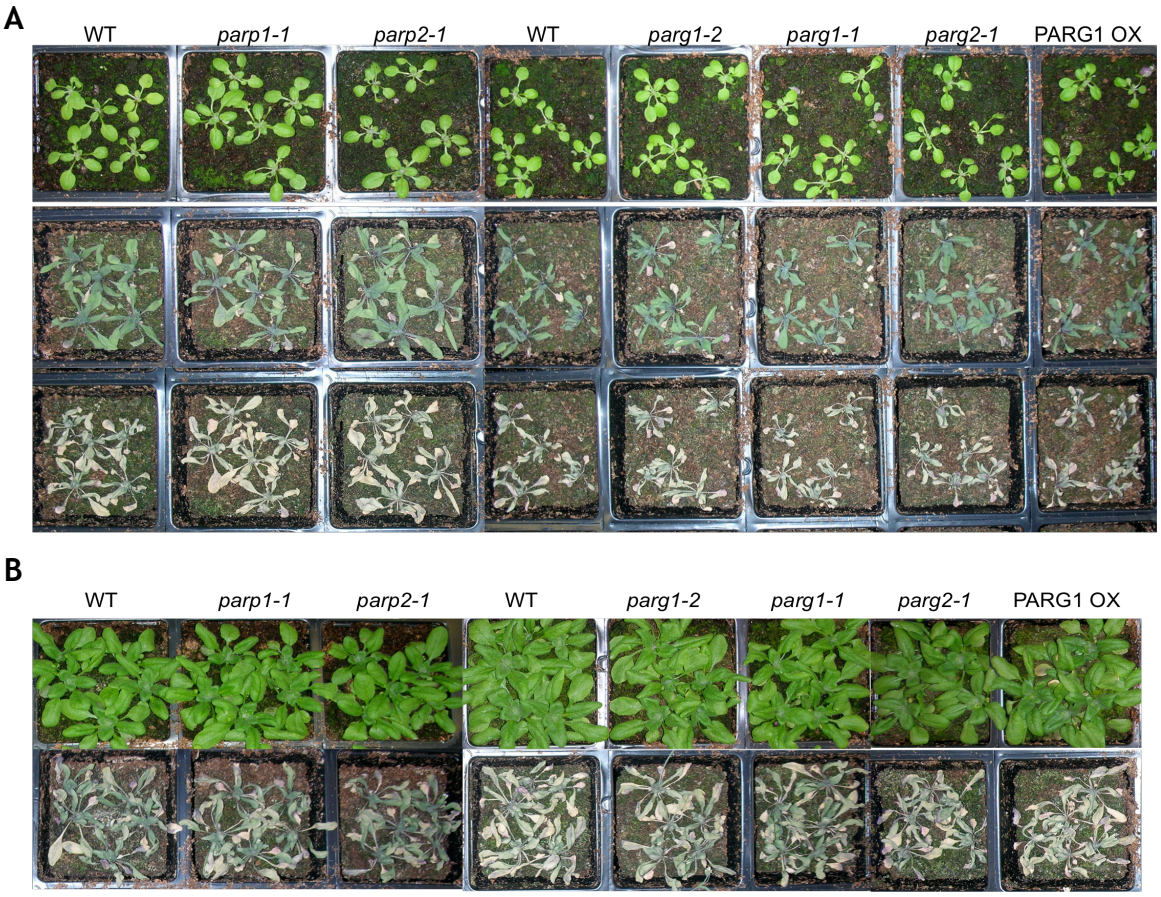

Figure 3.20 Drought treatment of T-DNA insertion lines
Seeds were sown on soil and grown in long day conditions.
A) Plants were grown for two weeks before watering was stopped. Plants are shown before (top panels), 10 days (middle panels), and 17 days (bottom panels) after watering stopped.
B) Plants were grown for three weeks before watering was stopped. Plants are shown before (top panels) and 10 days (bottom panels) after watering stopped.

3.2.9 Double mutant lines

Double PARP1/PARP2 knock-out mammalian lines are embryonic lethal (Menissier de Murcia *et al*., 2003), while single knock outs are viable, but hypersensitive to genotoxic stress (de Murcia *et al*., 1997; Schreiber *et al*., 2002). There is only one gene coding for PARG in mammals, although this gene exists in several isoforms with different subcellular localisations as described earlier in this chapter. Cell lines deficient in PARG are embryonic lethal (Koh *et al*., 2004). Earlier in this chapter it was demonstrated that single knock-outs of AtPARP1 or AtPARP2 do not display sensitivity to genotoxic stress, indicating the functional redundancy observed in mammals under genotoxic conditions is not found in *Arabidopsis* AtPARP1 and ATPARP2.

3.2.9.1 Genotyping of AtPARP-1/AtPARP-2 double knock-outs

The T-DNA insertion lines *parp1-1* and *parp2-1* were grown to the flowering stage and cross-fertilization was performed between female *parp2-1* and male *parp1-1* parents. After crossing plants, the seeds from the successful crosses were collected and the T1 generation grown up as usual and T2 seeds collected. These were then left to grow for 3 weeks before genomic DNA was extracted from each individual plant. Each sample was then PCR genotyped as described in section 3.2.3 for the presence of both T-DNA inserts showing a homozygous knock-out genotype for both AtPARP1 and AtPARP2 (figure 3.21). There was insufficient time to characterise any phenotypes of this double mutant line, however it was determined that no developmental differences to wild type Col-0 could be seen and the plants were fertile.

Figure 3.21. Isolation of *parp1-1/parp2-1* homozygous plants through genotyping
Ai) Gene structure of AtPARP1 and AtPARP2 where exons and introns are represented as black boxes and black lines, respectively. Location of *parp2-1* and *parp1-1* T-DNA insertions are indicated by a triangle, wherein an arrow indicates the position of the T-DNA left border
ii) PCR genotyping results for *parp2-1* allele. PCR reactions were completed using Col-0 or *parp1-1/parp2-1* genomic DNA with primers for the region flanking the insert (LP RP) as well as for the T-DNA left border and genomic flanking region (GK8409 RP, respectively).
iii) PCR genotyping results for *parp1-1* allele. PCR reactions were completed using Col-0 or *parp1-1/parp2-1* genomic DNA with primers for the region flanking the insert (LP RP) as well as for the T-DNA left border and genomic flanking region (GK8409 RP, respectively)

3.2.9.2 Genotyping of AtPARG1/AtPARG2 knock-outs

The T-DNA insertion lines *parg1-2* and *parg2-1* were grown to the flowering stage and cross-fertilization was performed between female *parg2-1* and male *parg1-2* parents. After crossing plants, the seeds from the successful crosses were collected and the T1 generation grown up as usual and T2 seeds collected. These were then left to grow for 3 weeks before genomic DNA was extracted from each individual plant. Each sample was then PCR genotyped as described in section 3.2.3 for the presence of both T-DNA inserts. In total 75 lines of T2 crossed mutant lines were genotyped, but no double mutants were found, and double mutants would be expected at a ratio of 1:16. However, due to the fact that these genes are closely linked (526 bp between them) the probability of a chiasmatic event taking place within this intergenic region is very small, and several thousands of plants would have to be genotyped to find one wherein this event had taken place.

3.3 Discussion

Arabidopsis contains three PARPs with different structures. AtPARP1 and AtPARP2 show high identitity to the mammalian PARP catalytic signature motif (88 and 92%, respectively) and both contain all the residues previously identified as important for activity. All the higher plant homologues of PARP1 show similar levels of identities to mammalian PARP1 (37-39%), and 73-76% similarity to each other. The same is true for AtPARP2, which along with other higher plant homologues of PARP2 show 37-39% identity to mammalian PARP2, and 72-73% similarities with each other. AtPARP3 shows only 40% identity to the PARP catalytic signature, and is missing several residues shown to be important for activity. The highest level of similarity to AtPARP3 is seen in other higher plant PARPs, but even these values are relatively low at ~40 %. *Arabidopsis* contains two PARGs, which share 51% amino acid identity, the largest stretch of conserved residues being found around the catalytic PARG signature motif and show a similar level of identity to other higher plant PARG homologues. The AtPARGs resemble the shorter protein isoforms of human PARG as these do not contain the N-terminal regulatory domain.

T-DNA insertion lines were obtained from stock centres. Plants homozygous for the insertion were identified through PCR genotyping of genomic DNA, as well as lack of transcript. However, it was not possible to isolate a homozygous AtPARP3 T-DNA insertion line, as although the genotyping results came up positive for a homozygous insertions of the T-DNA in the correct position, when further transcript analysis was conducted, the plants were found to contain transcript. A second AtPARP3 T-DNA insertion line was recently acquired, but so far the genotyping results have revealed only wild type and heterozygous plants (data not shown) despite more than 20 plants being genotyped. Since AtPARP3 is expressed mainly during seed development and germination, these results could perhaps indicate a requirement for AtPARP3 in early development. In addition to the T-DNA insertion lines, a homozygous AtPARG1 overexpressing line was also generated through stable transformation of wild type Col-0 plants. A second AtPARG1 overexpressing line as well as a line transformed with the empty vector should have been generated as controls to demonstrate that any phenotypes observed were not simply due to positional insertion effects.

The general appearance of the T-DNA insertion lines and overexpressing line were no different to wild type plants when grown in long or short day conditions. When examining general developmental phenotypes of the T-DNA insertions, it was not possible to compare across all genotypes, as significant differences were found between the wild type Col-0 control plants in the different trays, despite efforts to rotate the trays to circumvent any problems of differential light intensity and airflow. The difficulty in producing consistent growth data in wild type plants was highlighted in a recent paper (Massonnet *et al.*, 2010), where large variation was observed between laboratories supplied with the same seed stock and using the same methodology.

Previously a link between AtPARG1 and circadian rhythm was established as Panda *et al.* (2002) showed the lengthening of period in the *tej* mutant, which was found to be due to a single amino acid mutation, altering a conserved residue in the PARG catalytic signature. This phenotype was rescued in a dose dependent manner by the application of the PARP inhibitor 3-AB. This mutant also displayed an early flowering phenotype in both long and short day light conditions, although much more prominent under the latter conditions. A similar early flowering phenotype to that of *tej,* was observed in both *parg1-1* and *parg1-2* under long day, but not short day conditions. In the *tej* mutants there is still protein present, but the plants are less able to process the PAR polymers (Panda *et al.*, 2002). The AtPARG1 T-DNA insertion lines used in this study do not contain AtPARG1 transcript and thus do not express AtPARG1 protein. This difference between the mutants could perhaps account for the difference observed in flowering time phenotypes. The *tej* mutant could thus represent a dominant negative protein, still able to bind to any potential interactors or promoter regions but not able to act catalytically.

Differences in early development were examined using a germination assay, where it was observed that *parp2-1* showed an increased rate of germination. This could be due to a decrease in energy consumption during germination in these seedlings as the replenishment of NAD^+, through the *de novo* pathway, or the salvage pathway, uses five and three molecules of ATP, respectively, per molecule of NAD^+ (DeBlock *et al.*, 2005). The reduction of consumption of NAD^+ through PAR production would therefore leave more energy free for cell

divisions. Previously AtPARP3 has been suggested as being involved in regulation of germination (Hunt *et al.*, 2007; Beccera *et al.*, 2006).

3.3.1 AtPARG1 deficient plants are hypersensitive to genotoxic stress

The removal of poly(ADP-ribose) is catalysed by the enzyme PARG. There is only one single PARG gene in most organisms and knocking out this gene results in embryonic lethality (Koh *et al.*, 2004). The mammalian PARG gene does however have several isoforms of different sizes, which are found in different subcellular compartments (Meyer-Ficca *et al.*, 2004; Meyer *et al.*, 2007). Knocking out the largest isoform (110 KDa) by removing exons 2 and 3 (Δ2-3), does not affect the turnover of PAR, as these mutant cells showed similar kinetics to wild type cells when exposed to H_2O_2 (Cortes *et al.*, 2004). However, transgenic mice carrying the same mutation or one eliminating exon 1 were hypersensitive to γ-irradiation and other genotoxic agents (Cortes *et al.*, 2004; Fujihara *et al.*, 2009). The Δ2-3 mutant cell line displayed a reduction in the amount of auto-modification of PARP1, which might affect the ability of PARP1 to shuttle off damaged DNA and thus preventing the access of other members of the repair machinery (Cortes *et al.*, 2004; Gao *et al.*, 2007). A similar hypersensitive phenotype was observed in cells, which overexpressed PARP1, when DNA damaging agents were applied (Van Gool *et al*, 1997). The hypersensitivity of the overexpressing cell lines was not due to depletion of NAD^+ or ATP (Van Gool *et al.*, 1997). Inhibition of PARP has also been shown to sensitise cells to DNA damaging agents (Durkacz *et al.*, 1980). The findings above thus highlight the need for tight control of cellular PAR-levels upon activation of PARP1.

When the T-DNA insertion lines were examined under genotoxic stress conditions AtPARG1 T-DNA insertion lines were found to be sensitive to DNA damaging agents, as both *parg1* alleles used in this study, display the same phenotype. The phenotype manifests as early as the maturing seed, as germination rates on solid media containing DNA damaging agents are reduced compared with those of WT and *parg2-1* seeds. This hypersensitive phenotype can also be seen in later development, when one week old seedlings are exposed to DNA damaging agents in liquid media. The germination rate for the 35S:HA:AtPARG1 is similar to that of wild type seeds on 0.5 mM MMS, while it is lowered on 1 mM MMS. One

hypothesis to explain this phenotype could be that when AtPARG1 is knocked out there is not enough glycohydrolase activity to process the PAR polymers generated upon DNA damage. If the mode of activation in plants is the same as in mammals, i.e. inactivation of PARP when automodified, then with no enzyme to remove the polymer and thus no way of returning to the active PARP enzyme state. This would lower NAD^+ consumption and limit death through necrosis, but at the same time would limit DNA-repair. In plants over expressing AtPARG1 you would expect the PARP enzyme to remain in the active state, as polymers attached to the automodification domain and thus leaving the enzyme in an active state and free to consume NAD^+. Alternatively, if too much of the polymer is removed from PARP, it might not be able to form the protein interactions required for DNA damage repair, thus leaving the site un-repaired. It could be a case of a threshold that needs to be reached in terms of DNA damage for any phenotype to be seen. While both alleles of *parg1* showed the same level of hypersensitivity to the DNA damaging agents MMS and bleomycin, the response to abiotic stress and UVB treatment in the *parg1-2* allele was more severe. This could indicate the presence of a truncated protein in the *parg1-1* line, which is still able to perform some of the functions of AtPARG1 in response to these stresses. To further elucidate the difference between the two *parg1* alleles it would therefore be desirable to design an antibody specific to AtPARG1 to detect the presence of any truncated versions of AtPARG1 that might persist in these T-DNA insertion lines. It would be interesting to measure the extent of DNA damage inflicted in these as well as the other T-DNA insertion lines. This could be done using the Comet assay.

Double strand breaks such as those caused by irradiation or radiomimetics, like bleomycin, are repaired by NHEJ (non-homologous end joining) or HR (homologous recombination). MMS causes more simple single strand breaks, which are normally repaired by the BER (base excision repair) pathway. The mechanisms of repair in plants are less well characterized, although *Arabidopsis* does contain homologues of many of the genes showed to interact with PARP1 and PARP2 in both NHEJ and BER (Bleuyard *et al*., 2006), and thus could very likely perform a similar role in plants. Similar hypersensitive phenotypes as described for AtPARG1 deficient lines have been observed in mutants of AtKu80 (Gallego *et al*, 2003; West *et al*., 2002) and AtKu70 (Bundock *et al*., 2002; Riha

et al, 2002). In AtKu80 mutants treated with bleomycin, AtPARP2 transcript levels were significantly higher than in bleomycin treated WT, which could indicate that AtPARP2 has a role in putative DSB backup repair pathways (West *et al.*, 2004).

3.3.2 PARylation in oxidative stress

Oxidative stress has previously been shown to induce poly(ADP-ribosyl)ation both in mammals (Blenn *et al.*, 2006) and plants, where pre-treatment with PARP inhibitors (3-AB and nicotinamide) reduced cell death in soybean cell cultures after H_2O_2 application (Amor *et al.*, 1998). Later an upregulation of both AtPARP1 and AtPARP2 transcript levels in response to H_2O_2 was also observed in *A. thaliana* (Doucet-Chabeaud *et al*, 2001). The herbicide methyl viologen (MV) causes oxidative stress by generating ROS through transferring electrons from photosystem I to molecular oxygen. It has been shown to induce PAR formation in plants (Ishigawa *et al.*, 2009; Ogawa *et al.*, 2009). Chlorophyll content has been shown to be higher in AtPARP1 and AtPARP2 knock down plants compared to wild type plants (De Block *et al.*, 2005) and lower in the *parg1-3* mutant (Li *et al.*, 2011) after treatment with methyl viologen for 24 hours. However, the T-DNA insertion lines examined in this study showed no difference in their chlorophyll content compared with wild type.

3.3.3 PARylation in abiotic stress

Poly(ADP-ribosyl)ation in plants has been shown to have links to abiotic stresses such as high light and drought (Deblock *et al.*, 2005, Li *et al.*, 2011). AtPARP1 knock down lines had increased transcript levels of ABA, cold, and drought responsive genes compared to wild type in a microarray examining high light stress responses (Vanderauwera *et al.*, 2007). However, when the transcript levels of all AtPARPs and AtPARGs were examined in response to salt, high light and drought, only AtPARP3 transcript levels were significantly increased in response to these stresses (Ogawa *et al.*, 2009).

The tolerance to both salt and osmotic stress was investigated by growing the seeds on vertical plates containing increasing concentrations of NaCl and mannitol, respectively. No distinctive differences could be observed between

the AtPARP T-DNA insertion lines and the wild type on mannitol or NaCl. When the AtPARG T-DNA insertion lines were examined, both AtPARG1 and AtPARG2 null lines were more sensitive to salt stress, as they were smaller and more chlorotic. This trend is seen at 50 mM NaCl, but is much clearer at 100 mM NaCl. At this highest concentration, the 35S:HA:AtPARG1 line also displayed sensitivity to salt. This observation could further support the idea that there is a threshold for AtPARG1 expression at high levels of stress, and increasing PAR degradation above this, is detrimental to the cell. There was a noticeable variation in the appearance of wild type Col-0 on the plates, even at the control conditions. One way to amend this problem, could be to grow all the genotypes on control medium for a few days and transfer those similar in size and appearance to the stress plates.

The ability of *Arabidopsis* with altered PARylation activity to withstand drought has previously been investigated. An AtPARG1 T-DNA insertion line not used in this study, *parg1-3* showed reduced survival compared to wild type plants when re-watered after two weeks of drought (Li *et al.*, 2011), while AtPARP1 and AtPARP2 knockdown lines had higher tolerance to two week drought than wild type plants (DeBlock *et al.*, 2005). However, we found that no differences to the wild type plants could be seen in any of the T-DNA insertion lines. However, when commencing drought treatment, the plants should be monitored more closely i.e. on a daily basis to avoid missing any differences between genotypes. The exact conditions for drought used in other studies are hard to replicate as several factors can affect the outcome of the experiment, such as the heterogeneity of the soil that the plants are grown on and its water retention as well as the airflow around the growth chamber. The two studies mentioned above also withhold water for different lengths of time, and start drought at different plant ages.

3.3.4 Double knock-out lines

In this study, homozygous double knockouts of *parp1-1* and *parp2-1* were isolated. While no phenotypic data has yet been derived from these, it could be determined that they are viable, fertile and show no obvious phenotypes during development. Double PARP1/PARP2 knock-outs in mice are embryonic lethal

(Menissier de Murcia *et al.*, 2003), while the single knockouts are viable, but sensitive to genotoxic stress (de Murcia *et al.*, 1997; Schreiber *et al.*, 2002). AtPARP3 is expressed at high levels in seed development and germination (Becerra *et al.*, 2006; Hunt *et al.*, 2007), and so could be the protein that carries out PARylation activity during early development and any phenotypes as a result of the double *parp1-1*/*parp2-1* mutation would not be seen until the plants are challenged with stress.

In *C. elegans* there are also two PARGs, and RNAi knockdown through microinjection demonstrated no significant reduction in survival rates of progeny in single or double knock down worms under control conditions. However, when the worms were exposed to γ-irradiation after microinjection, there was a significant reduction in the survival rates of the progeny (St-Laurent *et al.*, 2007). The potential functional redundancy between AtPARG1 and AtPARG2 was investigated using genetic crosses to obtain double mutants. When PCR genotyping 75 T2 crossed lines (data not shown), no double mutants were found. This is more than likely due to the close linkage of AtPARG1 and AtPARG2. An alternative way to try and investigate the effect of a double AtPARG deficiency, would be to make dexamethasone/ethanol-inducible silencing constructs (Wielopolska *et al.*, 2005; Lo *et al.*, 2005) and stably transform them into a single mutant background.

In the next chapter, the potential cause of the genotoxin hypersensitive phenotype of the *parg1-1* and *parg1-2* is explored through the determination of PAR-levels in the T-DNA insertion lines, the activity and subcellular localisation of the AtPARG1 and AtPARG2 proteins, as well as identification of any AtPARG1-specific interactors.

4 Biochemical Analysis of AtPARGs

4.1 Introduction

It has been demonstrated that poly(ADP-ribose) levels increase in response to DNA damage, but the level of poly(ADP-ribosyl)ation attributed to individual PARPs differs significantly in mammals. In PARP1 deficient mammalian cells, PARP2 alone was only able to generate 5-20% of the amount of polymer produced in wild type cells in response to DNA damaging agents (Amé et al., 1999). In *Arabidopsis*, several studies have shown that AtPARP2 transcript is more upregulated than AtPARP1 transcript as a response to DNA damage caused by γ-irradiation (Doucet-Chabeaud *et al.*, 2001; Culligan *et al.*, 2006). In *A. thaliana* suspension cultures exposed to a combination of the genotoxins bleomycin and mitomycin C, AtPARP2 mRNA was upregulated 50-fold, and AtPARP1 mRNA only showed a 5.5-fold increase (Chen *et al.*, 2003). However, none of these papers described a similar upregulation at the protein level, nor do any of them explore any putative post-translational control of activity. Plant lines wherein AtPARP1 and AtPARP2 were knocked-down individually through the use of dsRNA constructs did not show significant difference in PAR content to control lines or each other when grown in low light. However, both RNAi lines did not display a similar increase in PAR content upon exposure to high light as was observed in the control plants (DeBlock *et al.*, 2005). As described previously, this study does not state the level of decrease achieved neither at the transcript nor protein level, but only shows an overall reduction in PAR polymer build-up (DeBlock *et al.*, 2005), and therefore the PAR production in response to abiotic stress can not be attributed to either AtPARP.

While the research on activity of the mammalian PARG has been impaired somewhat by the difficulty in purification of the full-length PARG protein isoform (Haketeyama *et al.*, 1986; Lin *et al.*, 1997), a study by Patel *et al.* (2005) identified residues vital for glycohydrolase activity by analysing a truncated version of the protein containing the C-terminal catalytic region. (figure 4.1B). This region displays high homology across several organisms, despite their very different N-terminal regions (figure 4.1A). In addition to the acidic residues described in the study above, Panda *et al.* (2002) showed that a

single residue mutation in AtPARG1, denoted *tej*, which contains the amino acid substitution of the conserved glycine at position 262 to a glutamate (G262E), resulted in a 20-fold higher PAR content in the mutant, indicating a slower turnover of the polymer. As described in the previous chapter a hypersensitive phenotype in response to genotoxic stress was found only in T-DNA insertion lines of AtPARG1, but not AtPARG2, which indicates that these proteins may have different levels of activity or different roles in plants in spite of their high level of similarity at the amino acid sequence level (66.9%). So far there have been no studies investigating the differences of AtPARGs at a molecular level.

This chapter initially investigates the production of PAR in T-DNA insertion lines. The difference in *in vitro* glycohydrolase activity of the two AtPARGs and their subcellular localisation as well as investigating the role of AtPARG1 through identification of potential interactors *in vitro* as well as *in vivo*.

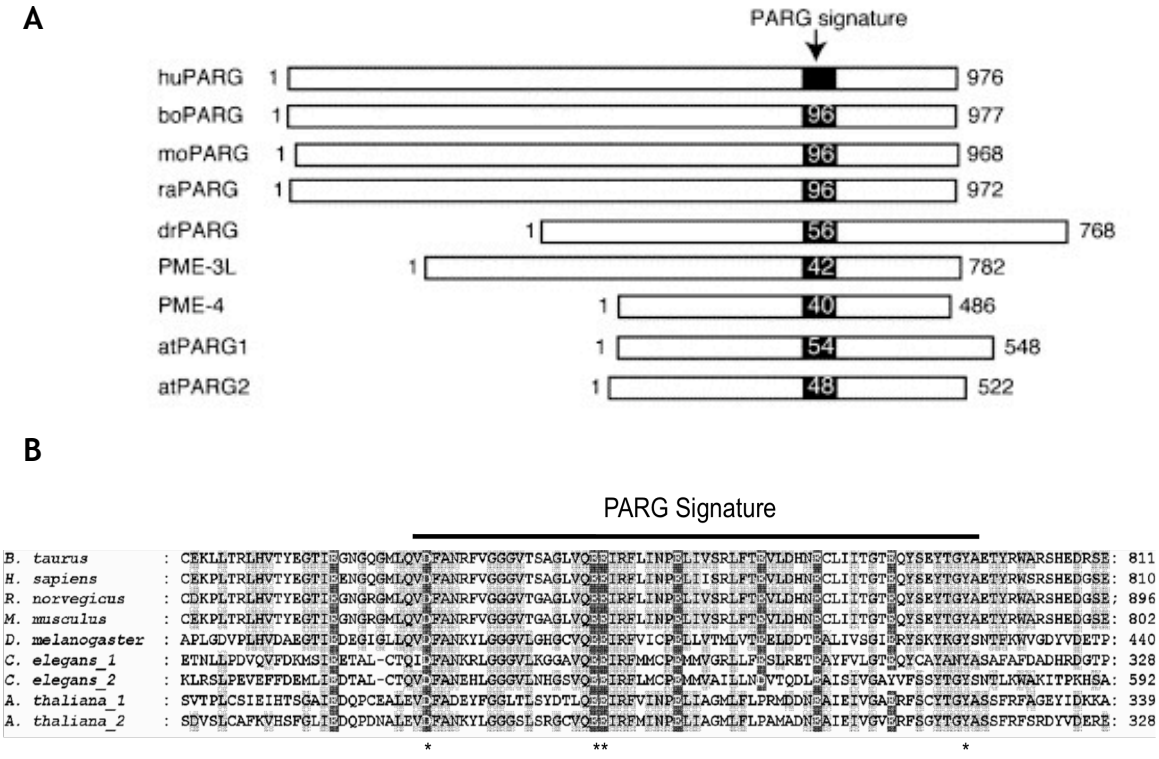

Figure 4.1. Amount of conservation in PARG structure across species
A) Differences in length of N-terminal regulatory domains of PARGs from different organisms. The percentage amino acid identity to the human PARG signature indicated in the black box. Figure taken from (St-Laurent *et al.*, 2007).
B) Alignment of the PARG signatures with residues identical to the human PARG highlighted in black, residues similar to human PARG highlighted in grey, and non-conserved residues in white. Asterisks indicate residues found to be important for activity through mutagenesis in bovine and nematode PARGs. Figure taken from (Patel *et al.*, 2005).

4.2 Results

4.2.1 Determination of poly(ADP-ribose) content of T-DNA insertion lines

In the previous chapter, AtPARG1 deficient lines were seen to be hypersensitive to DNA damaging agents. To find out whether the phenotype seen in the AtPARG1 T-DNA insertion lines is directly related to the amount of polymer present in the plants, a polyclonal antibody for the detection of the PAR polymer was obtained, which has previously been used on plants (DeBlock *et al.*, 2005; Adams-Phillips *et al.*, 2010). Seedlings were grown for 14 days in ½ MSMO + sucrose in constant light (section 2.2.4). Control samples were harvested before fresh media containing the alkylating agent MMS (1.18 mM) and the radiomimetic bleomycin (0.5 μg/ml) were used to induce poly(ADP-ribosyl)ation in seedlings over a time course with samples harvested at 4 and 8 hours exposure. The PAR levels of the total protein extracts from the seedlings were then examined by western blot and analysed using Image J.

PAR levels at time 0 were lower in *parp1-1* than wild type and *parp2-1*, indicating that AtPARP1 may actually be the more active of the two AtPARPs when no DNA damaging agent is present (figure 4.2A and B). The PAR levels in the *parp2-1* mutant remained virtually constant after exposure to both MMS and bleomycin, while those in *parp1-1* were lower than wild type initially, but increased after 4 and 8 hours, indicating that the majority of the polymer produced in response to DNA damaging stress is from AtPARP2 (figure 4.2A and B).

The PAR levels in *parg1-2* protein extracts showed the same pattern as wild type after exposure to bleomycin, while after MMS exposure they did not show the same increase after 8 hours. While *parg2-1* PAR levels were overall lower than wild type in response to bleomycin, they did not show any increase over time (figure 4.2B). In response to MMS, the PAR levels in *parg2-1* were opposite to those observed in wild type (figure 4.2A).

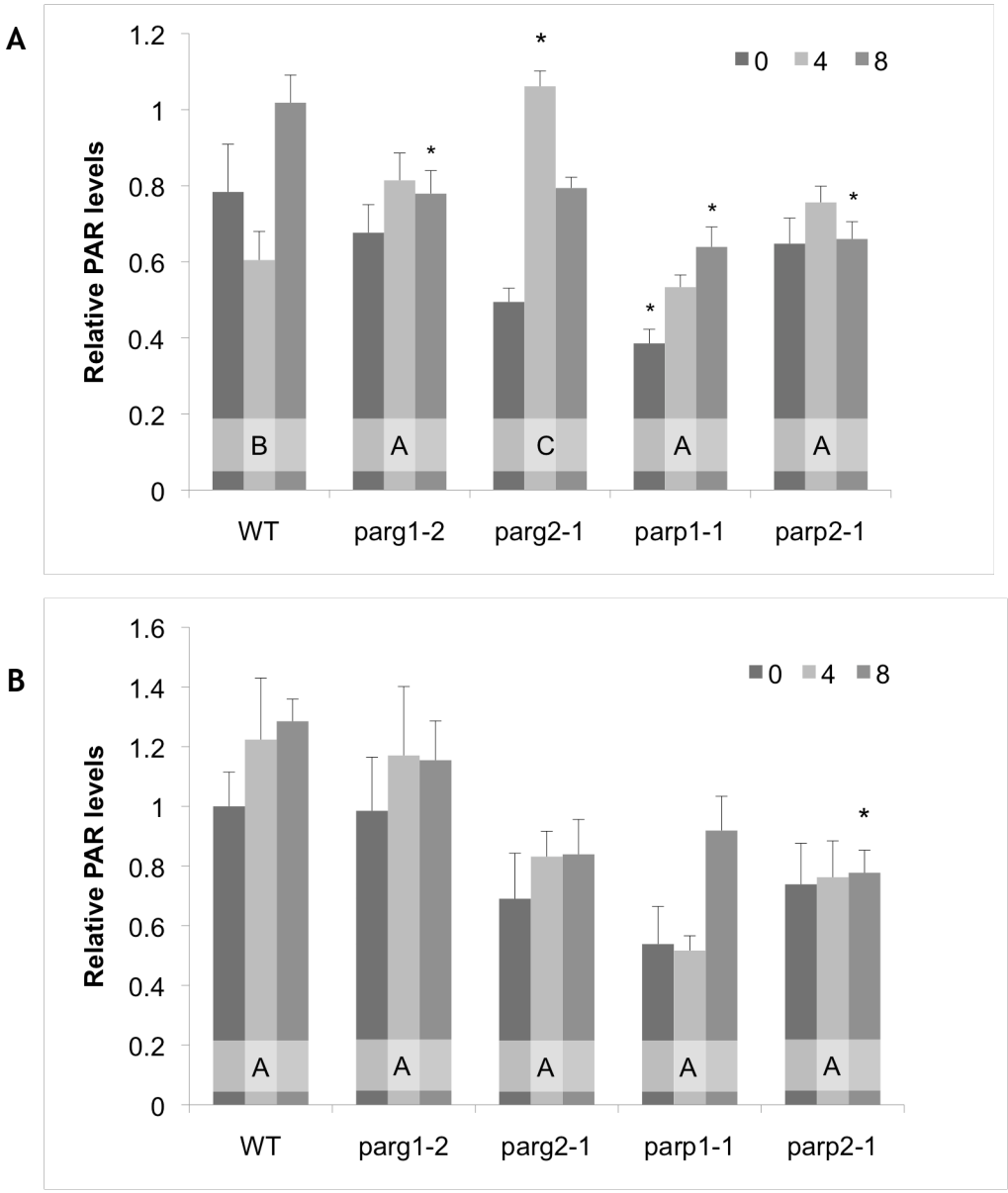

Figure 4.2. PAR levels after exposure to DNA damaging agents
A) Exposure to MMS. Levels of poly(ADP-ribose) in whole seedling protein extract after 0, 4, and 8 hours exposure to 1.18 mM MMS were measured by dot-blot analysis. Nitrocellulose membranes were dotted with 1 μg of protein from each of the genotypes at a given time of exposure and probed using anti-PAR antibodies. All values were normalised to the average WT time 0 value. Bars represent standard error.
B) Exposure to bleomycin. Levels of poly(ADP-ribose) in whole seedling protein extract after 0, 4, and 8 hours of exposure to 0.5 μg/ml bleomycin were measured by dot-blot analysis. Nitrocellulose membranes were dotted with 1 μg of protein from each of the genotypes at a given time of exposure and probed using anti-PAR antibodies. All values were normalised to the average WT time 0 value. Bars represent standard error.
Image J software was used for densitometry measurements. Asterisks show significant differences (ANOVA) between lines at each timepoint (0, 4, and 8 hours; $p < 0.05$, Tukey's test). Different letter codes indicate significant differences in the Line by Time interaction ($p < 0.05$; Tukey's test). See appendix A2.16 for tables.

4.2.2 AtPARP1 does not interact with AtXRCC1 *in vitro*

PARP1 has been shown to interact with the BER scaffold protein XRCC1 in mammals, and the domain identified by deletion analysis to be required for the interaction was show to be one of the two breast cancer 1 protein (BRCA1) C-terminus (BRCT) motifs (Masson *et al.*, 1998). *Arabidopsis* contains a homologue of this gene, and although AtXRCC1 only contains one BRCT motif (Taylor *et al.*, 2002), as opposed to the two found in mammalian XRCC1 (Bork *et al.*, 1997), it is the one shown to be required for interaction. The domain shows 53.8% sequence identity to the mammalian homologue (Taylor *et al.*, 2002). Yeast two-hybrid experiments using a GAL4 based system (figure 4.3A) were performed to see whether AtPARP1 interacts with AtXRCC1. Previously problems have been encountered with toxicity when expressing PARP1 in yeast (Kaiser *et al.*, 1992), although this was removed by addition of the PARP inhibitor 3-AB in the medium or by using proteins carrying catalytically inactivating mutations (Kaiser *et al.*, 1992; Masson *et al.*, 1998; Storozhenko *et al.*, 2001).

The full-length AtPARP1 and AtXRCC1 cDNAs were cloned into the Gateway entry vector pENTR-D-TOPO followed by introduction into the Gateway adapted Clontech yeast-two-hybrid bait vectors pGADT7-dest and pGBKT7-dest (C. Grefen, unpublished), respectively, through the LR recombination reaction. In addition a site directed mutant of AtPARP1 glutamic acid residue E960A was cloned as above to try and avoid the potential toxicity of PARPs in yeast as observed in the studies mentioned previously. This mutation was previously shown to abolish activity in human PARP1 by reduction in polymer formation more than 2000-fold (Marsischky *et al.*, 1995). Vectors containing the AtXRCC1 BD-fusion proteins were co-transformed into the yeast strain Pj69-4α with the empty pGADT7 vector. Yeast cell growth was seen on non-selective media (-L, -W) to confirm successful transformation. No growth was observed on selective media (-L, -W, -A, -H), demonstrating that the BD-fusion does not autoactivate the GAL4 system (figure 4.3B). As a positive control the p53-BD and SV40 T antigen-AD (Clontech) were used.

When testing for interactions using N-terminal fusion constructs, there was no interaction observed between N-terminally fused AtPARP1 and AtXRCC1 or between N-terminally fused AtPARP2 and XRCC1 (figure 4.3B). The interaction

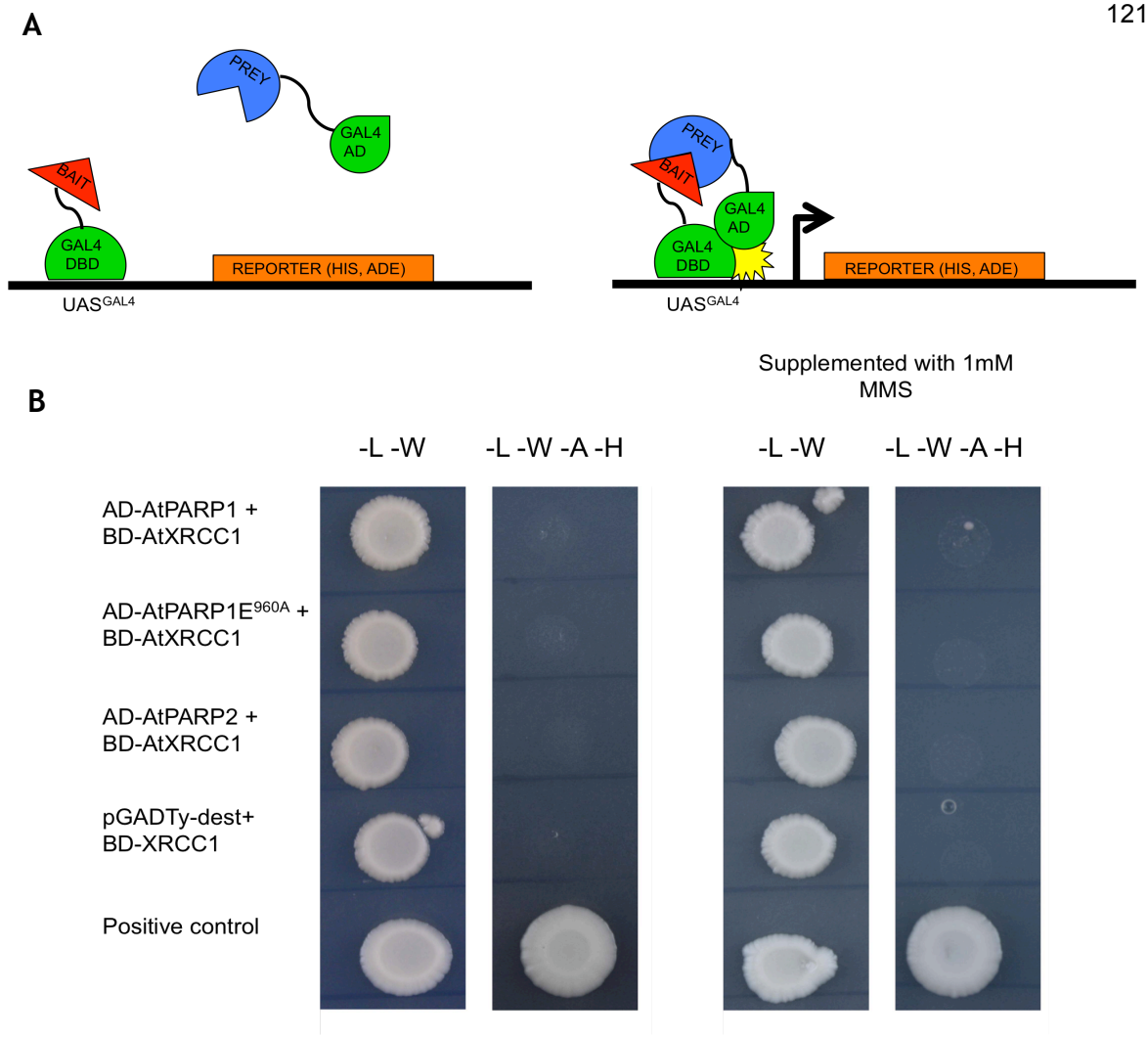

Figure 4.3. AtPARPs do not interact with AtXRCC1 *in vitro*
A) The principles of the GAL4 yeast two-hybrid system. A bait protein is fused to the DNA binding domain (DBD) of the GAL4 transcription factor. Any suspected interacting proteins (prey) are fused to the activation domain (AD) and co-transformed into yeast with several auxotrophic mutations. If the prey and bait interact, the two parts of the GAL4 transcription factor are close enough to activate transcription of a reporter protein.
B) Full length AtPARP1, AtPARP1^{E906A}, and AtPARP2 were expressed as activation domain (AD) and full length AtXRCC1 as DNA-binding domain (BD) N-terminal fusion proteins. The AD and BD fusions were provided by pGADT7-dest and pGBKT7-dest, respectively. Transformed PJ69-4α cells were grown on non-selective media (-L, -W) to check the transformation efficiency, and on selective media (-L, -W, -A, -H) to test for interaction (left hand panels). The cells were also grown on the same media containing 1 mM MMS (right hand panels).

was also tested on media supplemented with 1 mM MMS to see if an interaction could be induced by the presence of a DNA damaging agent. Weak interaction could be seen between AtPARP1 and AtXRCC1, but no growth was observed with any of the other construct combinations (figure 4.3B).

4.2.3 *In vitro* expression of AtPARGs

While human PARP1 is commercially available, it has been hard to express and purify full length PARG protein due to its low abundance in the cell. Only rat, bovine, and recently human versions of the catalytic region of the PARG protein, which is slightly longer than the 60 KDa isofom, have been purified to a high degree (Lin *et al.*, 1997; Shimokawa *et al.*, 1999; Okita *et al.*, 2011). So far there has been no work on the activity of AtPARGs. The following sections describe how we were able to express the full-length AtPARGs *in vitro* in order to determine whether they have glycohydrolase activity.

4.2.3.1 Generation of histidine tagged AtPARG1 protein for *E. coli* based expression

Full length AtPARG1 and AtPARG2 were PCR amplified from *A. thaliana* cDNA using Gateway compatible primers and cloned into the Gateway entry vector pENTR-D-TOPO. Full-length cDNA from the entry vector was transferred into the pDEST17 destination vector (figure 4.4A) by Gateway LR based recombination to generate bacterially expressed N-terminal histidine tagged AtPARG1 and AtPARG2. N-terminal tagging was chosen, as a paper described the loss of activity of bovine PARG[103], when a GFP tag was fused to the C-terminal (Haince *et al.*, 2006).

4.2.3.2 Expression of AtPARG proteins in *E. coli*

Both the His-AtPARG1 and His-AtPARG2 constructs were transformed into *E. coli* Rosetta-Gami 2 pLysS cells and protein expression was induced using IPTG. This strain is designed for optimisation of expression of eukaryotic proteins. It combines features from the BL21 derivative Rosetta 2, which supplies the tRNAs for seven codons rarely used in E. coli, and Origami 2, carrying two mutations (trxB/gor) that allow disulphide bond formation in the bacterial cytoplasm.

Expression trials at 37°C with increasing concentrations of IPTG (figure 4.4B) resulted in the proteins being in the insoluble fraction. Lowering temperature during expression slows the rate of protein synthesis, possibly keeping recombinant proteins from saturating cellular folding machinery and aggregating, and therefore might exclude them from being in inclusion bodies. Expression was therefore performed at 20°C for 16 hours. However, His-AtPARG2 was still in the insoluble fraction, while expression of His-AtPARG1 could no longer be detected (figure 4.4C). Purification using both a native and a hybrid protocol were attempted on cultures grown at 20°C and 37°C respectively, but none of these resulted in any detectable protein of the right size in the elutes (data not shown).

4.2.3.3 Generation of Histidine tagged AtPARG proteins for *S. frugiperda* based expression

Due to the potential limitations of *E.coli* based expression such as codon bias and lack of eukaryotic post-translational modifications, the Baculovirus insect cell expression system was used. To investigate any differences between AtPARGs in glycohydrolase activity, histidine tagged fusion proteins corresponding to the two AtPARGs as well as site-specific mutants of residues found to be important for activity in the mammalian PARG were generated.

Full length AtPARG1 and AtPARG2 were PCR amplified from *A.thaliana* cDNA using primers containing restriction sites (NcoI and PstI) and cloned into pCRtopo 4.0 (Invitrogen). The genes were then subcloned into the pACHLTA baculovirus transfer vector (BD Biosciences) (figure 4.5A) using ligation to generate N-terminal His-tagged AtPARG fusion proteins under the control of the strong polyhedrin promoter, which is expressed during the very late phase of viral infection. These constructs were used to generate recombinant Baculovius encoding AtPARGs using the BaculoGold transfection kit (BD biosciences), which were used to infect *Spodoptera frugiperda* (Sf9) insect cells for protein expression. Crude cell lysates were analysed by SDS-PAGE and western blot to confirm expression of the recombinant proteins.

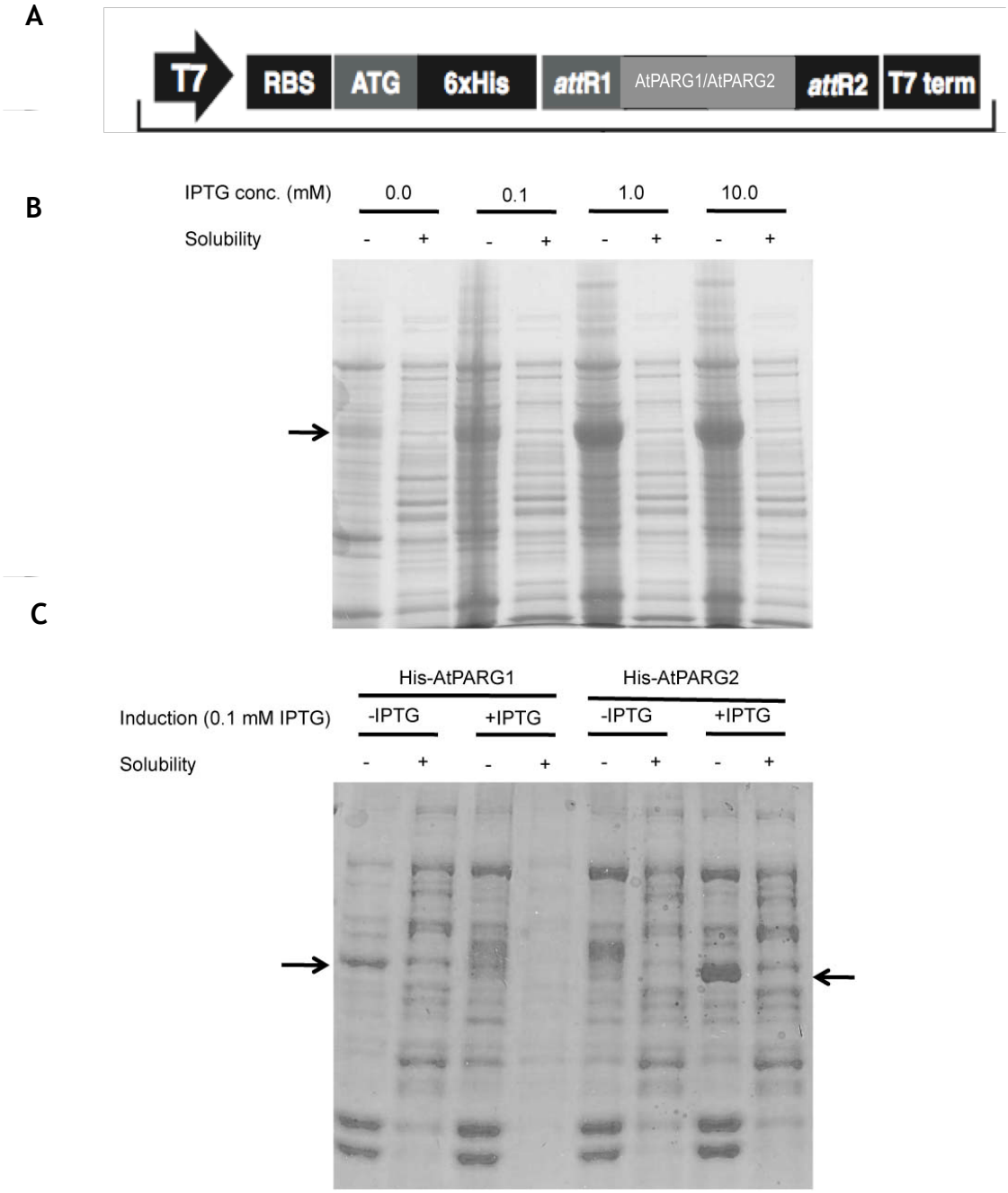

Figure 4.4 Expression of AtPARG-1 in *E.coli*
A) Schematic representation of the pDest17 vector carrying AtPARG1 or AtPARG2.
B) Coomassie stained SDS-PAGE gel showing IPTG-induced expression of the His-AtPARG1 protein in *E. coli* Rosetta-Gami Bl21 cells grown at 37°C. Lanes are alternately insoluble (-) and soluble (+) fractions, and the IPTG concentration is increasing towards the right as indicated. The arrow indicates the expected size of His-AtPARG1 (62 KDa).
C) Coomassie stained SDS-PAGE gel showing IPTG-induced expression of the His-AtPARG2, but not His-AtPARG1 protein in *E. coli* Rosetta-Gami Bl21. Cells were induced with 0.1 mM IPTG and grown at 20°C for 16 hours. Lanes are alternately insoluble (-) and soluble (+) fractions. Arrows on the left and right side indicate the expected sizes of His-AtPARG1 (62 KDa) and His-AtPARG2 (60 KDa), respectively.

4.2.3.4 Purification of recombinant AtPARGs.

Purification of the recombinant His-AtPARGS was tried using a 6xHis Purification Kit (BD Biosciences), but this did not result in high enough amounts of pure protein as a high proportion of the recombinant protein was eluted in the flow through (figure 4.5B). Despite making adjustments to the imidazole concentration in the wash and elution buffers, too much contaminating protein was present in the final elutes (figure 4.5C). The majority of all the recombinant PARGs expressed in insect cells were found to be insoluble (data not shown), but enough recombinant protein was detected through western blot in the soluble fraction to be able to perform the *in vitro* glycohydrolase activity assay (Trevigen). Initial trials showed that the activity generated in lysates containing recombinant proteins, was significantly different to the native background activity of uninfected lysates. Therefore the activity assays were performed using the crude soluble *Sf9* cell lysate, with untransfected *Sf9* cell lysate as a control to account for any native *Sf9* insect cell PARG activity.

4.2.3.5 Generation of AtPARG site directed mutants

Site directed mutagenesis of the three acidic residues Asp^{738}, Glu^{756}, and Glu^{757} into asparagine lowered bovine PARG activity to below a detectable level (Patel *et al.*, 2005). All these acidic residues are conserved in both AtPARGs (figure 4.1). Site directed mutations were introduced to change all three acidic residues, identified as critical for activity, in AtPARG1, D^{255}, E^{273}, and E^{274}, to asparagine. Among the residues conserved in the PARG catalytic region in all organisms, AtPARG2 is the only one, which does not have the third glycine in a triplet, but instead contains a leucine (figure 4.1). This residue L^{275} was changed into a glycine to examine the effect of this mutation on the activity of ATPARG2. Site directed mutagenesis was performed using primers listed in table 2.11, and after verification through sequencing, the constructs were used to generate recombinant Baculovius encoding AtPARGs using the BaculoGold transfection kit (BD biosciences) for protein expression. Crude cell lysates were analysed by SDS-PAGE and western blot to confirm expression of the recombinant proteins (data not shown). The E273N mutant protein did not express at levels comparable to any of the other recombinant proteins (data not shown), and therefore was not included in the glycohydrolase activity assay.

A

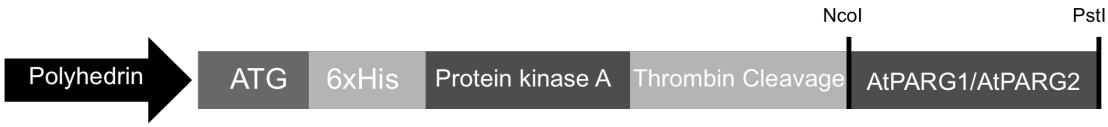

B

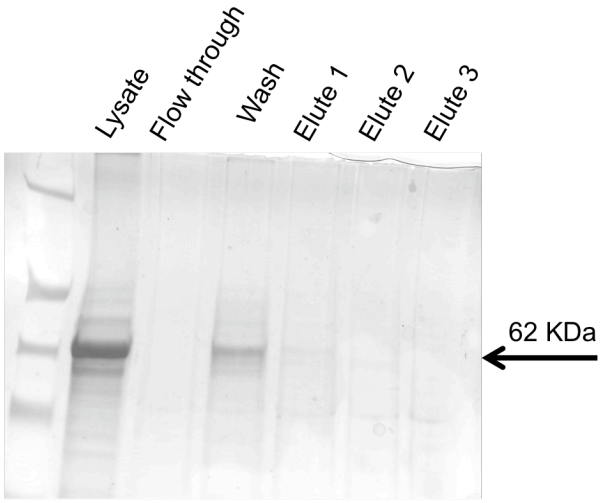

C

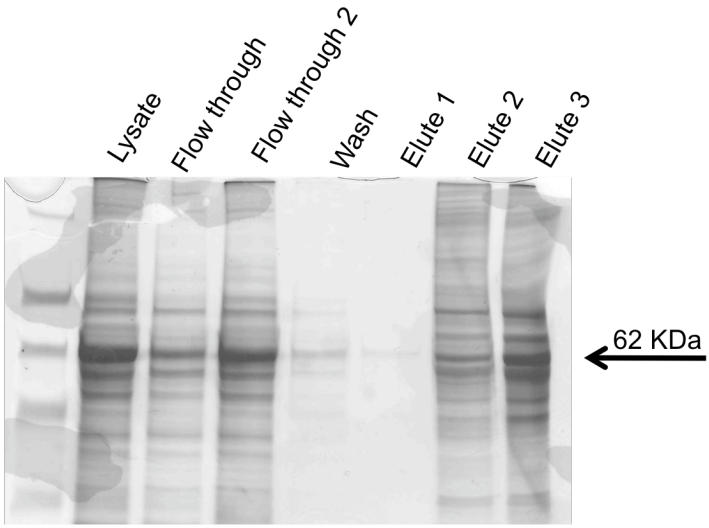

Figure 4.5 Purification of AtPARGs expressed in *Sf9* cells
A) Schematic representation of the pAcHLTA vector carrying AtPARG1 or AtPARG2.
B) Coomassie stain of fractions from protein purification of AtPARG1 using nickel resin. 16 μl of each fraction was loaded onto the gel. Fraction contents are indicated above the lanes. Half of the washes contained 20 mM imidazole and the other half none. Proteins were eluted using 0.3, 0.4, and 0,5 M imidazole, respectively.
C) Coomassie stain of fractions from protein purification of AtPARG1 using nickel resin. 16 μl of each fraction was loaded onto the gel. Fraction contents are indicated above the lanes No imidazole was used in the wash buffer. Proteins were eluted using 0.3 M imidazole.

4.2.4 Glycohydrolase activity assay

To assay the glycohydrolase activity of the AtPARGs, an ELISA-like plate assay was used (Trevigen). Briefly a 96 well plate has histones immobilised at the bottom of the well. Recombinant human PARP along with activated DNA is then incubated in the wells which, using biotinylated NAD as a substrate, attaches PAR polymers to the histones. *Sf9* lysate containing recombinant AtPARG1, AtPARG2 and mutants, along with positive control recombinant bovine PARG catalytic domain, and untransfected *Sf9* lysate used as a negative control and to monitor any native activity, were added to the wells. Finally the amount of PAR polymer remaining attached to the histones is measured by the absorbance at 450 nm.

Expression of the different recombinant proteins was optimised to a similar expression level by varying the amount of recombinant Baculovirus used for infection of *Sf9* cells prior to the activity assay by comparison of signal intensity in α-His western blots. A negative control of native *Sf9* lysate was included in the western blot to show that there was no contaminating signal present in the native *Sf9* lysate (figure 4.6A).

Recombinant His-AtPARGs displayed glycohydrolase activity when expressed through the Baculovirus system. The level of activity measured in protein extracts containing active recombinant proteins was significantly different to the activity measured in protein extracts from cells not transfected, but treated the same way. AtPARG1 had significantly higher glycohydrolase activity (20%) than AtPARG2, even with ten-fold the amount of lysate (figure 4.6B). The mutant proteins E274N, and TEJ (G262E) both showed significantly lower activity compared with the wild type AtPARG1 level, making them only slightly higher in activity than the native lysate (figure 4.6C). The D255N mutant protein displayed an activity comparable with the wild type AtPARG1 protein, thus indicating that this residue is not as important for activity in the plant PARG as was seen in mammals (Patel *et al.*, 2005) (figure 4.6C). The AtPARG2 mutant protein L275G showed levels of activity comparable to that of the native lysate for the same amount (figure 4.6D).

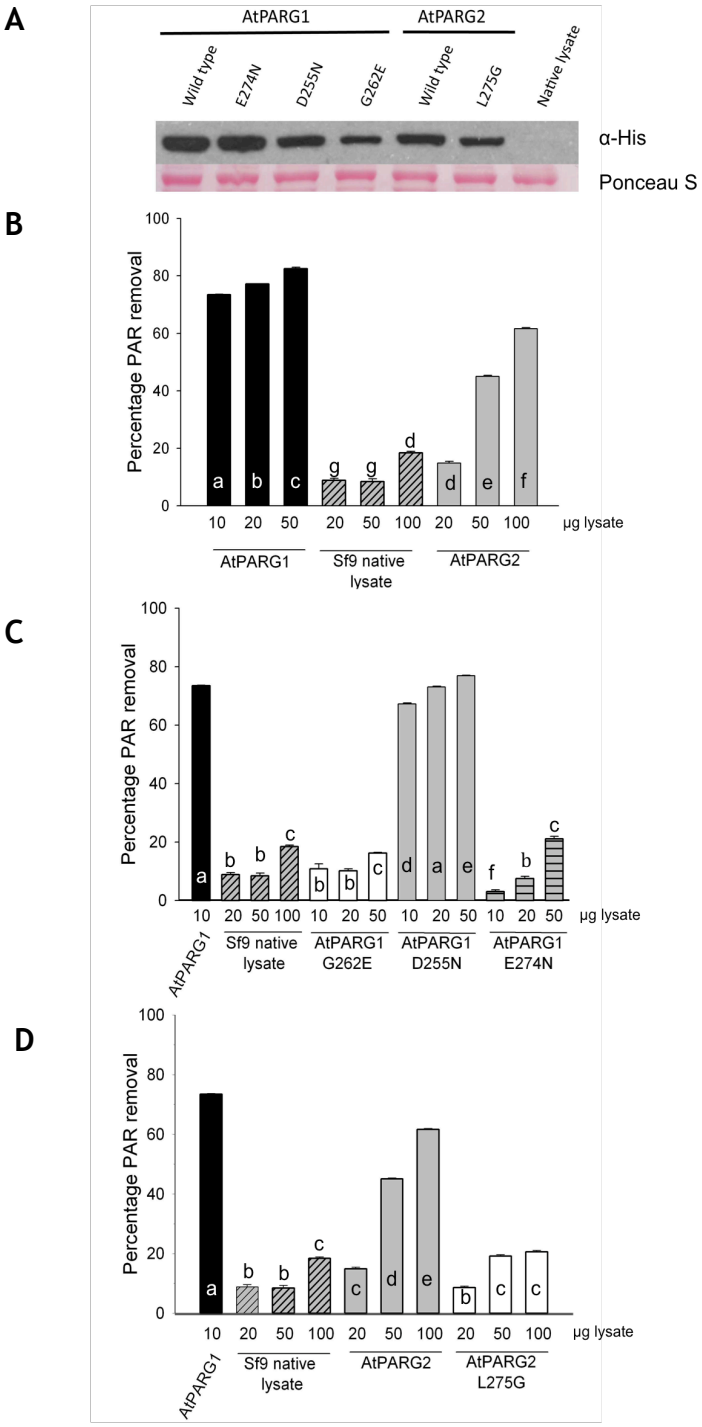

Figure 4.6. Glycohydrolase activity of AtPARGs

A) Western blot showing expression levels of the recombinant constructs in *Sf9* cell lysate. Ponceau S staining to show equal loading.

B) Glycohydrolase activity of AtPARG1 and AtPARG2 measured in *in vitro* assays. Numbers under each bar on the horizontal axis represents the amount of lysate used in μg in wells. All wells were in triplicate and values measured three times on plate reader. Bars represent standard error.

C) Glycohydrolase activity of AtPARG1, and mutant proteins G262E, D255N, and E274N measured in *in vitro* assays. Numbers under each bar on the horizontal axis represents the amount of lysate used in μg in wells. All wells were in triplicate and values measured three times on plate reader. Bars represent standard error.

D) Glycohydrolase activity of AtPARG1, AtPARG2 and AtPARG2 L275G measured in *in vitro* assays. Numbers under each bar on the horizontal axis represents the amount of lysate used in μg in wells. All wells were in triplicate and values measured three times on plate reader. Bars represent standard error.

Different letter codes indicate significant differences using ANOVA ($p < 0.05$, Tukey's test). See appendix A2.17 for table.

4.2.5 Analysis of AtPARG subcellular localisation by confocal microscopy

Human PARG has several isoforms with different subcellular localisations, each of which have different lengths (Meyer-Ficca *et al.*, 2004; Meyer *et al.*, 2007). A nuclear localisation signal (NLS), a nuclear export signal (NES) and a mitochondrial localisation signal (MTS) (Botta and Jacobson, 2010) have been identified in the N-terminal part of the mammalian gene, while the C-terminal also contains an NLS and an NES. Several of the PARG isoforms have been shown to re-localise upon DNA damage; the $PARG^{110}$ isoform moves from the nucleus to the cytoplasm and vice versa for $PARG^{103}$ isoform (Haince *et al.*, 2006). The $PARG^{110}$ and $PARG^{103}$ isoforms have also been found to be associated with the membrane rich fraction after ultracentrifugation and western blots (Bonicalzi *et al.*, 2003) using an antibody for a peptide in the C-terminal domain of PARG (Winstall *et al.*, 1999). GFP-tagged $PARG^{103}$ displayed perinuclear distribution and was found to co-localize with a Golgi marker (Bonicalzi *et al.*, 2003).

The AtPARGs are shorter than mammalian versions of the gene and do not contain the N-terminal regulatory domain. *In silico* analysis was performed on the AtPARG protein amino acid sequences using the predictive localisation programs NLSPredict and LOCtree (http://www.predictprotein.org/) as well as TargetP (http://www.cbs.dtu.dk/services/TargetP/) and found no known NLS, nor any significant likelihood of either protein being targeted to a subcellular compartment based on known motifs.

4.2.5.1 Transient expression of GFP-tagged AtPARGS in *N. benthamiana*

To determine the localisation of AtPARGs *in planta*, *Agrobacterium*-mediated transient transformation of *N. benthamiana* epidermal cells was employed (Sparkes *et al.*, 2006). Full-length AtPARG cDNAs were cloned into the Gateway® compatible plant binary vector pH7WGF2 and pH7FWG2 (Karimi *et al.*, 2007) which add an N-terminally and C-terminally fused GFP molecule to the protein, respectively, under the control of the constitutive cauliflower mosaic virus (CaMV) 35S promoter. The localisation of the GFP signal was analysed by transient expression in *N. benthamiana*.

Confocal microscopy showed that GFP-AtPARG1 was distributed throughout the cytoplasm as well as in the nucleus, while no signal was seen in the nucleolus (figure 4.7A). The same pattern of distribution was seen with the C-terminal fusion construct AtPARG-GFP (figure 4. 7B). Both N- and C-terminal tagged AtPARG2 GFP fusions also localise to the cytoplasm and nucleus (figure 4.7C and D). Both fusion proteins also showed nucleolar exclusion (figure 4.7). Cells transformed with a vector expressing only 35S:GFP showed a similar GFP signal distribution signal in nucleus and cytoplasm (figure 4.7E).

4.2.5.2 Stable expression of AtPARG1 in *A. thaliana*

Stably transformed *Arabidopsis* lines were made using the floral dip method (Clough and Bent, 1998), by cloning of the full-length AtPARG1 cDNA into the Gateway® compatible binary vector pGWB6 (Nakagawa *et al.*, 2007) to generate an N-terminal GFP fusion protein under the control of the CaMV 35S promoter. T3 seedlings were selected on antibiotics, and expression of the GFP fusion protein was examined using confocal microscopy. Nuclear and cytoplasmic localisation of 35S:GFP:AtPARG1 was observed although with a weak signal (figure 4.8A). To examine whether the presence of GFP signal in the nucleus was due to diffusion of the recombinant protein through the nuclear pores, fluorescence resonance after photobleaching (FRAP) was employed. In FRAP experiments, nuclei were exposed to laser intensities that photobleached the fluorophores. Cells were then imaged over time and the fluorescent signals in the bleached area and a background control area were recorded. As a separate control, plants stably transformed with the 35S:GFP were also examined. These control plants showed a significant signal recovery after nuclear bleaching (figure 4.8B). When the stable 35S:GFP:AtPARG1 plants were analysed, the GFP signal did not recover in the nucleus after bleaching (figure 4.8B). In addition, the mobile fraction signal, that contributed to fluorescence recovery, as well as the immobile fraction were determined for GFP-AtPARG1 and GFP. The mobile fraction for GFP-AtPARG1 (65%) was considerably lower than that of GFP (84%). The indicates that the presence of nuclear GFP:AtPARG1 signal is not simply down to diffusion. Moreover, analysis of the amino acid sequence of both AtPARGs, revealed a stretch of basic residues $^{333/344}$K/R-R-R-R/K-T-R$^{338/349}$ (figure 4.9), which showed similarity to the monopartite NLS identified in mammalian PARG (Shimokawa *et al.*, 1999; Haince *et al.*, 2006) and fits well with the

propsed consensus sequence for monopartite nuclear localisation signals (K/R-R-X-K/R) (Hodel *et al.*, 2001).

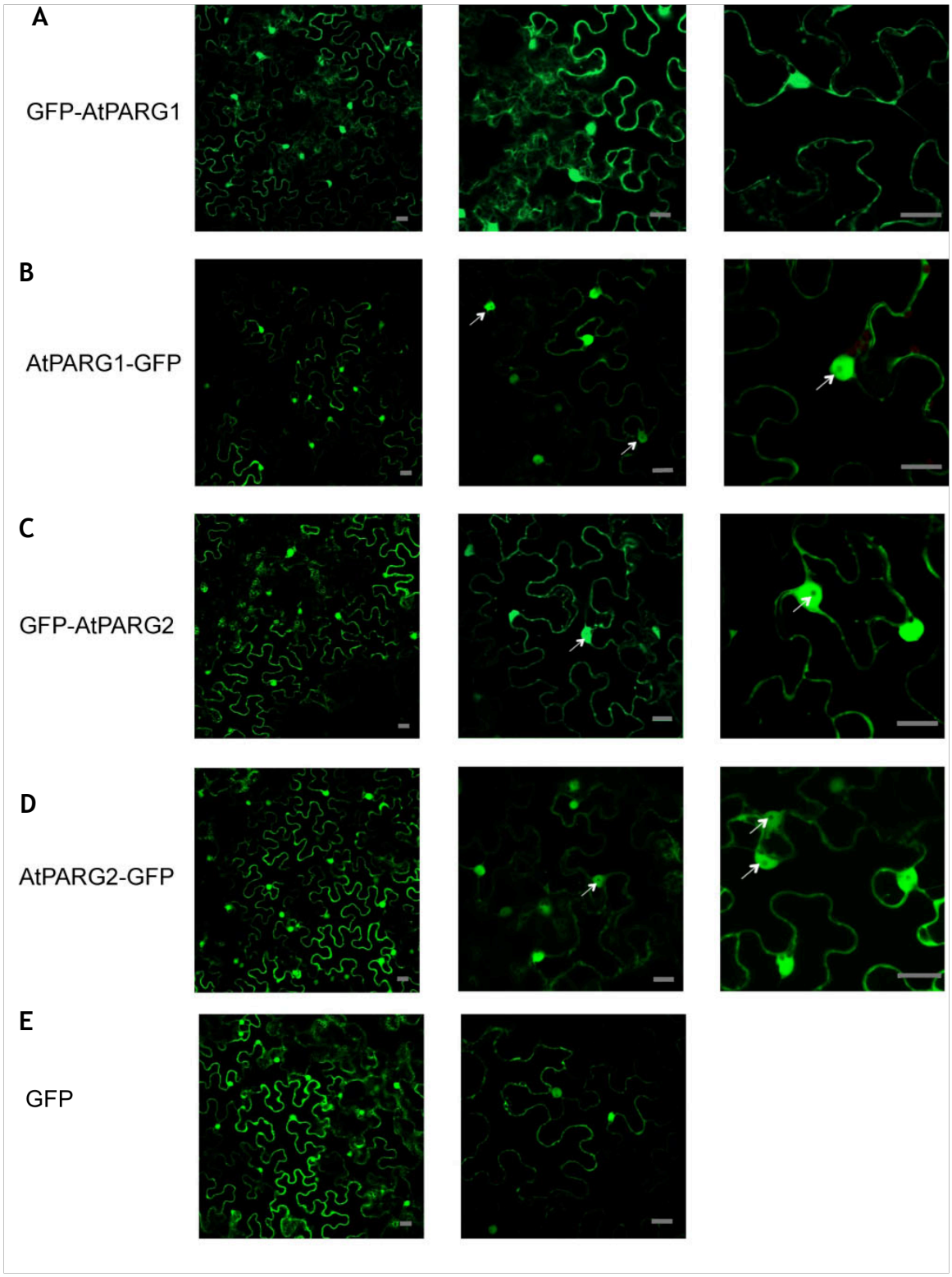

Figure 4.7. Subcellular localisation of AtPARG1
Confocal images of transient expression of AtPARG1 and AtPARG2 tagged N (A and C)-or C (B and D)-terminally with GFP under the control of CaMV 35S in *N. benthamiana* epidermal cells 3 days post infiltration. Confocal images of 35S-GFP are presented in the (E) for comparison. White arrows show nucleolar exclusion. Scale bars represent 20 μm.

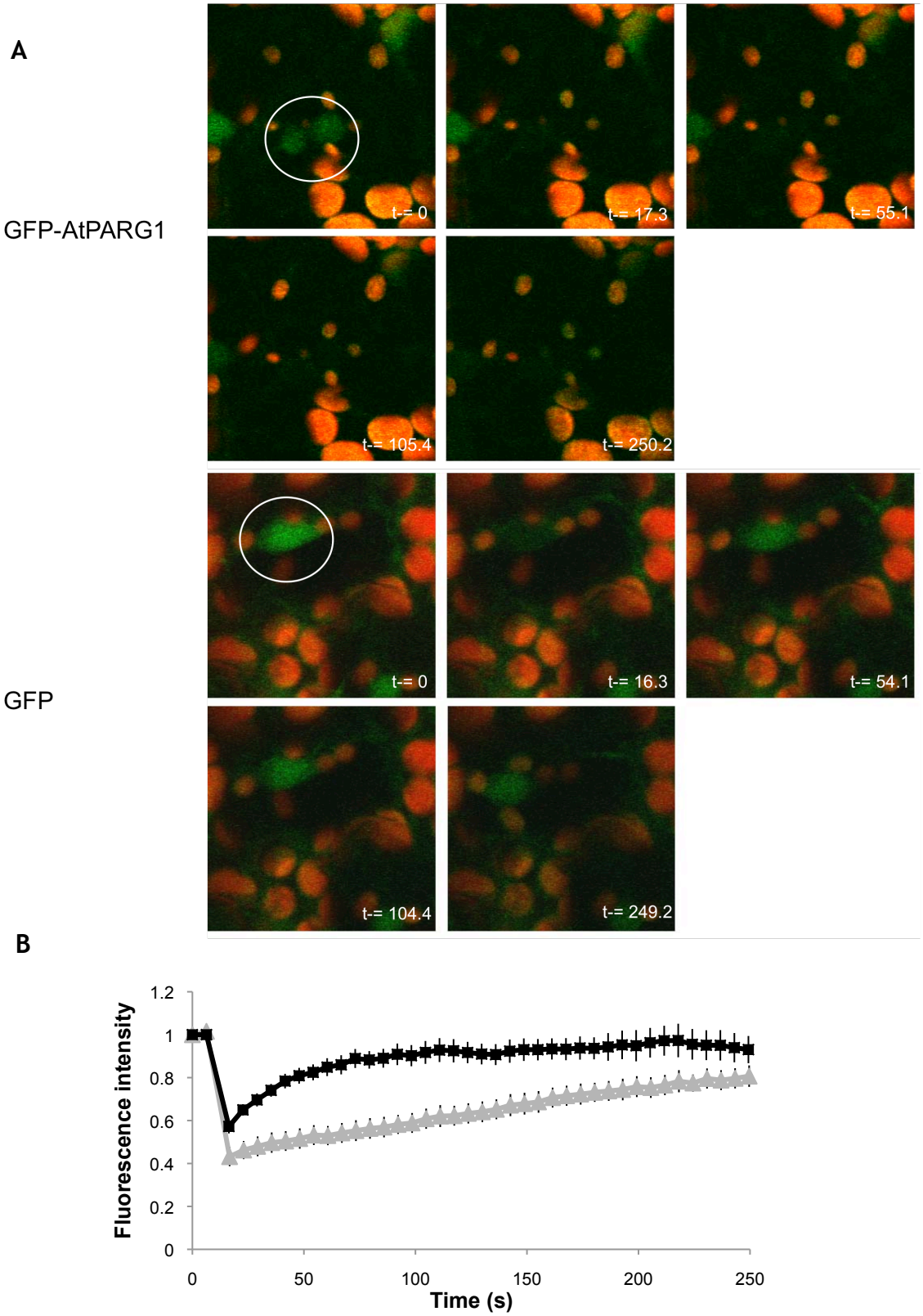

Figure 4.8.. FRAP analysis
A) FRAP analysis of nuclei in stable *Arabidopsis* lines of GFP-AtPARG1 (top) or GFP (bottom). A region of interest (ROI) in a nucleus was defined (indicated by the white circle) before FRAP experiments commenced (0 s) and the fluorescence of the ROI as well as of the background was continuously recorded at intervals.
B) Graph showing the background-corrected relative fluorescence (arbitrary units) of both GFP-ATPARG1 (grey) and GFP (black) plant lines over time during FRAP. Bars represent standard error (n=8).

Figure 4.9. Alignment of *Arabidopsis* PARGs
The alignment was performed using ClustalW2. Underlined in green is the catalytic PARG signature, in yellow the putative mitochondrial targeting sequence, in red the putative nuclear localisation signal. Asterisks indicate conserved residues.

4.2.6 Yeast Two Hybrid Screen for AtPARG1 interactors

To identify any putative interactors of AtPARG1, a LexA/GAL4 based yeast two-hybrid screen using an *Arabidopsis thaliana* cDNA library was carried out by Dualsystems Biotech (Switzerland). The cDNA library was generated using tissue from plants at a wide variety of developmental stages all pooled in equal quantities. For a full description of tissues used for library generation, see table 4.1 below. Full-length AtPARG1 was used as bait and cloned into pLexA-dir, generating a BD-AtPARG1 fusion protein. The *A. thaliana* cDNA library fragments were cloned into pGADT7-RecAB to give AD fusion proteins.

The interactors were categorized according to how many times they appeared in the screen. Class A were found three or more times, B two times and C were found once. These positive prey plasmids were then isolated and amplified in *E. coli*, before being sequenced. All sequencing results were translated using all three reading frames and searched against the Swissprot database using the BLASTX algorithm. A list of Class A and B interactors, their accession number and their predicted function in *Arabidopsis* as described by TAIR (www.arabidopsis.org) is presented in table 4.2 and a full list including the Class C interactors are listed in appendix 1.

A recent comprehensive investigation of the human PARG interactome using affinity purification mass spectrometry found PARG to interact with several heat shock proteins, proteins involved in RNA metabolism, and DNA repair (Isabelle *et al.*, 2010), although some interactors might have been missed out due to the conditions under which the cells were grown (non stressed) and so any interactions requiring the presence of PAR would not be present. Interactors of human PARP1 and human PARP2 were also examined and both, but not PARG, were found to interact with Ku70 DNA helicase 2 subunit (Isabelle *et al.*, 2010), the plant homologue of which was found in the yeast two hybrid screen of AtPARG1 interactors.

Plant developmental stage
Whole seedling samples taken every 4 hours over 24 hour period short and long day conditions
10 day old seedling samples taken every 4 hours over 24 hour period short and long day conditions
Etiolated seedlings grown for 5 days in the dark
Pollen from unfertilized, emasculated pistils
Unopened buds
Flowers (open 1-2 days)
Siliques from all stages (not dry)
Adult leaves from soil grown plants before and after bolting
Stems

Table 4.1. List of mRNA sources used for generating *A. thaliana* cDNA library used in Dual Systems Yeast-Two-Hybrid screen.

Class	Number of "hits"	Gene	Description
A	11	At5g01310	Basic helix-loop-helix protein family (bHLH) Trancription factor
A	10	At5g08530	51 KDa subunit of respiratory chain complex 1 (C151), NADH dehydrogenase
A	5	At1g16970	AtKu70, Involved in DNA repair, response to heat, telomere maintenance
A	4	At3g09840	Cell division cycle protein (AtCDC48), member of AAA-ATPase family
A	3	At1g43130	LCV2 (like Cov2). Involved in stem vascular tissue pattern formation
A	3	At1g01080	Nucleotide binding, RNA binding
B	2	At3g05345	Heat shock protein binding

Table 4.2. List of putative AtPARG1 interactors found in the Dual Systems Yeast-Two-Hybrid screen.
The table lists all interactors found more than once in the yeast-two hybrid screen as well as their TAIR accession number and predicted function (www.arabidopsis.org).

4.2.7 Confirmation of interactions with full-length proteins

Yeast two-hybrid experiments, using a GAL4 based system (figure 4.4A), were repeated to test whether the interactions were specific to the protein region identified in the Dual Systems screen. Cloning of the full-length cDNA from the 4 genes observed most frequently in the screen (Table 4.2) was attempted. However, despite optimisation of PCR, no product of the right size could be obtained for the most frequent interactor At5g01310. Three of the interactors from the screen were amplified from *A. thaliana* cDNA using full length gene specific primers with attB sites attached at their 5' ends and cloned into the Gateway entry vector pDONR207 through the BP recombination reaction, followed by introduction into the Gateway adapted Clontech yeast-two-hybrid bait vector pGBKT7-dest (Grefen, unpublished), through the LR recombination reaction. The resulting destination vectors were co-transformed into the yeast strain Pj69-4α with full-length AtPARG1 in the prey vector pGADT7-dest (Grefen, unpublished). Auto-activation tests were carried out for each BD-fusion protein to test whether they induce expression of the reporter genes in the absence of an interacting partner. Vectors containing the interactor BD-fusion proteins were co-transformed into the yeast strain Pj69-4α with the empty pGADT7 vector. Yeast cell growth was seen in all cases on non-selective media (-L, -W) to confirm successful transformation. No growth was observed on selective media (-L, -W, -A, -H), demonstrating that none of the BD-fusions autoactivate the GAL4 system (figure 4.10C, 4.11C and 4.12C). As a positive control the p53-BD and SV40 T antigen-AD (Clontech) were used.

4.2.7.1 AtPARG1, but not AtPARG2 interacts with At5g08530 *in vitro*

From the sequencing results provided by the Dual Systems screen, the prey sequence for At5g08530 was identified as amino acids 112 to 280 (figure 4.10A). The results of the LacZ assay performed by Dual Systems are shown for each of the positive interactions found in the screen (figure 4.10B). Full-length At5g08530 was cloned into the bait vector pGBKT7-dest as described above and tested in the yeast-two-hybrid system to confirm the interaction of the full-length protein with AtPARG1 (figure 4.10C). As yeast two hybrid vectors allowing C-terminal tagging with the activation and binding domains became available,

interactions were tested in four permutations (NN, NC, CC, CN) as this has been shown to reduce the number of false negatives (Stellberger *et al*., 2010).

Since the full-length At5g08530 interacted with AtPARG1, the bait vector was also tested to see whether it would interact with the close relative AtPARG2. Full-length AtPARG2 was cloned into the prey vector pGADT7-dest and this was co-transformed with BD-At5g08530 into the yeast strain. No interaction was observed between AD-AtPARG2 and BD-At5g08530, thus showing that interaction was specific to AtPARG1 (figure 4.10C). Unfortunately, upon examination of yeast protein extracts, it was found that no expression of C-terminally fused At5g08530 could be detected in western blots (data not shown), which would explain why no interactions could be seen in co-transformations with this construct.

4.2.7.2 AtPARG1, but not AtPARG2 interacts with At3g09840 *in vitro*

From the sequencing results provided by the Dual Systems screen, the prey sequence for At3g09840 was identified as amino acids 1-126 (figure 4.11A). Full-length At3g09840 was cloned into the bait vector pGBKT7-dest as described above and tested in the yeast two-hybrid system to confirm the interaction of the full-length protein with AtPARG1. As with At5g08530, the interaction of At3g09840 with AtPARG1 was also tested in four permutations (figure 4.11C).

Since the full-length BD-At3g09840 interacted with AtPARG1, the bait vector was also tested to see whether it would interact with the close relative AtPARG2. The interaction was found to be specific to AtPARG1 (figure 4.11C). As with the At5g08530 mentioned earlier, it was found that no expression of C-terminally fused At3g09840 could be detected in western blots (data not shown).

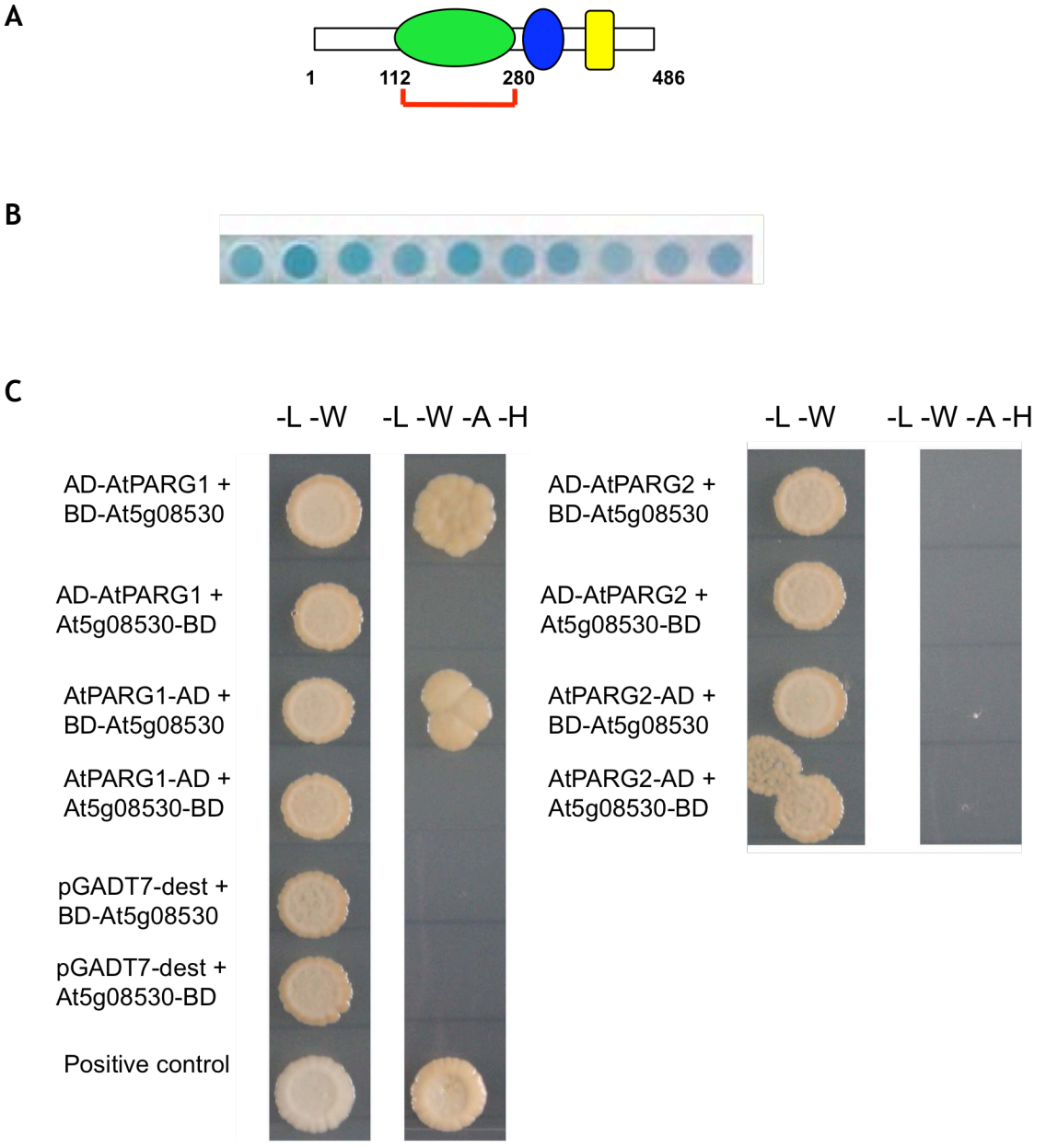

Figure 4.10. AtPARG1, but not AtPARG2, interacts with At5g08530 *in vitro*.
A) Using full-length AtPARG1 as bait, the central region of At5g08530 was isolated from the yeast-two-hybrid screen (amino acids 112-280). The red underline indicates the region identified and amino acids are indicated numerically. Green NADH ubiquinone oxidoreductase, 51 KDa subunit: Pfam PF01512. Blue soluble ligand binding: Pfam PF10531. Yellow NADH ubiquinone oxireductase F subunit iron-sulphur binding domain: Pfam PF10589
B) Positive clones from the yeast two-hybrid screen were passaged five times in liquid medium to remove any non-specific interactions. The clones were then assayed for activity of the second reporter gene, lacZ, using a quantitative ß-galactosidase assay. LacZ assay results from the Dual Systems yeast-two-hybrid screen containing At5g08530 clones are shown.
C) AtPARG1 and AtPARG2 were expressed as activation domain (AD) fusion proteins and At5g08530 as DNA-binding domain (BD) fusion proteins. The AD and BD fusions were provided by pGADT7-dest and pGBKT7-dest, respectively. Transformed PJ69-4α cells were grown on non-selective media (-L, -W) to check the transformation efficiency, and on selective media (-L, -W, -A, -H) to test for interaction.

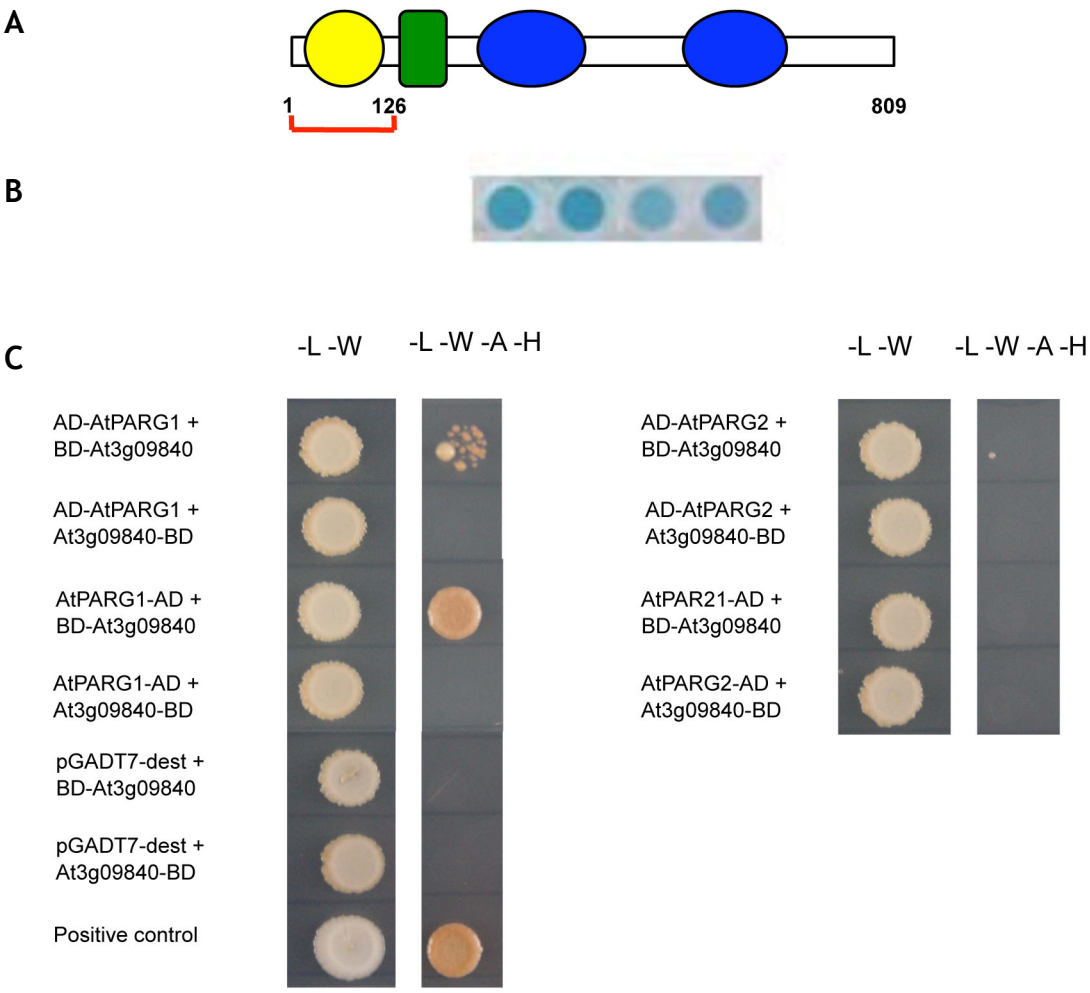

Figure 4.11. AtPARG1 interacts with At3g09840 *in vitro*.

A) Using full-length AtPARG1 as bait, the N-terminal region of At3g09840 was isolated from the yeast-two-hybrid screen (amino acids 1-126). The red underline indicates the region identified and amino acids are indicated numerically. In yellow AAA-ATPase VAT N-term: Pfam PF02359. In blue AAA-ATPase ATP binding: Pfam PF00004.

B) Positive clones from the yeast two-hybrid screen were passaged five times in liquid medium to remove any non-specific interactions. The clones were then assayed for activity of the second reporter gene, lacZ, using a quantitative ß-galactosidase assay. LacZ assay results from yeast-two-hybrid screen containing At3g09840 clones are shown.

C) AtPARG1 and AtPARG2 were expressed as activation domain (AD) fusion proteins and At3g98040 as DNA-binding domain (BD) fusion protein. The AD and BD fusions were provided by pGADT7-dest and pGBKT7-dest, respectively. Transformed PJ69-4α cells were grown on non-selective media (-L, -W) to check the transformation efficiency, and on selective media (-L, -W, -A, -H) to test for interaction.

4.2.7.3 AtKu does not interact with AtPARG1 or AtPARP1 *in vitro*

From the sequencing results provided by the Dual Systems screen, the prey sequence for AtKu70 (At1g16970) was identified as amino acids 201 to 369 (figure 4.12A). Full length AtKu70 was cloned in the bait vector pGBKT7-dest as described earlier and tested in the yeast-two-hybrid system to confirm the interaction of the full-length protein with AtPARG1. In addition, potential interaction with full-length AtPARP1 was also tested as this interaction has previously been observed in mammalian cells (Galande and Kohwi-Shigematsu, 1999; Isabelle *et al.*, 2010). No growth was observed on selective media or on selective media supplemented with 1 mM MMS when tested with either AtPARG1 or AtPARP1 (figure 4.12C) although western blots of the cultures tested on selective media were not able to detect expression of AtKu (data not shown). On closer inspection of the results delivered by Dual Systems, the ß-galactosidase plate assay measuring activation of the LacZ reporter gene conducted on all interactors (figure 4.12B), revealed that all interactions of AtPARG1 with AtKu were very faint blue and thus likely to not interact very strongly. No further work was done with this gene.

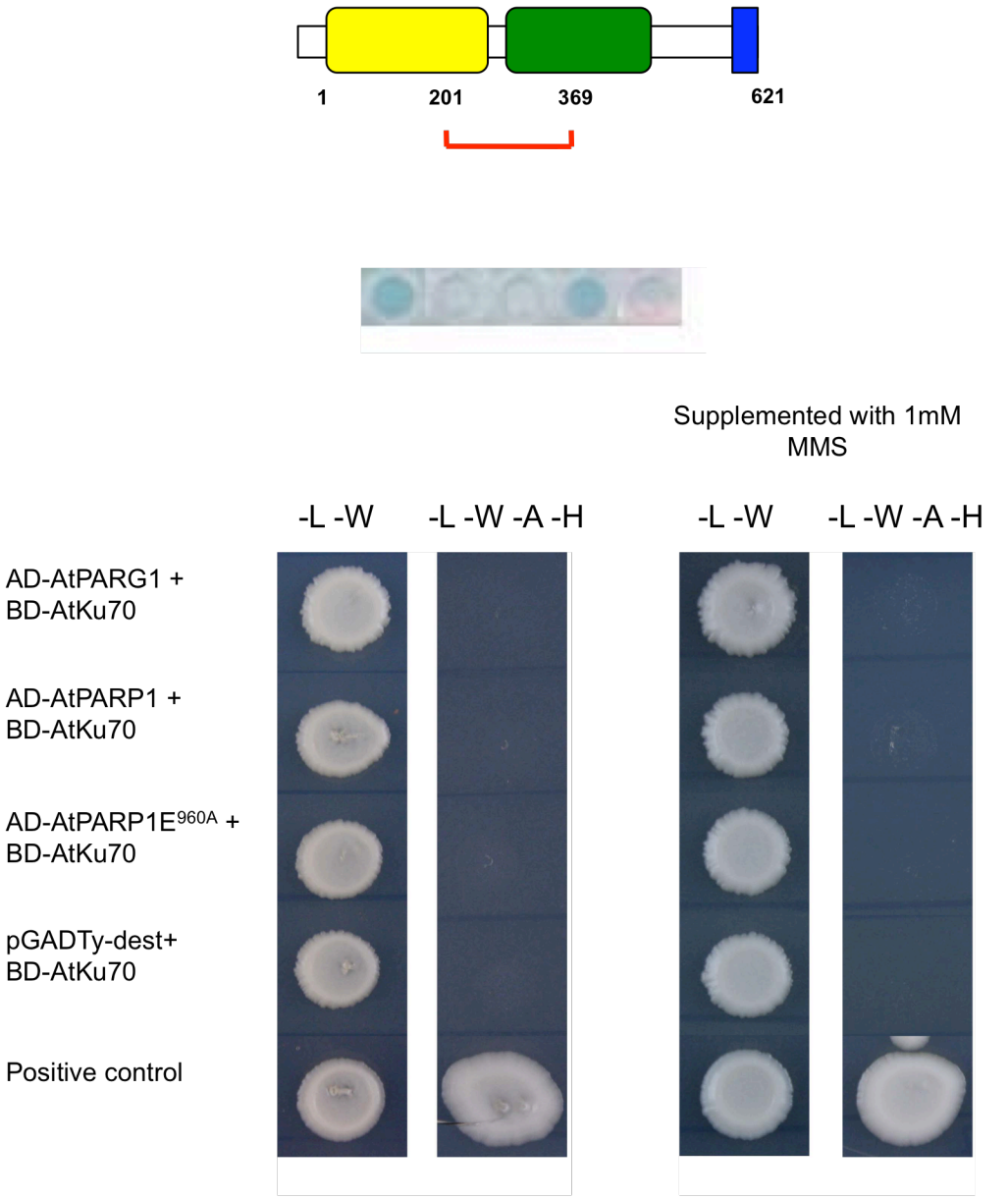

Figure 4.12. AtPARG1 and AtPARP1 do not interact with AtKU *in vitro*.
A) Using full length AtPARG1 as bait, the central region of AtKu70 was isolated from the yeast-two-hybrid screen (amino acids 201-369). The red underline indicates the region identified and amino acids are indicated numerically. Blue SAP DNA binding domain: Pfam PF02037. Green ATP-dependent DNA helicase: Pfam PF02735. Yellow Ku70/80 Nterminal α/ß: Pfam PF03731.
B) Positive clones from the yeast two-hybrid screen were passaged five times in liquid medium to remove any non-specific interactions. The clones were then assayed for activity of the second reporter gene, lacZ, using a quantitative ß-galactosidase assay. LacZ assay results from the Dual Systems yeast-two-hybrid screen containing AtKu clones are shown.
C) Full length AtPARG1, AtPARP1 and AtPARP1^{E960A} were expressed as activation domain (AD) and full length AtKU as DNA-binding domain (BD) N-terminal fusion proteins. The AD and BD fusions were provided by pGADT7-dest and pGBKT7-dest, respectively. Transformed PJ69-4α cells were grown on non-selective media (-L, -W) to check the transformation efficiency, and on selective media (-L, -W, -A, -H) to test for interaction (left hand panels). The cells were also grown on the same media containing 1 mM MMS (right hand panels).

4.2.8 Interactions *in planta*

Positive yeast two-hybrid interactors were tested *in planta* co-localisation from *N.benthamiana* plants infiltrated with *A. tumefasciens* cultures containing full-length fusion proteins. Full-length interactors were cloned into the entry vector pDONR207 and transferred into the Gateway® compatible plant binary pB7WGR2 vector (Karimi *et al.*, 2007) through the Gateway® LR based recombination generating an N-terminal RFP tagged putative interactors. AtPARG1 and AtPARG2 were cloned into pENTR D-TOPO and transferred into the Gateway® compatible plant binary pH7WGF2 and pH7FWG2 vectors (Karimi *et al.*, 2007) which add an N- or C-terminal GFP sequence, respectively. All fusion proteins were under the control of the constitutive CaMV 35S promoter. To circumvent initial problems of low transient expression, the silencing suppressor p19 of tomato bushy stunt virus (TBSV) (Voinnet, 2003) was co-infiltrated with the expression constructs to increase expression of the recombinant proteins under the control of the CaMV35S promoter. *Agrobacteria* containing each of the expression vectors and the p19 vector were mixed at a 1:1:1 ratio, prior to pressure infiltration of *N. benthamiana* at a final OD_{600} of 0.3-0.5.

4.2.8.1 AtPARG1 and AtPARG2 co-localise with At5g08530 *in planta*

The At5g08530 N-terminal RFP-fusion protein was transiently co-expressed in *N. bethamiana* with AtPARG1-GFP or AtPARG2-GFP fusion proteins, and their subcellular localisation was analysed using confocal microscopy 3 days post-infiltration. While only AtPARG1 could be seen in the nucleus, both AtPARG1 and At5g08530 were observed in the cytoplasm of transformed cells (figure 4.13A, B, C, F, G, H), which corresponds to the Pearson's correlation coefficient values measured for each of the subcellular compartments (figure 4.13E and J). At5g08530 is localised to the mitochondria (the subcellular localisation of proteins in *Arabidopsis* database (SUBA) www.suba.plantenergy.uwa.edu.au), which was not observed during these experiments. The N-terminal tag could thus be masking a subcellular localisation signal and result in mislocalisation. While expression with a C-terminal RFP tag was attempted to circumvent the signal masking issue, no expression could be detected under confocal microscopy when these constructs were transiently expressed in *N. benthamiana* (data not shown).

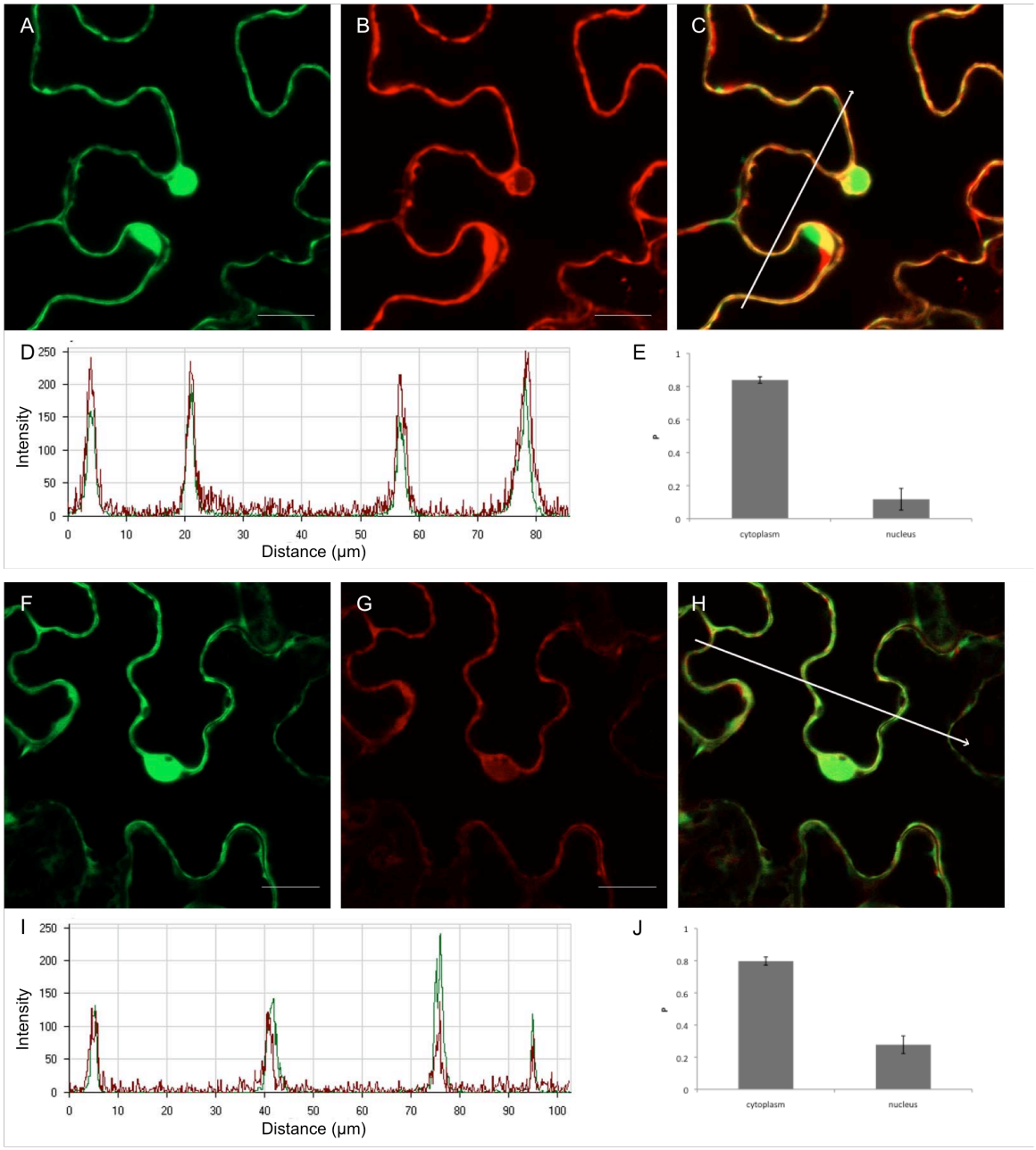

Figure 4.13. AtPARG1 and AtPARG2 co-localise with At5g08530 in tobacco
Tobacco leaf epidermal cells co-expressing either GFP-AtPARG1 and RFP-At5g08530 (A-E) or GFP-AtPARG2 and RFP-At5g08530 (F-J). Cells were transformed by agroinfitration and analysed by confocal microscopy 3 days post-transformation.
Frames show (A, F) GFP fluorescence, (B, G) RFP fluorescence and (C, H) GFP and RFP overlay (yellow colour). In D and I the fluorescence intensities of GFP (green line) and RFP (red line) are plotted against position on a line scan (white arrow in C and H) and are represented in arbitrary units. In E and J Pearson's coefficients (P) of colocalisation in different subcellular compartments are represented. Error bars represent SE (n=4-14). Scale bars = 20 µm.

4.2.8.2 AtPARG1 and AtPARG2 colocalise with At3g09840 *in planta*

The At3g09840 N-terminal RFP-fusion protein was transiently co-expressed in *N. bethamiana* with AtPARG1 or AtPARG2 N and C-terminal GFP fusion proteins, and their subcellular localisation was analysed using confocal microscopy 3 days post-infiltration. While only AtPARG1 could be seen in the nucleus, both AtPARG1 and At3g09840 were observed in the cytoplasm of transformed cells (figure 4.14A, B, C, F, G, H) and the fluorescence intensity of the RFP and GFP signals correlate across the cell (figure 4.14D and I). This was reflected in the Pearson's correlation coefficient values for colocalisation obtained for each both subcellular compartments (figure 4.14E and J). Similar subcellular distributions were observed for AtPARG2 and At3g09840 (figure 4.15A, B, C, F, G, H), although the difference between Pearson's correlation coefficients for the cytoplasm and the nucleus was much higher than for AtPARG1 and At3g09840 (figure 4.15D and I).

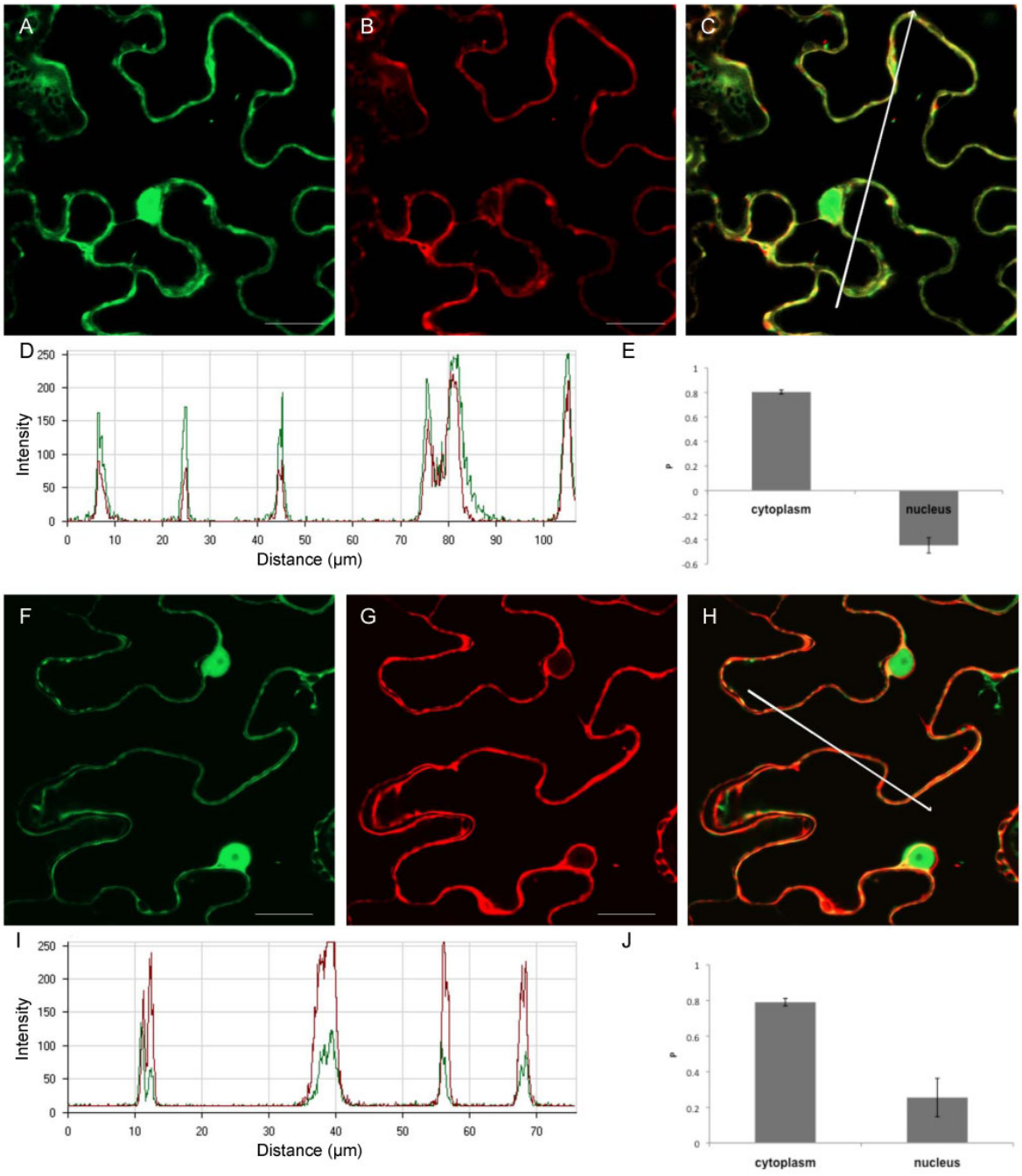

Figure 4.14. AtPARG1 colocalises with At3g09840 in the tobacco
Tobacco leaf epidermal cells co-expressing either GFP-AtPARG1 and RFP-At3g09840 (A-E) or AtPARG1-GFP and RFP-At3g09840 (F-J). Cells were transformed by agroinfitration and analysed by confocal microscopy 3 days post-transformation.
Frames show (A, F) GFP fluorescence, (B, G) RFP fluorescence and (C, H) GFP and RFP overlay (yellow colour). In D and I the fluorescence intensities of GFP (green line) and RFP (red line) are plotted against position on a line scan (white arrow in C and H) and are represented in arbitrary units. In E and J Pearson's coefficients (P) of colocalisation in different subcellular compartments are represented. Error bars represent SE (n=3-15). Scale bars = 20 μm.

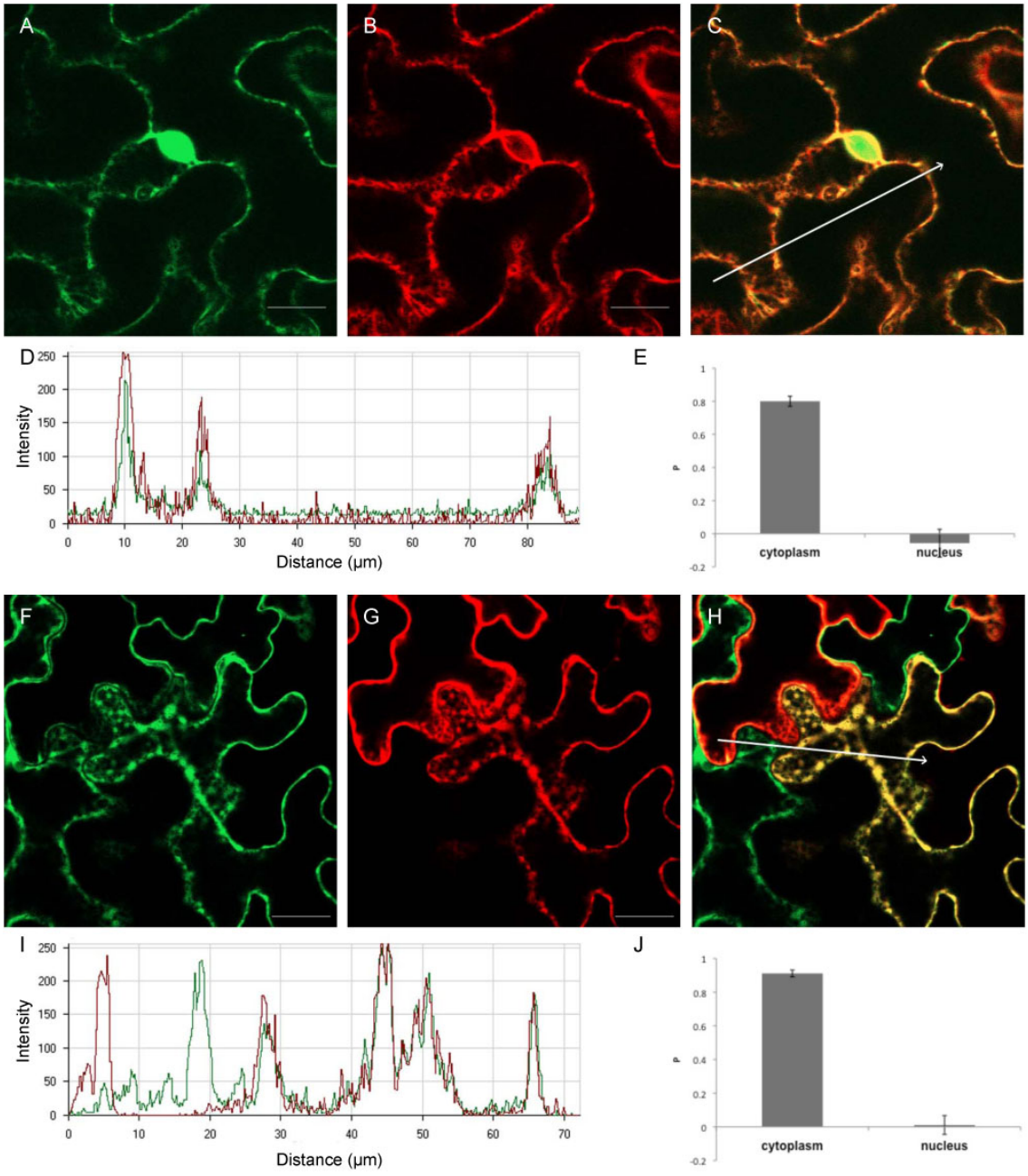

Figure 4.15. AtPARG2 colocalises with At3g09840 in tobacco
Tobacco leaf epidermal cells co-expressing either GFP-AtPARG2 and RFP-At3g09840 (A-E) or AtPARG2-GFP and RFP-At3g09840 (F-J). Cells were transformed by agroinfitration and analysed by confocal microscopy 3 days post-transformation.
Frames show (A, F) GFP fluorescence, (B, G) RFP fluorescence and (C, H) GFP and RFP overlay (yellow colour). In D and I the fluorescence intensities of GFP (green line) and RFP (red line) are plotted against position on a line scan (white arrow in C and H) and are represented in arbitrary units. In E and J Pearson's coefficients (P) of colocalisation in different subcellular compartments are represented. Error bars represent SE (n=3-15). Scale bars = 20 μm..

4.3 Discussion

4.3.1 PAR content

It has previously been shown that the AtPARPs are transcriptionally regulated (Garcia *et al.*, 2003; Culligan *et al.*, 2006), unlike those found in mammals, which have been shown to be expressed constitutively and are regulated at the post-translational level. So far there has been no evidence found to indicate the same type of post-transcriptional control in plants, although analysis of the AtPARP protein sequences indicate several possible phosphorylation targets (data not shown). It has been shown that PARP1 is responsible for 80-90% of the activity in mammals, while PARP2 contributes the remaining 10-20% of activity (Amé *et al.*, 1999; Schreiber *et al.*, 2002). Deficiencies in either gene result in mouse lines that are viable but hypersensitive to genotoxic stress (de Murcia *et al.*, 1997; Schreiber *et al.*, 2002), while double knockouts are embryonic lethal (Menissier de Murcia *et al.*, 2003). In the previous chapter it was found that T-DNA insertion lines in either AtPARP1 or AtPARP2 are viable and show no notable difference to the wild type in tolerance or sensitivity to genotoxic stress. It has however been shown that both AtPARP1 and AtPARP2 expression is regulated by the plant homologue of the serine/threonine protein kinase ATM, as both AtPARP1 and ATPARP2 transcripts are abolished in *Atatm* mutants (Garcia *et al.*, 2003). The examination of PAR-content of WT and T-DNA insertion lines protein extracts, both before and after two different forms of genotoxic stresses, has shown that the majority of PAR polymer is produced by AtPARP1. To fully determine which AtPARPs are responsible for the majority of PAR production, they would have to be expressed and their activity measured. This could be done in *E. coli* or an insect cell system and applied to a commercially available *in vitro* activity assay.

With an MMS and bleomycin hypersensitive phenotype observed in AtPARG1 T-DNA insertion lines, it was expected that this enzyme is responsible for the majority of the breakdown of PAR in the plant cell. Thus when examining levels of PAR in plant seedlings, more PAR polymer was expected in the AtPARG1 deficient lines, which was not the case. One likely explanation is that, in these plants autopoly(ADP-ribosyl)ation occurs quicker than normal, which also inhibits

the PARPs and thus results in less polymer being produced. One way to resolve this question would be to examine the NAD levels from the same samples, since the NAD content should be relatively lower in cells with active PARPs. The 20-fold increase in polymer levels observed in the *tej* mutant of AtPARG1, was determined from nuclear extracts (Panda *et al.*, 2002). The extracts used here for estimation of polymer level were from whole seedlings and would thus also include any polymer present in the cytoplasm. Any ADP-ribose generated after PARG activity is exported to the cytoplasm to be broken down and thus not included in the total ADP-ribose content of the cell. This difference in methodology could account for the difference in PAR-levels between the *tej* mutant and the *parg1* alleles used in this study. In addition, the presence of a dominant negative version of AtPARG in the *tej* mutant could also be disrupting the processing of polymers. Although the method of PAR level determination used in this study quantitatively estimates the amount of polymer present in the seedlings, it does not account for the length or branching of polymer present in the protein extracts.

It would be interesting to see whether any differences can be seen in PAR polymer structure generated in the T-DNA insertion lines. Previously, polymer size has been measured by incubation of protein extracts with radio-labelled NAD^+, and measuring the resulting PAR levels by the incorporation of NAD^+ and running the samples on a 20% polyacrylamide DNA sequencing gel, which would also determine the sizes of polymer generated, but not the extent of branching (Affar *et al.*, 1999). This method would determine the size of polymer generated by the individual AtPARPs, as well as determine the type of product resulting from the individual AtPARG activity *in vivo*, which would provide clues to the exo and endoglycosidase activity.

4.3.2 Putative interactors of AtPARP1 and AtPARP2

The *Arabidopsis* homologues of PARP1 and XRCC1 both contain a BRCT motif, which has been shown to be site of interaction in mammals (Masson *et al.*, 1998). Due to the structural resemblance of AtPARP1 to its mammalian homologue (figure 3.1) and the existence of a plant homologue of AtXRCC1, the putative interaction between these proteins were tested *in vitro* using yeast two-hybrid. A very weak interaction was observed between N-terminally fused

AtPARP1 and AtXRCC1, while no growth was observed on selective media when testing the catalytically inactive AtPARP1^{E960A} mutant protein. While interaction has previously been observed between PARP2 and XRCC1 in mammals (Schreiber *et al.*, 2002), AtPARP2 and AtXRCC1 did not interact using the yeast two-hybrid system.

The role of XRCC1 in plants may be different to the one described in mammals as homologues for genes involved in BER (DNA ligase III, DNA polymerase ß) as well as the major protein for genome maintenance in mammals, p53, have not been found in plants (Charbonnel *et al.*, 2010; Tuteja *et al.*, 2009). Transcript of a rice homologue (OsXRCC1) was upregulated after treatment with the DSB inducing agent bleomycin, but not the alkylating agent MMS or oxidative stress in the form of H_2O_2 (Uchiyama *et al.*, 2008). Moreover, AtXRCC1 deficient seedlings were shown to be sensitive to γ-irradiation (Charbonnel *et al.*, 2010), and the OsXRCC1 was shown to interact with the proliferating cell nuclear antigen (PCNA) (Uchiyama *et al.*, 2008), a protein previously implicated in NHEJ in mammals through its interaction with the heterodimer Ku70/Ku80 (Balajee and Geard, 2001).

4.3.3 Putative AtPARG1 and AtPARG2 shown to definitively have glycohydrolase activity

The mammalian catalytic domain has been well characterized and residues required for function have been indentified (Patel *et al.*, 2005). The catalytic region is highly conserved, which was demonstrated by the fact that the same residues were also required for the activity of the nematode PARGs, and the larger PARG (PME-3) was found to have higher glycohydrolase activity than the shorter protein PME-4 (St-Laurent *et al.* 2007). Nematodes are the only other organism known to contain two genes encoding for PARGs. A difference in the two AtPARGs was established in the form of the hypersensitive phenotype of *parg1* insertion lines in response to DNA damaging agents. To see whether this was due to a similar difference in activity, as was observed in the two proteins in nematodes, the two AtPARGs were cloned for recombinant expression.

As with previous attempts by other groups to purify the full-length PARG protein from other organisms, we did not succeed in purifying the AtPARG proteins when

using prokaryotic or eukaryotic expression systems. This could be due to toxicicty of the protein to prokaryotes, as they do not contain native PARG genes. In addition, we found that even when expressed as part of an insect cell lysate, the recombinant AtPARG proteins were repeatedly unstable with break down products observed shortly after protein extraction, even when kept on ice (data not shown).

The glycohydrolase activity of the two AtPARGs was therefore determined using recombinant proteins expressed in the insect cell system and the cell lysates in an *in vitro* assay. AtPARG1 showed 20% higher glycohydrolase activity than AtPARG2 in this assay, when the values from wells with the highest amount of AtPARG2 were compared with the lowest amount of AtPARG1. Single basepair mutations of AtPARG1 identified that the conserved aspartate residue D^{255}, unlike in the mammalian enzyme is not required for activity as introduction of this mutation did not significantly lower glycohydrolase activity compared with the WT AtPARG1 protein. In the nematode which also contains two distinct PARG genes, the mutation of this aspartate residue only completely abolishes activity in one of the two PARG proteins, while it is only lowered slightly in the other when compared with the activity of the wild type protein (St-Laurent *et al.*, 2007). Within the conserved PARG signature the two AtPARGs show very high sequence identity and all of the acidic residues analysed in mammals and worms are also conserved. However, AtPARG2 does not have the third residue in an otherwise conserved glycine triplet. Introducing the third glycine through mutation of the lysine residue present at this position (L275G) lowered the activity to background levels, demonstrating that the L^{275} residue is required for glycohydrolase activity of AtPARG2.

The different subcellular localised isoforms of mammalian PARG all contain a regulatory region (aa 461-476) upstream of the PARG catalytic domain, in which a 16-residue mitochondrial targeting sequence is located (Whatcott *et al.*, 2009; Botta and Jacobson, 2010). Several of the residues in this sequence were shown to be required for catalytic activity of both the shorter mitochondrially localised and the full-length nuclear localised PARG (Botta and Jacobson, 2010). Part of this sequence is conserved in the *Arabidopsis* PARGs. It would therefore be interesting to see if residues within this partially conserved motif are also required for activity in the *Arabidopsis* orthologues.

4.3.4 Subcellular localisation

PARG in mammals are localised throughout the cell in isoforms of different lengths (Meyer-Ficca *et al.*, 2004; Meyer *et al.*, 2007). In the worm *C. elegans*, which like *A. thaliana* has two distinct PARGs, one PARG is predominantly nuclear and while the other is mostly cytoplasmic (St-Laurent *et al.*, 2007). Subcellular localisation experiments analysing both transiently expressed N-terminally GFP-tagged AtPARG1 in *N. benthamiana* as well as stably transformed *A. thaliana* lines indicate the presence of this protein in the nucleus as well as in the cytoplasm. N-terminal fusions can sometimes mask any potential signal peptides present in the N-terminal region of a protein, and the subcellular distribution of the fusion protein could thus be a false representation of its real localisation. To rule this out, fluorescence recovery after photobleaching (FRAP) experiments were employed to examine the mobility of the fluorescent fusion proteins. FRAP experiments performed on *Arabidopsis* stably transformed with N-terminally GFP-tagged AtPARG1 under the control of the constitutive promoter CaMV 35S (pGWB6) demonstrated that the 35S:GFP:AtPARG1 recombinant proteins do not diffuse back into the nucleus after bleaching as the GFP-signal does not recover, which is the case for GFP, therefore any potential NLS does not seem to be affected be the presence of an N-terminal tag. In addition it has been found that large proteins (>50 KDa) are too big to enter the nucleus through the nuclear pore complex (Poon and Jans, 2005) and GFP-AtPARG1 is 80-90 KDa. Unfused GFP is only 27 KDa and is thus able to enter the nucleus through passive diffusion (Niwa, 2002). AtPARG2 also localises to both the nucleus and cytoplasm. In addition to the nuclear localisation, AtPARG1 and AtPARG2 could also be seen in net-like patterns throughout the cell (data not shown). This type of pattern has previously been observed with ER-localised proteins, so to investigate the putative localisation of AtPARGs in the ER, further confocal microscopy on plants co-infiltrated with the ER marker protein HDEL (Gomord *et al.*, 1997) could be performed. Ultracentrifugation or sucrose gradients could also be used to determine the presence of the AtPARGs in these fractions (again, specific anti-bodies would be desirable). Several of the mammalian isoforms of PARG have been shown to shuttle between subcellular compartments in response to stress (Haince *et al.*, 2006). As mentioned previously, a putative mitochondrial localisation signal has recently been identified in mammalian PARG (Niere *et al.*, 2008), which has also been shown to contain residues

required for activity (Botta and Jacobson, 2010). Some of these residues are conserved in the AtPARGs. Site directed mutagenesis of this motif in GFP fusion proteins would help determine the importance of these residues in the Arabidopsis proteins. Analysis of the AtPARG protein sequences and comparison to their mammalian homologues revealed a stretch of basic residues with high similarity to a consensus motif for an NLS. Deletion analysis of this stretch would reveal whether it is responsible for the nuclear localisation observed when transiently expressing AtPARG GFP fusion proteins in *N. bethamiana*.

4.3.5 Putative interactors of AtPARG1

Several proteins were isolated in a LexA/GAL4 based yeast-two-hybrid screen for AtPARG1 interactors carried out by Dual Systems (Switzerland). These included proteins previously found to be involved in DNA repair and cell cycle. In addition, the protein with the second highest frequency of interaction localises to the mitochondria. The yeast-two-hybrid experiments were repeated using full-length clones of the interactors identified in the screen. One of three proteins, which was successfully cloned, AtKu70, has previously been shown to be involved in DNA damage repair in Arabidopsis (Bundock *et al.*, 2002; Riha *et al*, 2002). While the initial screen identified this protein 4 times, the approach of using the full-length protein in the GAL4 system did not result in interaction, nor did it express at a high enough level to detect using western blots. This is, however, not necessarily directly indicative of a negative result. The lack of interaction could be due to steric effects incurred by the folding of the full-length protein, obscuring the exosed part of the protein in found in the truncated version, which was identified in the initial screen, or that the N-terminal fusion of AtKu is preventing the correct folding. The results of the initial screen could have been confirmed by extracting and sequencing the plasmids used and performing the yeast-two-hybrid experiment as in the screen. The AtKu could also be tested directly *in vivo* using BiFC or pulldown methods.

Two of the full-length proteins cloned showed expression, At5g08530, an NADH dehydrogenase which is a subunit of respiratory complex 1, and At3g09840, an AAA-ATPase (ATPases associated with various cellular activities), which has previously been shown to be involved in regulation of the cell cycle in *Arabidopsis* (Park *et al.*, 2008). These interacted solely with AtPARG1 and not

the closely related AtPARG2, thus further supporting the theory of separate roles for the two AtPARG homologues in plants, as was suggested in the previous chapter, where only T-DNA insertion lines of AtPARG1 displayed a phenotype in response to genotoxic stress. However, the conditions of yeast two-hybrid screens "force" proteins into the nucleus and can therefore yield false positives. Therefore it was important to confirm the interactions *in planta* as well. Due to the conditions under which the *A. thaliana* cDNA library were constructed, a lot of the genes normally associated with DNA damage in plants, would not have been expressed at a high enough level if at all and so would not be present in such a library. Therefore any interactions of AtPARG1 with such proteins would not be found using this screen. Had time allowed, the screen could have been expanded by using cDNA library derived from seedlings exposed to DNA damaging agents. As an alternative or a compliment to an expanded yeast two hybrid cDNA library screen, pull-down assays using stressed and non-stressed *Arabidopsis* plants transformed with tagged AtPARG1 could be used and mass spectrometry used for identification of any interacting proteins.

To test the interactions *in planta* co-immunoprecipitation of tagged proteins transiently expressed in *N. benthamiana* were undertaken to save time. GFP-tagged AtPARG1 under the control of the constitutive CaMV 35S promoter were transformed into *A. tumefasciens* and co-infiltrated into *N. benthamiana* with RFP-tagged interactors confirmed as positive in the full-length yeast two-hybrid experiments.

The RFP-At5g08530 NADH dehydrogenase was found to co-localise with GFP-AtPARG1 and GFP-AtPARG2 in the cytoplasm of transiently transformed *N. benthamiana* cells. However, At5g08530 localises to the mitochondria (according to SUBA) where it forms part of respiratory complex 1. This mislocalisation could be due to the overexpression levels resulting in saturation of the trafficking pathway from the cytoplasm into the mitochondria (Sparkes *et al.*, 2006). Since the correct subcellular distribution for this protein was not observed using these conditions, no further work was done with this protein in this study.

The RFP-At3g09840 AAA-ATPase was found to co-localise with N and C-terminally GFP tagged AtPARG1 and AtPARG2 in the cytoplasm of transiently transformed *N. benthamiana* cells. This AAA-ATPase protein has been shown in mammals to

play a role in cell cycle control, cell proliferation, and is involved in proteasome- and ER-associated degradation of proteins (reviewed in Woodman *et al.*, 2003). In *Arabidopsis* it has been shown to localize to the nucleus, ER, plasma membrane, and cytoplasm (Rancour *et al.*, 2002; Aker *et al.*, 2007; Park *et al.*, 2008) and is required for seedling development and cytokinesis (Park *et al.*, 2008).

A smear at the top of western blots on RFP-At3g09840 would always appear in protein extract gels. It is currently unclear what causes this, it could have something to do with the native hexameric conformation of the fusion protein (Aker *et al.*, 2007), or the fact that it exists as both soluble and membrane bound in the cell.

The interactions were also examined using C-terminally tagged RFP interactor protein fusions, as it has previously been discussed that the subcellular localisation signals of proteins can be masked by N-terminal fusions, but no expression of C-terminally tagged At3g09840 could be detected under confocal microscopy. Therefore no further investigation into this potential limitation for correct subcellular distribution could be made at this time. This problem has since been found to potentially be due to the length of the linker between the protein of interest and the fusion protein, and can therefore be addressed in future analyses, by re-cloning into a different subcloning vector, such as pENTR-D-TOPO, which did not show the same problems.

To circumvent the problem of AtPARG2 being expressed at higher levels consistently in transient transformation of tobacco, the split-YFP BiFC approach could be employed. This system usually provides a yes or no answer on interaction, and with the development of a system containing internal controls for expression levels (C. Grefen, personal communication) even the problem of incomparable expression levels could be solved.

In future deletion analysis can be used to determine which parts of the proteins are interacting, and following on from that, any specific residues required can be identified by site directed mutagenesis.

While the results in this chapter showed that there is a difference in the activity of the two AtPARGs, their subcellular distribution is similar. In addition, there does not seem to be any differences in the PAR content of the *parg1-2* and the *parg2-1* lines that can explain the hypersensitive phenotypes seen in chapter 3. The next chapter looks into any differences in regulation of the two AtPARGs at the transcriptional level as well as trying to establish any alterations in the transcriptome of the *parg1-2* knock-out line.

5 Transcriptomics

5.1 Introduction

In the mammalian poly(ADP-ribosyl)ation model, the control of mechanism is at the protein level, with transcript and protein level remaining constant and the activity being induced by DNA strand breaks (Johansson, 1999). The poly(ADP-ribose) polymer as well as the autoribosylated PARP are known to act as a modulator of chromatin structure (Tulin *et al*., 2002; Tulin and Spradling, 2003) and binds to several promoter elements in human genomic DNA (Krishnakumar *et al* ., 2008). A 20-amino acid consensus PAR-binding motif, consisting of a cluster rich in basic residues and a pattern of hydrophobic amino acids interspersed with basic residues has been indentified, and several DNA damage check-point proteins such as p53 and p21, as well as proteins involved in BER, NER and NHEJ, contain this motif (Pleschke *et al*., 2000). PARP1 has been shown to function as a transcriptional co-regulator, and as both an enhancer and repressor (Reviewed in Kraus, 2008). In plants, the regulation of PARPs has so far only been demonstrated at the transcriptional level as transcript levels of AtPARP1 and AtPARP2 showed significant increases after treatment with DNA damaging agents such as γ-irradiation, and bleomycin (Doucet-Chabeaud *et al*., 2001; Culligan *et al*., 2006; Chen *et al*., 2003) as well as oxidative stress (Doucet-Chabeaud *et al*., 2001).

Much less is known about the transcriptional regulation of AtPARGs. AtPARG1 has already been implicated in the control of circadian rhythm in *Arabidopsis,* as a single basepair mutant (G262E) showed an increase in circadian period length as well as an earlier flowering time (Panda *et al*., 2002). Transcript levels of AtPARG1 were increased after γ-irradiation (Culligan *et al*., 2006). AtPARG2 transcript levels were upregulated after treatment with the bacterial pathogen *Pseudomonas syringae* pv. *tomato* (Adams-Phillips *et al*., 2008) and the necrotrophic fungus *Botrytis cinerea* (Adams-Phillips *et al*. 2010).

In this chapter the putative upstream promoter regions of the genes in the PARylation family were analysed for the presence of specific response elements. The effects of abiotic and genotoxic stress on AtPARP and AtPARG transcript

levels in the wild type plant were examined both using semi-quantitative RT-PCR as well as through *in sillico* analysis using online microarray data from the eFP Browser. Their upstream regions were analysed using online software to see if any common promoter elements exist within these. This chapter also highlights differences in the transcriptomes of wild type and *parg1-1* through SAGE analysis of seedlings of both genotypes under normal conditions and under genotoxic stress.

5.2 Results

5.2.1 Promoter sequences of AtPARPs and AtPARGs

Putative regulatory motifs in the promoter regions of AtPARPs and AtPARGs were analysed using the Athena program (O'Connor *et al*., 2005). The region 1 kb (or to the adjacent gene if less than 1 kb) immediately 5' of the start codon was queried against a database of known regulatory elements (Table 5.1). Although the software determines that none of these promoter elements are enriched, it is noticeable that all the genes, except AtPARG2, contain CCA1 binding motifs and AtPARP2 also has an Evening Element. Both of these promoter elements have been shown to be involved in the regulation of clock controlled or circadian genes in *A. thaliana* (Michael and McClung, 2002). There are also several promoters involved in the response to ABA-induced stress and water stress, a high number of which were present in the AtPARP3 promoter. In addition, this promoter region also contains motifs that are involved in germination. W-boxes, which are involved in plant immunity (Eulgem and Somssich, 2007), were found in all but AtPARP3.

Gene	Element	Function
AtPARP1	Ibox promoter motif	Light response
	TATA-box (2)	
	W-box	Pathogen defense, senescence, trichome formation
	LEAFYATAG	
	MYB2AT	Water stress
	CARGCW8GAT (4)	Flower development
	CCA1 binding site motif(2)	Circadian rhythm
	GAREAT (2)	Giberellin responsive element
	MYB4 binding site motif	Environmental stress
	MYB1LEPR	Plant defense
	ATHB6	Hormone response
	ARF binding site motif	Auxin response factor
	BoxII	
	Hexamer promoter motif	Histone H4 regulation
AtPARP2	T-box	Light induced transcription
	W-box	Pathogen defense, senescence, trichome formation
	BoxII	
	TATA-box (3)	
	MYB4 binding site motif (3)	Environmental stress
	MYB1AT (3)	Water stress
	CARGCW8GAT(4)	Flower development
	CCA1 (2)	Circadian rhythm
	EveningElement	Circadian rhythm
	RY-repeat promoter motif (2)	legume seed protein genes
	AtMYB2 BS in RD22	Drought and ABA
AtPARP3	CACGTGMOTIF (2)	Embryogenesis, defense related
	MYB1AT (4)	Water stress
	BoxII (2)	
	TATA-box (4)	
	MYB3 binding site motif	Environmental stresses
	MYB4 binding site motif (3)	Environmental stress
	GADOWNAT	Germination, Giberellin response
	ABFs binding site motif	ABA response
	ABRE binding site motif	ABA response
	ABRE-Like binding site motif (2)	Dehydration and cold
	AtMYB2 BS in RD22	Drought and ABA
	RAV1-B binding site motif	
	UPRMOTIFIIAT	Unfolded protein response
	ACGTABREMOTIFA2OSEM (2)	ABA response
	GBOXLERBCS	Light regulation
	CCA1	Circadian rhythm
	MYB1LEPR	Plant defense
AtPARG1	MYB1AT (5)	Water stress
	T-box	Light induced transcription
	W-box (4)	Pathogen defense, senescence, trichome formation
	TATA-box (2)	
	GAREAT (2)	Giberellin responsive element
	MYB4 binding site motif	Environmental stress
	Ibox	Light response
	BoxII	
	CARGCW8GAT (4)	Flower development

	CCA1	Circadian rhythm
AtPARG2	W-box (4)	Pathogen defense, senescence, trichome formation
	T-box	Light induced transcription
	AtMYB2 BS in RD22	Drought and ABA
	MYCATERD1	Water stress

Table 5.1. Known promoter response elements found in the upstream sequence of poly(ADP) ribosylation family member genes.
The promoter response elements were located using the Athena software, 1000 bp upstream of the start codon of each gene. Further information about the transcription factor families was obtained through links from Athena to PLACE or AtCis (Agris) databases. Numbers in parentheses indicate the number of times, if more than once, the response elements are found in the upstream region.

5.2.2 Semi-quantitative RT-PCR

To investigate the transcript levels of PARylation gene family members in *A. thaliana* under biotic, abiotic and genotoxic stress, initial semi-quantitative RT-PCR experiments were undertaken in collaboration with Dr Sarah Henry. *Arabidopsis* Col-0 seedlings were grown in liquid media in constant light for 12 days after which stress chemicals were applied at the concentrations listed in table 5.2. Tissue was harvested at 0, 2, 4, 8, 24 and 48-hour time points. The transcript levels were analysed by measuring PCR product band intensity after gel electrophoresis using Image J software. The transcript levels were normalised to *ACTIN2* transcript levels, and the normalised intensities for each of the treatments are presented in tables 5.3 to 5.7, with each table representing separate transcript levels for each PARylation family member. S. Henry (2008) later confirmed these initial observations for UV-B, ABA, MMS, and bleomycin treatment using qPCR (data not shown).

Stress chemical	Final concentration
Mannitol	2.5 M
NaCl	200 mM
Abscisic Acid	50 µM
Jasmonic Acid	50 µM
LPS	1 µg/ml
NAA	5 µM
ACC	200 µM
Salicylic Acid	10 µM
MMS	1.2mM
Bleomycin	0.5µg/ml
UV-B	Plates grown in 3µE
Wounding	Seedling crushed twice with forceps

Table 5.2. Final concentrations of stress chemical for *Arabidopsis* treatments.

The levels of AtPARP1 transcript after stress treatments are displayed in table 5.3 below. The application of the DNA damaging agents MMS and bleomycin induced significant increases in AtPARP1 transcript levels. This increase showed a similar temporal profile for both treatments, with a peak at 5 to 5.5-fold increase after 4 hours of exposure. The levels remained high at 3 to 4-fold increase after 48 hours. Treatment with lipopolysaccarides, which induces plant defense responses, lowered the transcript levels to 60 to 70% of basal levels for 8 hours. Transcript levels in response to the phytohormones ABA, ethylene and auxin were lowered to 40 to 50% of basal levels after 48 hours.

Stress	**AtPARP1 fold-change in expression level**					
Time point in hours	**0**	**2**	**4**	**8**	**24**	**48**
Salt	1.00	1.06	1.16	1.07	1.10	0.62
Mannitol	1.00	0.75	0.82	0.76	1.04	0.81
Abscisic acid	1.00	0.95	0.48	1.20	0.82	0.42
Ethylene (ACC)	1.00	1.09	1.18	1.13	1.19	0.50
Auxin (NAA)	1.00	0.95	0.84	0.82	0.76	0.40
Lipopolysaccharide	1.00	0.68	0.61	0.68	1.05	1.34
Jasmonic acid	1.00	0.92	1.22	1.19	1.19	0.60
Salicylic acid	1.00	0.88	0.89	0.98	1.02	0.64
Wounding	1.00	0.49	0.71	1.12	0.82	0.26
MMS	1.00	1.30	5.03	4.37	2.90	3.18
Bleomycin	1.00	2.90	5.47	3.81	3.13	3.95
UV-B	1.00	0.93	1.87	0.67	1.72	0.59

Table 5.3. SQRT-PCR determined AtPARP1 expression levels under stress treatments
Transcript levels were taken at time points 0, 2, 4, 8, 24 and 48 hours. Transcript levels are expressed normalised to Actin2 expression. NA indicates transcript levels too low to measure.

The AtPARP2 transcript levels after stress treatments are displayed in table 5.4 below. The transcript levels of AtPARP2 show the highest induction in response to the DNA damaging agent bleomycin. It increases to nearly 16-fold after 4 hours, after which it decreases to 9.5-fold and remains high at 12.6-fold after 48 hours. The transcriptional response to alkylating agent MMS shows a similar response to that seen for bleomycin, although slightly less pronounced with a peak of 8.5-fold upregulation seen after 8 hours and remains high at 8-fold after 48 hours. More than a 2-fold increase was observed after 24 and 48 hours of UV-B exposure. Both jasmonic and salicylic acid, known signalling molecules in the plant immune response, lowers the transcript levels to 40 to 50% of basal levels after 48 hours.

Stress	**AtPARP2 fold change in expression level**					
Time point in hours	**0**	**2**	**4**	**8**	**24**	**48**
Salt	1.00	1.95	2.13	1.76	1.75	1.52
Mannitol	1.00	2.09	1.77	1.76	1.65	1.61
Abscisic acid	1.00	1.40	0.94	1.00	0.86	2.55
Ethylene (ACC)	1.00	1.11	1.20	1.01	1.22	0.43
Auxin (NAA)	1.00	1.01	1.17	0.88	0.62	0.47
Lipopolysaccharide	1.00	0.93	0.66	0.96	0.70	0.92
Jasmonic acid	1.00	0.60	0.82	0.64	0.57	0.37
Salicylic acid	1.00	0.61	0.95	0.82	0.62	0.51
Wounding	1.00	0.49	0.75	0.85	0.64	0.26
MMS	1.00	1.74	8.43	8.53	5.65	8.06
Bleomycin	1.00	7.01	15.87	9.53	10.21	12.61
UV-B	1.00	0.86	1.44	1.09	2.40	2.30

Table 5.4. SQRT-PCR determined AtPARP2 expression levels under stress treatments
Transcript levels were taken at time points 0, 2, 4, 8, 24 and 48 hours. Transcript levels are expressed normalised to Actin2 expression.

The transcript levels of AtPARP3 after stress treatments are displayed in table 5.5 below. They showed a similar temporal profile to that of AtPARP1 and AtPARP2 in response to MMS and bleomycin, peaking at 2.8-fold and 5.6-fold, respectively, after 4 hours of exposure. The highest increases in transcript levels were observed after treatment with ABA, salt and osmotic stress, with 32, 12 and 6-fold, respectively, after 4 hours exposure. Treatment with auxin also induced AtPARP3 transcript levels nearly 20-fold which peak after 4 hours of treatment.

Stress	**AtPARP3 fold-change in expression level**					
Time point in hours	**0**	**2**	**4**	**8**	**24**	**48**
Salt	1.00	7.62	12.23	8.31	6.06	0.48
Mannitol	1.00	2.91	6.23	5.55	3.51	2.18
Abscisic acid	1.00	11.64	32.44	22.28	13.19	8.43
Ethylene (ACC)	1.00	0.95	2.09	NA	NA	NA
Auxin (NAA)	1.00	11.66	19.22	5.11	6.48	NA
Lipopolysaccharide	1.00	0.94	2.70	1.41	0.21	1.18
Jasmonic acid	1.00	0.80	1.06	1.96	1.28	1.09
Salicylic acid	1.00	0.80	1.84	0.50	1.55	1.04
Wounding	1.00	0.53	2.42	3.14	0.96	0.84
MMS	1.00	1.35	2.80	2.27	1.12	1.36
Bleomycin	1.00	3.55	5.66	4.57	2.22	2.37
UV-B	1.00	2.20	2.70	1.57	1.96	0.82

Table 5.5. SQRT-PCR determined AtPARP3 expression levels under stress treatments
Transcript levels were taken at time points 0, 2, 4, 8, 24 and 48 hours. Transcript levels are expressed normalised to Actin2 expression.

The AtPARG1 transcripts levels after stress treatments are displayed in table 5.6 below. The level of AtPARG1 transcript were increased with both DNA damaging agent, MMS and bleomycin, with a peak after 4 hours of treatment at 2.8 and 5.6-fold increase, respectively. A similar temporal profile was also seen with UV-B stress application. A decrease in transcript levels could be seen after treatment with phytohormones. Treatment with ABA, ethylene and auxin lowered AtPARG1 transcript levels to half and quarter of the levels of the control, respectively. Treatment with jasmonic and salicylic acid, which are key signalling molecules in plant disease resistance, decreased expression levels to less than half after 48 hours of treatment.

Stress	**AtPARG1 fold-change in expression levels**					
Time point in hours	**0**	**2**	**4**	**8**	**24**	**48**
Salt	1.00	1.02	0.96	0.99	0.92	0.18
Mannitol	1.00	0.85	0.91	1.47	2.19	1.97
Abscisic acid	1.00	0.96	0.56	0.42	0.74	0.58
Ethylene (ACC)	1.00	0.66	0.69	0.25	0.23	0.20
Auxin (NAA)	1.00	0.92	1.03	0.23	0.67	NA
Lipopolysaccharide	1.00	1.68	1.16	0.72	0.57	0.61
Jasmonic acid	1.00	0.71	0.68	0.62	0.57	0.44
Salicylic acid	1.00	1.54	1.66	1.43	1.00	0.47
Wounding	1.00	0.72	0.99	0.83	0.85	0.18
MMS	1.00	1.35	2.80	2.27	1.12	1.36
Bleomycin	1.00	3.55	5.66	4.57	2.22	2.37
UV-B	1.00	2.20	2.70	1.57	1.96	0.82

Table 5.6. SQRT-PCR determined expression levels of AtPARG1 in response to stress treatment
Transcript levels were taken at time points 0, 2, 4, 8, 24 and 48 hours. Transcript levels are expressed normalised to Actin2 expression. NA indicates transcript levels too low to measure.

The AtPARG2 expression levels after stress treatments are displayed in table 5.7 below. The DNA damaging agents MMS and bleomycin both induced transcript levels of AtPARG2. The peak of transcript after MMS treatment at 4.2-fold is seen after 8 hours, while the peak after bleomycin treatment at 4-fold was seen after 4 hours. UV-B treatment also increased AtPARG2 treatment with a peak of 3.7-fold seen after 24 hours of treatment, but the levels remained high at 3.5-fold after 48 hours.

Stress	**AtPARG2 fold-change in expression level**					
Time point in hours	**0**	**2**	**4**	**8**	**24**	**48**
Salt	1.00	1.77	2.30	2.50	3.46	1.67
Mannitol	1.00	1.05	1.10	1.35	1.27	1.18
Abscisic acid	1.00	1.84	0.96	1.23	1.27	1.18
Ethylene (ACC)	1.00	0.81	1.21	1.01	0.71	0.61
Auxin (NAA)	1.00	1.03	1.31	1.10	0.66	0.61
Lipopolysaccharide	1.00	0.83	1.03	0.91	0.80	0.87
Jasmonic acid	1.00	1.53	1.93	1.48	1.11	3.16
Salicylic acid	1.00	1.86	2.61	2.96	2.16	2.15
MMS	1.00	2.34	3.85	4.26	2.45	2.96
Bleomycin	1.00	2.36	4.00	3.24	2.60	3.04
UV-B	1.00	1.20	2.30	1.39	3.71	3.53

Table 5.7. SQRT-PCR determined expression levels of AtPARG2 in response to stress treatments
Transcript levels were taken at time points 0, 2, 4, 8, 24 and 48 hours. Transcript levels are expressed normalised to Actin2 expression.

5.2.3 Expression levels of AtPARPs and AtPARGs from public microarray data

There are many publicly available microarray databases. One of these is the eFP browser ((Winter *et al.*, 2007) http://www.bar.utoronto.ca/efp). This tool provides comprehensive transcript level analysis of *Arabidopsis* genes, through the collation of data from many different groups, and the information ranges from developmental and tissue specific data to hormone, chemical, biotic and abiotic treatments. The data showing transcriptional regulation of AtPARG1, AtPARP1, AtPARP2, and AtPARP3 was accessed at this site and is presented in the following sections. AtPARG2 (At2g31865) does not feature on the ATH1 affymetrix chip, most commonly used for microarray on *Arabidopsis* tissue, and so is therefore not included in this analysis. The average expression level data obtained from the eFP Browser was normalised to the levels of control samples taken at the same time points, to enable comparison between the fold-change of the different genes.

5.2.3.1 Expression levels in response to phytohormones

Wild type Col-0 seedlings were grown in liquid media for 7 days before phytohormone and mock treatment was applied for 30 minutes, 1 hour and 3 hours (Shimada lab) before the transcript levels were analysed by microarray. The relative normalised expression levels of PARylation family members for plants treated with 10 μM ethylene (ACC), 10 μM abscisic acid (ABA) and 1 μM Auxin (IAA) can be seen in figure 5.1. ABA is as mentioned in chapter 3, involved in the regulation of stomatal closing in response to water stress, as well as inducing seed dormancy. Auxin is involved in cell elongation and cell division. Ethylene is involved in the triple response of shoot and root growth and differentiation as well as the release of dormancy. While the transcript levels of AtPARP1, AtPARP2 and AtPARG1 remain invariant across the treatment times, AtPARP3 is up regulated by both treatment with ethylene and ABA. AtPARP3 transcript levels more than 5-fold increase after 1 hour of exposure, but then returns to basal levels after 3 hours. After 1 hour of ABA treatment, AtPARP3 levels increased by more than 4-fold, and this increased to more than 7-fold after 3 hours. No noticeable changes could be with application of Auxin.

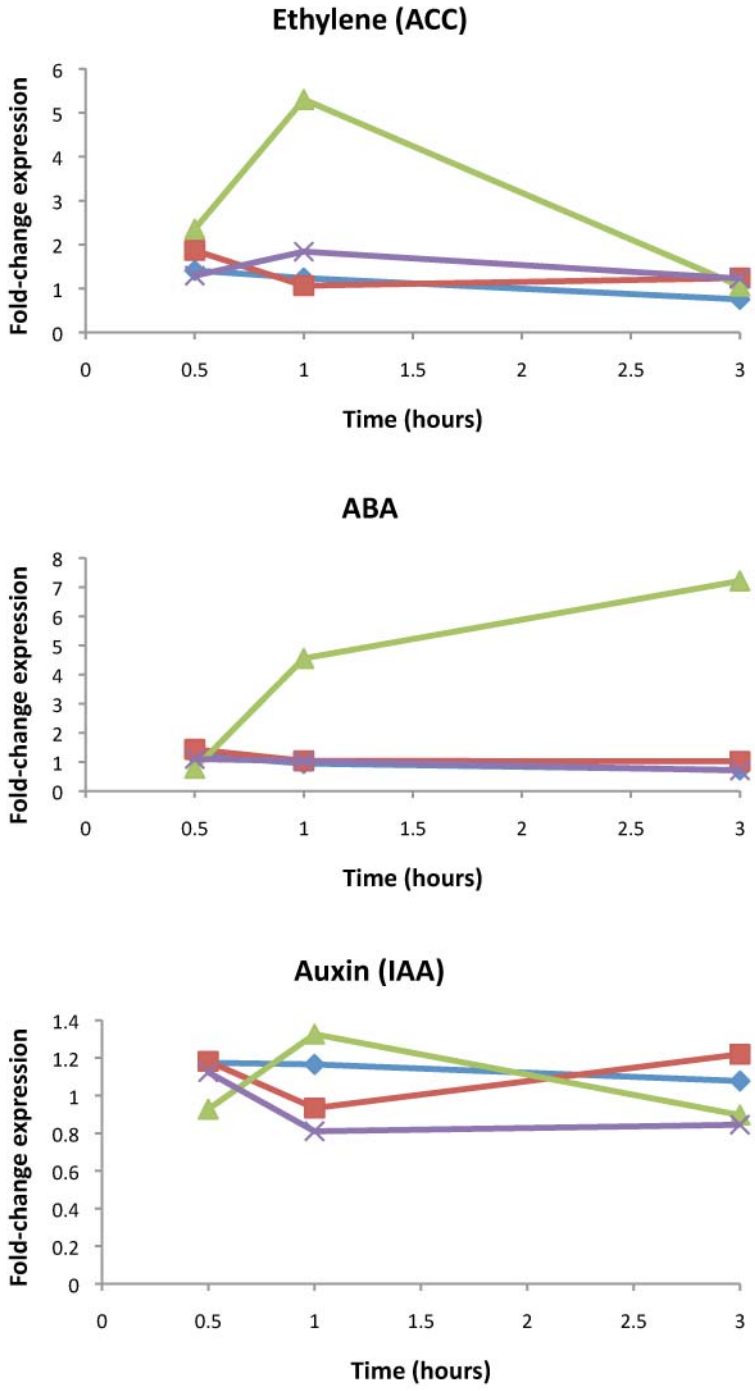

Figure 5.1. Changes in response to treatment with phytohormones
Wild type plants were grown for 7 days in liquid media before phytohormones were added. Plants were mock-treated or treated with ABA at 10 μM, ethylene at 10 μM and auxin (IAA) at 1 μM final concentration. Tissue was harvested after 30 min, one hour and 3 hours of exposure. Graphs represent the average fold-change in expression of AtPARP1 (blue), AtPARP2 (red), AtPARP3 (green) and AtPARG1 (purple) (n=2).

5.2.3.2 Expression levels in response to abiotic stresses

Stresses were applied to plants grown on rafts in liquid media in magenta boxes for 18 days in long day conditions. Transcript levels in separate shoot and root material were analysed by microarray after treatments with abiotic stress over a time course of 24 hours (Kilian *et al.*, 2007). The relative normalised expression levels of PARylation family members under the abiotic stress conditions are presented in figure 5.2. No distinct difference fromcontrol transcript levels for AtPARP1 or AtPARG1. For cold (rafts placed on crushed ice), salt (rafts floated in 150 mM NaCl) and osmotic (rafts floated in 300 mM mannitol) treatments the transcript levels of AtPARP3 in roots were upregulated after 12 hours. In shoots a rise in the AtPARP3 transcript was not seen until 24 hours after treatment began. Slight increases were see in the transcript levels of AtPARP2 in roots after 24-hour exposure to salt and mannitol, while no changes were observed in the roots. After heat treatment (38°C for 3 hours followed by continuous temperature of 25°C), a peak of AtPARP3 mRNA expression can be seen in shoots after 3 hours at the recovery temperature, after which it is returned to basal levels, while the mRNA expression in the root peaks after 12 hours. A slight peak in AtPARP2 expression levels is observed after 3 hours at the recovery temperature and the levels go down gradually until they reach basal levels after 24 hours. Drought stress (rafts placed in airstream for 15 minutes and back in liquid media for recovery) induced slight increases in transcript levels for AtPARP2, AtPARP3 and AtPARG1 after 30 minutes in both shoots and roots.

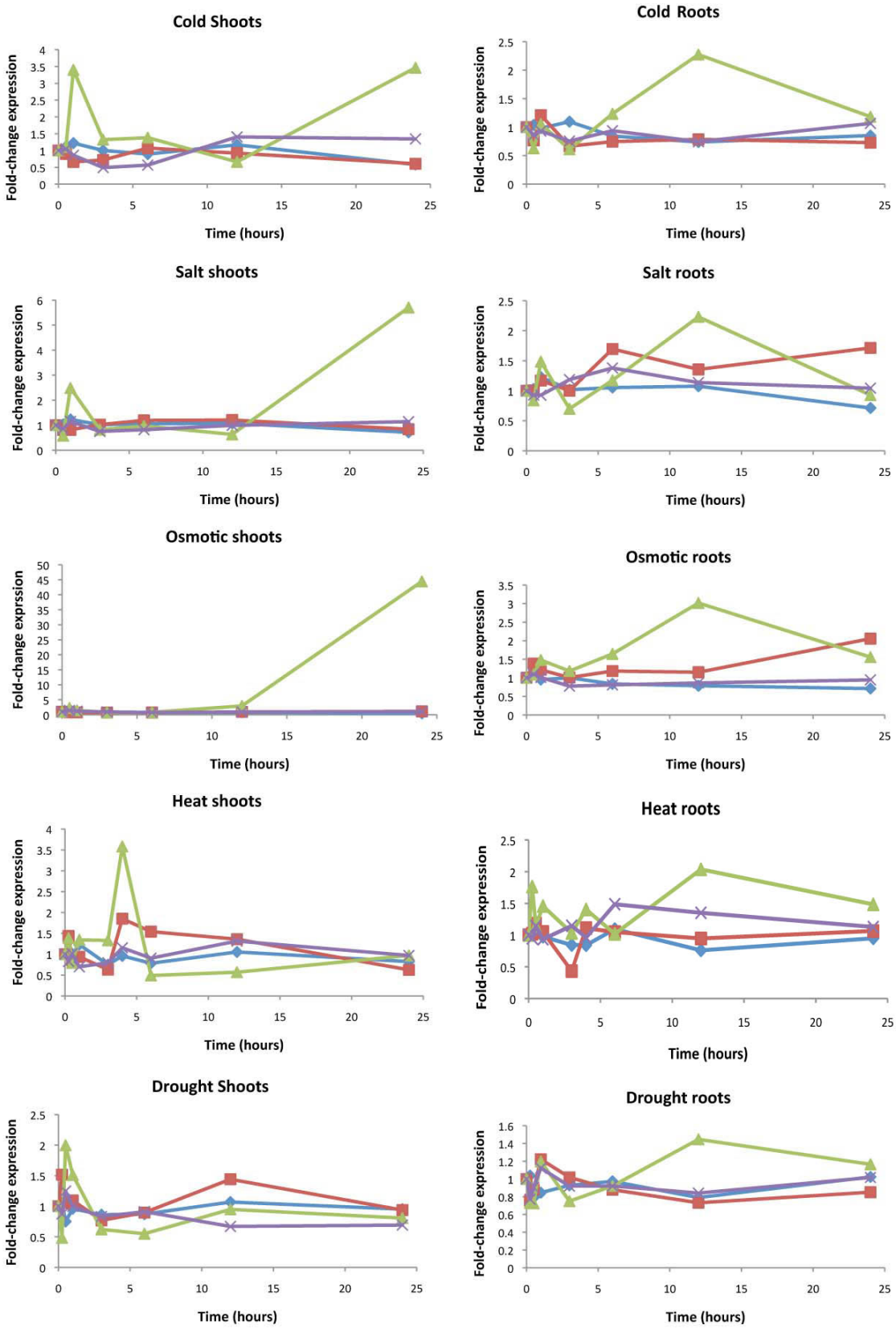

Figure 5.2. Changes in transcript levels in response to abiotic stress.
Abiotic stress treatments of 18 day old wild type plants grown in rafts. Cold 4°C on crushed ice, salt 150 mM NaCl, osmotic 300 mM mannitol, Heat 38°C 3 hours then 25°C continuous, drought 15 mins exposure to airstream. Graphs represent the average fold-change in expression of AtPARP1 (blue), AtPARP2 (red), AtPARP3 (green) and AtPARG1 (purple) (n=2)

5.2.3.3 Expression levels response to DNA damaging agents

Stresses were applied to plants grown on rafts in liquid media in magenta boxes for 18 days in long day conditions. Transcript levels in separate shoot and root material were analysed by microarray after treatments with DNA damaging agents over a time course of 24 hours (Kilian *et al.*, 2007). The relative normalised expression levels of PARylation family members under the genotoxic stress conditions are presented in figure 5.3. Genotoxic stress was applied as a combination of the double strand inducer bleomycin (1.5 μg/ml) and the DNA cross-linking agent mitomycin C (22μg/ml), a treatment, which had previously been shown to induce DNA damage (Chen *et al.*, 2003). This treatment induced a significant increase in the levels of AtPARP2 transcript in both shoots and roots after 30 minutes of treatment and this increase persisted until 24 hours after application of stress at which point it was still significantly different to basal levels. A less pronounced, but equally persistent, increase in AtPARP2 transcript levels in shoots was seen in response to UV-B treatment (15 mins of UV-B at 1.18 W m^{-2}, after which the boxes were placed back in control conditions), while in roots an increase was seen after 30 mins after which the transcript returned to basal levels. AtPARP1 also showed a persisting increase in transcript levels after exposure to DNA damaging agents, but this increase was much less pronounced than the one observed for AtPARP2, and was only found in roots and the temporal profile of expression was equal to AtPARP2 transcript levels. AtPARG1 transcript levels do not change in response to application of DNA damaging agents, but does show a slight increase initially after UV-B treatment in the shoots, and again after 24 hours in recovery conditions. An increase in ATPARP3 transcript levels was seen in shoots after 30 mins, and in roots after 12 hours. None of the genes showed any significant changes in response to oxidative stress treatment in the form of methyl viologen (10 μM).

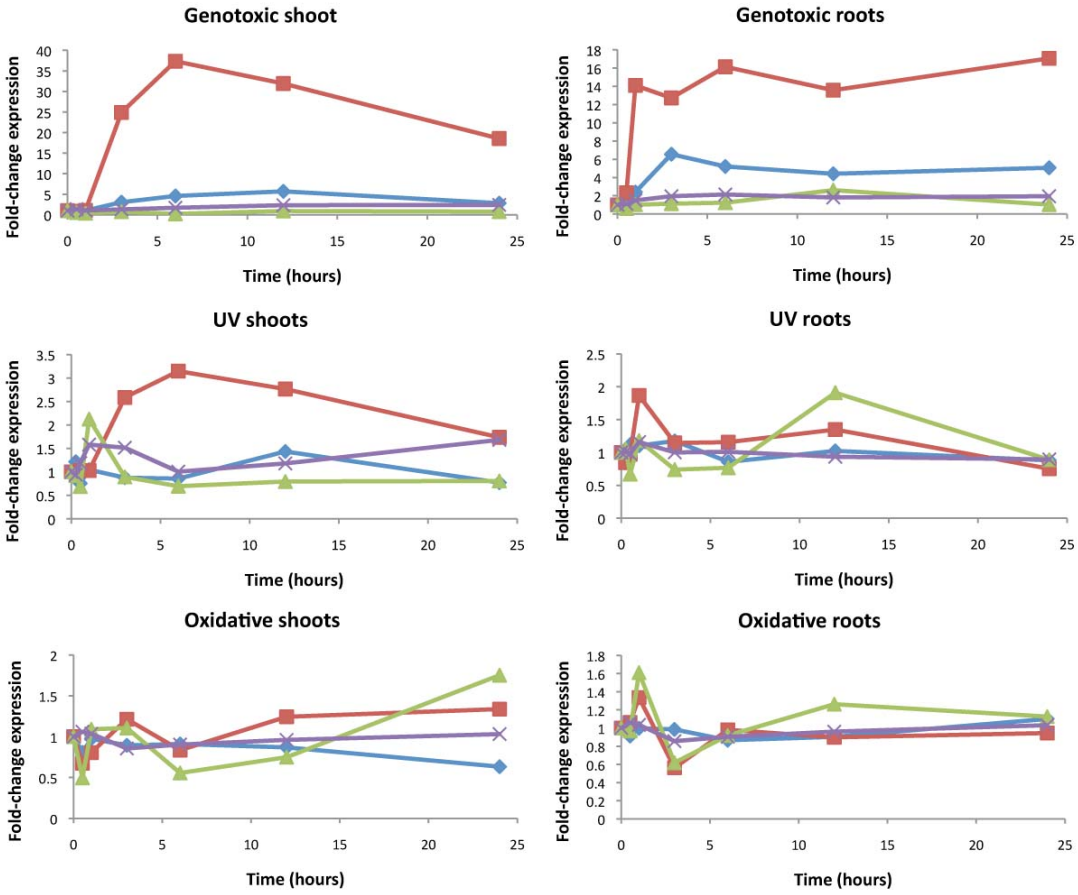

Figure 5.3. Changes in transcript levels in response to DNA damaging stresses
Genotoxic: 1.5 μg/ml bleomycin and 22 μg/ml mitomycin C, Oxidative 10 μM methyl viologen, UV-B: 15 minutes of UV-B light (1.18 W m^{-2}). Graphs represent the average fold-change in expression of AtPARP1 (blue), AtPARP2 (red), AtPARP3 (green) and AtPARG1 (purple) (n=2).

5.2.4 Serial analysis of gene expression (SAGE)

Similar to microarrays, serial analysis of gene expression (SAGE) (Velculescu *et al.*, 1995) provides quantitative information on gene expression but, unlike microarrays, SAGE detects unknown transcripts because it does not require prior knowledge of what is present in the sample under analysis, it can also detect alternatively spliced transcripts and antisense transcripts (Wang 2006). SAGE generates absolute rather than relative measurements of gene expression without the bias of predesigned hybridization probes for known genes. Although it does provide high sensitivity, the specificity of SAGE is lower than microarrays. The cost of SAGE is also currently lower than microarray, but it does require the right, very expensive, equipment. In addition, not all *Arabidopsis* genes are represented on the Affymetrix chips currently used to perform microarrays on Arabidopsis cDNA. For example, as mentioned earlier, AtPARG2 is not present. However, SAGE fails to detect 8% of the 33602 genes due to lack of a CATG site. The basic premise of SAGE is described in figure 5.4.

Serial analysis of gene expression (SAGE) was performed in collaboration with Mads Sønderkær and Dr Kåre Lehmann Nielsen at Aalborg University, Denmark.

For comparative transcript profiling, RNA was isolated from more than 200 two week old seedlings in control conditions as well as after 4 hours exposure to the alkylating agent MMS at a final concentration of 1.18 mM, as the RT-PCR data on wild type seedlings in table 5.6 revealed this to be the time point with the highest fold increase in expression after exposure. Quadruplicate biological replicate samples were extracted for each condition and prepared for DeepSAGE (Nielsen *et al.*, 2008) sequencing. Ultra-high-throughout sequencing of the samples resulted in between 4182964 and 13363987 sequence tags for each pooled sample library (WT, WTMMS, *parg1-2*, *parg1-2*MMS). Tags were discarded which were not seen in at least 4 replicates. Due to the short tag sequence length (21 bp), a number of tags were assigned to multiple genes. Therefore, all further analysis was restricted to tags that had been unambiguously assigned to a single gene. Tag counts were normalised to counts per million, to allow comparison across the libraries. This left 9186 genes, which were annotated to

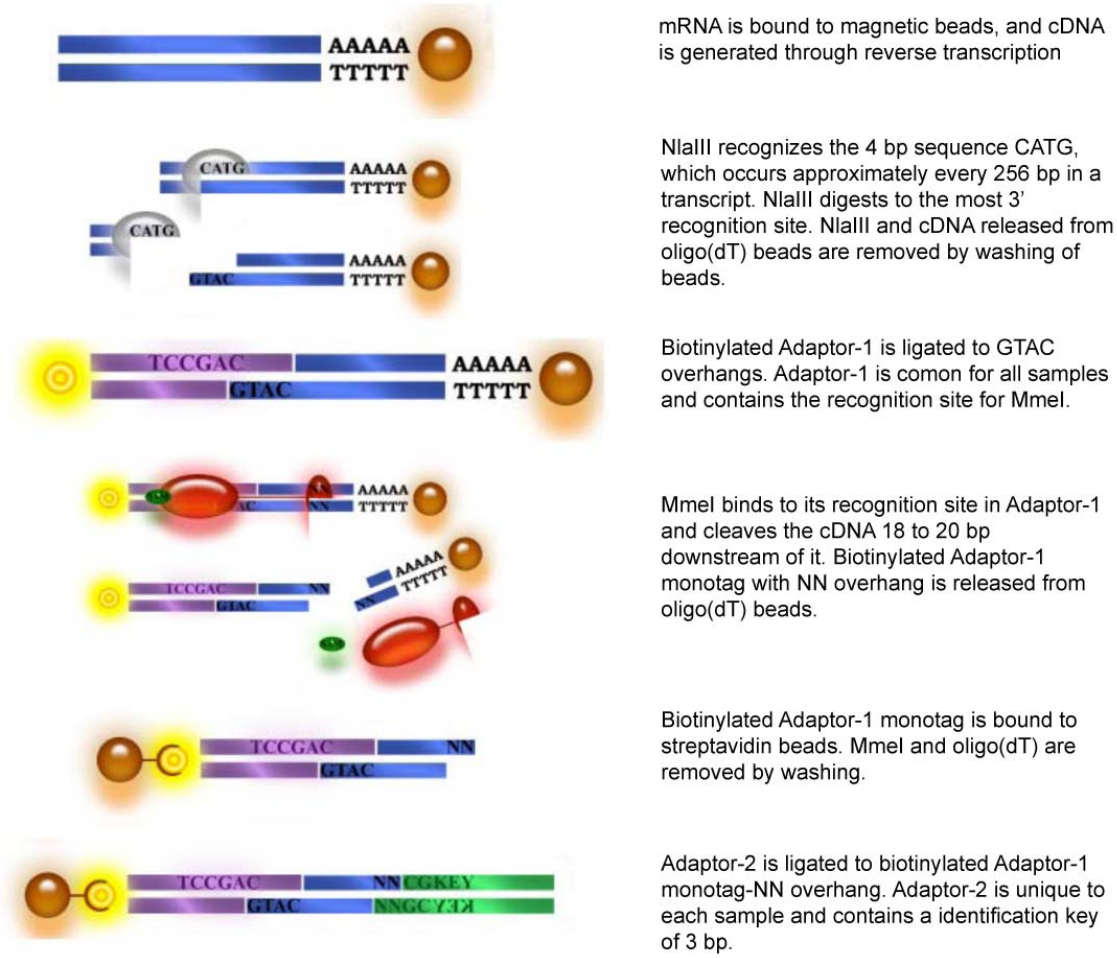

Figure 5.4. DeepSAGE methodology.

The basic premise of SAGE is explained in the figure. RNA from samples is made into double stranded cDNA which is attached to oligo(dT) beads. The enzyme NlaIII cuts at the most 3' recognition site and the most 3' cDNA attached to the oligo beads is ligated to a biotinylated Adaptor-1, which is common for all samples. A second restriction enzyme, MmeI, binds to a recognition site in the Adaptor-1 and cuts 18 to 20bp downstream of this site. A second sample specific adaptor-2 molecule, containing a 3 bp identification key, is then ligated to the opposite end of Adaptor-1. Using primers for the known sequences of Adaptor-1 and -2, PCR reactions are performed, which are then diluted to equimolar concentrations before running in a sequencer.

the *Arabidopsis* genome. Genes were considered differentially regulated, if they showed more than a 2-fold change in expression values ($p \leq 0.01$).

5.2.4.1 Comparison of transcriptomes of untreated wild type and *parg1-2*

A comparison of the wild type and *parg1-2* control libraries, revealed 1796 genes to be differentially regulated. Of these genes 133 were found to be ≥5-fold down-regulated in *parg1-2* libraries compared with wild type, while 566 genes were ≥5-fold up-regulated. To assess regulation of groups of functionally related genes in these two data sets, the genes were analysed using the DAVID online functional annotation tool (www.david.abcc.ncifcrf.gov), and the most enriched gene ontology (GO) terms ($p<0.01$) are listed in table 5.8 and 5.9 below. An over-representation of genes involved in proteasomal degradation, transcriptional regulation and auxin signalling was seen in up-regulated genes (table 5.8), while the down-regulated genes represented were involved in oxidative and abiotic stress as well as JA-signalling (table 5.9).

GO term	*p*-value
proteolysis involved in cellular protein catabolic process (GO:0051603)	1.97E-04
proteasome complex (GO:0000502)	0.009864596
regulation of translation (GO:0006417)	0.006946272
auxin mediated signaling pathway (GO:0009734)	0.009449998

Table 5.8. Gene ontologies for genes up-regulated more than 5-fold in *parg1-2* compared with wild type

GO term	*p*-value
oxidation reduction (GO:0055114)	0.006141294
response to abiotic stimulus (GO:0009628)	0.006652456
jasmonic acid mediated signaling pathway (GO:0009867)	9.94E-04

Table 5.9. Gene ontologies for genes down-regulated more than 5-fold in *parg1-2* compared with wild type

As mentioned earlier, the number of genes that are more than 5-fold up-regulated in *parg1-2* compared with wild type is more than 4 times higher. The 20 most differentially regulated genes are listed in table 5.10 and 5.11. Of the up-regulated genes, not very many have been characterised. Among the most down-regulated proteins, one of the only proteins described in the literature is the Cop9 signalosome 5A subunit, which is involved in proteasomal degradation.

Gene ID	Name	Fold change
AT3G54970	D-aminoacid aminotransferase-like PLP-dependent enzymes superfamily protein	646.2
AT4G39150	DNAJ heat shock N-terminal domain-containing protein	389.0
AT3G57610	adenylosuccinate synthase	341.3
AT1G71270	Vps52 / Sac2 family	219.1
AT2G01710	Chaperone DnaJ-domain superfamily protein	164.3
AT5G50430	ubiquitin-conjugating enzyme 33	158.8
AT4G08035	other RNA	121.9
AT1G80210	Mov34/MPN/PAD-1 family protein	110.7
AT1G29355	unknown protein	97.6
AT2G31730	basic helix-loop-helix (bHLH) DNA-binding superfamily protein	95.3
AT3G11550	Uncharacterised protein family (UPF0497)	95.3
AT1G80570	RNI-like superfamily protein	89.7
AT4G28780	GDSL-like Lipase/Acylhydrolase superfamily protein	86.5
AT5G63480	unknown protein	83.1
AT5G63200	tetratricopeptide repeat (TPR)-containing protein	62.1
AT5G40460	unknown protein	58.3
AT2G39050	hydroxyproline-rich glycoprotein family protein	52.9
AT4G14550	indole-3-acetic acid inducible 14	50.9
AT3G24820	BSD domain-containing protein	49.3
AT4G26160	atypical CYS HIS rich thioredoxin 1	47.3

Table 5.10. The 20 most up-regulated genes in *parg1-2* control

Gene ID	Name	Fold change
AT5G10040	unknown protein	-722.5
AT4G17510	ubiquitin C-terminal hydrolase 3	-222.0
AT2G44090	Ankyrin repeat family protein	-218.8
AT4G27730	oligopeptide transporter 1	-153.4
AT2G33430	differentiation and greening-like 1	-125.8
AT3G09100	mRNA capping enzyme family protein	-109.4
AT1G22920	COP9 signalosome 5A	-105.0
AT3G47630	CONTAINS InterPro DOMAIN/s: Mitochondrial matrix Mmp37	-105.0
AT3G56050	Protein kinase family protein	-101.9
AT1G17420	lipoxygenase 3	-92.4
AT5G44730	Haloacid dehalogenase-like hydrolase (HAD) superfamily protein	-86.1
AT4G30260	Integral membrane Yip1 family protein	-84.3

AT1G61770	Chaperone DnaJ-domain superfamily protein	-83.0
AT3G13040	myb-like HTH transcriptional regulator family protein	-81.1
AT3G52790	peptidoglycan-binding LysM domain-containing protein	-74.8
AT3G10330	Cyclin-like family protein	-67.9
AT2G38360	prenylated RAB acceptor 1.B4	-61.3
AT1G66350	RGA-like 1	-61.0
AT5G26280	TRAF-like family protein	-56.1
AT5G01270	carboxyl-terminal domain (ctd) phosphatase-like 2	-55.3

Table 5.11. The 20 most down-regulated genes in *parg1-2* control

5.2.4.2 Comparison of transcriptomes of MMS treated wild type and *parg1-2*

To examine any differences in the transcriptomes of the *parg1-2* and the WT when treated with MMS, the fold differences in tag counts between treated and the control libraries were used. When examining MMS treated WT seedlings it was found that 4467 genes were differentially regulated. For the MMS treated *parg1-2* seedlings 3448 genes were differentially regulated. Of these 1305 were found to be unique for *parg1-1*, and 2324 were unique for WT. The data set contained 2143 genes that were significantly differentially regulated, 88 of which were regulated in opposite directions for each genotype (figure 5.4).

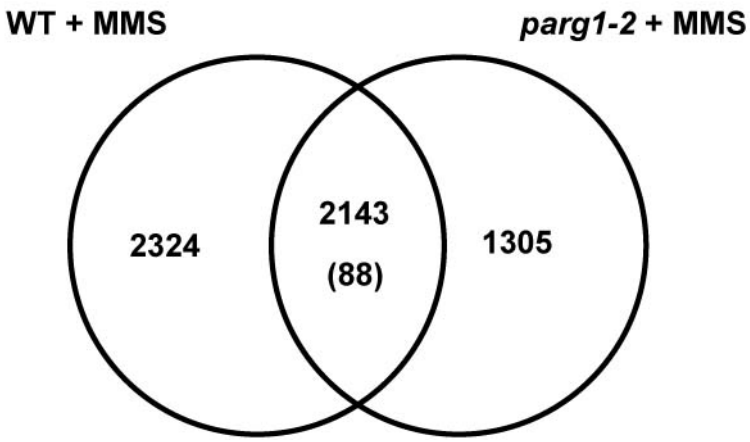

Figure 5.5. Comparative transcript profiling of MMS treated wild type and *parg1-2* seedlings
Venn diagram showing the number of genes with more than a 2-fold change ($p \leq 0.01$), which differentially regulated between wild type and *parg1-2* seedlings treated with MMS. The number in parentheses represents the number of genes that are common to both genotypes, but regulated in different directions.

To assess regulation of groups of functionally related genes in these two data sets, the genes were analysed using the DAVID online functional annotation tool The most enriched gene ontology (GO) terms (p<0.01) in genes up-regulated more than 5-fold in MMS treated wild type and *parg1-2* are listed in tables 5.12 and 5.13 below. The number of genes down-regulated in both data sets were too few to generate any significantly enriched clusters of GO terms. The GO term categories in which genes unique for MMS treated wild type were over-represented, included protein degradation and translational regulation. When analysing the up-regulated genes unique for *parg1-2* treated with MMS, a significant over-representation of genes involved in co-factor synthesis, responses to stresses, and photosynthetic regulation was observed.

GO term	*p*-value
membrane-enclosed lumen (GO:0031974)	2.13E-07
nuclear body (GO:0016604)	1.76E-04
RNA processing (GO:0006396)	1.81E-05
translation factor activity, nucleic acid binding (GO:0008135)	2.24E-04
proteasome complex (GO:0000502)	5.22E-05
protein serine/threonine phosphatase activity (GO:0004722)	8.75E-04
ubiquitin-dependent protein catabolic process (GO:0006511)	0.002030761
CUL4 RING ubiquitin ligase complex (GO:0080008)	0.007427974
regulation of translation (GO:0006417)	0.006801482

Table 5.12. Gene ontologies for genes upregulated more than five-fold in wild type seedlings treated with MMS

GO term	*p*-value
cofactor biosynthetic process (GO:0051188)	0.002685451
response to organic substance (GO:0010033)	0.009396805
response to abiotic stimulus (GO:0009628)	0.007031904
chloroplast part (GO:0044434)	3.67E-04

Table 5.13. Gene ontologies for genes up-regulated more than five-fold in *parg1-2* seedlings treated with MMS

To further analyse the difference in transcriptomes between MMS treated wild type and *parg1-2*, the 88 genes that that were regulated in opposite directions in the two data sets were examined closer, as there were too few present to generate valid data using the gene ontology analysis tool (table 5.14). Among these was the circadian clock regulator time for coffee (TIC) (Ding *et al.*, 2007), which was decreased by nearly 4-fold in *parg1-2*, but 22-fold up-regulated in wild type. Another gene was oxidative stress 3 (OXS3), which is involved in tolerance to a range of metals (Blanvillain *et al.*, 2008). This gene was decreased by more than 8-fold in *parg1-2*, but showed more than 10-fold increase in wild type.

Gene ID	Name	Fold change WT MMS	Fold change *parg1-2* MMS
AT2G44090	Ankyrin repeat family protein	0.42	355.58
AT3G52790	peptidoglycan-binding LysM domain-containing protein	0.23	93.08
AT4G35480	RING-H2 finger A3B	0.44	16.51
AT5G52540	Protein of unknown function (DUF819)	0.29	12.57
AT1G13880	ELM2 domain-containing protein	0.47	12.56
AT3G47000	Glycosyl hydrolase family protein	0.27	10.18
AT4G33700	CBS domain-containing protein with a domain of unknown function (DUF21)	0.32	10.13
AT4G01050	thylakoid rhodanese-like	0.27	8.74
AT5G27420	carbon/nitrogen insensitive 1	0.20	7.49
AT3G17185	TAS3/TASIR-ARF (TRANS-ACTING SIRNA3); other RNA	0.39	5.01
AT3G01670	unknown protein	0.41	4.71
AT5G08260	serine carboxypeptidase-like 35	0.32	4.56
AT3G18250	Putative membrane lipoprotein	0.34	4.54
AT5G41340	ubiquitin conjugating enzyme 4	0.26	4.31
AT1G55670	photosystem I subunit G	0.23	3.84
AT1G45201	triacylglycerol lipase-like 1	0.18	3.63
AT5G62360	Plant invertase/pectin methylesterase inhibitor superfamily protein	0.29	3.54
AT1G31330	photosystem I subunit F	0.38	3.30
AT1G72610	germin-like protein 1	0.38	2.84
AT3G12500	basic chitinase	0.19	2.75
AT5G23060	calcium sensing receptor	0.22	2.68
AT5G23940	HXXXD-type acyl-transferase family protein	0.39	2.60
AT2G45130	SPX domain gene 3	0.32	2.51
AT2G23670	homolog of Synechocystis YCF37	0.40	2.13

AT3G20250	pumilio 5	3.55	0.48
AT4G02500	UDP-xylosyltransferase 2	4.06	0.48
AT1G19660	Wound-responsive family protein	9.78	0.46
AT1G06240	Protein of unknown function DUF455	7.94	0.45
AT1G64680	unknown protein	2.59	0.44
AT5G49080	transposable element gene	2.72	0.42
AT1G21670	CONTAINS InterPro DOMAIN/s: WD40-like Beta Propeller (InterPro:IPR011659), Six-bladed beta-propeller, TolB-like (InterPro:IPR011042)	4.24	0.42
AT2G45990	unknown protein	4.46	0.41
AT4G24805	S-adenosyl-L-methionine-dependent methyltransferases superfamily protein	5.75	0.41
AT2G42890	MEI2-like 2	5.55	0.40
AT3G18560	unknown protein	10.42	0.40
AT2G33730	P-loop containing nucleoside triphosphate hydrolases superfamily protein	3.74	0.39
AT5G45480	Protein of unknown function (DUF594)	2.59	0.39
AT3G11530	Vacuolar protein sorting 55 (VPS55) family protein	4.77	0.37
AT5G41790	COP1-interactive protein 1	2.23	0.37
AT1G73060	Low PSII Accumulation 3	3.44	0.37
AT1G05785	Got1/Sft2-like vescicle transport protein family	3.89	0.36
AT3G28920	homeobox protein 34	8.16	0.36
AT5G06560	Protein of unknown function, DUF593	3.05	0.36
AT2G30700	unknown protein	4.21	0.36
AT2G43410	RNA binding	5.20	0.35
AT1G10910	Pentatricopeptide repeat (PPR) superfamily protein	13.15	0.35
AT5G03970	F-box associated ubiquitination effector family protein	5.10	0.35
AT5G47080	casein kinase II beta chain 1	7.99	0.33
AT3G24550	proline extensin-like receptor kinase 1	15.80	0.29
AT5G15190	unknown protein	6.23	0.29
AT3G22380	time for coffee	22.28	0.28
AT1G10270	glutamine-rich protein 23	9.06	0.28
AT3G08020	PHD finger family protein	6.86	0.27
AT2G18370	Bifunctional inhibitor/lipid-transfer protein/seed storage 2S albumin superfamily protein	2.11	0.27
AT1G30000	alpha-mannosidase 3	3.06	0.27
AT5G62680	Major facilitator superfamily protein	2.74	0.25
AT4G40065	other RNA	2.53	0.24
AT5G39530	Protein of unknown function (DUF1997)	5.19	0.24
AT2G22970	serine carboxypeptidase-like 11	3.91	0.23
AT5G18120	APR-like 7	3.78	0.23
AT1G47550	exocyst complex component sec3A	6.54	0.23
AT4G26190	Haloacid dehalogenase-like hydrolase (HAD) superfamily protein	31.47	0.22

AT1G67230	little nuclei1	4.55	0.22
AT4G27040	EAP30/Vps36 family protein	7.08	0.22
AT3G22290	Endoplasmic reticulum vesicle transporter protein	6.70	0.20
AT4G13720	Inosine triphosphate pyrophosphatase family protein	10.51	0.20
AT3G54840	Ras-related small GTP-binding family protein	17.58	0.20
AT5G65110	acyl-CoA oxidase 2	28.97	0.20
AT3G10572	3-phosphoinositide-dependent protein kinase-1, putative	15.35	0.20
AT2G45210	SAUR-like auxin-responsive protein family	2.81	0.19
AT4G39150	DNAJ heat shock N-terminal domain-containing protein	131.76	0.19
AT4G02720	unknown protein	50.48	0.19
AT2G19180	unknown protein	4.62	0.19
AT4G24680	modifier of snc1	5.64	0.18
AT1G48240	novel plant snare 12	25.00	0.18
AT4G38120	ARM repeat superfamily protein	4.36	0.18
AT1G44800	nodulin MtN21 /EamA-like transporter family protein	3.37	0.16
AT4G35850	Pentatricopeptide repeat (PPR) superfamily protein	26.21	0.16
AT1G32160	Protein of unknown function (DUF760)	8.89	0.13
AT3G59990	methionine aminopeptidase 2B	3.62	0.13
AT5G56550	oxidative stress 3	10.45	0.11
AT2G20142	Toll-Interleukin-Resistance (TIR) domain family protein	9.39	0.05
AT1G80160	Lactoylglutathione lyase / glyoxalase I family protein	3.82	0.03
AT4G14550	indole-3-acetic acid inducible 14	29.92	0.01
AT1G32190	alpha/beta-Hydrolases superfamily protein	5.46	0.01
AT1G11210	Protein of unknown function (DUF761)	5.13	0.01
AT1G32900	UDP-Glycosyltransferase superfamily protein	6.44	0.01
AT1G20160	Subtilisin-like serine endopeptidase family protein	5.35	0.00

Table 5.14. Genes regulated in opposite directions in MMS-treated WT and *parg1-2* seedlings

5.3 Discussion

The first three sections of this chapter analysed the transcriptional response of PARylation gene family members to different stress treatments. Analysis of promoter regions, public microarray data and SQRT-PCR gave both consistent and inconsistent results. Both AtPARP1 and AtPARP2 transcript levels were increased after treatment with genotoxic stress agents. AtPARP2 transcript levels were shown to be more abundant than AtPARP1 in response to genotoxic stress both from the microarray data obtained using eFP Browser as well as from the RT PCR data. These results are similar to those previously found by others (Culligan *et al.*, 2006; Chen *et al.*, 2003; Doucet-Chabeaud *et al.*, 2001). AtPARP3 also shows slight upregulation in response to genotoxic stress, but not to the same levels as seen with the other two AtPARPs. AtPARP3 showed a similar fold increase to AtPARP1 in response to bleomycin in the SQRT-PCR data, while the microarray data showed a distinct difference between the fold increases of these two genes. In addition, UV-B treatment elicited an increase AtPARP3 levels in both data sets. Since AtPARP3 does not contain any known DNA binding domains, it would be interesting to find out if this gene is involved in the response to DNA damage or if it just displays a general stress response.

Any information concerning regulation and function of AtPARP3, has so far been very limited. This gene has been shown to be abundantly transcribed in the developing seed (Hunt *et al.*, 2007; Becerra *et al.*, 2006). While analysis of the promoter regions revealed the presence of several ABA response, abiotic and water stress elements in all the genes, only AtPARP3 transcripts were noticeably upregulated by the abiotic stress treatments in both public microarray data and our SQRT-PCR experiments. A pronounced upregulation of AtPARP3 transcript is seen in samples treated with ABA, salt, mannitol and auxin. The only abiotic treatment, which did not induce a clear increase in AtPARP3 transcript in the public databases, was drought. However, the protocol used for drought treatment consisted of exposing seedlings to an airstream for 15 minutes, which may not be sufficient to induce the expression of genes normally associated with drought, as it is a very short and extreme treatment, that may not optimally emulate the type of drought stress normally experienced in a soil grown plant. A recent paper showed that AtPARP3 transcript was significantly induced by both

salt and high light stress (Ishigawa *et al.*, 2009). As mentioned previously this PARP contains no known DNA binding domains, so considering the data presented here, a role for AtPARP3 outside conventional DNA damage repair could be proposed. The SQ-RTPCR data described in this thesis were obtained from two week old seedlings, while the data presented on the eFP browser were generated using tissue from 18 day old plants, and neither reveal any tissue specificity. We have cloned the putative promoter region from AtPARP3 and generated transgenic lines, which contain this region upstream of a GUS reporter gene. These lines could help determine any tissue specificity with regards to transcript abundance in response to ABA, salt, mannitol and other abiotic stresses.

AtPARG1 contains several abiotic stress response elements in its putative promoter region. Despite this, no noticeable changes in transcript levels could be seen after treatment with abiotic stress.

For AtPARG2, the levels were highest in samples treated with genotoxins, but also UV-B and salt treated samples showed an increase in transcript level. A link between plant pathogen reponse and PARylation has been shown (Adams-Phillips *et al.*, 2008; Adams-Phillips *et al.*, 2010). All promoter regions except AtPARP3, contain W-boxes, which are involved in plant immunity (Pandey *et al.*, 2009). In addition AtPARG2 levels were also increased after exposure to JA and SA, which are phytohormones used in signalling in response to pathogens. AtPARG2 transcript levels were upregulated in response to treatment with bacterial pathogens and fungi (Adams-Phillips *et al.*, 2008; Adams-Phillips *et al*. 2010). Since AtPARG2 is not present on the Affymetrix chips most commonly used for *Arabidopsis* microarrays, there is limited information available on transcriptional responses to stresses for this gene. The information obtained in this study, could help in providing a clue to potential functions of AtPARG2 in stress responses.

A microarray study describing the types of genes differentially regulated in response to MMS treatment (100 ppm) for 24 hours has previously been published (Kim *et al.*, 2006). Most of the genes identified as highly up-regulated by this microarray were not present in the SAGE data generated for this study. However, the study by Kim (2006) revealed that several genes involved in the ubiquitin 26S proteasome pathway were up-reglated. Similar categories of genes

were increased in the MMS treated wild type data presented here. Notably, the microarray found 3 chlorophyll A/B binding proteins were down-regulated in response to MMS, while the SAGE data here showed 4 chlorophyll A/B binding proteins to be more than two-fold up-regulated in MMS treated *parg1-2*. The lack of upregulation of similar genes to this microarray in our study could be due to the differences in methodology or perhaps the length and intensity of the MMS treatment applied. None of the genes normally associated with DNA repair were seen to be up-regulated in the our MMS treated data sets. This could be due to a lack of desired effect of the treatment. The duration of treatment chosen was due to the transcript levels of AtPARG1 observed during the SQRT-PCR time series, where it showed the highest levels over the period measured. Since the MMS hypersensitive phenotype of *parg1-2* seedlings do not manifest until 5-6 days after starting treatment, a later time point for harvesting the tissue should perhaps have been chosen. Alternatively, treatment with a different DNA damaging agent could be employed.

Of the genes regulated in opposite directions after MMS treatment were two genes known to be involved in circadian rhythm. Time for Coffee (TIC), a nucleus acting clock regulator, which works close to the central oscillator (Ding *et al.*, 2007) was 3.4-fold down regulated in *parg1-2* seedlings exposed to MMS, but 22.1-fold upregulated in wild type. CCA1 was increased more than 4-fold in *parg1-2*, but more than 4-fold reduced in the wild type. However, the value for the CCA1 levels in wild type were not significant (p= 0.08). These observations may represent a link to the altered circadian phenotype observed in the AtPARG1 mutant *tej* (Panda *et al.*, 2002). Interestingly, AtNUDX7 was down-regulated by 5.6-fold in *parg1-2* without stress, but was increased in both treated *parg1-2* and wild type by 15 and 3.5-fold respectively. This protein breaks down ADP-ribose, which is generated by AtPARG activity (Ishikawa *et al.*, 2009). In mammals, the types of PAR seen when no external DNA damage is present, are metabolically stable mono or oligo ADP-ribose units on target proteins. When stimulated by DNA strand breaks, much longer and more complicated structures are produced (Benjamin and Gill, 1980 a), and these two types of polymer differ greatly in their turnover rate (Wielckens *et al.*, 1983; Alvarez-Gonzalez and Althaus, 1989). The difference in levels of AtNUDX7

observed could perhaps be due to a change in the normal PAR polymer composition.

6 Final Discussion

Post-translational protein modifications all involve the attachment of smaller chemical groups or moieties. The most well known types of modification include phosphorylation, which is involved in the activation or deactivation of enzymes, methylation, best known for its action on histones, which influences the availability of DNA for transcription, and ubiquitination, which targets proteins for degradation. The lesser known post-translational modification mechanism of poly(ADP-ribosyl)ation has been well characterized in mammals, where it is involved in many different cellular processes such as cell division, telomere maintenance, programmed cell death, chromatin structure, gene expression and DNA damage repair (for review see Hassa and Hottiger, 2008; D'Amours *et al.*, 1999). The functions of this modification in organisms other than mammals are much less known. The overall aims of this study was to expand the current knowledge on PARylation in plants initially through the first collective characterisation of insertionally inactivated lines of all the different members of the plant PARylation family members so far identified.

6.1 Roles of poly(ADP-ribosyl)ation in response to DNA damaging agents

PARP expression in mammals is constitutive, and the regulation of activity takes place at the protein level. In plants, however, the regulation takes place at the transcriptional level as both AtPARP1 and AtPARP2 transcripts are up-regulated after application of DNA damaging agents (Chen *et al.*, 2003; Culligan *et al.*, 2006; Doucet-Chabeaud *et al.*, 2001) and AtPARP2 is in fact one of the genes that show the highest increase (50 to 100-fold, depending on the type of DNA damaging agent applied and the methodology). The transcriptional profiles of these genes in response to genotoxic stress were confirmed in this study. In mammals, single PARP1 and PARP2 null mice are viable, but hypersensitive to genotoxic stress (de Murcia *et al.*, 1997; Schreiber *et al.*, 2002), while double mutants are embryonic lethal (Menissier de Murcia *et al.*, 2003). Since AtPARP2 is one of the most up-regulated genes in response to genotoxic stress, a phenotype in mutants of this gene would be predicted after exposure to DNA damaging agents. However, exposure of both *parp1-1* and *parp2-1* T-DNA

insertion lines to DNA damaging stress, failed to show a phenotype. This indicates the redundancy between the two genes. When insertional mutants were germinated on media containing the alkylating agent MMS, *parp2-1* had higher germination rates than wild type. This could indicate that the energy consumption during germination in these seedlings is decreased as the replenishment of NAD^+, through the *de novo* pathway, or the salvage pathway, uses five and three molecules of ATP, respectively, per molecule of NAD^+. The reduction in energy expenditure could therefore result in an increase in cell division.

The protein kinase ataxia telangiectasia mutated (ATM) is a key regulator of several DNA damage response pathways in mammals (Shiloh, 2006). The plant homologue AtATM is involved in changing gene expression following DNA damage and controls the expression of AtPARP1 and AtPARP2 as well as AtPARG1 as no increases in transcript of these genes were observed in *Atatm* mutants (Culligan *et al.*, 2006). AtATM also controls the expression of the plant specific transcription factor suppressor of gamma response 1 (AtSOG1), which was proposed to function as a plant analogue to the animal p53. It is responsible for most of the changes in transcription such as after DNA damage and was also shown to control the expression of AtPARP1 and AtPARP2 (Yoshiyama *et al.*, 2009). When mutants of AtKu80, the plant protein homologue of a protein involved in double strand break repair Ku80, were treated with bleomycin, AtPARP2 transcript levels were significantly higher in these plants, than in bleomycin treated WT. This could indicate that AtPARP2 has a role in putative DSB backup repair pathways (West *et al.*, 2004). In mammals, the DNA scaffold protein X-ray repair cross-complementing 1 (XRCC1) is involved in the assembly of DNA damage repair complexes at sites of breaks in response to single strand breaks, and its interaction with PARP1 is well documented (Masson *et al.*, 1998). The rice homologue OsXRCC1 was upregulated in response to the DSB-inducing agent bleomycin, while no change could be observed in transcript levels after treatment with the single strand inducing agents MMS or H_2O_2 (Uchiyama *et al.*, 2008). Moreover, a mutant line of AtXRCC1 displayed a hypersensitive phenotype in response to γ-irradiation (Charbonnel *et al.*, 2010), but also showed an increase in transcript levels in response to oxidative stress (Ishigawa *et al.*, 2009). These differences from mammals in the assignment of proteins to DNA

repair pathway could perhaps explain why the well-established interaction of PARP1 and XCRR1 could not be seen in *in vitro* yeast two-hybrid experiments in this study.

AtPARG1 and AtPARG2 transcript levels were increased after treatment with both MMS and bleomycin, but only *parg1* lines were shown to be hypersensitive to these stresses. The levels of PAR in these lines were examined using an anti-PAR antibody. While an increase in PAR levels could be seen in the wild type seedlings after application of both MMS and bleomycin, the levels in the *parg1-2* seedlings remained unchanged. The *parg2-1* seedlings, however, contained lower PAR content under control conditions. Moreover, while the levels of PAR in *parg2-1* showed no change after application of bleomycin, after 4 hours of MMS exposure they increased to a level comparable to that observed in wild type after 8 hours. The anti-PAR antibody used has a 10-fold greater affinity for polymers above 15 units. Since the longest chain length described in plants is 45 units (Chen *et al.*, 1994; Mahajan and Zuo, 1998), this method may not have detected shorter polymers.

6.2 Poly(ADP-ribosyl)ation in abiotic stress

The link of PARylation to abiotic stress, which had previously been proposed in several papers, was further established in this study. All of the upstream promoter regions of the 5 PARylation genes were found to contain several abiotic stress response elements, and in AtPARP3 in particular. Transcriptional analysis conducted for this study as well as microarray database entries revealed AtPARP3 to be differentially regulated by ABA treatment, salt and osmotic stress, while none of the other genes analysed showed similar increases. Sensitivity to abiotic stress in the form of salt and osmotic stress was seen in *parg1* and *parg2* lines. These results indicate that PARylation is involved in plant responses to abiotic stress. In a recent study in mouse cells, PARP1 and PARG were shown to control extracellular Ca^{2+} fluxes into the cell after exposure to oxidative stress (Blenn *et al.*, 2011). The calcium channel melastatin-like transient receptor potential 2 (TRPM2) contains a NUDIX box sequence motif with a binding site for ADP-ribose, the breakdown product of PARG activity on PAR. The gating of this channel was shown to be sensitive to intracellular ADP-

ribose concentration. Ca^{2+} influx was reduced in cells in which PARP1 activity had been abolished and in cells with reduced levels of PARG. Abiotic stress in plants is a form of oxidative stress as it triggers the formation of ROS, and the regulation of stomatal closure in response to abiotic stress is triggered by an increase in intracellular Ca^{2+} concentration. It has been shown that *parg1-3* plants show reduced stomatal closure in response to drought stress (Li *et al*., 2011). Measuring stomatal apertures as well as Ca^{2+} flux in response to abiotic stress and application of ABA in the T-DNA insertion lines used in this study could help elucidate the role of PARylation in the response to abiotic stress. In addition, analysis of Ca^{2+} channels in *Arabidopsis* for NUDIX motifs and regulation of channels after application of ADP-ribose would determine whether the same type of mechanism observed in mammals after oxidative stress operates in plants.

6.3 Activity and localisation of AtPARGs

PARG in mammals exists as a single gene with several isoforms. So far, the only organisms found to contain more than one PARG gene are nematodes and plants. Due to the fact that AtPARG2 is not present on the microarray chips most commonly used for plant transcriptional studies, this study provides new clues towards the function of this virtually uncharacterised gene. Through the expression of recombinant AtPARG1 and AtPARG2 in the insect cell system it was demonstrated for the first time that both AtPARGs have glycohydrolase activity. AtPARG1 displayed a 20% higher *in vitro* activity than AtPARG2, when the lowest amount of AtPARG1 used in the assay was compared with the highest amount of AtPARG2. Residues previously identified as necessary for activity in mammalian and worm PARG enzymes (Patel *et al*., 2005; St-Laurent *et al*., 2007) showed conserved function in AtPARG1. One of the mutations of AtPARG1, D255N, did not result in significant loss of activity. Nematodes are the only other organism known to contain two genes encoding PARGs. Interestingly, mutation of the corresponding amino acid in the nematode PME-4, also failed to lower activity (St-Laurent *et al*, 2007). In addition, the non-conserved L275 residue of AtPARG2 was shown to be required for activity. However, while the differences in activity *in vitro* may go some way in examining why the sensitivity to DNA damaging agents was only observed in the *parg1* lines, it may not be reflective of their

true activity *in planta*, as the relative endo and exoglycosidic activities could not be determined.

While the isoforms of human PARG and the two PARG enzymes in *C. elegans* show different subcellular localisation (Meyer-Ficca *et al.*, 2004; Meyer *et al.*, 2007; Whatcott *et al.*, 2009; St-Laurent *et al.*, 2007), transient transformation of tobacco and stable transformation of *Arabidopsis* showed for the first time that AtPARG1 and AtPARG2 to localise to both cytoplasm and nucleus, and that both were found to contain a putative nuclear localisation signal (NLS). Overexpression of fusion proteins *in planta* can sometimes lead to saturation of a trafficking pathway, which can result in the accumulation of fusion proteins in an earlier trafficking compartment (Sparkes *et al.*, 2006). The localisation could be examined again, either by expressing the protein under a less powerful constitutive promoter such as ubiquitin10 or under their native promoter. Localisation of the AtPARGs could be further investigated to see if they change compartments upon DNA damaging stress, which has been shown to be the case for several of the mammalian PARG protein isoforms (Haince *et al.*, 2006). The N-terminal domain of mammalian PARGS, which is not represented in the AtPARGs, has been proposed to regulate this mobility, but since the full-length human PARG protein has yet to be purified due to instability and low cellular abundance of the protein (Haketeyama *et al.*, 1986; Lin *et al.*, 1997) this has not been confirmed experimentally.

6.4 Conclusions

This study is the first to undertake simultaneous characterisation of insertional lines of all the known members of the plant poly(ADP-ribosyl)ation, and the first to use insertional lines of the AtPARPs. Here, recombinant AtPARG1 and AtPARG2 were also presented for the first time. These approaches have established novel findings, that contributes to the field of plant poly(ADP-ribosyl)ation, which so far limited.

AtPARP1 and AtPARP2 showed compensatory effects in response to genotoxic, abiotic and oxidative stress as insertional mutants of either gene did not show a phenotype under any of these stresses. The regulation of AtPARP1 and AtPARP2

at the transcriptional level, observed in previous studies, was confirmed, as well as AtPARP2 being the more up-regulated of the two. The majority of PAR polymer produced under control conditions, was found to be produced by AtPARP1, as *parp1-1* seedlings had less polymer content than wild type and *parp2-1*.

AtPARG1 was shown to be required for the response to genotoxic stress, as two separate alleles of *parg1* displayed hypersensitive phenotypes. Both AtPARG1 and AtPARG2 were required for the response to salt stress. A transcriptional profile of AtPARG2 was also generated, which demonstrated an up-regulation in response to genotoxic stress to the same degree as AtPARG1. In addition, an increase in transcript level was observed in response to salt, and the two phytohormones, jasmonic acid and salicylic acid, which are involved in plant pathogen response. Both AtPARGs were shown to localise to the nucleus and the cytoplasm through stable and transient expression of GFP-fusion proteins. Recombinant AtPARG1 and AtPARG2 were expressed in insect cells, and through a commercial glycohydrolase assay, it was found that AtPARG1 has higher activity than AtPARG2. Residues in the catalytic domain of AtPARG1, which are conserved across species, were shown to be required for its activity. In addition, a residue not conserved in PARGs in any other species was shown to be required for the activity of AtPARG2.

A putative role for AtPARP3 in the response to abiotic stress was established as its transcript levels were increased in response to treatment with salt, mannitol, cold, heat and the phytohormone ABA, the latter a regulator in the response to many abiotic stresses. Moreover, the putative promoter region of this gene was found to contain many abiotic stress response elements.

6.5 Future work

Mammalian PARG exists as a single gene with several isoforms. PARG null mice are embryonic lethal (Koh *et al.*, 2004), and depleting cells of the full-length nuclear isoform results in mice that are viable, but hypersensitive to genotoxic stress (Cortes *et al.*, 2004). While this study suggests the involvement of AtPARG1 in the genotoxic stress response and both the AtPARGs in the response

to abiotic stress, it still leaves the question of whether the glycohydrolase activity contributed by these two proteins is required for development, in the same manner as is seen in mammals. Due to the close linkage of AtPARG1 and AtPARG2, the probability of finding homozygous double mutants by crossing plants is very small and would be very time consuming. An alternative way to try and investigate the effect of a double AtPARG deficiency, would be to make dexamethasone/ethanol-inducible silencing constructs (Wielopolska *et al.*, 2005; Lo *et al.*, 2005) and stably transform them into a single mutant background. By creating inducible silencing lines for AtPARG1 in a *parg2-1* background, the effect of complete loss of PARG activity, and any putative functional redundancy could be examined.

Poly(ADP-ribosyl)ation has been shown to have roles in regulation of transcription in mammals (for reviews see Kraus, 2008; Kraus and Lis, 2003). To try and identify any putative transcriptional regulation by PARylation in plants, a chromatin immunoprecipitation (ChIP) assay on plants transformed with a tagged version of AtPARP1 or AtPARP2 could reveal whether they regulate other genes at the transcriptional level.

The bonds in cyclic ADP-ribose (cADPr) are similar to those in PAR. A putative role for AtPARG in the turnover of cADPr could be investigated by HPLC. Since cADPr is thought to be a key second messenger molecule in circadian rhythm and abiotic stress, this would provide a link to the circadian phenotype observed *tej* (Panda *et al.*, 2002) as well as provide explanation as to why only *parg*1 and *parg2-1* lines displayed sensitivity to abiotic stress.

The lack of any stress responsive phenotypes in the *parp1-1* and *parp2-1* lines, indicate an overlap in function between the two genes. The double *parp1-1/parp2-1* lines isolated in this study were viable and fertile, and therefore indicates that functional non-redundancy is not found in *Arabidopsis* DNA binding domain-containing PARPs under normal conditions. It will be interesting to see if phenotypes will be observed in this double mutant line in response to stress and compare them to PARP inhibitor treated plants.

Following on from the fact that *parp1-1/parp2-1* plants are viable and fertile, it would be interesting to establish a role for AtPARP3. So far, no homozygous

insertional mutants of this gene, in which transcript is completely abolished have been identified. Genotyping PCR of the second AtPARP3 insertional line acquired for this study has so far only yielded wild type and heterozygote PCR profiles. When analysing expression across developmental stages, transcript of this gene has so far only been observed at high levels in the developing seed (Becerra *et al.*, 2006), it would therefore not seem unreasonable to propose an essential role for this gene in germination. This could be examined by germinating the double *parp1-1*/*parp2-1* in the presence of a PARP inhibitor, and by analysing the siliques of heterozygous AtPARP3 insertional lines for aborted seeds. Any roles of AtPARP3 outside early development, could be investigated by RNAi, using one of the inducible silencing constructs mentioned earlier. Since AtPARP3 has several changes in the amino acid sequnce in the conserved catalytic domain, it would be interesting to see how they affect any poly(ADP-ribose) polymerase activity this protein might have. Attempts were made to clone this gene, but sequencing results revealed two separate versions of the gene. One corresponding to the sequence described on TAIR, and one which included the intron between exons 5 and 6. This could indicate alternative splicing events, which could be explored using 5' rapid amplification of cDNA ends (RACE).

The putative nuclear localisation signal in the AtPARGs identified in this study could be mutated to determine its validity. In addition, exposing transgenic tobacco or *Arabidopsis* to genotoxic stress or exogenous ABA would enable visualization of any changes in the subcellular localisation in response to stress, similar to what been observed for PARG in human cells (Haince *et al.*, 2006). One approach might be to add an NLS or nuclear exclusion signal to AtPARG1 and stabily transform into a *parg1-2* background to see if this alters the PAR polymer levels or changes the phenotype. Recently a mitochondrial targeting sequence (MTS) was identified in the short isoforms of human PARG, which contained several residues found to be required for activity (Botta and Jacobson, 2010). Several of these residues are conserved in both AtPARGs, and site directed mutagenesis of these residues would reveal whether they are also required for activity of the AtPARGs.

Comet assays are frequently to measure the extent of DNA damage in plants (Menke *et al.*, 2001). This method could be used to determine DNA damage

levels in T-DNA insertion lines in response to both genotoxic and abiotic stresses, which would help elucidate whether the DNA damaging agent hypersensitive phenotype observed in *parg1* alleles is directly related to the amount of DNA damage present after treatment. In addition, this method could be used to examine any potential temporal delays in the repair of DNA damage in the T-DNA insertions lines.

Although the interaction of AtPARP1 and AtXRCC1 was not seen in the yeast two-hybrid experiments in this study, repeating this experiment in a different system, such as insect cells, would perhaps provide a more accurate *in vitro* system, since yeast is one of the only organisms not to contain native PARPs and PARGs. To explore differences in activity of the two DNA damage induced AtPARPs, these proteins could be expressed recombinantly *in vitro* to determine any differences in activity. Several commercial assay kits are available for testing PARP activity. However, this method might not reflect the true *in vivo* activity. Previously, the extent of polymer produced has been measured by incubation of protein extracts with radio-labelled NAD^+, and measuring the resulting PAR levels by the incorporation of NAD^+ and running the samples on a 20% polyacrylamide DNA sequencing gel, which would also determine the sizes of polymer generated, but not the extent of branching (Affar *et al.*, 1995). This method could also be used for measuring if there are any differences in polymer size between the nuclear and cytoplasmic fractions. The same method could also be used to determine any difference in length of polymers generated in the *parg1* and *parg2-1* lines, to see if this could go some way in explaining the difference in hypersensitive phenotype of the *parg1* line.

Appendix I

Class	Number of times identified	Gene	Description
A	11	At5g01310	Basic helix-loop-helix protein family (bHLH) Trancription factor
A	10	At5g08530	51 KDa subunit of respiratory chain complex 1 (C151), NADH dehydrogenase
A	5	At1g16970	AtKu70, Involved in DNA repair, response to heat, telomere maintenance
A	4	At3g09840	Cell division cycle protein (AtCDC48), member of AAA-ATPase family
A	3	At1g43130	LCV2 (like Cov2). Involved in stem vascular tissue pattern formation
A	3	At1g01080	Nucleotide binding, RNA binding
B	2	At3g05345	Heat shock protein binding
C	1	At1g01240	unknown protein, involved in N-terminal protein myristoylation
C	1	At1g04690	KAB1 potassium channel subunit
C	1	At2g45990	unknown protein, located in chloroplast
C	1	At2g31160	Light Sensitive Hypocotyls 3 (LSH3) function unknown
C	1	At5g48990	F-box protein. Involved in ubiquitin-dependent protein catabolic process. Located in the chloroplast
C	1	At1g53290	protein amino acid glycosylation. Located in the membrane.
C	1	At5g13050 5-	Formyltetrahydrofolate cycloligase (5-FCL)
C	1	At1g01090	PDH-E1 α, pyruvate dehydrogenase E1 α subunit. Involved in metabolic process, glycolysis, oxidation reduction. Located in plastid, choroplast, chloroplast envelope
C	1	At4g39280	Involved in phenylalanyl-tRNA aminoacylation, tRNA aminoacylation for protein translation, translation. Located in the cytoplasm. ATP binding.
C	1	At4g32270	unknown protein, unknown function

List of putative AtPARG1 interactors found in the Dual Systems Yeast-Two-Hybrid screen. The table lists all interactors found in the yeast-two hybrid screen as well as their TAIR accession number and predicted function (www.arabidopsis.org).

Appendix II

Table A2.1. Long day flowering PARG mutants

General Linear Model: Leaves versus Genotype

```
Factor     Type    Levels  Values
Genotype   fixed        5  35SHA, parg1-1, parg1-2, parg2-1, Wt

Analysis of Variance for Leaves, using Adjusted SS for Tests
Source     DF   Seq SS  Adj SS  Adj MS     F      P
Genotype    4   75.480  75.480  18.870  8.65  0.000
Error      45   98.200  98.200   2.182
Total      49  173.680

S = 1.47723   R-Sq = 43.46%   R-Sq(adj) = 38.43%

Grouping Information Using Tukey Method and 95.0% Confidence

Genotype   N  Mean  Grouping
parg2-1   10  14.0  A
Wt        10  12.9  A B
35SHA     10  11.6    B C
parg1-2   10  11.4    B C
parg1-1   10  10.5      C

Means that do not share a letter are significantly different.
```

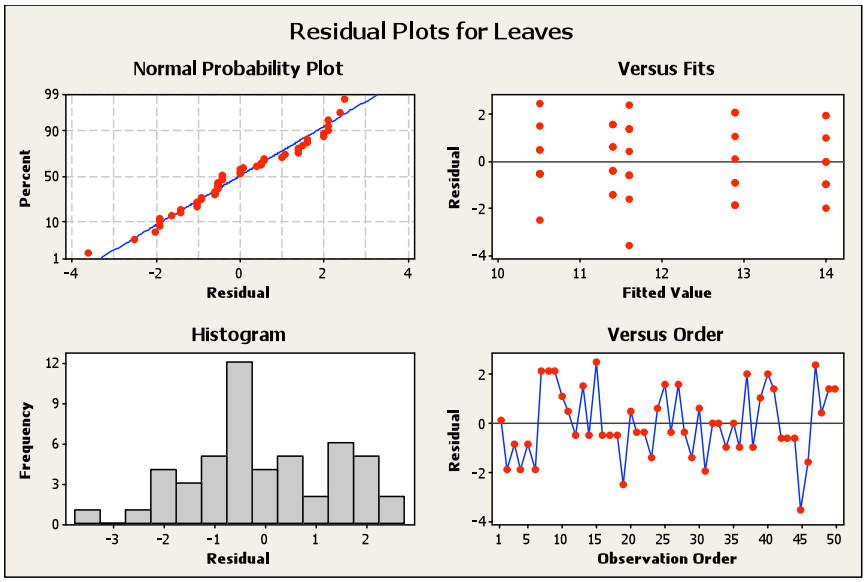

Table A2.2. Short day flowering PARG mutants

General Linear Model: Leaves versus Genotype

```
Factor    Type   Levels  Values
Genotype  fixed       5  35SHA, parg1-1, parg1-2, parg2-1, WT

Analysis of Variance for Leaves, using Adjusted SS for Tests
Source    DF   Seq SS   Adj SS  Adj MS     F      P
Genotype   4   5387.0   5387.0  1346.7  6.68  0.000
Error     70  14110.5  14110.5   201.6
Total     74  19497.5

S = 14.1979   R-Sq = 27.63%   R-Sq(adj) = 23.49%

Grouping Information Using Tukey Method and 95.0% Confidence

Genotype   N   Mean  Grouping
parg1-1   15  103.5  A
35SHA     15  102.7  A
WT        15   87.9     B
parg1-2   15   87.6     B
parg2-1   15   82.9     B

Means that do not share a letter are significantly different.
```

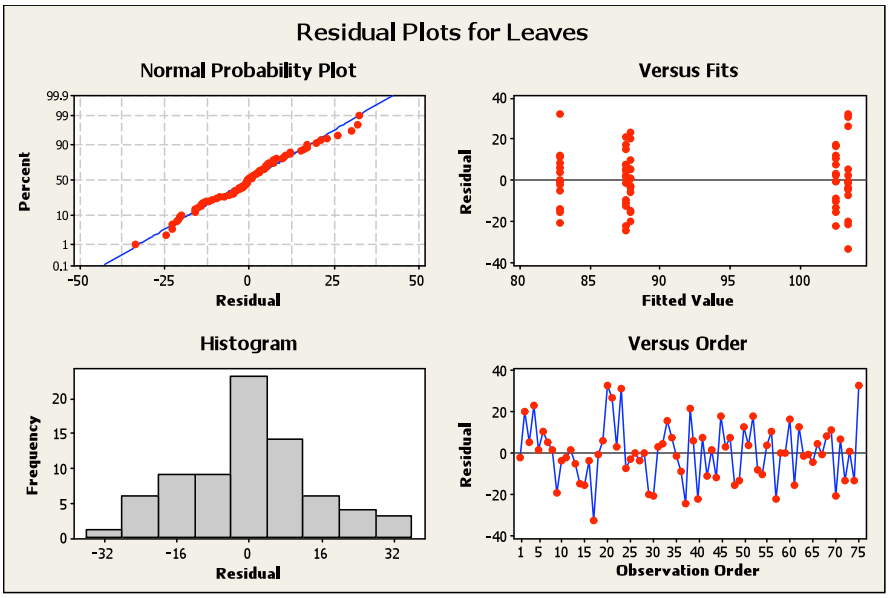

Table A2.3 Short day flowering PARP mutants

General Linear Model: leaves versus genotype

```
Factor    Type   Levels  Values
genotype  fixed       3  parp1-1, parp2-1, WT

Analysis of Variance for leaves, using Adjusted SS for Tests
Source    DF  Seq SS  Adj SS  Adj MS     F      P
genotype   2   793.2   793.2   396.6  3.46  0.041
Error     42  4817.6  4817.6   114.7
Total     44  5610.8

S = 10.7100   R-Sq = 14.14%   R-Sq(adj) = 10.05%

Grouping Information Using Tukey Method and 95.0% Confidence

genotype   N  Mean  Grouping
parp1-1   15  97.7  A
parp2-1   15  90.1  A B
WT        15  87.9    B

Means that do not share a letter are significantly different.
```

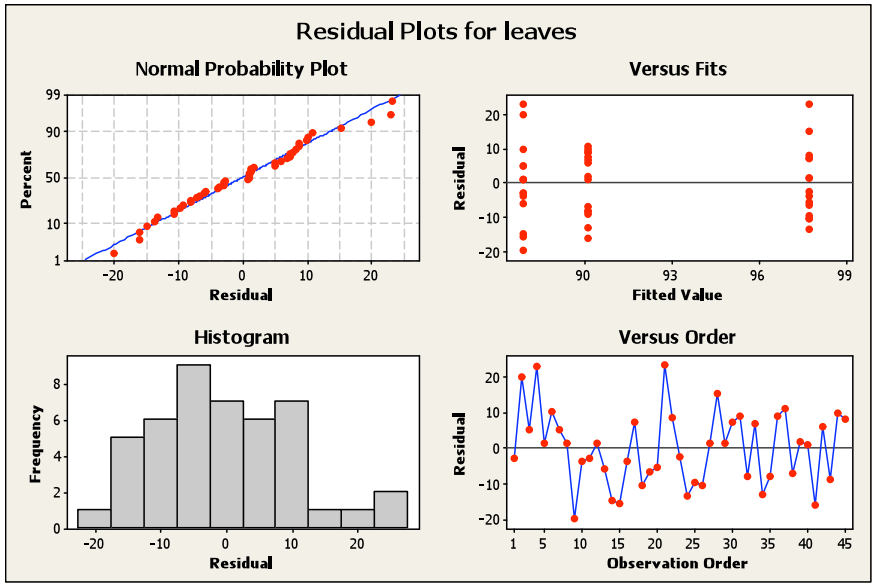

Table A2.4 Germination PARP 38 hours

General Linear Model: DATA versus Genotype

```
Factor    Type   Levels  Values
Genotype  fixed       3  parp1-1, parp2-1, WT

Analysis of Variance for DATA, using Adjusted SS for Tests
Source    DF  Seq SS  Adj SS  Adj MS      F      P
Genotype   2  2047.6  2047.6  1023.8  31.05  0.001
Error      6   197.9   197.9    33.0
Total      8  2245.5

S = 5.74263   R-Sq = 91.19%   R-Sq(adj) = 88.25%

Grouping Information Using Tukey Method and 95.0% Confidence

Genotype  N  Mean  Grouping
parp2-1   3  96.4  A
parp1-1   3  70.4     B
WT        3  60.7     B

Means that do not share a letter are significantly different.
```

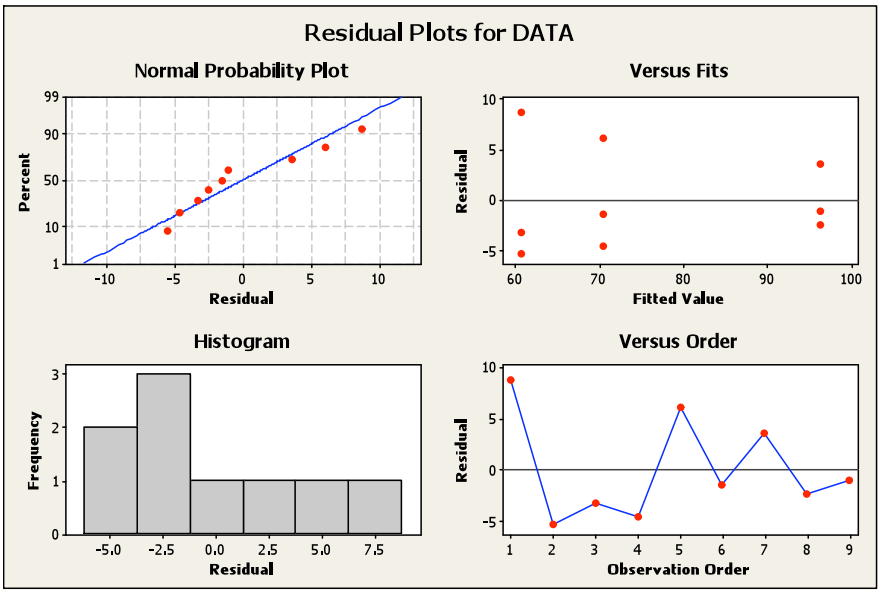

Table A2.5 Germination PARP 47 hours

General Linear Model: DATA versus Genotype

```
Factor    Type   Levels  Values
Genotype  fixed       3  parp1-1, parp2-1, WT

Analysis of Variance for DATA, using Adjusted SS for Tests
Source    DF  Seq SS  Adj SS  Adj MS      F      P
Genotype   2  527.89  527.89  263.94  21.83  0.002
Error      6   72.55   72.55   12.09
Total      8  600.44

S = 3.47739   R-Sq = 87.92%   R-Sq(adj) = 83.89%

Grouping Information Using Tukey Method and 95.0% Confidence

Genotype  N  Mean  Grouping
parp2-1   3  99.0  A
parp1-1   3  84.8     B
WT        3  81.2     B

Means that do not share a letter are significantly different.
```

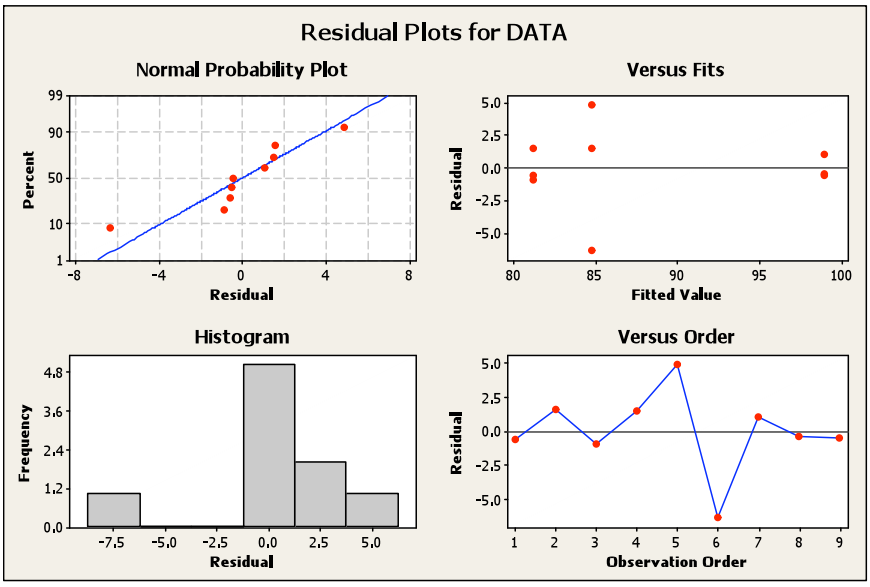

Table A2.6 Germination 0.5 mM MMS PARG 37 hours

General Linear Model: DATA versus genotype

```
Factor    Type   Levels  Values
genotype  fixed       5  35SHA, parg1-1, parg1-2, parg2-1, WT

Analysis of Variance for DATA, using Adjusted SS for Tests
Source    DF   Seq SS   Adj SS  Adj MS      F      P
genotype   4  13025.1  13025.1  3256.3  69.82  0.000
Error     10    466.4    466.4    46.6
Total     14  13491.5

S = 6.82902   R-Sq = 96.54%   R-Sq(adj) = 95.16%

Grouping Information Using Tukey Method and 95.0% Confidence

genotype  N  Mean  Grouping
parg2-1   3  73.0  A
WT        3  70.3  A
35SHA     3  55.8  A
parg1-2   3   9.2     B
parg1-1   3   5.8     B

Means that do not share a letter are significantly different.
```

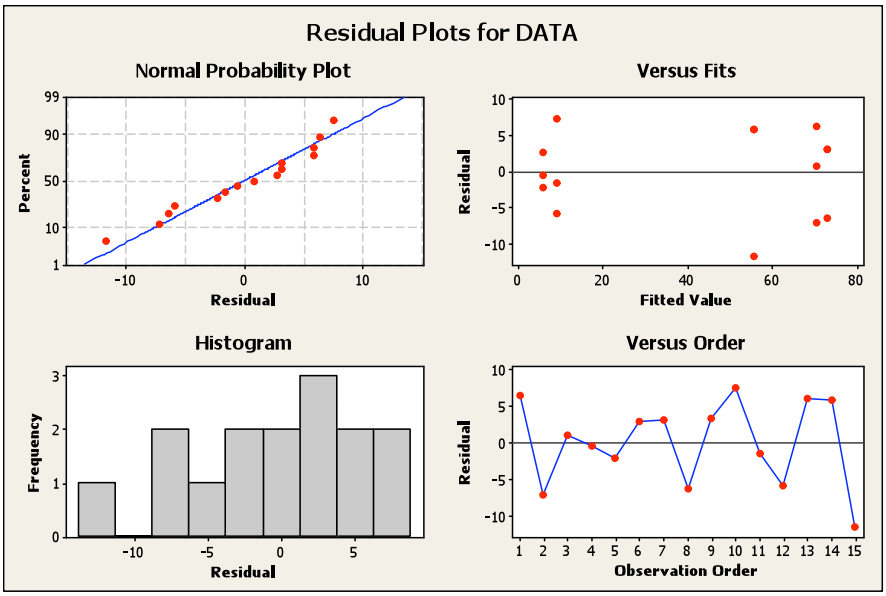

Table A2.7 Germination 0.5 mM MMS PARG 46 hours

General Linear Model: DATA versus genotype

```
Factor    Type   Levels  Values
genotype  fixed       5  35SHA, parg1-1, parg1-2, parg2-1, WT

Analysis of Variance for DATA, using Adjusted SS for Tests
Source    DF  Seq SS  Adj SS  Adj MS      F      P
genotype   4  8678.6  8678.6  2169.6  24.95  0.000
Error     10   869.6   869.6    87.0
Total     14  9548.2

S = 9.32548   R-Sq = 90.89%   R-Sq(adj) = 87.25%

Grouping Information Using Tukey Method and 95.0% Confidence

genotype  N  Mean  Grouping
WT        3  88.0  A
35SHA     3  86.2  A
parg2-1   3  84.0  A
parg1-1   3  46.9     B
parg1-2   3  29.8     B

Means that do not share a letter are significantly different.
```

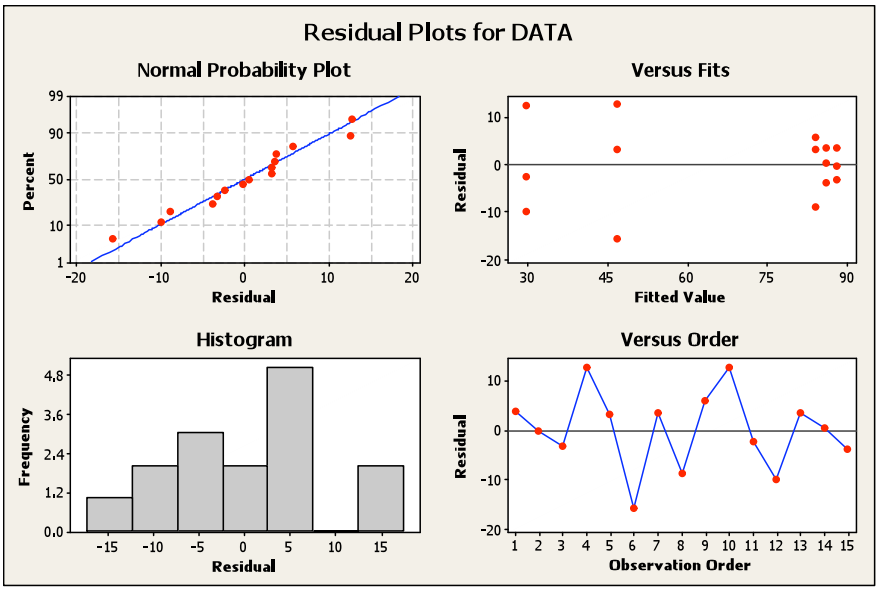

Table A2.8 Germination 0.5 mM MMS PARG 60 hours

General Linear Model: DATA versus genotype

```
Factor    Type   Levels  Values
genotype  fixed       5  35SHA, parg1-1, parg1-2, parg2-1, WT

Analysis of Variance for DATA, using Adjusted SS for Tests
Source    DF  Seq SS  Adj SS  Adj MS     F      P
genotype   4  366.15  366.15   91.54  3.59  0.046
Error     10  255.25  255.25   25.53
Total     14  621.41

S = 5.05226   R-Sq = 58.92%   R-Sq(adj) = 42.49%

Grouping Information Using Tukey Method and 95.0% Confidence

genotype  N  Mean  Grouping
WT        3  93.2  A
parg2-1   3  90.1  A B
35SHA     3  89.3  A B
parg1-1   3  87.1  A B
parg1-2   3  78.5    B

Means that do not share a letter are significantly different.
```

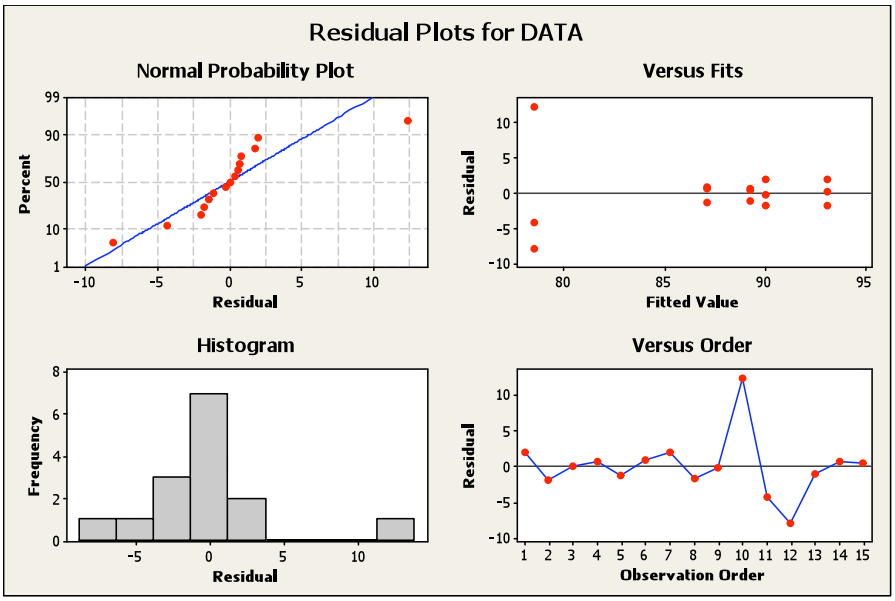

Table A2.9 Germination 1.0 mM MMS PARG 37 hours

General Linear Model: DATA versus genotype

```
Factor    Type   Levels  Values
genotype  fixed       5  35SHA, parg1-1, parg1-2, parg2-1, WT

Analysis of Variance for DATA, using Adjusted SS for Tests
Source    DF   Seq SS  Adj SS  Adj MS     F      P
genotype   4   714.36  714.36  178.59  5.42  0.014
Error     10   329.64  329.64   32.96
Total     14  1044.00

S = 5.74143   R-Sq = 68.43%   R-Sq(adj) = 55.80%

Grouping Information Using Tukey Method and 95.0% Confidence

genotype  N  Mean  Grouping
WT        3  18.9  A
parg2-1   3  10.1  A B
35SHA     3   2.8    B
parg1-2   3   1.7    B
parg1-1   3   0.6    B

Means that do not share a letter are significantly different.
```

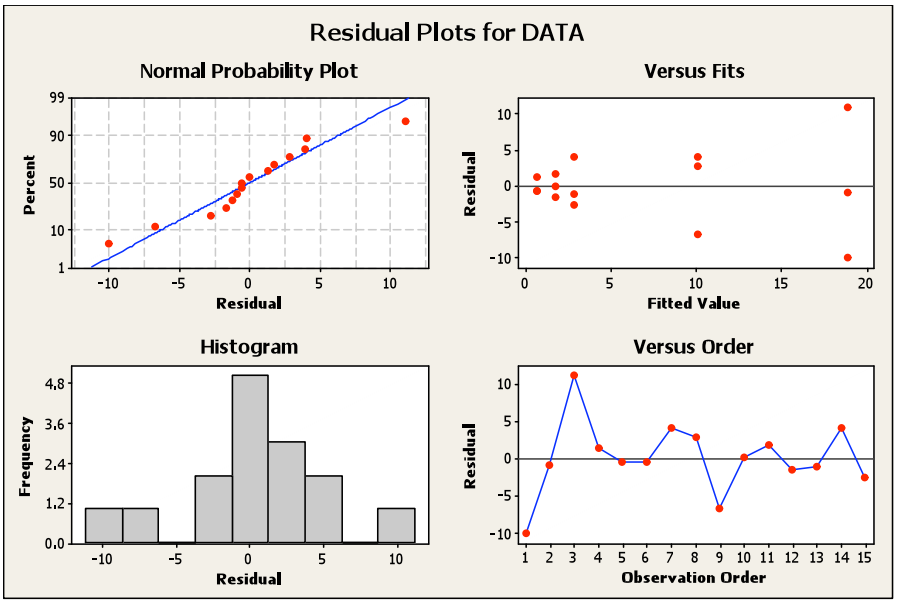

Table A2.10 Germination 1.0 mM MMS PARG 46 hours

General Linear Model: DATA versus genotype

```
Factor    Type   Levels  Values
genotype  fixed       5  35SHA, parg1-1, parg1-2, parg2-1, WT

Analysis of Variance for DATA, using Adjusted SS for Tests
Source    DF   Seq SS   Adj SS  Adj MS      F      P
genotype   4  11551.8  11551.8  2887.9  17.05  0.000
Error     10   1693.8   1693.8   169.4
Total     14  13245.6

S = 13.0146   R-Sq = 87.21%   R-Sq(adj) = 82.10%

Grouping Information Using Tukey Method and 95.0% Confidence

genotype  N  Mean  Grouping
parg2-1   3  72.0  A
WT        3  59.0  A
35SHA     3  52.8  A
parg1-2   3   9.5     B
parg1-1   3   3.0     B

Means that do not share a letter are significantly different.
```

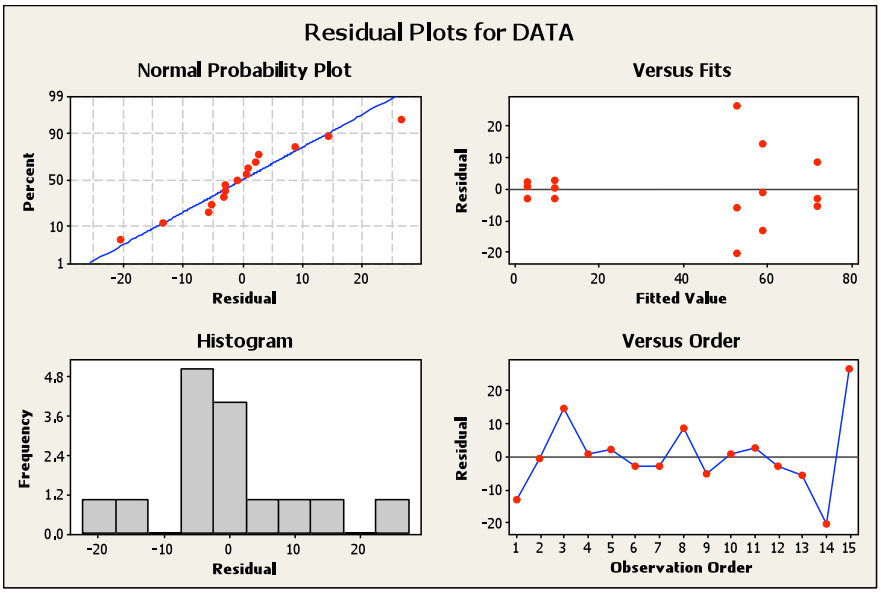

Table A2.11 Germination 1.0 mM MMS PARG 60 hours

General Linear Model: DATA versus genotype

```
Factor    Type   Levels  Values
genotype  fixed       5  35SHA, parg1-1, parg1-2, parg2-1, WT

Analysis of Variance for DATA, using Adjusted SS for Tests
Source    DF  Seq SS  Adj SS  Adj MS      F      P
genotype   4  4284.0  4284.0  1071.0  10.05  0.002
Error     10  1065.7  1065.7   106.6
Total     14  5349.6

S = 10.3231   R-Sq = 80.08%   R-Sq(adj) = 72.11%

Grouping Information Using Tukey Method and 95.0% Confidence

genotype  N  Mean  Grouping
WT        3  87.2  A
parg2-1   3  84.9  A
35SHA     3  67.3  A B
parg1-2   3  49.7    B
parg1-1   3  46.9    B

Means that do not share a letter are significantly different.
```

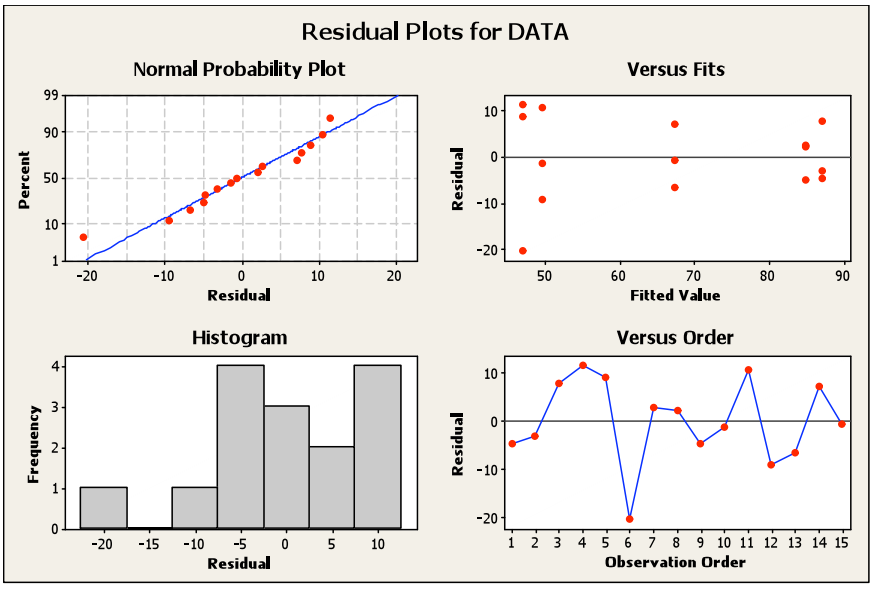

Table A2.12 Germination 1.0 mM MMS PARG 70 hours

General Linear Model: DATA versus genotype

```
Factor    Type   Levels  Values
genotype  fixed       5  35SHA, parg1-1, parg1-2, parg2-1, WT


Analysis of Variance for DATA, using Adjusted SS for Tests
Source    DF   Seq SS  Adj SS  Adj MS     F      P
genotype   4   818.05  818.05  204.51  5.40  0.014
Error     10   378.57  378.57   37.86
Total     14  1196.62

S = 6.15280   R-Sq = 68.36%   R-Sq(adj) = 55.71%

Grouping Information Using Tukey Method and 95.0% Confidence

genotype  N  Mean  Grouping
WT        3  93.3  A
parg2-1   3  90.2  A B
35SHA     3  82.9  A B
parg1-2   3  76.8  A B
parg1-1   3  74.2    B

Means that do not share a letter are significantly different.
```

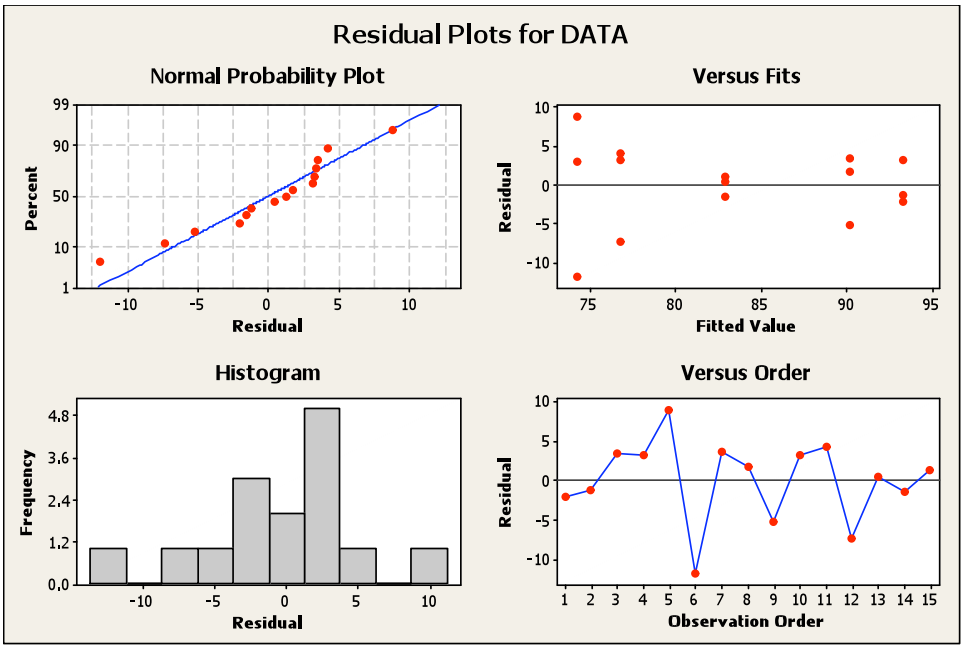

Table A2.13 Germination 0.5 mM MMS PARP 47 hours

General Linear Model: Data versus genotype

```
Factor     Type   Levels  Values
genotype   fixed       3  parp1-1, parp2-1, WT

Analysis of Variance for Data, using Adjusted SS for Tests
Source     DF   Seq SS  Adj SS  Adj MS     F      P
genotype    2   999.74  999.74  499.87  8.70  0.017
Error       6   344.86  344.86   57.48
Total       8  1344.60

S = 7.58134   R-Sq = 74.35%   R-Sq(adj) = 65.80%

Grouping Information Using Tukey Method and 95.0% Confidence

genotype  N  Mean  Grouping
parp2-1   3  95.8  A
parp1-1   3  82.1  A B
WT        3  70.0    B

Means that do not share a letter are significantly different.
```

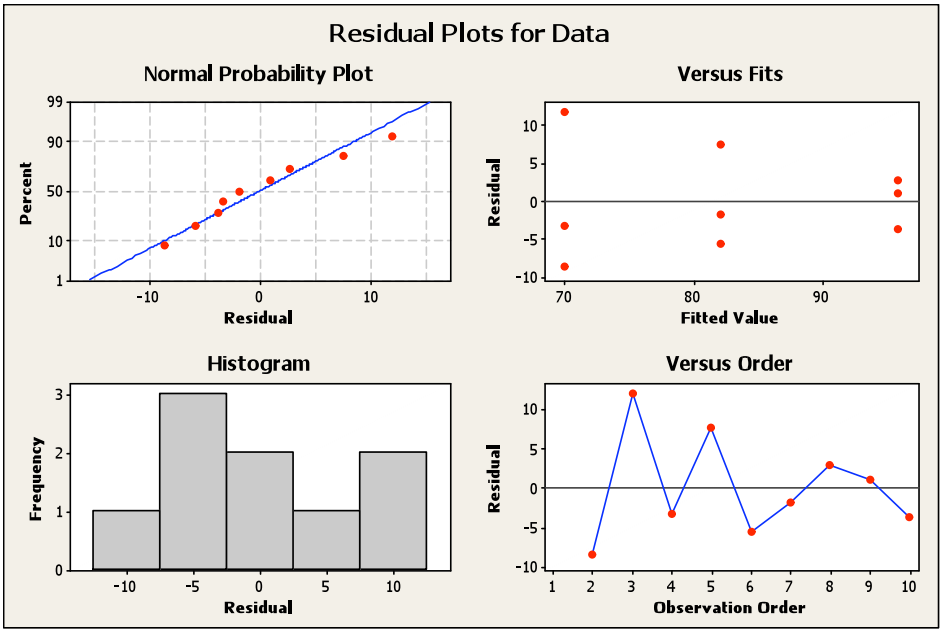

Table A2.14 Germination 0.5 mM MMS PARP 71 hours

General Linear Model: DATA versus genotype

```
Factor    Type   Levels  Values
genotype  fixed       3  parp1-1, parp2-1, WT

Analysis of Variance for DATA, using Adjusted SS for Tests
Source    DF  Seq SS  Adj SS  Adj MS     F      P
genotype   2  194.34  194.34   97.17  6.10  0.036
Error      6   95.59   95.59   15.93
Total      8  289.93

S = 3.99152   R-Sq = 67.03%   R-Sq(adj) = 56.04%

Grouping Information Using Tukey Method and 95.0% Confidence

genotype  N  Mean  Grouping
parp2-1   3  98.9  A
WT        3  90.9  A B
parp1-1   3  87.9    B

Means that do not share a letter are significantly different.
```

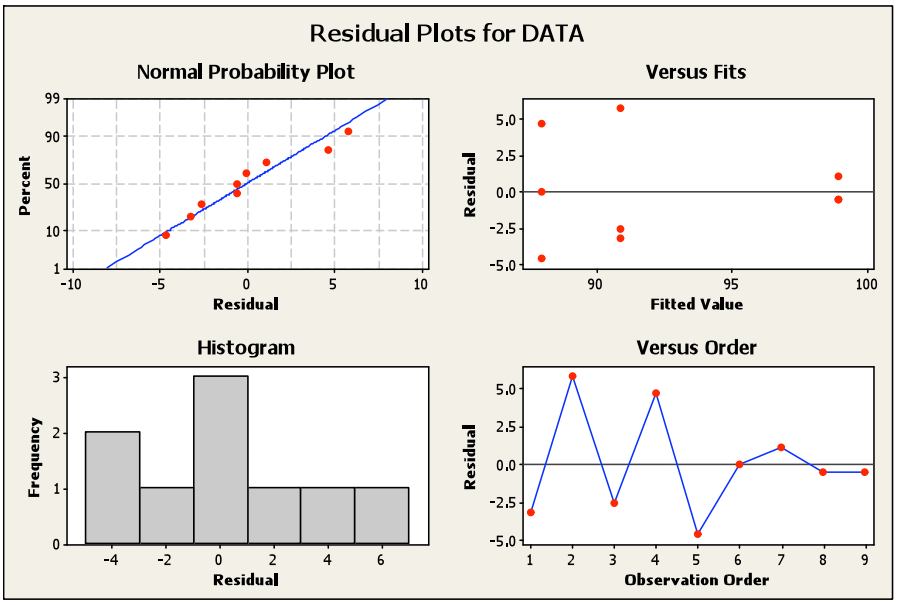

Table A2.15 Chlorophyll content

General Linear Model: chlorophyll versus genotype, treatment

```
Factor     Type   Levels  Values
genotype   fixed       7  35SHA, parg1-1, parg1-2, parg2-1, parp1-1, parp2-1,
                          Wt
treatment  fixed       2  con, MV


Analysis of Variance for chlorophyll, using Adjusted SS for Tests
Source              DF     Seq SS     Adj SS     Adj MS       F      P
genotype             6  0.0010707  0.0010707  0.0001785   24.18  0.000
treatment            1  0.0032003  0.0032003  0.0032003  433.70  0.000
genotype*treatment   6  0.0004619  0.0004619  0.0000770   10.43  0.000
Error               28  0.0002066  0.0002066  0.0000074
Total               41  0.0049396

S = 0.00271645   R-Sq = 95.82%   R-Sq(adj) = 93.88%

Grouping Information Using Tukey Method and 95.0% Confidence

genotype  treatment  N  Mean  Grouping
parg1-2   con        3   0.1  A
parg2-1   con        3   0.1  A B
parp1-1   con        3   0.1  A B
parp2-1   con        3   0.1  A B
parg1-1   con        3   0.1  A B
Wt        con        3   0.1    B
parg1-2   MV         3   0.1      C
parp1-1   MV         3   0.1      C
parg2-1   MV         3   0.1      C
35SHA     con        3   0.1      C
parp2-1   MV         3   0.1      C
parg1-1   MV         3   0.1      C
35SHA     MV         3   0.1      C
Wt        MV         3   0.1      C

Means that do not share a letter are significantly different.
```

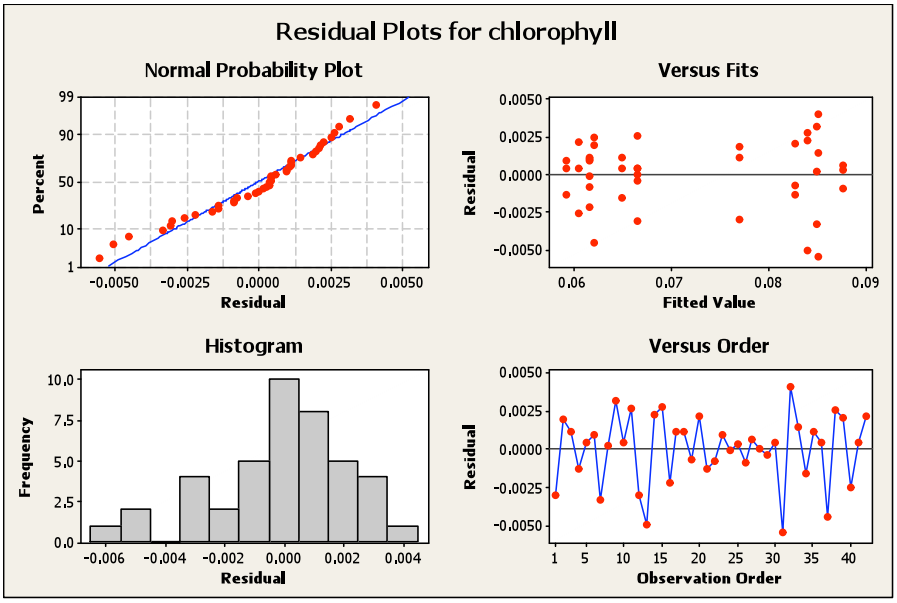

Table A2.16 PAR levels MMS treatment

General Linear Model: DATA versus LINE, TIME

```
Factor  Type   Levels  Values
LINE    fixed       5  parg1-2, parg2-1, parp1-1, parp2-1, WT
TIME    fixed       3  0, 4, 8

Analysis of Variance for DATA, using Adjusted SS for Tests
Source     DF   Seq SS   Adj SS   Adj MS      F      P
LINE        4  0.79336  0.79336  0.19834  10.24  0.000
TIME        2  0.48050  0.48050  0.24025  12.40  0.000
LINE*TIME   8  1.00321  1.00321  0.12540   6.47  0.000
Error      60  1.16236  1.16236  0.01937
Total      74  3.43943

S = 0.139186   R-Sq = 66.20%   R-Sq(adj) = 58.32%

Grouping Information Using Tukey Method and 95.0% Confidence

LINE      N  Mean  Grouping
WT       15   0.8  A
parg2-1  15   0.8  A
parg1-2  15   0.8  A
parp2-1  15   0.7  A
parp1-1  15   0.5    B

Means that do not share a letter are significantly different.
```

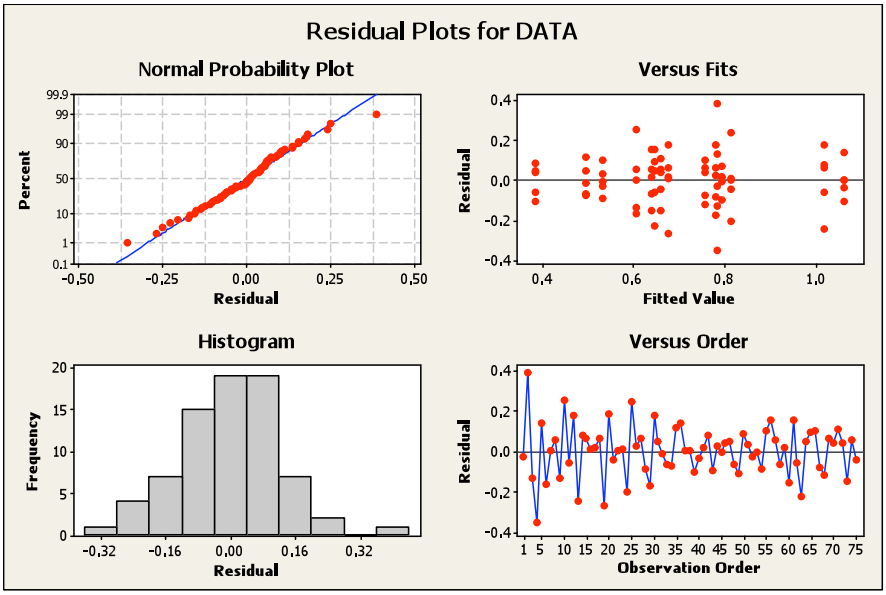
Residual Plots for DATA
Normal Probability Plot
Percent
99.9
99
90
50
10
1
0.1
-0,50
-0,25
0,00
0,25
0,50
Residual
Versus Fits
Residual
0,4
0,2
0,0
-0,2
-0,4
0,4
0,6
0,8
1,0
Fitted Value
Histogram
Frequency
20
15
10
5
0
-0,32
-0,16
0,00
0,16
0,32
Residual
Versus Order
Residual
0,4
0,2
0,0
-0,2
-0,4
1 5 10 15 20 25 30 35 40 45 50 55 60 65 70 75
Observation Order

Table A2.17 PARG activity assay

General Linear Model: Dat_2 versus Line_2, Time_2

```
Factor  Type   Levels  Values
Line_2  fixed      25  1, 2, 3, 4, 5, 6, 7, 8, 9, 10, 11, 12, 13, 14, 15, 16,
                       17, 18, 19, 20, 21, 22, 23, 24, 25
Time_2  fixed       2  2, 3

Analysis of Variance for Dat_2, using Adjusted SS for Tests
Source          DF    Seq SS    Adj SS  Adj MS        F      P
Line_2          24  119294.3  119294.3  4970.6  1764.92  0.000
Time_2           1       0.8       0.5     0.5     0.19  0.663
Line_2*Time_2   24      46.1      46.1     1.9     0.68  0.857
Error           96     270.4     270.4     2.8
Total          145  119611.6

S = 1.67819   R-Sq = 99.77%   R-Sq(adj) = 99.66%

Tukey 99.0% Simultaneous Confidence Intervals
```

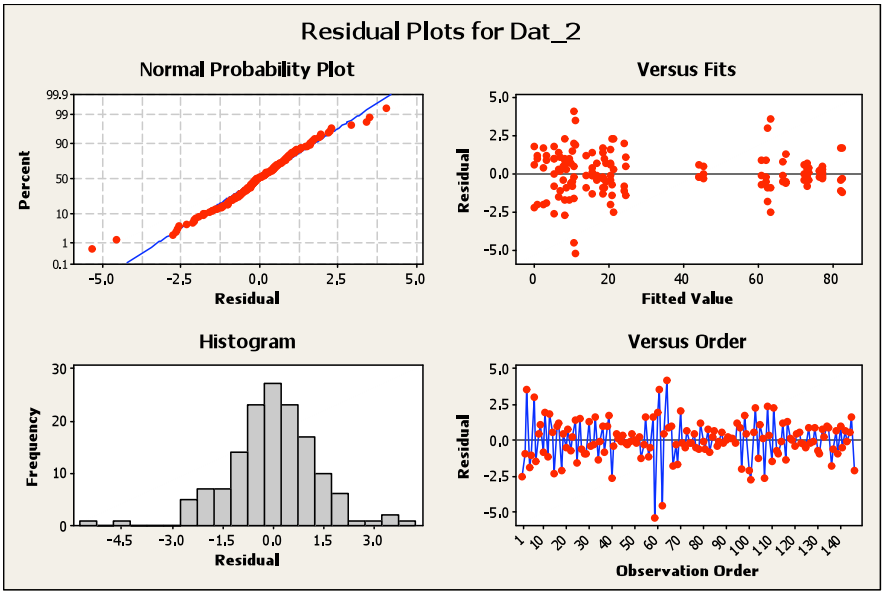

Appendix III

Table A3.1 Genes down regulated more than 10-fold in *parg1-2* seedlings compared to wild type seedlings in control conditions.

Gene ID	Name	Fold change
AT5G10040	unknown protein	-722.5
AT4G17510	ubiquitin C-terminal hydrolase 3	-222.0
AT2G44090	Ankyrin repeat family protein	-218.8
AT4G27730	oligopeptide transporter 1	-153.4
AT2G33430	differentiation and greening-like 1	-125.8
AT3G09100	mRNA capping enzyme family protein	-109.4
AT1G22920	COP9 signalosome 5A	-105.0
AT3G47630	CONTAINS InterPro DOMAIN/s: Mitochondrial matrix Mmp37 (InterPro:IPR015222)	-105.0
AT3G56050	Protein kinase family protein	-101.9
AT1G17420	lipoxygenase 3	-92.4
AT5G44730	Haloacid dehalogenase-like hydrolase (HAD) superfamily protein	-86.1
AT4G30260	Integral membrane Yip1 family protein	-84.3
AT1G61770	Chaperone DnaJ-domain superfamily protein	-83.0
AT3G13040	myb-like HTH transcriptional regulator family protein	-81.1
AT3G52790	peptidoglycan-binding LysM domain-containing protein	-74.8
AT3G10330	Cyclin-like family protein	-67.9
AT2G38360	prenylated RAB acceptor 1.B4	-61.3
AT1G66350	RGA-like 1	-61.0
AT5G26280	TRAF-like family protein	-56.1
AT5G01270	carboxyl-terminal domain (ctd) phosphatase-like 2	-55.3
AT1G48920	nucleolin like 1	-47.8
AT4G01870	tolB protein-related	-34.9
AT4G25340	FK506 BINDING PROTEIN 53	-34.6
AT2G35960	NDR1/HIN1-like 12	-33.1
AT2G28390	SAND family protein	-31.8
AT3G15040	Protein of unknown function, DUF584	-30.6
ATMG01170	ATPase, F0 complex, subunit A protein	-30.4
AT2G02990	ribonuclease 1	-26.2
AT1G24148	unknown protein	-23.1
AT5G48540	receptor-like protein kinase-related family protein	-21.3
AT1G10370	Glutathione S-transferase family protein	-21.0
AT5G17230	PHYTOENE SYNTHASE	-20.0
AT4G09010	ascorbate peroxidase 4	-16.1
AT1G19730	Thioredoxin superfamily protein	-15.9
AT3G26210	cytochrome P450, family 71, subfamily B, polypeptide 23	-15.7
AT1G08180	unknown protein	-15.0
AT4G08960	phosphotyrosyl phosphatase activator (PTPA) family protein	-14.4
AT4G35480	RING-H2 finger A3B	-14.0
AT2G38290	ammonium transporter 2	-13.7
AT1G77120	alcohol dehydrogenase 1	-13.6
AT1G14610	valyl-tRNA synthetase / valine--tRNA ligase (VALRS)	-13.3
AT2G37690	phosphoribosylaminoimidazole carboxylase, putative / AIR carboxylase, putative	-12.6
AT4G22470	protease inhibitor/seed storage/lipid transfer protein (LTP) family protein	-12.4
AT3G54040	PAR1 protein	-12.1
AT3G21215	RNA-binding (RRM/RBD/RNP motifs) family protein	-12.1

AT1G35516	myb-like transcription factor family protein	-11.9
AT1G18300	nudix hydrolase homolog 4	-11.6
AT1G43800	Plant stearoyl-acyl-carrier-protein desaturase family protein	-11.6
AT5G36925	unknown protein	-11.6
AT1G69070	CONTAINS InterPro DOMAIN/s: Nop14-like protein (InterPro:IPR007276)	-11.2
AT5G62360	Plant invertase/pectin methylesterase inhibitor superfamily protein	-11.1
AT3G20395	RING/U-box superfamily protein	-11.1
AT1G80510	Transmembrane amino acid transporter family protein	-10.9
AT2G29450	glutathione S-transferase tau 5	-10.9

Table A3.2 Genes more than 10-fold upregulated in *parg1-2* seedlings compared to wild type seedlings in control conditions

Gene ID	Name	Fold change
AT3G54970	D-aminoacid aminotransferase-like PLP-dependent enzymes superfamily protein	646.2
AT4G39150	DNAJ heat shock N-terminal domain-containing protein	389.0
AT3G57610	adenylosuccinate synthase	341.3
AT1G71270	Vps52 / Sac2 family	219.1
AT2G01710	Chaperone DnaJ-domain superfamily protein	164.3
AT5G50430	ubiquitin-conjugating enzyme 33	158.8
AT4G08035	other RNA	121.9
AT1G80210	Mov34/MPN/PAD-1 family protein	110.7
AT1G29355	unknown protein	97.6
AT2G31730	basic helix-loop-helix (bHLH) DNA-binding superfamily protein	95.3
AT3G11550	Uncharacterised protein family (UPF0497)	95.3
AT1G80570	RNI-like superfamily protein	89.7
AT4G28780	GDSL-like Lipase/Acylhydrolase superfamily protein	86.5
AT5G63480	unknown protein	83.1
AT5G63200	tetratricopeptide repeat (TPR)-containing protein	62.1
AT5G40460	unknown protein	58.3
AT2G39050	hydroxyproline-rich glycoprotein family protein	52.9
AT4G14550	indole-3-acetic acid inducible 14	50.9
AT3G24820	BSD domain-containing protein	49.3
AT4G26160	atypical CYS HIS rich thioredoxin 1	47.3
AT5G05230	RING/U-box superfamily protein	46.2
AT2G17230	EXORDIUM like 5	45.4
AT2G42160	zinc finger (ubiquitin-hydrolase) domain-containing protein	45.2
AT3G26670	Protein of unknown function (DUF803)	44.4
AT5G10370	helicase domain-containing protein / IBR domain-containing protein / zinc finger protein-related	44.2
AT5G35570	O-fucosyltransferase family protein	43.9
AT5G16715	ATP binding;valine-tRNA ligases;aminoacyl-tRNA ligases;nucleotide binding;ATP binding;aminoacyl-tRNA ligases	42.9
AT1G57770	FAD/NAD(P)-binding oxidoreductase family protein	41.4
AT5G58390	Peroxidase superfamily protein	41.1
AT4G28070	AFG1-like ATPase family protein	39.5
AT4G11910	Unknown protein, BEST Arabidopsis thaliana protein match is: non-yellowing 1 (TAIR:AT4G22920.1)	39.1
AT4G17950	AT hook motif DNA-binding family protein	38.4
AT3G10572	3-phosphoinositide-dependent protein kinase-1, putative	37.6
AT2G46680	homeobox 7	37.4
AT5G27950	P-loop containing nucleoside triphosphate hydrolases superfamily	37.2

	protein	
AT5G65110	acyl-CoA oxidase 2	36.9
AT3G23990	heat shock protein 60	35.8
AT1G26180	unknown protein	35.4
AT2G20830	transferases;folic acid binding	35.2
AT5G24060	Pentatricopeptide repeat (PPR) superfamily protein	35.0
AT1G04990	Zinc finger C-x8-C-x5-C-x3-H type family protein	34.7
AT1G80380	P-loop containing nucleoside triphosphate hydrolases superfamily protein	34.7
AT1G03970	G-box binding factor 4	33.8
AT4G30580	Phospholipid/glycerol acyltransferase family protein	33.3
AT2G02960	RING/FYVE/PHD zinc finger superfamily protein	33.1
AT2G40820	Unknown protein, BEST Arabidopsis thaliana protein match is: myosin heavy chain-related (TAIR:AT3G56480.1)	32.4
AT4G10090	elongator protein 6	32.2
AT1G10700	phosphoribosyl pyrophosphate (PRPP) synthase 3	31.8
AT2G17670	Tetratricopeptide repeat (TPR)-like superfamily protein	31.8
AT3G03440	ARM repeat superfamily protein	31.1
AT3G02640	unknown protein	31.0
AT2G17500	Auxin efflux carrier family protein	30.7
AT3G01370	CRM family member 2	30.6
AT1G78995	unknown protein	30.3
AT1G78210	alpha/beta-Hydrolases superfamily protein	29.6
AT1G21630	Calcium-binding EF hand family protein	29.4
AT3G22680	RNA-DIRECTED DNA METHYLATION 1	28.6
AT3G58750	citrate synthase 2	28.5
AT1G12480	C4-dicarboxylate transporter/malic acid transport protein	27.8
AT5G04810	pentatricopeptide (PPR) repeat-containing protein	27.8
AT1G50450	Saccharopine dehydrogenase	27.7
AT4G37180	Homeodomain-like superfamily protein	27.6
AT1G20300	Pentatricopeptide repeat (PPR) superfamily protein	27.3
AT4G21090	MITOCHONDRIAL FERREDOXIN 2	26.6
AT4G15640	unknown protein	26.2
AT3G58560	DNAse I-like superfamily protein	26.1
AT1G06070	Basic-leucine zipper (bZIP) transcription factor family protein	26.0
AT4G35850	Pentatricopeptide repeat (PPR) superfamily protein	25.9
AT4G31860	Protein phosphatase 2C family protein	25.9
AT1G60000	RNA-binding (RRM/RBD/RNP motifs) family protein	25.8
AT1G12270	stress-inducible protein, putative	25.7
AT5G20000	AAA-type ATPase family protein	25.7
AT1G50410	SNF2 domain-containing protein / helicase domain-containing protein / zinc finger protein-related	25.5
AT3G24506	unknown protein	25.3
AT3G45230	hydroxyproline-rich glycoprotein family protein	25.0
AT3G10915	Reticulon family protein	24.9
AT1G48240	novel plant snare 12	24.8
AT4G22910	FIZZY-related 2	24.5
AT5G08160	serine/threonine protein kinase 3	24.4
AT1G14790	RNA-dependent RNA polymerase 1	24.3
AT2G15695	Protein of unknown function DUF829, transmembrane 53	24.2
AT4G26190	Haloacid dehalogenase-like hydrolase (HAD) superfamily protein	24.2
AT1G74290	alpha/beta-Hydrolases superfamily protein	23.3
AT3G18535	tubulin-tyrosine ligases	23.3
AT2G25590	Plant Tudor-like protein	22.9
AT5G16040	Regulator of chromosome condensation (RCC1) family protein	22.2
AT1G75850	VPS35 homolog B	22.1
AT1G33490	unknown protein	21.8

AT5G26240	chloride channel D	21.5
AT3G22380	time for coffee	21.2
AT1G28490	syntaxin of plants 61	21.1
AT3G19720	P-loop containing nucleoside triphosphate hydrolases superfamily protein	20.8
AT1G71820	SEC6	20.7
AT2G38450	CONTAINS InterPro DOMAIN/s: Sel1-like (InterPro:IPR006597)	20.5
AT1G51740	syntaxin of plants 81	20.4
AT5G49660	Leucine-rich repeat transmembrane protein kinase family protein	20.4
AT1G10910	Pentatricopeptide repeat (PPR) superfamily protein	20.1
AT1G73100	SU(VAR)3-9 homolog 3	19.8
AT5G35210	metalloendopeptidases;zinc ion binding;DNA binding	19.6
AT4G34310	alpha/beta-Hydrolases superfamily protein	19.6
AT5G65270	RAB GTPase homolog A4A	19.5
AT5G20730	Transcriptional factor B3 family protein / auxin-responsive factor AUX/IAA-related	19.4
AT5G10940	transducin family protein / WD-40 repeat family protein	19.4
AT5G05210	Surfeit locus protein 6	19.3
AT1G54570	Esterase/lipase/thioesterase family protein	19.1
AT1G75780	tubulin beta-1 chain	19.0
AT4G38760	Protein of unknown function (DUF3414)	18.6
AT2G25110	stromal cell-derived factor 2-like protein precursor	18.6
AT5G30490	CONTAINS InterPro DOMAIN/s: Craniofacial development protein 1/Bucentaur (InterPro:IPR011421)	18.5
AT3G53480	pleiotropic drug resistance 9	18.3
AT1G23380	KNOTTED1-like homeobox gene 6	18.3
AT2G18193	P-loop containing nucleoside triphosphate hydrolases superfamily protein	18.2
AT1G72170	Domain of unknown function (DUF543)	17.8
AT1G42470	Patched family protein	17.7
AT3G60830	actin-related protein 7	17.5
AT3G63390	unknown protein	17.3
AT1G04250	AUX/IAA transcriptional regulator family protein	17.2
AT3G11880	Protein of unknown function DUF2359, transmembrane	17.2
AT5G37070	Protein of unknown function, DUF538	17.2
AT2G41500	WD-40 repeat family protein / small nuclear ribonucleoprotein Prp4p-related	17.1
AT5G56180	actin-related protein 8	17.0
AT5G51150	Mitochondrial import inner membrane translocase subunit Tim17/Tim22/Tim23 family protein	16.8
AT3G08590	Phosphoglycerate mutase, 2,3-bisphosphoglycerate-independent	16.7
AT1G53650	CTC-interacting domain 8	16.7
AT5G44710	CONTAINS InterPro DOMAIN/s: Ribosomal protein S27/S33, mitochondrial (InterPro:IPR013219)	16.7
AT5G25810	Integrase-type DNA-binding superfamily protein	16.6
AT2G02070	indeterminate(ID)-domain 5	16.4
AT4G37660	Ribosomal protein L12/ ATP-dependent Clp protease adaptor protein ClpS family protein	16.3
AT3G48380	Peptidase C78, ubiquitin fold modifier-specific peptidase 1/ 2	15.9
AT1G29357	other RNA	15.8
AT5G45620	Proteasome component (PCI) domain protein	15.7
AT3G12400	Ubiquitin-conjugating enzyme/RWD-like protein	15.7
AT3G27100	Unknown protein, CONTAINS InterPro DOMAIN/s: Transcription factor, enhancer of yellow 2 (InterPro:IPR018783)	15.4
AT5G28640	SSXT family protein	15.4
AT3G13740	Ribonuclease III family protein	15.3
AT4G02720	unknown protein	15.1
AT4G02340	alpha/beta-Hydrolases superfamily protein	15.1

AT3G06650	ATP-citrate lyase B-1	15.0
AT1G71790	Subunits of heterodimeric actin filament capping protein Capz superfamily	15.0
AT2G26550	heme oxygenase 2	15.0
AT5G56220	P-loop containing nucleoside triphosphate hydrolases superfamily protein	14.9
AT4G22570	adenine phosphoribosyl transferase 3	14.9
AT3G60350	ARABIDILLO-2	14.9
AT2G04110	pseudogene of unknown protein	14.8
AT2G37020	Translin family protein	14.8
AT1G34630	Unknown protein, BEST Arabidopsis thaliana protein match is: Mitochondrial import inner membrane translocase subunit Tim17/Tim22/Tim23 family protein (TAIR:AT5G51150.1)	14.6
AT5G58450	Tetratricopeptide repeat (TPR)-like superfamily protein	14.6
AT4G29030	Putative membrane lipoprotein	14.5
AT1G56290	CwfJ-like family protein	14.5
AT1G17720	Protein phosphatase 2A, regulatory subunit PR55	14.4
AT4G20300	Protein of unknown function (DUF1639)	14.1
AT1G30910	Molybdenum cofactor sulfurase family protein	14.1
AT2G41900	CCCH-type zinc finger protein with ARM repeat domain	14.1
AT5G46170	F-box family protein	14.0
AT2G27140	HSP20-like chaperones superfamily protein	13.9
AT1G77130	plant glycogenin-like starch initiation protein 2	13.9
AT5G19630	alpha/beta-Hydrolases superfamily protein	13.9
AT5G64090	Unknown protein	13.8
AT1G04620	coenzyme F420 hydrogenase family / dehydrogenase, beta subunit family	13.8
AT2G25605	unknown protein, LOCATED IN: chloroplast	13.7
AT1G63700	Protein kinase superfamily protein	13.6
AT2G43235	unknown protein, LOCATED IN: chloroplast	13.6
AT2G34720	nuclear factor Y, subunit A4	13.3
AT1G06240	Protein of unknown function DUF455	13.3
AT5G57930	Arabidopsis thaliana protein of unknown function (DUF794)	13.3
AT4G24310	Protein of unknown function (DUF679)	13.1
AT5G49970	pyridoxin (pyrodoxamine) 5'-phosphate oxidase	13.1
AT5G03900	Iron-sulphur cluster biosynthesis family protein	12.9
AT4G00390	DNA-binding storekeeper protein-related transcriptional regulator	12.8
AT3G55640	Mitochondrial substrate carrier family protein	12.7
AT1G50020	unknown protein, LOCATED IN: chloroplast thylakoid membrane, chloroplast	12.7
AT3G02520	general regulatory factor 7	12.7
AT1G21770	Acyl-CoA N-acyltransferases (NAT) superfamily protein	12.6
AT4G22830	unknown protein	12.6
AT5G49710	unknown protein	12.6
AT5G03552	MIR822a; miRNA	12.6
AT5G47080	casein kinase II beta chain 1	12.6
AT5G02200	far-red-elongated hypocotyl1-like	12.6
AT1G02690	importin alpha isoform 6	12.6
AT1G68190	B-box zinc finger family protein	12.5
AT3G20060	ubiquitin-conjugating enzyme19	12.5
AT3G06060	NAD(P)-binding Rossmann-fold superfamily protein	12.5
AT3G49790	Carbohydrate-binding protein	12.4
AT3G24550	proline extensin-like receptor kinase 1	12.3
AT3G52840	beta-galactosidase 2	12.3
AT4G39235	unknown protein	12.3
AT3G55040	glutathione transferase lambda 2	12.2
AT1G54220	Dihydrolipoamide acetyltransferase, long form protein	12.2

AT3G27180	S-adenosyl-L-methionine-dependent methyltransferases superfamily protein	12.2
AT1G18160	Protein kinase superfamily protein	12.2
AT1G26650	unknown protein	12.1
AT4G30360	cyclic nucleotide-gated channel 17	12.1
AT3G15530	S-adenosyl-L-methionine-dependent methyltransferases superfamily protein	12.0
AT3G55420	unknown protein	12.0
AT1G06470	Nucleotide/sugar transporter family protein	12.0
AT5G51960	Unknown protein, CONTAINS InterPro DOMAIN/s: Complex 1 LYR protein (InterPro:IPR008011	12.0
AT1G31350	KAR-UP F-box 1	11.9
AT1G56300	Chaperone DnaJ-domain superfamily protein	11.8
AT5G01740	Nuclear transport factor 2 (NTF2) family protein	11.8
AT1G77770	Protein of unknown function (DUF1644)	11.8
AT1G19740	ATP-dependent protease La (LON) domain protein	11.7
AT3G27906	unknown protein	11.7
AT4G39510	cytochrome P450, family 96, subfamily A, polypeptide 12	11.7
AT3G53530	Chloroplast-targeted copper chaperone protein	11.7
AT5G51640	Plant protein of unknown function (DUF828)	11.7
AT3G52180	dual specificity protein phosphatase (DsPTP1) family protein	11.6
AT1G54060	6B-interacting protein 1-like 1	11.6
AT3G46290	hercules receptor kinase 1	11.6
AT3G53340	nuclear factor Y, subunit B10	11.5
AT3G27570	Sucrase/ferredoxin-like family protein	11.5
AT5G20200	nucleoporin-related	11.5
AT1G67890	PAS domain-containing protein tyrosine kinase family protein	11.4
AT3G03305	Calcineurin-like metallo-phosphoesterase superfamily protein	11.4
AT1G16570	UDP-Glycosyltransferase superfamily protein	11.3
AT5G02800	Protein kinase superfamily protein	11.1
AT1G31410	putrescine-binding periplasmic protein-related	11.1
AT2G42910	Phosphoribosyltransferase family protein	11.0
AT5G06950	bZIP transcription factor family protein	11.0
AT5G59500	protein C-terminal S-isoprenylcysteine carboxyl O-methyltransferases	10.9
AT4G08290	nodulin MtN21 /EamA-like transporter family protein	10.9
AT5G51280	DEAD-box protein abstrakt, putative	10.9
AT2G31820	Ankyrin repeat family protein	10.9
AT5G16270	sister chromatid cohesion 1 protein 4	10.8
AT2G42680	multiprotein bridging factor 1A	10.8
AT1G10270	glutamine-rich protein 23	10.8
AT2G29320	NAD(P)-binding Rossmann-fold superfamily protein	10.8
AT1G36370	serine hydroxymethyltransferase 7	10.8
AT1G56500	haloacid dehalogenase-like hydrolase family protein	10.8
AT1G49820	S-methyl-5-thioribose kinase	10.8
AT2G06990	RNA helicase, ATP-dependent, SK12/DOB1 protein	10.6
AT3G48060	BAH domain ;TFIIS helical bundle-like domain	10.6
AT4G38360	Protein of unknown function (DUF300)	10.5
AT4G32190	Myosin heavy chain-related protein	10.4
AT1G07010	Calcineurin-like metallo-phosphoesterase superfamily protein	10.4
AT5G61500	autophagy 3 (APG3)	10.3
AT2G28470	beta-galactosidase 8	10.3
AT3G18560	unknown protein	10.3
AT3G24120	Homeodomain-like superfamily protein	10.3
AT3G26890	unknown protein	10.2
AT5G25890	indole-3-acetic acid inducible 28	10.1
AT3G10620	nudix hydrolase homolog 26	10.1
AT1G63900	E3 Ubiquitin ligase family protein	10.1

AT3G23620	Ribosomal RNA processing Brix domain protein	10.1
AT5G37310	Endomembrane protein 70 protein family	10.0
AT2G43350	glutathione peroxidase 3	10.0
AT4G20130	plastid transcriptionally active 14	10.0
AT1G04680	Pectin lyase-like superfamily protein	10.0

Table A3.3 1 Genes upregulated more than 10-fold in wild type seedlings compared to *parg1-2* seedlings when treated with MMS.

Gene ID	Name	Fold change
AT5G24640	unknown protein	1048.22
AT3G57610	adenylosuccinate synthase	339.08
AT2G19560	proteasome family protein	317.76
AT2G35390	Phosphoribosyltransferase family protein	265.44
AT1G71270	Vps52 / Sac2 family	226.69
AT4G10730	Protein kinase superfamily protein	217.01
AT2G29350	senescence-associated gene 13	201.50
AT2G16070	plastid division2	200.54
AT5G50430	ubiquitin-conjugating enzyme 33	188.91
AT3G23990	heat shock protein 60	183.39
AT5G41740	Disease resistance protein (TIR-NBS-LRR class) family	143.38
AT1G17690	Unknown	135.99
AT4G37370	cytochrome P450, family 81, subfamily D, polypeptide 8	123.29
AT5G36920	unknown protein;	122.06
AT3G07300	NagB/RpiA/CoA transferase-like superfamily protein	118.19
AT3G57765	U2.3; snRNA	116.25
AT5G27400	S-adenosyl-L-methionine-dependent methyltransferases superfamily protein	115.28
AT1G28490	syntaxin of plants 61	113.79
AT1G04990	Zinc finger C-x8-C-x5-C-x3-H type family protein	99.46
AT5G17930	MIF4G domain-containing protein / MA3 domain-containing protein	97.20
AT1G71260	WHIRLY 2	94.80
AT4G03120	C2H2 and C2HC zinc fingers superfamily protein	93.71
AT2G29500	HSP20-like chaperones superfamily protein	89.41
AT1G76070	unknown protein;	87.96
AT4G00620	Amino acid dehydrogenase family protein	87.22
AT4G21090	MITOCHONDRIAL FERREDOXIN 2	77.63
AT1G14130	2-oxoglutarate (2OG) and Fe(II)-dependent oxygenase superfamily protein	71.80
AT3G51050	FG-GAP repeat-containing protein	71.56
AT3G07750	3'-5'-exoribonuclease family protein	68.77
AT1G28540	unknown protein	67.46
AT3G15090	GroES-like zinc-binding alcohol dehydrogenase family protein	67.46
AT3G24820	BSD domain-containing protein	66.83
AT3G54010	FKBP-type peptidyl-prolyl cis-trans isomerase family protein	66.00
AT1G28240	Protein of unknown function (DUF616)	65.37
AT1G31220	Formyl transferase	64.40
AT1G04625	Polynucleotidyl transferase, ribonuclease H-like superfamily protein	62.21
AT2G42160	zinc finger (ubiquitin-hydrolase) domain-containing protein	60.98
AT1G80210	Mov34/MPN/PAD-1 family protein	60.75
AT1G67950	RNA-binding (RRM/RBD/RNP motifs) family protein	60.26
AT2G20940	Protein of unknown function (DUF1279)	60.04
AT3G15650	alpha/beta-Hydrolases superfamily protein	59.22

AT4G28070	AFG1-like ATPase family protein	59.05
AT1G72470	exocyst subunit exo70 family protein D1	58.36
AT3G08590	Phosphoglycerate mutase, 2,3-bisphosphoglycerate-independent	58.25
AT3G53480	pleiotropic drug resistance 9	57.60
AT2G17500	Auxin efflux carrier family protein	56.99
AT1G23410	Ribosomal protein S27a / Ubiquitin family protein	56.96
AT5G24060	Pentatricopeptide repeat (PPR) superfamily protein	55.40
AT4G19190	zinc knuckle (CCHC-type) family protein	54.49
AT2G31730	basic helix-loop-helix (bHLH) DNA-binding superfamily protein	54.25
AT5G63480	unknown protein	53.23
AT5G23880	cleavage and polyadenylation specificity factor 100	51.91
AT3G54420	homolog of carrot EP3-3 chitinase	49.61
AT1G70790	Calcium-dependent lipid-binding (CaLB domain) family protein	49.57
AT1G71940	SNARE associated Golgi protein family	48.60
AT4G20860	FAD-binding Berberine family protein	48.56
AT4G20010	plastid transcriptionally active 9	48.05
AT1G77000	RNI-like superfamily protein	47.79
AT4G08035	other RNA	47.62
AT1G30040	gibberellin 2-oxidase	47.40
AT2G42360	RING/U-box superfamily protein	47.30
AT2G26550	heme oxygenase 2	47.28
AT5G20730	Transcriptional factor B3 family protein / auxin-responsive factor AUX/IAA-related	46.36
AT4G35730	Regulator of Vps4 activity in the MVB pathway protein	46.28
AT3G58750	citrate synthase 2	45.85
AT4G25630	fibrillarin 2	45.14
AT5G65270	RAB GTPase homolog A4A	44.49
AT5G04180	alpha carbonic anhydrase 3	44.11
AT1G18580	galacturonosyltransferase 11	44.09
AT1G67490	glucosidase 1	44.01
AT2G37770	NAD(P)-linked oxidoreductase superfamily protein	44.01
AT5G16290	VALINE-TOLERANT 1	43.81
AT1G65030	Transducin/WD40 repeat-like superfamily protein	43.54
AT2G45023	other RNA	43.04
AT2G36800	don-glucosyltransferase 1	41.83
AT4G36400	FAD-linked oxidases family protein	41.51
AT3G29270	RING/U-box superfamily protein	40.77
AT4G31860	Protein phosphatase 2C family protein	40.62
AT1G64350	Transducin/WD40 repeat-like superfamily protein	40.45
AT5G20000	AAA-type ATPase family protein	40.37
AT3G52050	5'-3' exonuclease family protein	40.02
AT4G25710	Galactose oxidase/kelch repeat superfamily protein	39.93
AT5G33320	Glucose-6-phosphate/phosphate translocator-related	38.87
AT2G25180	response regulator 12	38.73
AT2G31410	unknown protein	38.67
AT4G02280	sucrose synthase 3	38.21
AT1G63260	tetraspanin10	37.99
AT1G10700	phosphoribosyl pyrophosphate (PRPP) synthase 3	37.54
AT3G58560	DNAse I-like superfamily protein	36.60
AT5G35320	unknown protein	36.60
AT1G21630	Calcium-binding EF hand family protein	35.35
AT3G52200	Dihydrolipoamide acetyltransferase, long form protein	35.27
AT1G63780	Ribosomal RNA processing Brix domain protein	35.24
AT4G36680	Tetratricopeptide repeat (TPR)-like superfamily protein	34.82
AT5G27395	Mitochondrial inner membrane translocase complex, subunit Tim44-related protein	34.76

AT5G54380	protein kinase family protein	34.72
AT1G50410	SNF2 domain-containing protein / helicase domain-containing protein / zinc finger protein-related	34.66
AT2G17670	Tetratricopeptide repeat (TPR)-like superfamily protein	34.63
AT1G76510	ARID/BRIGHT DNA-binding domain-containing protein	34.63
AT1G26650	unknown protein (source: NCBI BLink).	34.50
AT3G10815	RING/U-box superfamily protein	34.43
AT1G26460	Tetratricopeptide repeat (TPR)-like superfamily protein	34.11
AT4G26160	atypical CYS HIS rich thioredoxin 1	33.96
AT2G19950	golgin candidate 1	33.46
AT2G32030	Acyl-CoA N-acyltransferases (NAT) superfamily protein	33.33
AT5G25110	CBL-interacting protein kinase 25	33.08
AT5G21280	hydroxyproline-rich glycoprotein family protein	32.68
AT4G17950	AT hook motif DNA-binding family protein	32.25
AT5G67130	PLC-like phosphodiesterases superfamily protein	31.95
AT5G48950	Thioesterase superfamily protein	31.95
AT4G27650	Eukaryotic release factor 1 (eRF1) family protein	31.78
AT2G32020	Acyl-CoA N-acyltransferases (NAT) superfamily protein	31.74
AT1G78210	alpha/beta-Hydrolases superfamily protein	31.47
AT3G59820	LETM1-like protein	31.06
AT3G07565	Protein of unknown function (DUF3755)	30.80
AT4G11740	Ubiquitin-like superfamily protein	30.69
AT5G56660	IAA-leucine resistant (ILR)-like 2	30.69
AT4G08150	KNOTTED-like from Arabidopsis thaliana	30.56
AT3G53720	cation/H+ exchanger 20	30.44
AT2G24250	Protein of unknown function (DUF295)	30.43
AT4G30580	Phospholipid/glycerol acyltransferase family protein	30.22
AT3G26670	Protein of unknown function (DUF803)	30.01
AT3G16560	Protein phosphatase 2C family protein	29.93
AT1G04980	PDI-like 2-2	29.74
AT5G66760	succinate dehydrogenase 1-1	29.65
AT3G49860	ADP-ribosylation factor-like A1B	29.45
AT2G34900	Transcription factor GTE6	29.32
AT2G40400	Protein of unknown function (DUF399 and DUF3411)	28.96
AT2G03350	Protein of unknown function, DUF538	28.95
AT2G29190	pumilio 2	28.89
AT1G24340	FAD/NAD(P)-binding oxidoreductase family protein	28.80
AT2G45950	SKP1-like 20	28.71
AT1G20300	Pentatricopeptide repeat (PPR) superfamily protein	28.62
AT1G31550	GDSL-like Lipase/Acylhydrolase superfamily protein	28.56
AT1G69980	unknown protein	28.52
AT1G48570	zinc finger (Ran-binding) family protein	28.50
AT5G47970	Aldolase-type TIM barrel family protein	28.37
AT1G04770	Tetratricopeptide repeat (TPR)-like superfamily protein	28.36
AT1G17180	glutathione S-transferase TAU 25	28.33
AT5G52060	BCL-2-associated athanogene 1	28.28
AT1G49170	Protein of unknown function (DUF167)	28.25
AT1G28520	vascular plant one zinc finger protein	27.32
AT3G61380	Phosphatidylinositol N-acetyglucosaminlytransferase subunit P-related	27.01
AT1G72730	DEA(D/H)-box RNA helicase family protein	26.96
AT2G20370	Exostosin family protein	26.88
AT2G34170	Protein of unknown function (DUF688)	26.86
AT5G24030	SLAC1 homologue 3	26.58
AT1G77550	tubulin-tyrosine ligases;tubulin-tyrosine ligases	26.55
AT1G62430	CDP-diacylglycerol synthase 1	26.53
AT5G05560	E3 ubiquitin ligase, putative	26.53

AT4G37180	Homeodomain-like superfamily protein	26.39
AT1G05575	unknown protein	26.34
AT2G44180	methionine aminopeptidase 2A	26.34
AT2G20180	phytochrome interacting factor 3-like 5	26.10
AT3G48880	RNI-like superfamily protein	26.06
AT2G20020	RNA-binding CRS1 / YhbY (CRM) domain-containing protein	25.95
AT1G73965	CLAVATA3/ESR-RELATED 13	25.90
AT1G74250	DNAJ heat shock N-terminal domain-containing protein	25.56
AT5G58980	Neutral/alkaline non-lysosomal ceramidase	25.56
AT1G52320	Protein of unknown function DUF632	25.47
AT2G37020	Translin family protein	25.45
AT1G09150	pseudouridine synthase and archaeosine transglycosylase (PUA) domain-containing protein	25.42
AT5G50370	Adenylate kinase family protein	25.13
AT1G29790	S-adenosyl-L-methionine-dependent methyltransferases superfamily protein	24.97
AT3G57710	Protein kinase superfamily protein	24.95
AT3G63390	unknown protein	24.62
AT5G61060	histone deacetylase 5	24.61
AT1G49620	Cyclin-dependent kinase inhibitor family protein	24.47
AT3G02320	N2,N2-dimethylguanosine tRNA methyltransferase	24.26
AT4G14040	selenium-binding protein 2	24.18
AT1G53650	CTC-interacting domain 8	23.67
AT3G18770	Autophagy-related protein 13	23.62
AT3G03340	LUC7 related protein	23.44
AT5G16270	sister chromatid cohesion 1 protein 4	23.30
AT3G27180	S-adenosyl-L-methionine-dependent methyltransferases superfamily protein	23.30
AT3G49000	RNA polymerase III subunit RPC82 family protein	23.29
AT1G50450	Saccharopine dehydrogenase	23.14
AT2G37990	ribosome biogenesis regulatory protein (RRS1) family protein	23.14
AT1G58180	beta carbonic anhydrase 6	23.05
AT5G62760	P-loop containing nucleoside triphosphate hydrolases superfamily protein	22.88
AT3G20500	purple acid phosphatase 18	22.81
AT3G05970	long-chain acyl-CoA synthetase 6	22.68
AT1G63900	E3 Ubiquitin ligase family protein	22.66
AT1G80245	Spc97 / Spc98 family of spindle pole body (SBP) component	22.46
AT3G19290	ABRE binding factor 4	22.45
AT5G08360	Protein of unknown function (DUF789)	22.42
AT5G65400	alpha/beta-Hydrolases superfamily protein	22.31
AT1G63810	CONTAINS InterPro DOMAIN/s: Nrap protein (InterPro:IPR005554)	22.07
AT1G74290	alpha/beta-Hydrolases superfamily protein	22.00
AT3G62370	heme binding	21.91
AT2G23170	Auxin-responsive GH3 family protein	21.84
AT2G41730	unknown protein	21.83
AT5G61770	PETER PAN-like protein	21.82
AT5G40460	unknown protein	21.71
AT2G04040	MATE efflux family protein	21.68
AT1G74910	ADP-glucose pyrophosphorylase family protein	21.59
AT1G64220	translocase of outer membrane 7 kDa subunit 2	21.52
AT1G20370	Pseudouridine synthase family protein	21.37
AT3G53940	Mitochondrial substrate carrier family protein	21.37
AT4G37990	elicitor-activated gene 3-2	21.36
AT1G02330	CONTAINS InterPro DOMAIN/s: Hepatocellular carcinoma-associated antigen 59 (InterPro:IPR010756)	21.35
AT5G42150	Glutathione S-transferase family protein	21.27

AT5G61030	glycine-rich RNA-binding protein 3	21.15
AT2G06990	RNA helicase, ATP-dependent, SK12/DOB1 protein	21.12
AT4G28480	DNAJ heat shock family protein	21.12
AT4G25225	unknown protein	21.10
AT5G16070	TCP-1/cpn60 chaperonin family protein	21.10
AT4G25730	FtsJ-like methyltransferase family protein	20.93
AT3G17450	hAT dimerisation domain-containing protein	20.92
AT2G24100	unknown protein	20.79
AT4G14965	membrane-associated progesterone binding protein 4	20.72
AT5G10300	methyl esterase 5	20.67
AT3G08950	electron transport SCO1/SenC family protein	20.62
AT3G19720	P-loop containing nucleoside triphosphate hydrolases superfamily protein	20.61
AT1G77030	hydrolases, acting on acid anhydrides, in phosphorus-containing anhydrides;ATP-dependent helicases;nucleic acid binding;ATP binding;RNA binding;helicases	20.39
AT1G68920	basic helix-loop-helix (bHLH) DNA-binding superfamily protein	20.38
AT1G10870	ARF-GAP domain 4	20.38
AT3G06820	Mov34/MPN/PAD-1 family protein	20.37
AT5G35940	Mannose-binding lectin superfamily protein	19.86
AT3G06430	Tetratricopeptide repeat (TPR)-like superfamily protein	19.82
AT2G25605	unknown proteinPlants - 36; Viruses - 0; Other Eukaryotes - 33 (source: NCBI BLink).	19.78
AT2G45730	eukaryotic initiation factor 3 gamma subunit family protein	19.52
AT1G34630	BEST Arabidopsis thaliana protein match is: Mitochondrial import inner membrane translocase subunit Tim17/Tim22/Tim23 family protein (TAIR:AT5G51150.1)	19.49
AT3G10690	DNA GYRASE A	19.42
AT5G13020	Emsy N Terminus (ENT)/ plant Tudor-like domains-containing protein	19.41
AT5G63780	RING/FYVE/PHD zinc finger superfamily protein	19.31
AT5G15740	O-fucosyltransferase family protein	19.21
AT4G32400	Mitochondrial substrate carrier family protein	19.15
AT5G40980	Protein of unknown function (DUF 3339)	19.09
AT5G03160	homolog of mamallian P58IPK	19.04
AT5G29000	Homeodomain-like superfamily protein	19.02
AT5G41670	6-phosphogluconate dehydrogenase family protein	18.98
AT1G29810	Transcriptional coactivator/pterin dehydratase	18.96
AT1G02690	importin alpha isoform 6	18.87
AT1G72710	casein kinase 1-like protein 2	18.87
AT1G67630	DNA polymerase alpha 2	18.53
AT1G30070	SGS domain-containing protein	18.39
AT4G22830	Protein of unknown function DUF2499	18.39
AT3G03740	BTB-POZ and MATH domain 4	18.39
AT5G10940	transducin family protein / WD-40 repeat family protein	18.32
AT1G15200	protein-protein interaction regulator family protein	18.29
AT1G76300	snRNP core protein SMD3	18.26
AT5G65900	DEA(D/H)-box RNA helicase family protein	18.24
AT4G22920	non-yellowing 1	18.22
AT4G18740	Rho termination factor	18.19
AT3G53810	Concanavalin A-like lectin protein kinase family protein	18.18
AT1G21640	NAD kinase 2	18.18
AT1G21980	phosphatidylinositol-4-phosphate 5-kinase 1	18.13
AT1G30510	root FNR 2	18.12
AT5G18270	Arabidopsis NAC domain containing protein 87	18.09
AT2G41960	unknown protein	18.08
AT1G12800	Nucleic acid-binding, OB-fold-like protein	17.97
AT2G34720	nuclear factor Y, subunit A4	17.82

AT3G51870	Mitochondrial substrate carrier family protein	17.74
AT5G07900	Mitochondrial transcription termination factor family protein	17.74
AT1G07400	HSP20-like chaperones superfamily protein	17.71
AT1G03910	CONTAINS InterPro DOMAIN/s: Cactin protein, cactus-binding domain, C-terminal (InterPro:IPR019134), Cactin, central region (InterPro:IPR018816)	17.67
AT2G17230	EXORDIUM like 5	17.67
AT1G61800	glucose-6-phosphate/phosphate translocator 2	17.62
AT4G02430	RNA-binding (RRM/RBD/RNP motifs) family protein	17.61
AT5G35210	metalloendopeptidases;zinc ion binding;DNA binding	17.58
AT3G13080	multidrug resistance-associated protein 3	17.57
AT5G48290	Heavy metal transport/detoxification superfamily protein	17.57
AT5G63440	Protein of unknown function (DUF167)	17.56
AT1G60680	NAD(P)-linked oxidoreductase superfamily protein	17.49
AT1G65032	unknown protein	17.48
AT5G45930	magnesium chelatase i2	17.47
AT5G02150	Fes1C	17.46
AT1G54380	spliceosome protein-related	17.42
AT2G37230	Tetratricopeptide repeat (TPR)-like superfamily protein	17.33
AT2G42810	protein phosphatase 5.2	17.31
AT4G06634	zinc finger (C2H2 type) family protein	17.22
AT4G38360	Protein of unknown function (DUF300)	17.22
AT1G55150	DEA(D/H)-box RNA helicase family protein	17.22
AT1G55590	RNI-like superfamily protein	17.15
AT2G25620	DNA-binding protein phosphatase 1	17.13
AT5G04900	NYC1-like	17.13
AT1G74530	unknown protein	17.1
AT3G13610	2-oxoglutarate (2OG) and Fe(II)-dependent oxygenase superfamily protein	17.05
AT1G75850	VPS35 homolog B	16.99
AT3G26090	G-protein coupled receptors;GTPase activators	16.98
AT4G28220	NAD(P)H dehydrogenase B1	16.89
AT3G28100	nodulin MtN21 /EamA-like transporter family protein	16.86
AT1G31810	Formin Homology 14	16.84
AT3G45230	hydroxyproline-rich glycoprotein family protein	16.80
AT5G08780	winged-helix DNA-binding transcription factor family protein	16.70
AT1G49820	S-methyl-5-thioribose kinase	16.62
AT4G31550	WRKY DNA-binding protein 11	16.61
AT1G74340	dolichol phosphate-mannose biosynthesis regulatory protein-related	16.50
AT1G54570	Esterase/lipase/thioesterase family protein	16.42
AT5G66950	Pyridoxal phosphate (PLP)-dependent transferases superfamily protein	16.36
AT5G45250	Disease resistance protein (TIR-NBS-LRR class) family	16.29
AT2G26200	S-adenosyl-L-methionine-dependent methyltransferases superfamily protein	16.26
AT4G02725	unknown protein	16.13
AT1G08125	S-adenosyl-L-methionine-dependent methyltransferases superfamily protein	16.09
AT5G53330	Ubiquitin-associated/translation elongation factor EF1B protein	16.06
AT3G22740	homocysteine S-methyltransferase 3	16.06
AT5G42130	Mitochondrial substrate carrier family protein	16.05
AT4G38710	glycine-rich protein	16.04
AT4G20380	LSD1 zinc finger family protein	16.04
AT1G77440	20S proteasome beta subunit C2	16.02
AT2G30550	alpha/beta-Hydrolases superfamily protein	16.00
AT3G15352	cytochrome c oxidase 17	15.98
AT1G15480	Tetratricopeptide repeat (TPR)-like superfamily protein	15.98
AT5G44785	organellar single-stranded DNA binding protein 3	15.90
AT1G19680	RING/U-box superfamily protein	15.83

AT3G52660	RNA-binding (RRM/RBD/RNP motifs) family protein	15.76
AT1G27840	Transducin/WD40 repeat-like superfamily protein	15.70
AT3G11660	NDR1/HIN1-like 1	15.67
AT3G09970	Calcineurin-like metallo-phosphoesterase superfamily protein	15.61
AT1G06180	myb domain protein 13	15.60
AT3G55040	glutathione transferase lambda 2	15.60
AT5G17520	root cap 1 (RCP1)	15.53
AT2G21300	ATP binding microtubule motor family protein	15.53
AT2G33810	squamosa promoter binding protein-like 3	15.46
AT2G30500	Kinase interacting (KIP1-like) family protein	15.46
AT3G59780	Rhodanese/Cell cycle control phosphatase superfamily protein	15.39
AT1G29550	Eukaryotic initiation factor 4E protein	15.38
AT5G05750	DNAJ heat shock N-terminal domain-containing protein	15.37
AT3G18535	tubulin-tyrosine ligases	15.36
AT5G44710	CONTAINS InterPro DOMAIN/s: Ribosomal protein S27/S33, mitochondrial (InterPro:IPR013219	15.28
AT1G06410	trehalose-phosphatase/synthase 7	15.26
AT3G21351	unknown protein	15.24
AT2G32850	Protein kinase superfamily protein	15.17
AT4G30800	Nucleic acid-binding, OB-fold-like protein	15.17
AT1G14580	C2H2-like zinc finger protein	15.16
AT5G51960	CONTAINS InterPro DOMAIN/s: Complex 1 LYR protein (InterPro:IPR0080110)	15.12
AT5G02200	far-red-elongated hypocotyl1-like	15.11
AT2G47000	ATP binding cassette subfamily B4	15.08
AT1G35460	basic helix-loop-helix (bHLH) DNA-binding superfamily protein	15.00
AT5G25560	CHY-type/CTCHY-type/RING-type Zinc finger protein	14.96
AT3G45260	C2H2-like zinc finger protein	14.95
AT5G35930	AMP-dependent synthetase and ligase family protein	14.93
AT3G06810	acyl-CoA dehydrogenase-related	14.92
AT5G17690	like heterochromatin protein (LHP1)	14.83
AT5G42730	pseudogene similar to ACT domain-containing protein, similar to F-box family protein	14.83
AT4G36010	Pathogenesis-related thaumatin superfamily protein	14.81
AT5G59140	BTB/POZ domain-containing protein	14.81
AT1G48540	Outer arm dynein light chain 1 protein	14.76
AT5G40510	Sucrase/ferredoxin-like family protein	14.73
AT2G41900	CCCH-type zinc finger protein with ARM repeat domain	14.69
AT3G59220	pirin	14.67
AT1G80130	Tetratricopeptide repeat (TPR)-like superfamily protein	14.58
AT2G46535	unknown protein	14.56
AT5G24740	Protein of unknown function (DUF1162)	14.56
AT3G02520	general regulatory factor 7	14.43
AT3G57480	zinc finger (C2H2 type, AN1-like) family protein	14.40
AT3G02070	Cysteine proteinases superfamily protein	14.34
AT5G51300	splicing factor-related	14.31
AT5G06950	bZIP transcription factor family protein	14.30
AT2G46510	ABA-inducible BHLH-type transcription factor	14.30
AT5G54900	RNA-binding protein 45A	14.30
AT5G10650	RING/U-box superfamily protein	14.27
AT2G32810	beta galactosidase 9	14.26
AT3G52940	Ergosterol biosynthesis ERG4/ERG24 family	14.26
AT3G18760	Translation elongation factor EF1B/ribosomal protein S6 family protein	14.25
AT5G19250	Glycoprotein membrane precursor GPI-anchored	14.24
AT5G23460	unknown protein	14.24
AT3G09650	Tetratricopeptide repeat (TPR)-like superfamily protein	14.20

AT5G39670	Calcium-binding EF-hand family protein	14.20
AT3G05990	Leucine-rich repeat (LRR) family protein	14.19
AT5G12310	RING/U-box superfamily protein	14.13
AT5G14520	pescadillo-related	14.12
AT1G79210	N-terminal nucleophile aminohydrolases (Ntn hydrolases) superfamily protein	14.12
AT2G19385	zinc ion binding	14.11
AT4G31750	HOPW1-1-interacting 2	14.10
AT1G07090	Protein of unknown function (DUF640)	14.07
AT2G03510	SPFH/Band 7/PHB domain-containing membrane-associated protein family	14.05
AT5G55300	DNA topoisomerase I alpha	13.99
AT3G43230	RING/FYVE/PHD-type zinc finger family protein	13.93
AT5G09770	Ribosomal protein L17 family protein	13.93
AT4G38760	Protein of unknown function (DUF3414)	13.93
AT2G18900	Transducin/WD40 repeat-like superfamily protein	13.93
AT3G42170	BED zinc finger ;hAT family dimerisation domain	13.91
AT1G07010	Calcineurin-like metallo-phosphoesterase superfamily protein	13.90
AT3G22570	Bifunctional inhibitor/lipid-transfer protein/seed storage 2S albumin superfamily protein	13.90
AT1G66900	alpha/beta-Hydrolases superfamily protein	13.89
AT5G04710	Zn-dependent exopeptidases superfamily protein	13.89
AT4G25260	Plant invertase/pectin methylesterase inhibitor superfamily protein	13.87
AT1G75510	Transcription initiation factor IIF, beta subunit	13.74
AT1G07910	RNAligase	13.71
AT2G31840	Thioredoxin superfamily protein	13.69
AT3G48760	DHHC-type zinc finger family protein	13.62
AT4G14710	RmlC-like cupins superfamily protein	13.59
AT3G26360	Ribosomal protein S21 family protein	13.59
AT2G37035	unknown protein	13.58
AT3G25410	Sodium Bile acid symporter family	13.51
AT1G04250	AUX/IAA transcriptional regulator family protein	13.46
AT3G28930	AIG2-like (avirulence induced gene) family protein	13.45
AT5G44430	plant defensin 1.2C	13.43
AT4G12340	copper ion binding	13.34
AT3G48200	unknown protein	13.31
AT3G48380	Peptidase C78, ubiquitin fold modifier-specific peptidase 1/ 2	13.26
AT5G23850	Arabidopsis thaliana protein of unknown function (DUF821)	13.24
AT3G22980	Ribosomal protein S5/Elongation factor G/III/V family protein	13.23
AT1G31860	histidine biosynthesis bifunctional protein (HISIE)	13.23
AT1G02150	Tetratricopeptide repeat (TPR)-like superfamily protein	13.18
AT5G57860	Ubiquitin-like superfamily protein	13.18
AT2G14045	unknown protein	13.17
AT1G01710	Acyl-CoA thioesterase family protein	13.12
AT4G13360	ATP-dependent caseinolytic (Clp) protease/crotonase family protein	13.03
AT3G47860	chloroplastic lipocalin	12.99
AT5G53045	unknown protein	12.99
AT3G06740	GATA transcription factor 15	12.98
AT1G78995	unknown protein	12.97
AT5G23340	RNI-like superfamily protein	12.95
AT5G49970	pyridoxin (pyrodoxamine) 5'-phosphate oxidase	12.87
AT1G54220	Dihydrolipoamide acetyltransferase, long form protein	12.87
AT1G23280	MAK16 protein-related	12.87
AT1G07830	ribosomal protein L29 family protein	12.86
AT2G07723	pseudogene, similar to orf454~homology with two ORFs from Marchantia polymorpha mtDNA (orf169 and orf322),	12.86
AT5G11340	Acyl-CoA N-acyltransferases (NAT) superfamily protein	12.85

AT1G80890	unknown protein	12.83
AT1G74090	desulfo-glucosinolate sulfotransferase 18	12.81
AT5G40440	mitogen-activated protein kinase kinase 3	12.80
AT3G24350	syntaxin of plants 32	12.78
AT2G33340	MOS4-associated complex 3B	12.76
AT1G80270	PENTATRICOPEPTIDE REPEAT 596	12.69
AT4G02150	ARM repeat superfamily protein	12.63
AT4G24730	Calcineurin-like metallo-phosphoesterase superfamily protein	12.61
AT3G17120	unknown protein	12.54
AT2G46420	Plant protein 1589 of unknown function	12.52
AT2G42540	cold-regulated 15a	12.51
AT5G03780	TRF-like 10	12.39
AT3G56070	rotamase cyclophilin 2	12.37
AT2G27460	sec23/sec24 transport family protein	12.36
AT1G07030	Mitochondrial substrate carrier family protein	12.32
AT3G12400	Ubiquitin-conjugating enzyme/RWD-like protein	12.30
AT1G14560	Mitochondrial substrate carrier family protein	12.27
AT2G09800	transposable element gene	12.23
AT5G64090	CONTAINS InterPro DOMAIN/s: Hyccin (InterPro:IPR018619)	12.20
AT2G40095	Alpha/beta hydrolase related protein	12.18
AT5G49400	zinc knuckle (CCHC-type) family protein	12.17
AT3G19520	Protein of unknown function (DUF626)	12.17
AT2G41460	apurinic endonuclease-redox protein	12.14
AT4G39838	Potential natural antisense gene, locus overlaps with AT4G39840	12.11
AT5G35740	Carbohydrate-binding X8 domain superfamily protein	12.11
AT3G53340	nuclear factor Y, subunit B10	12.11
AT1G06380	Ribosomal protein L1p/L10e family	12.10
AT1G53540	HSP20-like chaperones superfamily protein	12.10
AT4G38960	B-box type zinc finger family protein	12.08
AT5G62480	glutathione S-transferase tau 9	12.07
AT5G16040	Regulator of chromosome condensation (RCC1) family protein	12.05
AT2G46580	Pyridoxamine 5'-phosphate oxidase family protein	12.05
AT5G03660	Family of unknown function (DUF662)	12.02
AT3G20060	ubiquitin-conjugating enzyme19	11.99
AT4G34640	squalene synthase 1	11.95
AT2G04080	MATE efflux family protein	11.92
AT3G03090	vacuolar glucose transporter 1	11.91
AT3G27906	unknown protein	11.89
AT5G04830	Nuclear transport factor 2 (NTF2) family protein	11.89
AT1G06470	Nucleotide/sugar transporter family protein	11.84
AT1G33060	NAC 014	11.84
AT5G18940	Mo25 family protein	11.82
AT4G10470	unknown protein	11.81
AT1G74800	Galactosyltransferase family protein	11.81
AT2G28550	related to AP2.7	11.80
AT5G42590	cytochrome P450, family 71, subfamily A, polypeptide 16	11.78
AT4G30990	ARM repeat superfamily protein	11.78
AT5G47980	HXXXD-type acyl-transferase family protein	11.76
AT1G08350	Endomembrane protein 70 protein family	11.75
AT1G19080	GINS complex protein	11.74
AT2G41500	WD-40 repeat family protein / small nuclear ribonucleoprotein Prp4p-related	11.72
AT5G16340	AMP-dependent synthetase and ligase family protein	11.71
AT2G35020	N-acetylglucosamine-1-phosphate uridylyltransferase 2	11.65
AT2G34680	Outer arm dynein light chain 1 protein	11.65
AT1G09130	ATP-dependent caseinolytic (Clp) protease/crotonase family protein	11.65

AT1G52730	Transducin/WD40 repeat-like superfamily protein	11.56
AT3G52840	beta-galactosidase 2	11.54
AT3G21080	ABC transporter-related	11.54
AT5G06110	DnaJ domain ;Myb-like DNA-binding domain	11.54
AT5G10920	L-Aspartase-like family protein	11.53
AT3G02065	P-loop containing nucleoside triphosphate hydrolases superfamily protein	11.52
AT1G31070	N-acetylglucosamine-1-phosphate uridylyltransferase 1	11.50
AT2G14900	Gibberellin-regulated family protein	11.50
AT3G60370	FKBP-like peptidyl-prolyl cis-trans isomerase family protein	11.49
AT5G35730	EXS (ERD1/XPR1/SYG1) family protein	11.48
AT3G18210	2-oxoglutarate (2OG) and Fe(II)-dependent oxygenase superfamily protein	11.48
AT4G14900	FRIGIDA-like protein	11.44
AT2G41830	Uncharacterized protein	11.40
AT5G08100	N-terminal nucleophile aminohydrolases (Ntn hydrolases) superfamily protein	11.39
AT4G36515	unknown protein	11.39
AT2G29440	glutathione S-transferase tau 6	11.38
AT5G62620	Galactosyltransferase family protein	11.37
AT1G03110	Transducin/WD40 repeat-like superfamily protein	11.37
AT5G64420	DNA polymerase V family	11.36
AT2G03120	signal peptide peptidase	11.35
AT4G13670	plastid transcriptionally active 5	11.35
AT2G46340	SPA (suppressor of phyA-105) protein family	11.35
AT5G37370	PRP38 family protein	11.34
AT3G19260	LAG1 homologue 2	11.32
AT2G18230	pyrophosphorylase 2	11.28
AT1G29940	nuclear RNA polymerase A2	11.26
AT1G75990	PAM domain (PCI/PINT associated module) protein	11.25
AT1G51950	indole-3-acetic acid inducible 18	11.24
AT2G40570	initiator tRNA phosphoribosyl transferase family protein	11.24
AT5G20590	TRICHOME BIREFRINGENCE-LIKE 5	11.20
AT5G14600	S-adenosyl-L-methionine-dependent methyltransferases superfamily protein	11.17
AT3G06435	Expressed protein	11.14
AT5G53940	Yippee family putative zinc-binding protein	11.12
AT2G32960	Phosphotyrosine protein phosphatases superfamily protein	11.09
AT4G09670	Oxidoreductase family protein	11.03
AT3G19990	unknown protein	11.00
AT1G77140	vacuolar protein sorting 45	11.0
AT5G50200	nitrate transmembrane transporters	10.93
AT1G01930	zinc finger protein-related	10.91
AT3G49570	response to low sulfur 3	10.89
AT4G32551	LisH dimerisation motif;WD40/YVTN repeat-like-containing domain	10.87
AT3G50530	CDPK-related kinase	10.87
AT4G22150	plant UBX domain-containing protein 3	10.86
AT2G17410	ARID/BRIGHT DNA-binding domain-containing protein	10.85
AT1G17510	unknown protein	10.85
AT3G01750	Ankyrin repeat family protein	10.85
AT3G09270	glutathione S-transferase TAU 8	10.84
AT3G57220	Glycosyl transferase family 4 protein	10.83
AT3G44200	NIMA (never in mitosis, gene A)-related 6	10.82
AT1G61870	pentatricopeptide repeat 336	10.79
AT1G55020	lipoxygenase 1	10.76
AT2G33850	unknown protein	10.76
AT4G02450	HSP20-like chaperones superfamily protein	10.76
AT5G18550	Zinc finger C-x8-C-x5-C-x3-H type family protein	10.75

AT3G62260	Protein phosphatase 2C family protein	10.73
AT1G10580	Transducin/WD40 repeat-like superfamily protein	10.73
AT5G23610	BEST Arabidopsis thaliana protein match is: SWITCH1 (TAIR:AT5G51330.1)	10.72
AT5G01290	mRNA capping enzyme family protein	10.71
AT1G16560	Per1-like family protein	10.66
AT4G31360	selenium binding	10.63
AT4G17140	pleckstrin homology (PH) domain-containing protein	10.61
AT5G50210	quinolinate synthase	10.57
AT4G26080	Protein phosphatase 2C family protein	10.56
AT5G24340	3'-5' exonuclease domain-containing protein	10.53
AT5G09380	RNA polymerase III RPC4	10.51
AT5G66070	RING/U-box superfamily protein	10.49
AT1G30210	TEOSINTE BRANCHED 1, cycloidea, and PCF family 24	10.47
AT1G42440	BEST Arabidopsis thaliana protein match is: P-loop containing nucleoside triphosphate hydrolases superfamily protein (TAIR:AT1G06720.1)	10.47
AT2G42070	nudix hydrolase homolog 23	10.46
AT1G80930	MIF4G domain-containing protein / MA3 domain-containing protein	10.46
AT3G63000	NPL4-like protein 1	10.46
AT4G14990	Topoisomerase II-associated protein PAT1	10.46
AT3G58180	ARM repeat superfamily protein	10.44
AT2G25110	stromal cell-derived factor 2-like protein precursor	10.44
AT5G10140	K-box region and MADS-box transcription factor family protein	10.44
AT4G01060	CAPRICE-like MYB3	10.40
AT1G19190	alpha/beta-Hydrolases superfamily protein	10.39
AT3G12370	Ribosomal protein L10 family protein	10.39
AT4G00660	RNAhelicase-like 8	10.38
AT3G03490	peroxin 19-1	10.37
AT2G47580	spliceosomal protein U1A	10.35
AT1G34210	somatic embryogenesis receptor-like kinase 2	10.35
AT1G22510	RING/U-box protein with domain of unknown function (DUF 1232)	10.35
AT4G09970	unknown protein	10.30
AT3G16170	AMP-dependent synthetase and ligase family protein	10.30
AT5G04550	Protein of unknown function (DUF668)	10.27
AT5G56260	Ribonuclease E inhibitor RraA/Dimethylmenaquinone methyltransferase	10.27
AT2G17350	unknown protein	10.25
AT1G29357	other RNA	10.23
AT1G64040	type one serine/threonine protein phosphatase 3	10.22
AT5G19180	E1 C-terminal related 1	10.20
AT3G54120	Reticulon family protein	10.19
AT3G29350	histidine-containing phosphotransmitter 2	10.19
AT5G04750	F1F0-ATPase inhibitor protein, putative	10.18
AT1G75660	5'-3' exoribonuclease 3	10.17
AT2G36850	glucan synthase-like 8	10.16
AT2G17340	Uncharacterised conserved protein (UCP030210)	10.12
AT2G34300	S-adenosyl-L-methionine-dependent methyltransferases superfamily protein	10.12
AT4G32240	unknown protein	10.11
AT3G47430	peroxin 11B	10.11
AT1G78410	VQ motif-containing protein	10.09
AT5G49710	unknown protein	10.08
AT5G16140	Peptidyl-tRNA hydrolase family protein	10.08
AT5G38200	Class I glutamine amidotransferase-like superfamily protein	10.04
AT1G24996	unknown protein	10.04
AT3G13440	S-adenosyl-L-methionine-dependent methyltransferases superfamily protein	10.04

AT1G77810	Galactosyltransferase family protein	10.02
AT2G02090	SNF2 domain-containing protein / helicase domain-containing protein	10.01
AT1G09200	Histone superfamily protein	10.00

Table A3.4 Genes downregulated more than 10-fold in wild type seedlings compared to *parg1-2* seedlings when treated with MMS.

Gene ID	Name	Fold change
AT5G20410	monogalactosyldiacylglycerol synthase 2	-141.91
AT3G05920	Heavy metal transport/detoxification superfamily protein	-102.17
AT4G14060	Polyketide cyclase/dehydrase and lipid transport superfamily protein	-85.15
AT4G12590	Protein of unknown function DUF106, transmembrane	-47.47
AT1G11840	glyoxalase I homolog	-18.53
AT5G12150	Rho GTPase activation protein (RhoGAP) with PH domain	-11.51

Table A3.5 Genes upregulated more than 10-fold in *parg1-2* seedlings compared to wild type seedlings when treated with MMS.

Gene ID	Name	Fold change
AT5G10040	unknown protein	1141.1
AT1G22920	COP9 signalosome 5A	604.7
AT5G51350	Leucine-rich repeat transmembrane protein kinase family protein	355.6
AT2G27450	nitrilase-like protein 1	343.5
AT3G13290	varicose-related	309.4
AT1G16960	Ubiquitin domain-containing protein	291.3
ATCG00330	chloroplast ribosomal protein S14	289.3
AT2G19870	tRNA/rRNA methyltransferase (SpoU) family protein	287.3
AT3G17300	unknown protein	251.1
AT3G09100	mRNA capping enzyme family protein	245.1
AT2G03670	cell division cycle 48B	243.1
AT1G75490	Integrase-type DNA-binding superfamily protein	241.1
AT5G66000	unknown protein	241.1
AT2G21180	unknown protein	227.0
AT3G47630	CONTAINS InterPro DOMAIN/s: Mitochondrial matrix Mmp37 (InterPro:IPR015222)	223.0
AT2G07798	unknown protein	212.9
AT4G14145	unknown protein	192.9
AT5G26280	TRAF-like family protein	190.3
AT5G04160	Nucleotide-sugar transporter family protein	180.8
AT5G44730	Haloacid dehalogenase-like hydrolase (HAD) superfamily protein	164.7
AT3G12270	protein arginine methyltransferase 3	138.6
AT2G38360	prenylated RAB acceptor 1.B4	98.9
AT2G35960	NDR1/HIN1-like 12	91.7
AT5G48540	receptor-like protein kinase-related family protein	81.4
ATMG01170	ATPase, F0 complex, subunit A protein	77.7
AT1G17050	solanesyl diphosphate synthase 2	74.8
AT2G03470	ELM2 domain-containing protein	68.8
AT4G32960	unknown protein	64.8
AT2G21060	glycine-rich protein 2B	61.5
AT5G10730	NAD(P)-binding Rossmann-fold superfamily protein	53.8

AT5G65925	unknown protein	53.3
AT5G49690	UDP-Glycosyltransferase superfamily protein	46.9
AT3G15920	Phox (PX) domain-containing protein	46.6
AT1G69750	cytochrome c oxidase 19-2	43.9
AT5G60860	RAB GTPase homolog A1F	40.1
AT4G37790	Homeobox-leucine zipper protein family	39.5
AT3G18215	Protein of unknown function, DUF599	35.3
AT1G25280	tubby like protein 10	33.8
AT1G65380	Leucine-rich repeat (LRR) family protein	33.7
AT3G21215	RNA-binding (RRM/RBD/RNP motifs) family protein	33.4
AT2G47980	sister-chromatid cohesion protein 3	32.1
AT4G09010	ascorbate peroxidase 4	29.6
AT3G12290	Amino acid dehydrogenase family protein	29.2
AT1G80510	Transmembrane amino acid transporter family protein	28.6
AT3G08670	unknown protein	28.1
AT3G33530	Transducin family protein / WD-40 repeat family protein	27.6
AT5G25780	eukaryotic translation initiation factor 3B-2	26.1
AT3G20970	NFU domain protein 4	25.9
AT1G74410	RING/U-box superfamily protein	25.4
AT3G60800	DHHC-type zinc finger family protein	25.2
AT3G27280	prohibitin 4	24.7
AT4G39690	CONTAINS InterPro DOMAIN/s: Mitochondrial inner membrane protein Mitofilin (InterPro:IPR019133)	24.3
AT3G54040	PAR1 protein	24.2
AT5G05190	Protein of unknown function (DUF3133)	23.9
AT1G35516	myb-like transcription factor family protein	23.2
AT1G19730	Thioredoxin superfamily protein	23.1
AT3G48330	protein-l-isoaspartate methyltransferase 1	22.7
AT4G32440	Plant Tudor-like RNA-binding protein	22.5
AT1G22610	C2 calcium/lipid-binding plant phosphoribosyltransferase family protein	21.3
AT5G15640	Mitochondrial substrate carrier family protein	21.0
AT3G02875	Peptidase M20/M25/M40 family protein	20.5
AT3G01850	Aldolase-type TIM barrel family protein	20.3
AT4G13590	Uncharacterized protein family (UPF0016)	20.2
AT1G67190	F-box/RNI-like superfamily protein	19.8
AT2G16790	P-loop containing nucleoside triphosphate hydrolases superfamily protein	19.1
AT1G09530	phytochrome interacting factor 3	19.0
AT2G31750	UDP-glucosyl transferase 74D1	18.2
AT1G56060	unknown protein	17.8
AT2G21340	MATE efflux family protein	17.7
AT2G21940	shikimate kinase 1	17.6
AT4G12250	UDP-D-glucuronate 4-epimerase 5	17.4
AT5G56590	O-Glycosyl hydrolases family 17 protein	17.2
AT1G09850	xylem bark cysteine peptidase 3	17.1
AT3G49160	pyruvate kinase family protein	16.9
AT4G13245	snoRNA	16.8
AT1G18650	plasmodesmata callose-binding protein 3	16.8
AT1G77510	PDI-like 1-2	16.7
AT4G33070	Thiamine pyrophosphate dependent pyruvate decarboxylase family protein	16.6
AT1G21790	TRAM, LAG1 and CLN8 (TLC) lipid-sensing domain containing protein	16.5
AT1G80190	partner of SLD five 1	16.4
AT4G24960	HVA22 homologue D	16.3
AT1G11390	Protein kinase superfamily protein	16.2
AT5G27730	Protein of unknown function (DUF1624)	16.0

AT5G64410	oligopeptide transporter 4	15.9
AT1G11820	O-Glycosyl hydrolases family 17 protein	15.9
AT1G07985	Expressed protein	15.9
AT3G57260	beta-1,3-glucanase 2	15.6
AT5G48412		15.6
AT5G25220	KNOTTED1-like homeobox gene 3	15.5
AT4G29420	F-box/RNI-like superfamily protein	15.5
AT5G51740	Peptidase family M48 family protein	15.4
AT1G03220	Eukaryotic aspartyl protease family protein	15.4
AT3G05940	Protein of unknown function (DUF300)	15.4
AT3G19980	flower-specific, phytochrome-associated protein phosphatase 3	15.3
AT4G39420	unknown protein	15.3
AT5G19570	unknown protein	15.2
AT3G29575	ABI five binding protein 3	15.0
AT5G54490	pinoid-binding protein 1	14.9
AT1G58848	Disease resistance protein (CC-NBS-LRR class) family	14.7
AT3G04830	Protein prenylyltransferase superfamily protein	14.7
AT5G23440	ferredoxin/thioredoxin reductase subunit A (variable subunit) 1	14.6
AT5G63120	P-loop containing nucleoside triphosphate hydrolases superfamily protein	14.5
AT4G09580	SNARE associated Golgi protein family	14.4
AT1G78630	Ribosomal protein L13 family protein	14.4
AT1G49760	poly(A) binding protein 8	14.2
AT1G33265	Transmembrane proteins 14C	14.1
AT5G57000	unknown protein	13.9
AT5G53860	embryo defective 2737	13.9
AT4G21280	photosystem II subunit QA	13.8
AT2G01930	basic pentacysteine1	13.8
AT5G18660	NAD(P)-binding Rossmann-fold superfamily protein	13.8
AT5G03030	Chaperone DnaJ-domain superfamily protein	13.6
AT3G59970	methylenetetrahydrofolate reductase 1	13.5
AT3G56040	UDP-glucose pyrophosphorylase 3	13.5
AT2G35744	snoRNA	13.3
AT5G57050	Protein phosphatase 2C family protein	13.2
AT5G38520	alpha/beta-Hydrolases superfamily protein	13.2
AT4G35785	RNA-binding (RRM/RBD/RNP motifs) family protein	13.2
AT3G52470	Late embryogenesis abundant (LEA) hydroxyproline-rich glycoprotein family	13.1
AT4G33560	Wound-responsive family protein	13.1
AT3G10405	unknown protein	13.1
AT3G55400	methionyl-tRNA synthetase / methionine--tRNA ligase / MetRS (cpMetRS)	13.0
AT5G64470	Plant protein of unknown function (DUF828)	13.0
AT3G52280	general transcription factor group E6	12.8
AT5G45775	Ribosomal L5P family protein	12.7
AT1G06220	Ribosomal protein S5/Elongation factor G/III/V family protein	12.7
AT5G13225	snoRNA	12.7
AT5G24735	other RNA	12.7
AT3G03970	ARM repeat superfamily protein	12.6
AT4G30370	RING/U-box superfamily protein	12.5
AT1G20950	Phosphofructokinase family protein	12.5
AT1G59750	auxin response factor 1	12.5
AT1G53840	pectin methylesterase 1	12.5
AT5G67500	voltage dependent anion channel 2	12.5
AT5G47390	myb-like transcription factor family protein	12.4
AT3G61980	serine protease inhibitor, Kazal-type family protein	12.3
AT3G29370	unknown protein	12.2

AT5G14040	phosphate transporter 3;1	12.1
AT2G28290	P-loop containing nucleoside triphosphate hydrolases superfamily protein	12.0
AT3G02550	LOB domain-containing protein 41	11.8
AT5G62980	Dihydroneopterin aldolase	11.8
AT4G10130	DNAJ heat shock N-terminal domain-containing protein	11.7
AT4G20410	gamma-soluble NSF attachment protein	11.6
AT5G57990	ubiquitin-specific protease 23	11.6
AT4G17250	unknown protein.	11.4
AT5G08120	movement protein binding protein 2C	11.3
AT1G58370	glycosyl hydrolase family 10 protein / carbohydrate-binding domain-containing protein	11.3
AT4G02680	ETO1-like 1	11.2
AT2G26660	SPX domain gene 2	11.2
AT5G23140	nuclear-encoded CLP protease P7	11.2
AT3G50240	ATP binding microtubule motor family protein	11.2
AT5G62930	SGNH hydrolase-type esterase superfamily protein	11.2
AT1G63160	replication factor C 2	11.1
AT4G01880	methyltransferases	11.1
AT3G08510	phospholipase C 2	11.1
AT1G30440	Phototropic-responsive NPH3 family protein	11.0
AT3G04140	Ankyrin repeat family protein	11.0
AT1G49780	plant U-box 26	10.9
AT1G08800	Protein of unknown function, DUF593	10.8
AT5G42330	unknown protein	10.8
AT5G24120	sigma factor E	10.7
AT5G46850	CONTAINS InterPro DOMAIN/s: PIG-X/PBN1 (InterPro:IPR013233).	10.7
AT2G47020	Peptide chain release factor 1	10.7
AT4G20400	JUMONJI 14	10.5
AT3G51820	UbiA prenyltransferase family protein	10.5
AT1G22620	Phosphoinositide phosphatase family protein	10.4
AT2G17975	zinc finger (Ran-binding) family protein	10.4
AT5G16730	Plant protein of unknown function (DUF827)	10.4
AT2G22120	RING/FYVE/PHD zinc finger superfamily protein	10.4
AT4G08690	Sec14p-like phosphatidylinositol transfer family protein	10.4
AT4G25080	magnesium-protoporphyrin IX methyltransferase	10.4
AT4G27410	NAC (No Apical Meristem) domain transcriptional regulator superfamily protein	10.4
AT3G23250	myb domain protein 15	10.2
AT2G35620	Leucine-rich repeat protein kinase family protein	10.2
AT1G47480	alpha/beta-Hydrolases superfamily protein	10.2
AT2G40010	Ribosomal protein L10 family protein	10.1
AT3G24140	basic helix-loop-helix (bHLH) DNA-binding superfamily protein	10.1
AT3G24315	Sec20 family protein	10.0
AT1G80770	P-loop containing nucleoside triphosphate hydrolases superfamily protein	10.0
AT5G24314	plastid transcriptionally active7	10.0

Table A3.6 Genes downregulated more than 10-fold in *parg1-2* seedlings compared to wild type seedlings when treated with MMS.

Gene ID	Name	Fold change
AT1G21920	Histone H3 K4-specific methyltransferase SET7/9 family protein	-122.1
AT2G48070	resistance to phytophthora 1	-77.7

AT2G05260	alpha/beta-Hydrolases superfamily protein	-70.7
AT5G42146	unknown protein	-66.8
AT1G19720	Pentatricopeptide repeat (PPR-like) superfamily protein	-59.8
AT5G06850	C2 calcium/lipid-binding plant phosphoribosyltransferase family protein	-45.6
AT1G61210	Transducin/WD40 repeat-like superfamily protein	-32.9
AT3G13510	Protein of Unknown Function (DUF239)	-30.6
AT5G28640	SSXT family protein	-28.9
AT3G55260	beta-hexosaminidase 1	-23.0
AT1G32530	RING/U-box superfamily protein	-13.5
AT1G13380	Protein of unknown function (DUF1218)	-11.7
AT5G51970	GroES-like zinc-binding alcohol dehydrogenase family protein	-11.1
AT2G18290	anaphase promoting complex 10	-10.9

List of References

Adams-Phillips L, Briggs AG, Bent AF. Disruption of poly(ADP-ribosyl)ation mechanisms alters responses of Arabidopsis to biotic stress. Plant Physiol. 2010; 152 (1): 267-80.

Adams-Phillips L, Wan J, Tan X, Dunning FM, Meyers BC, Michelmore RW, Bent AF. Discovery of ADP-ribosylation and other plant defense pathway elements through expression profiling of four different Arabidopsis-Pseudomonas R-avr interactions. Mol Plant Microbe Interact. 2008; 21 (5): 646-57.

Affar EB, Germain M, Winstall E, Vodenicharov M, Shah RG, Salvesen GS, Poirier GG. Caspase-3-mediated processing of poly(ADP-ribose) glycohydrolase during apoptosis. J Biol Chem. 2001; 276 (4): 2935-42.

Affar EB, Duriez PJ, Shah RG, Winstall E, Germain M, Boucher C, Bourassa S, Kirkland JB, Poirier GG. Immunological determination and size characterization of poly(ADP-ribose) synthesized in vitro and in vivo. Biochim Biophys Acta. 1999; 1428 (2-3): 137-46.

Ahlfors R, Lång S, Overmyer K, Jaspers P, Brosché M, Tauriainen A, Kollist H, Tuominen H, Belles-Boix E, Piippo M, Inzé D, Palva ET, Kangasjärvi J. Arabidopsis RADICAL-INDUCED CELL DEATH1 belongs to the WWE protein-protein interaction domain protein family and modulates abscisic acid, ethylene, and methyl jasmonate responses. Plant Cell. 2004; 16 (7): 1925-37.

Aker J, Hesselink R, Engel R, Karlova R, Borst JW, Visser AJ, de Vries SC. In vivo hexamerization and characterization of the Arabidopsis AAA ATPase CDC48A complex using forster resonance energy transfer-fluorescence lifetime imaging microscopy and fluorescence correlation spectroscopy. Plant Physiol. 2007; 145 (2): 339-50.

Althaus FR, Richter C. ADP-ribosylation of proteins Enzymology and biological significance. Mol Biol Biochem Biophys. 1987; 37: 1-237.

Alvarez-Gonzalez R, Althaus FR. Poly(ADP-ribose) catabolism in mammalian cells exposed to DNA-damaging agents. Mutat Res. 1989; 218 (2): 67-74.

Amor Y, Babiychuk E, Inzé D, Levine A. The involvement of poly(ADP-ribose) polymerase in the oxidative stress responses in plants. FEBS Lett. 1998; 440 (1-2): 1-7.

Amé JC, Jacobson EL, Jacobson MK. Molecular heterogeneity and regulation of poly(ADP-ribose) glycohydrolase. Mol Cell Biochem. 1999; 193 (1-2): 75-81.

Amé JC, Spenlehauer C, de Murcia G. The PARP superfamily. Bioessays. 2004; 26 (8): 882-93.

Andrabi SA, Kim NS, Yu SW, Wang H, Koh DW, Sasaki M, Klaus JA, Otsuka T, Zhang Z, Koehler RC, Hurn PD, Poirier GG, Dawson VL, Dawson TM. Poly(ADP-ribose) (PAR) polymer is a death signal. Proc Natl Acad Sci U S A. 2006; 103 (48): 18308-13.

Aravind L, Koonin EV. SAP - a putative DNA-binding motif involved in chromosomal organization. Trends Biochem Sci. 2000; 25 (3): 112-4.

Ariumi Y, Masutani M, Copeland TD, Mimori T, Sugimura T, Shimotohno K, Ueda K, Hatanaka M, Noda M. Suppression of the poly(ADP-ribose) polymerase activity by DNA-dependent protein kinase in vitro. Oncogene. 1999; 18 (32): 4616-25.

Asher G, Reinke H, Altmeyer M, Gutierrez-Arcelus M, Hottiger MO, Schibler U. Poly(ADP-ribose) polymerase 1 participates in the phase entrainment of circadian clocks to feeding. Cell. 2010; 142 (6): 943-53.

Babiychuk E, Cottrill PB, Storozhenko S, Fuangthong M, Chen Y, O'Farrell MK, Van Montagu M, Inzé D, Kushnir S. Higher plants possess two structurally different poly(ADP-ribose) polymerases. Plant J. 1998; 15 (5): 635-45.

Babiychuk E, Van Montagu M, Kushnir S. N-terminal domains of plant poly(ADP-ribose) polymerases define their association with mitotic chromosomes. Plant J. 2001; 28 (3): 245-55.

Balajee AS, Geard CR. Chromatin-bound PCNA complex formation triggered by DNA damage occurs independent of the ATM gene product in human cells. Nucleic Acids Res. 2001; 29 (6): 1341-51.

Barlow C, Hirotsune S, Paylor R, Liyanage M, Eckhaus M, Collins F, Shiloh Y, Crawley JN, Ried T, Tagle D, Wynshaw-Boris A. Atm-deficient mice: a paradigm of ataxia telangiectasia. Cell. 1996; 86 (1): 159-71.

Becerra C, Puigdomenech P, Vicient CM. Computational and experimental analysis identifies Arabidopsis genes specifically expressed during early seed development. BMC Genomics. 2006; 7: 38.

Benjamin RC, Gill DM. (b) Poly(ADP-ribose) synthesis in vitro programmed by damaged DNA A comparison of DNA molecules containing different types of strand breaks. J Biol Chem. 1980; 255 (21): 10502-8.

Benjamin RC, Gill DM. (a) ADP-ribosylation in mammalian cell ghosts Dependence of poly(ADP-ribose) synthesis on strand breakage in DNA. J Biol Chem. 1980; 255 (21): 10493-501.

Blanvillain R, Kim JH, Wu S, Lima A, Ow DW. OXIDATIVE STRESS 3 is a chromatin-associated factor involved in tolerance to heavy metals and oxidative stress. Plant J. 2009; 57 (4): 654-65.

Blenn C, Althaus FR, Malanga M. Poly(ADP-ribose) glycohydrolase silencing protects against H2O2-induced cell death. Biochem J. 2006; 396 (3): 419-29

Bleuyard JY, Gallego ME, White CI. Recent advances in understanding of the DNA double-strand break repair machinery of plants. DNA Repair (Amst). 2006; 5 (1): 1-12.

Bonicalzi ME, Vodenicharov M, Coulombe M, Gagné JP, Poirier GG. Alteration of poly(ADP-ribose) glycohydrolase nucleocytoplasmic shuttling characteristics upon cleavage by apoptotic proteases. Biol Cell. 2003; 95 (9): 635-44.

Bork P, Hofmann K, Bucher P, Neuwald AF, Altschul SF, Koonin EV. A superfamily of conserved domains in DNA damage-responsive cell cycle checkpoint proteins. FASEB J. 1997; 11 (1): 68-76.

Botta D, Jacobson MK. Identification of a regulatory segment of poly(ADP-ribose) glycohydrolase. Biochemistry. 2010; 49 (35): 7674-82.

Briggs AG, Bent AF. Poly(ADP-ribosyl)ation in plants. Trends Plant Sci. 2011; 16 (7): 372-80.

Brochu G, Duchaine C, Thibeault L, Lagueux J, Shah GM, Poirier GG. Mode of action of poly(ADP-ribose) glycohydrolase. Biochim Biophys Acta. 1994; 1219 (2): 342-50.

Brown BA, Jenkins GI. UV-B signaling pathways with different fluence-rate response profiles are distinguished in mature Arabidopsis leaf tissue by requirement for UVR8, HY5, and HYH. Plant Physiol. 2008; 146 (2): 576-88.

Bryant HE, Schultz N, Thomas HD, Parker KM, Flower D, Lopez E, Kyle S, Meuth M, Curtin NJ, Helleday T. Specific killing of BRCA2-deficient tumours with inhibitors of poly(ADP-ribose) polymerase. Nature. 2005; 434 (7035): 913-7.

Bundock P, van Attikum H, Hooykaas P. Increased telomere length and hypersensitivity to DNA damaging agents in an Arabidopsis KU70 mutant. Nucleic Acids Res. 2002; 30 (15): 3395-400.

Caldecott KW, Tucker JD, Stanker LH, Thompson LH. Characterization of the XRCC1-DNA ligase III complex in vitro and its absence from mutant hamster cells. Nucleic Acids Res. 1995; 23 (23): 4836-43.

Carbone M, Rossi MN, Cavaldesi M, Notari A, Amati P, Maione R. Poly(ADP-ribosyl)ation is implicated in the G0-G1 transition of resting cells. Oncogene.

2008; 27 (47): 6083-92.

Chambon P, Weill JD, Mandel P. Nicotinamide mononucleotide activation of new DNA-dependent polyadenylic acid synthesizing nuclear enzyme. Biochem Biophys Res Commun. 1963; 11: 39-43.

Chang P, Jacobson MK, Mitchison TJ. Poly(ADP-ribose) is required for spindle assembly and structure. Nature. 2004; 432 (7017): 645-9.

Chang P, Coughlin M, Mitchison TJ. Interaction between Poly(ADP-ribose) and NuMA contributes to mitotic spindle pole assembly. Mol Biol Cell. 2009; 20 (21): 4575-85.

Chang W, Dynek JN, Smith S. NuMA is a major acceptor of poly(ADP-ribosyl)ation by tankyrase 1 in mitosis. Biochem J. 2005; 391 (2): 177-84.

Charbonnel C, Gallego ME, White CI. Xrcc1-dependent and Ku-dependent DNA double-strand break repair kinetics in Arabidopsis plants. Plant J. 2010; 64 (2): 280-90.

Chen IP, Haehnel U, Altschmied L, Schubert I, Puchta H. The transcriptional response of Arabidopsis to genotoxic stress - a high-density colony array study (HDCA). Plant J. 2003; 35 (6): 771-86.

Cherney BW, McBride OW, Chen DF, Alkhatib H, Bhatia K, Hensley P, Smulson ME. cDNA sequence, protein structure, and chromosomal location of the human gene for poly(ADP-ribose) polymerase. Proc Natl Acad Sci U S A. 1987; 84 (23): 8370-4.

Chi NW, Lodish HF. Tankyrase is a golgi-associated mitogen-activated protein kinase substrate that interacts with IRAP in GLUT4 vesicles. J Biol Chem. 2000; 275 (49): 38437-44.

Chiang YJ, Hsiao SJ, Yver D, Cushman SW, Tessarollo L, Smith S, Hodes RJ. Tankyrase 1 and tankyrase 2 are essential but redundant for mouse embryonic development. PLoS One. 2008; 3 (7): e2639.

Citarelli M, Teotia S, Lamb RS. Evolutionary history of the poly(ADP-ribose) polymerase gene family in eukaryotes. BMC Evol Biol. 2010; 10: 308.

Clough SJ, Bent AF. Floral dip: a simplified method for Agrobacterium-mediated

transformation of Arabidopsis thaliana. Plant J. 1998; 16 (6): 735-43.

Cohausz O, Blenn C, Malanga M, Althaus FR. The roles of poly(ADP-ribose)-metabolizing enzymes in alkylation-induced cell death. Cell Mol Life Sci. 2008; 65 (4): 644-55.

Cortes U, Tong WM, Coyle DL, Meyer-Ficca ML, Meyer RG, Petrilli V, Herceg Z, Jacobson EL, Jacobson MK, Wang ZQ. Depletion of the 110-kilodalton isoform of poly(ADP-ribose) glycohydrolase increases sensitivity to genotoxic and endotoxic stress in mice. Mol Cell Biol. 2004; 24 (16): 7163-78.

Cregan SP, Dawson VL, Slack RS. Role of AIF in caspase-dependent and caspase-independent cell death. Oncogene. 2004; 23 (16): 2785-96.

Culligan KM, Robertson CE, Foreman J, Doerner P, Britt AB. ATR and ATM play both distinct and additive roles in response to ionizing radiation. Plant J. 2006; 48 (6): 947-61.

d'Adda di Fagagna F, Hande MP, Tong WM, Lansdorp PM, Wang ZQ, Jackson SP. Functions of poly(ADP-ribose) polymerase in controlling telomere length and chromosomal stability. Nat Genet. 1999; 23 (1): 76-80.

D'Amours D, Desnoyers S, D'Silva I, Poirier GG. Poly(ADP-ribosyl)ation reactions in the regulation of nuclear functions. Biochem J. 1999; 342 (2): 249-68.

Dantzer F, de La Rubia G, Ménissier-De Murcia J, Hostomsky Z, de Murcia G, Schreiber V. Base excision repair is impaired in mammalian cells lacking Poly(ADP-ribose) polymerase-1. Biochemistry. 2000; 39 (25): 7559-69

Dantzer F, Giraud-Panis MJ, Jaco I, Amé JC, Schultz I, Blasco M, Koering CE, Gilson E, Ménissier-de Murcia J, de Murcia G, Schreiber V. Functional interaction between poly(ADP-Ribose) polymerase 2 (PARP-2) and TRF2: PARP activity negatively regulates TRF2. Mol Cell Biol. 2004; 24 (4): 1595-607.

David KK, Andrabi SA, Dawson TM, Dawson VL. Parthanatos, a messenger of death. Front Biosci. 2009; 14: 1116-28.

De Block M, Verduyn C, De Brouwer D, Cornelissen M. Poly(ADP-ribose) polymerase in plants affects energy homeostasis, cell death and stress

tolerance. Plant J. 2005; 41 (1): 95-106.

de Murcia G, Ménissier de Murcia J. Poly(ADP-ribose) polymerase: a molecular nick-sensor. Trends Biochem Sci. 1994; 19 (4): 172-6.

de Murcia G, Jongstra-Bilen J, Ittel ME, Mandel P, Delain E. Poly(ADP-ribose) polymerase auto-modification and interaction with DNA: electron microscopic visualization. EMBO J. 1983; 2 (4): 543-8.

de Murcia JM, Niedergang C, Trucco C, Ricoul M, Dutrillaux B, Mark M, Oliver FJ, Masson M, Dierich A, LeMeur M, Walztinger C, Chambon P, de Murcia G. Requirement of poly(ADP-ribose) polymerase in recovery from DNA damage in mice and in cells. Proc Natl Acad Sci U S A. 1997; 94 (14): 7303-7.

De Schutter K, Joubès J, Cools T, Verkest A, Corellou F, Babiychuk E, Van Der Schueren E, Beeckman T, Kushnir S, Inzé D, De Veylder L. Arabidopsis WEE1 kinase controls cell cycle arrest in response to activation of the DNA integrity checkpoint. Plant Cell. 2007; 19 (1): 211-25.

Doucet-Chabeaud G, Godon C, Brutesco C, de Murcia G, Kazmaier M. Ionising radiation induces the expression of PARP-1 and PARP-2 genes in Arabidopsis. Mol Genet Genomics. 2001; 265 (6): 954-63.

Druzhyna N, Smulson ME, LeDoux SP, Wilson GL. Poly(ADP-ribose) polymerase facilitates the repair of N-methylpurines in mitochondrial DNA. Diabetes. 2000; 49 (11): 1849-55.

Du L, Zhang X, Han YY, Burke NA, Kochanek PM, Watkins SC, Graham SH, Carcillo JA, Szabó C, Clark RS. Intra-mitochondrial poly(ADP-ribosylation) contributes to NAD+ depletion and cell death induced by oxidative stress. J Biol Chem. 2003; 278 (20): 18426-33.

Durkacz BW, Omidiji O, Gray DA, Shall S. (ADP-ribose)n participates in DNA excision repair. Nature. 1980; 283 (5747): 593-6.

Earle E, Saxena A, MacDonald A, Hudson DF, Shaffer LG, Saffery R, Cancilla MR, Cutts SM, Howman E, Choo KH. Poly(ADP-ribose) polymerase at active centromeres and neocentromeres at metaphase. Hum Mol Genet. 2000; 9 (2): 187-94.

Earley KW, Haag JR, Pontes O, Opper K, Juehne T, Song K, Pikaard CS. Gateway-compatible vectors for plant functional genomics and proteomics. Plant J. 2006; 45 (4): 616-29.

Eulgem T, Somssich IE. Networks of WRKY transcription factors in defense signaling. Curr Opin Plant Biol. 2007; 10 (4): 366-71.

Fahrer J, Kranaster R, Altmeyer M, Marx A, Bürkle A. Quantitative analysis of the binding affinity of poly(ADP-ribose) to specific binding proteins as a function of chain length. Nucleic Acids Res. 2007; 35 (21): e143.

Falsig J, Christiansen SH, Feuerhahn S, Bürkle A, Oei SL, Keil C, Leist M. Poly(ADP-ribose) glycohydrolase as a target for neuroprotective intervention: assessment of currently available pharmacological tools. Eur J Pharmacol. 2004; 497 (1): 7-16.

Farmer H, McCabe N, Lord CJ, Tutt AN, Johnson DA, Richardson TB, Santarosa M, Dillon KJ, Hickson I, Knights C, Martin NM, Jackson SP, Smith GC, Ashworth A. Targeting the DNA repair defect in BRCA mutant cells as a therapeutic strategy. Nature. 2005; 434 (7035): 917-21.

Filipovic DM, Meng X, Reeves WB. Inhibition of PARP prevents oxidant-induced necrosis but not apoptosis in LLC-PK1 cells. Am J Physiol. 1999; 277 (3 Pt 2): F428-36.

Fujihara H, Ogino H, Maeda D, Shirai H, Nozaki T, Kamada N, Jishage K, Tanuma S, Takato T, Ochiya T, Sugimura T, Masutani M. Poly(ADP-ribose) Glycohydrolase deficiency sensitizes mouse ES cells to DNA damaging agents. Curr Cancer Drug Targets. 2009; 9 (8): 953-62.

Galande S, Kohwi-Shigematsu T. Poly(ADP-ribose) polymerase and Ku autoantigen form a complex and synergistically bind to matrix attachment sequences. J Biol Chem. 1999; 274 (29): 20521-8.

Gallego ME, Bleuyard JY, Daoudal-Cotterell S, Jallut N, White CI. Ku80 plays a role in non-homologous recombination but is not required for T-DNA integration in Arabidopsis. Plant J. 2003; 35 (5): 557-65.

Gao H, Coyle DL, Meyer-Ficca ML, Meyer RG, Jacobson EL, Wang ZQ, Jacobson

MK. Altered poly(ADP-ribose) metabolism impairs cellular responses to genotoxic stress in a hypomorphic mutant of poly(ADP-ribose) glycohydrolase. Exp Cell Res. 2007; 313 (5): 984-96.

Garcia V, Bruchet H, Camescasse D, Granier F, Bouchez D, Tissier A. AtATM is essential for meiosis and the somatic response to DNA damage in plants. Plant Cell. 2003; 15 (1): 119-32.

Germain M, Affar EB, D'Amours D, Dixit VM, Salvesen GS, Poirier GG. Cleavage of automodified poly(ADP-ribose) polymerase during apoptosis Evidence for involvement of caspase-7. J Biol Chem. 1999; 274 (40): 28379-84.

Gietz RD, Woods RA. Genetic transformation of yeast. Biotechniques. 2001; 30 (4) :816-20, 822-6.

Gomord V, Denmat LA, Fitchette-Lainé AC, Satiat-Jeunemaitre B, Hawes C, Faye L. The C-terminal HDEL sequence is sufficient for retention of secretory proteins in the endoplasmic reticulum (ER) but promotes vacuolar targeting of proteins that escape the ER. Plant J. 1997; 11 (2): 313-25.

Gradwohl G, Ménissier de Murcia JM, Molinete M, Simonin F, Koken M, Hoeijmakers JH, de Murcia G. The second zinc-finger domain of poly(ADP-ribose) polymerase determines specificity for single-stranded breaks in DNA. Proc Natl Acad Sci U S A. 1990; 87 (8): 2990-4.

Gravel C, Stergiou L, Gagnon SN, Desnoyers S. The C elegans gene pme-5: molecular cloning and role in the DNA-damage response of a tankyrase orthologue. DNA Repair (Amst). 2004; 3 (2): 171-82.

Ha HC, Snyder SH. Poly(ADP-ribose) polymerase is a mediator of necrotic cell death by ATP depletion. Proc Natl Acad Sci U S A. 1999; 96 (24): 13978-82.

Haince JF, Ouellet ME, McDonald D, Hendzel MJ, Poirier GG. Dynamic relocation of poly(ADP-ribose) glycohydrolase isoforms during radiation-induced DNA damage. Biochim Biophys Acta. 2006; 1763 (2): 226-37.

Hanai S, Kanai M, Ohashi S, Okamoto K, Yamada M, Takahashi H, Miwa M. Loss of poly(ADP-ribose) glycohydrolase causes progressive neurodegeneration in Drosophila melanogaster. Proc Natl Acad Sci U S A. 2004; 101 (1): 82-6.

Hassa PO, Hottiger MO. The diverse biological roles of mammalian PARPS, a small but powerful family of poly-ADP-ribose polymerases. Front Biosci. 2008; 13: 3046-82.

Hassa PO, Haenni SS, Elser M, Hottiger MO. Nuclear ADP-ribosylation reactions in mammalian cells: where are we today and where are we going? Microbiol Mol Biol Rev. 2006; 70 (3): 789-829.

Hatakeyama K, Nemoto Y, Ueda K, Hayaishi O. Purification and characterization of poly(ADP-ribose) glycohydrolase Different modes of action on large and small poly(ADP-ribose). J Biol Chem. 1986; 261 (32): 14902-11.

Helleday T, Bryant HE, Schultz N. Poly(ADP-ribose) polymerase (PARP-1) in homologous recombination and as a target for cancer therapy. Cell Cycle. 2005; 4 (9): 1176-8.

Hodel MR, Corbett AH, Hodel AE. Dissection of a nuclear localization signal. J Biol Chem. 2001; 276 (2): 1317-25.

Huambachano O, Herrera F, Rancourt A, Satoh MS. Double-stranded DNA binding domain of poly(ADP-ribose) polymerase-1 and molecular insight into the regulation of its activity. J Biol Chem. 2011; 286 (9): 7149-60

Huber A, Bai P, de Murcia JM, de Murcia G. PARP-1, PARP-2 and ATM in the DNA damage response: functional synergy in mouse development. DNA Repair (Amst). 2004; 3 (8-9): 1103-8

Hunt L, Lerner F, Ziegler, M. NAD- New roles in signalling and gene regulation in plants. New Phytologist 2004; 163: 31-44

Hunt L, Holdsworth MJ, Gray JE. Nicotinamidase activity is important for germination. Plant J. 2007; 51 (3): 341-51.

Huyton T, Bates PA, Zhang X, Sternberg MJ, Freemont PS. The BRCA1 C-terminal domain: structure and function. Mutat Res. 2000; 460 (3-4): 319-32.

Isabelle M, Moreel X, Gagné JP, Rouleau M, Ethier C, Gagné P, Hendzel MJ, Poirier GG. Investigation of PARP-1, PARP-2, and PARG interactomes by affinity-purification mass spectrometry. Proteome Sci. 2010; 8: 22

Ishikawa K, Ogawa T, Hirosue E, Nakayama Y, Harada K, Fukusaki E, Yoshimura K, Shigeoka S. Modulation of the poly(ADP-ribosyl)ation reaction via the Arabidopsis ADP-ribose/NADH pyrophosphohydrolase, AtNUDX7, is involved in the response to oxidative stress. Plant Physiol. 2009; 151 (2): 741-54.

Jacobson EL, Meadows R, Measel J. Cell cycle perturbations following DNA damage in the presence of ADP-ribosylation inhibitors. Carcinogenesis. 1985; 6 (5): 711-4.

Jacobson EL, Antol KM, Juarez-Salinas H, Jacobson MK. Poly(ADP-ribose) metabolism in ultraviolet irradiated human fibroblasts. J Biol Chem. 1983; 258 (1): 103-7.

Jaspers P, Overmyer K, Wrzaczek M, Vainonen JP, Blomster T, Salojärvi J, Reddy RA, Kangasjärvi J. The RST and PARP-like domain containing SRO protein family: analysis of protein structure, function and conservation in land plants. BMC Genomics. 2010; 11: 170.

Johansson M. A human poly(ADP-ribose) polymerase gene family (ADPRTL): cDNA cloning of two novel poly(ADP-ribose) polymerase homologues. Genomics. 1999; 57 (3): 442-5.

John GB, Shang Y, Li L, Renken C, Mannella CA, Selker JM, Rangell L, Bennett MJ, Zha J. The mitochondrial inner membrane protein mitofilin controls cristae morphology. Mol Biol Cell. 2005; 16 (3): 1543-54.

Juarez-Salinas H, Levi V, Jacobson EL, Jacobson MK. Poly(ADP-ribose) has a branched structure in vivo. J Biol Chem. 1982; 257 (2) 607-9.

Kaiser P, Auer B, Schweiger M. Inhibition of cell proliferation in Saccharomyces cerevisiae by expression of human NAD+ ADP-ribosyltransferase requires the DNA binding domain ("zinc fingers"). Mol Gen Genet. 1992; 232 (2): 231-9.

Kal AJ, van Zonneveld AJ, Benes V, van den Berg M, Koerkamp MG, Albermann K, Strack N, Ruijter JM, Richter A, Dujon B, Ansorge W, Tabak HF. Dynamics of gene expression revealed by comparison of serial analysis of gene expression transcript profiles from yeast grown on two different carbon sources. Mol Biol Cell. 1999; 10 (6): 1859-72.

Kaminker PG, Kim SH, Taylor RD, Zebarjadian Y, Funk WD, Morin GB, Yaswen P, Campisi J. TANK2, a new TRF1-associated poly(ADP-ribose) polymerase, causes rapid induction of cell death upon overexpression. J Biol Chem. 2001; 276 (38): 35891-9.

Kanai M, Tong WM, Sugihara E, Wang ZQ, Fukasawa K, Miwa M. Involvement of poly(ADP-Ribose) polymerase 1 and poly(ADP-Ribosyl)ation in regulation of centrosome function. Mol Cell Biol. 2003; 23 (7): 2451-62.

Karimi M, Depicker A, Hilson P. Recombinational cloning with plant gateway vectors. Plant Physiol. 2007; 145 (4): 1144-54.

Kaufmann SH, Desnoyers S, Ottaviano Y, Davidson NE, Poirier GG. Specific proteolytic cleavage of poly(ADP-ribose) polymerase: an early marker of chemotherapy-induced apoptosis. Cancer Res. 1993; 53 (17): 3976-85.

Kawaichi M, Ueda K, Hayaishi O. Multiple autopoly(ADP-ribosyl)ation of rat liver poly(ADP-ribose) synthetase Mode of modification and properties of automodified synthetase. J Biol Chem. 1981; 256 (18): 9483-9.

Keil C, Gröbe T, Oei SL. MNNG-induced cell death is controlled by interactions between PARP-1, poly(ADP-ribose) glycohydrolase, and XRCC1. J Biol Chem. 2006; 281 (45): 34394-405.

Kilian J, Whitehead D, Horak J, Wanke D, Weinl S, Batistic O, D'Angelo C, Bornberg-Bauer E, Kudla J, Harter K. The AtGenExpress global stress expression data set: protocols, evaluation and model data analysis of UV-B light, drought and cold stress responses. Plant J. 2007; 50 (2): 347-63.

Kim YH, Koh JY. The role of NADPH oxidase and neuronal nitric oxide synthase in zinc-induced poly(ADP-ribose) polymerase activation and cell death in cortical culture. Exp Neurol. 2002; 177 (2): 407-18.

Kim YS. Analysis of gene expression upon DNA damage in Arabidopsis. J Plant Biol. 2006. 49 (4): 298-302.

Ko LJ, Prives C. p53: puzzle and paradigm. Genes Dev. 1996; 10 (9): 1054-72.

Koh DW, Lawler AM, Poitras MF, Sasaki M, Wattler S, Nehls MC, Stöger T, Poirier

GG, Dawson VL, Dawson TM. Failure to degrade poly(ADP-ribose) causes increased sensitivity to cytotoxicity and early embryonic lethality. Proc Natl Acad Sci U S A. 2004; 101 (51): 17699-704.

Koh DW, Patel CN, Ramsinghani S, Slama JT, Oliveira MA, Jacobson MK. Identification of an inhibitor binding site of poly(ADP-ribose) glycohydrolase. Biochemistry. 2003; 42 (17): 4855-63.

Koonin EV, Altschul SF, Bork P. BRCA1 protein products Functional motifs. Nat Genet. 1996; 13 (3): 266-8.

Kraus WL, Lis JT. PARP goes transcription. Cell. 2003; 113 (6): 677-83.

Krishnakumar R, Gamble MJ, Frizzell KM, Berrocal JG, Kininis M, Kraus WL. Reciprocal binding of PARP-1 and histone H1 at promoters specifies transcriptional outcomes. Science. 2008; 319 (5864): 819-21.

Kubota Y, Nash RA, Klungland A, Schär P, Barnes DE, Lindahl T. Reconstitution of DNA base excision-repair with purified human proteins: interaction between DNA polymerase beta and the XRCC1 protein. EMBO J. 1996; 15 (23): 6662-70.

Kumari SR, Mendoza-Alvarez H, Alvarez-Gonzalez R. Functional interactions of p53 with poly(ADP-ribose) polymerase (PARP) during apoptosis following DNA damage: covalent poly(ADP-ribosyl)ation of p53 by exogenous PARP and noncovalent binding of p53 to the M(r) 85,000 proteolytic fragment. Cancer Res. 1998; 58 (22): 5075-8.

Kun E, Zimber PH, Chang AC, Puschendorf B, Grunicke H. Macromolecular enzymatic product of NAD+ in liver mitochondria. Proc Natl Acad Sci U S A. 1975; 72 (4): 1436-40.

Kushnir S, Babiychuk E, Storozhenko S, Davey MW, Papenbrock J, De Rycke R, Engler G, Stephan UW, Lange H, Kispal G, Lill R, Van Montagu M. A mutation of the mitochondrial ABC transporter Sta1 leads to dwarfism and chlorosis in the Arabidopsis mutant starik. Plant Cell. 2001; 13 (1): 89-100.

Kwak JM, Mori IC, Pei ZM, Leonhardt N, Torres MA, Dangl JL, Bloom RE, Bodde S, Jones JD, Schroeder JI. NADPH oxidase AtrbohD and AtrbohF genes function in ROS-dependent ABA signaling in Arabidopsis. EMBO J. 2003; 22 (11): 2623-33.

Langelier MF, Planck JL, Roy S, Pascal JM. Crystal structures of poly(ADP-ribose) polymerase-1 (PARP-1) zinc fingers bound to DNA: structural and functional insights into DNA-dependent PARP-1 activity. J Biol Chem. 2011; 286 (12): 10690-701.

Langelier MF, Servent KM, Rogers EE, Pascal JM. A third zinc-binding domain of human poly(ADP-ribose) polymerase-1 coordinates DNA-dependent enzyme activation. J Biol Chem. 2008; 283 (7): 4105-14.

Lapucci A, Pittelli M, Rapizzi E, Felici R, Moroni F, Chiarugi A. Poly(ADP-ribose) polymerase-1 is a nuclear epigenetic regulator of mitochondrial DNA repair and transcription. Mol Pharmacol. 2011; 79 (6): 932-40.

Lehtiö L, Jemth AS, Collins R, Loseva O, Johansson A, Markova N, Hammarström M, Flores A, Holmberg-Schiavone L, Weigelt J, Helleday T, Schüler H, Karlberg T. Structural basis for inhibitor specificity in human poly(ADP-ribose) polymerase-3. J Med Chem. 2009; 52 (9): 3108-11.

Lepiniec L, Babiychuk E, Kushnir S, Van Montagu M, Inzé D. Characterization of an Arabidopsis thaliana cDNA homologue to animal poly(ADP-ribose) polymerase. FEBS Lett. 1995; 364 (2): 103-8.

Leppard JB, Dong Z, Mackey ZB, Tomkinson AE. Physical and functional interaction between DNA ligase IIIalpha and poly(ADP-Ribose) polymerase 1 in DNA single-strand break repair. Mol Cell Biol. 2003; 23 (16): 5919-27.

Li G, Nasar V, Yang Y, Li W, Liu B, Sun L, Li D, Song F. Arabidopsis poly(ADP-ribose) glycohydrolase 1 is required for drought, osmotic and oxidative stress responses. Plant Sci. 2011; 180 (2): 283-91.

Li J, Mahajan A, Tsai MD. Ankyrin repeat: a unique motif mediating protein-protein interactions. Biochemistry. 2006; 45 (51): 15168-78

Lin W, Amé JC, Aboul-Ela N, Jacobson EL, Jacobson MK. Isolation and characterization of the cDNA encoding bovine poly(ADP-ribose) glycohydrolase. J Biol Chem. 1997; 272 (18): 11895-901.

Liu Z, Hossain GS, Islas-Osuna MA, Mitchell DL, Mount DW. Repair of UV damage in plants by nucleotide excision repair: Arabidopsis UVH1 DNA repair gene is a

homolog of Saccharomyces cerevisiae Rad1. Plant J. 2000; 21 (6): 519-28.

Lo C, Wang N, Lam E. Inducible double-stranded RNA expression activates reversible transcript turnover and stable translational suppression of a target gene in transgenic tobacco. FEBS Lett. 2005; 579 (6): 1498-502.

Lonskaya I, Potaman VN, Shlyakhtenko LS, Oussatcheva EA, Lyubchenko YL, Soldatenkov VA. Regulation of poly(ADP-ribose) polymerase-1 by DNA structure-specific binding. J Biol Chem. 2005; 280 (17): 17076-83.

Ludwig A, Behnke B, Holtlund J, Hilz H. Immunoquantitation and size determination of intrinsic poly(ADP-ribose) polymerase from acid precipitates An analysis of the in vivo status in mammalian species and in lower eukaryotes. J Biol Chem. 1988; 263 (15): 6993-9.

Mahajan PB, Zuo Z. Purification and cDNA cloning of maize Poly(ADP)-ribose polymerase. Plant Physiol. 1998; 118 (3): 895-905.

Malanga M, Pleschke JM, Kleczkowska HE, Althaus FR. Poly(ADP-ribose) binds to specific domains of p53 and alters its DNA binding functions. J Biol Chem. 1998; 273 (19): 11839-43.

Malanga M, Althaus FR. The role of poly(ADP-ribose) in the DNA damage signaling network. Biochem Cell Biol. 2005; 83 (3): 354-64.

Marsischky GT, Wilson BA, Collier RJ. Role of glutamic acid 988 of human poly-ADP-ribose polymerase in polymer formation Evidence for active site similarities to the ADP-ribosylating toxins. J Biol Chem. 1995; 270 (7): 3247-54.

Masson M, Niedergang C, Schreiber V, Muller S, Menissier-de Murcia J, de Murcia G. XRCC1 is specifically associated with poly(ADP-ribose) polymerase and negatively regulates its activity following DNA damage. Mol Cell Biol. 1998; 18 (6): 3563-71.

Massonnet C, Vile D, Fabre J, Hannah MA, Caldana C, Lisec J, Beemster GT, Meyer RC, Messerli G, Gronlund JT, Perkovic J, Wigmore E, May S, Bevan MW, Meyer C, Rubio-Díaz S, Weigel D, Micol JL, Buchanan-Wollaston V, Fiorani F, Walsh S, Rinn B, Gruissem W, Hilson P, Hennig L, Willmitzer L, Granier C. Probing the reproducibility of leaf growth and molecular phenotypes: a

comparison of three Arabidopsis accessions cultivated in ten laboratories. Plant Physiol. 2010; 152 (4): 2142-57.

Masutani M, Nozaki T, Wakabayashi K, Sugimura T. Role of poly(ADP-ribose) polymerase in cell-cycle checkpoint mechanisms following gamma-irradiation. Biochimie. 1995; 77 (6): 462-5.

Mendoza-Alvarez H, Alvarez-Gonzalez R. Poly(ADP-ribose) polymerase is a catalytic dimer and the automodification reaction is intermolecular. J Biol Chem. 1993; 268 (30): 22575-80.

Menke M, Chen I, Angelis KJ, Schubert I. DNA damage and repair in Arabidopsis thaliana as measured by the comet assay after treatment with different classes of genotoxins. Mutat Res. 2001; 493 (1-2): 87-93.

Meyer R, Müller M, Beneke S, Küpper JH, Bürkle A. Negative regulation of alkylation-induced sister-chromatid exchange by poly(ADP-ribose) polymerase-1 activity. Int J Cancer. 2000; 88 (3): 351-5.

Meyer RG, Meyer-Ficca ML, Jacobson EL, Jacobson MK. Human poly(ADP-ribose) glycohydrolase (PARG) gene and the common promoter sequence it shares with inner mitochondrial membrane translocase 23 (TIM23). Gene. 2003; 314: 181-90.

Meyer RG, Meyer-Ficca ML, Whatcott CJ, Jacobson EL, Jacobson MK. Two small enzyme isoforms mediate mammalian mitochondrial poly(ADP-ribose) glycohydrolase (PARG) activity. Exp Cell Res. 2007; 313 (13): 2920-36.

Meyer-Ficca ML, Meyer RG, Coyle DL, Jacobson EL, Jacobson MK. Human poly(ADP-ribose) glycohydrolase is expressed in alternative splice variants yielding isoforms that localize to different cell compartments. Exp Cell Res. 2004; 297 (2): 521-32.

Meyer-Ficca ML, Meyer RG, Jacobson EL, Jacobson MK. Poly(ADP-ribose) polymerases: managing genome stability. Int J Biochem Cell Biol. 2005; 37 (5): 920-6.

Michael TP, McClung CR. Phase-specific circadian clock regulatory elements in Arabidopsis. Plant Physiol. 2002; 130 (2): 627-38.

Min W, Cortes U, Herceg Z, Tong WM, Wang ZQ. Deletion of the nuclear isoform of poly(ADP-ribose) glycohydrolase (PARG) reveals its function in DNA repair, genomic stability and tumorigenesis. Carcinogenesis. 2010; 31 (12): 2058-65.

Miwa M, Saikawa N, Yamaizumi Z, Nishimura S, Sugimura T. Structure of poly(adenosine diphosphate ribose): identification of 2'-[1"-ribosyl-2"-(or 3"-)(1'"-ribosyl)]adenosine-5',5",5'"-tris(phosphate) as a branch linkage. Proc Natl Acad Sci U S A. 1979; 76 (2): 595-9.

Miwa M, Sugimura T. Splitting of the ribose-ribose linkage of poly(adenosine diphosphate-robose) by a calf thymus extract. J Biol Chem. 1971; 246 (20): 6362-4.

Miwa M, Tanaka M, Matsushima T, Sugimura T. Purification and properties of glycohydrolase from calf thymus splitting ribose-ribose linkages of poly(adenosine diphosphate ribose). J Biol Chem. 1974; 249 (11): 3475-82.

Molinete M, Vermeulen W, Bürkle A, Ménissier-de Murcia J, Küpper JH, Hoeijmakers JH, de Murcia G. Overproduction of the poly(ADP-ribose) polymerase DNA-binding domain blocks alkylation-induced DNA repair synthesis in mammalian cells. EMBO J. 1993; 12 (5): 2109-17.

Monz D, Munnia A, Comtesse N, Fischer U, Steudel WI, Feiden W, Glass B, Meese EU. Novel tankyrase-related gene detected with meningioma-specific sera. Clin Cancer Res. 2001; 7 (1): 113-9.

Mortusewicz O, Amé JC, Schreiber V, Leonhardt H. Feedback-regulated poly(ADP-ribosyl)ation by PARP-1 is required for rapid response to DNA damage in living cells. Nucleic Acids Res. 2007; 35 (22): 7665-75.

Mueller-Dieckmann C, Kernstock S, Lisurek M, von Kries JP, Haag F, Weiss MS, Koch-Nolte F. The structure of human ADP-ribosylhydrolase 3 (ARH3) provides insights into the reversibility of protein ADP-ribosylation. Proc Natl Acad Sci U S A. 2006; 103 (41): 15026-31.

Ménisser-de Murcia J, Mark M, Wendling O, Wynshaw-Boris A, de Murcia G. Early embryonic lethality in PARP-1 Atm double-mutant mice suggests a functional synergy in cell proliferation during development. Mol Cell Biol. 2001; 21 (5): 1828-32.

Ménissier de Murcia J, Ricoul M, Tartier L, Niedergang C, Huber A, Dantzer F, Schreiber V, Amé JC, Dierich A, LeMeur M, Sabatier L, Chambon P, de Murcia G. Functional interaction between PARP-1 and PARP-2 in chromosome stability and embryonic development in mouse. EMBO J. 2003; 22 (9): 2255-63.

Nakagawa T, Kurose T, Hino T, Tanaka K, Kawamukai M, Niwa Y, Toyooka K, Matsuoka K, Jinbo T, Kimura T. Development of series of gateway binary vectors, pGWBs, for realizing efficient construction of fusion genes for plant transformation. J Biosci Bioeng. 2007; 104 (1): 34-41.

Nielsen KL. DeepSAGE: higher sensitivity and multiplexing of samples using a simpler experimental protocol. Methods Mol Biol. 2008; 387: 81-94.

Niere M, Kernstock S, Koch-Nolte F, Ziegler M. Functional localization of two poly(ADP-ribose)-degrading enzymes to the mitochondrial matrix. Mol Cell Biol. 2008; 28 (2): 814-24.

Nishizuka Y, Ueda K, Nakazawa K, Hayaishi O. Studies on the polymer of adenosine diphosphate ribose I Enzymic formation from nicotinamide adenine dinuclotide in mammalian nuclei. J Biol Chem. 1967; 242 (13): 3164-71.

O'Connor TR, Dyreson C, Wyrick JJ. Athena: a resource for rapid visualization and systematic analysis of Arabidopsis promoter sequences. Bioinformatics. 2005; 21 (24): 4411-3.

Ogata N, Ueda K, Kawaichi M, Hayaishi O. Poly(ADP-ribose) synthetase, a main acceptor of poly(ADP-ribose) in isolated nuclei. J Biol Chem. 1981; 256 (9): 4135-7.

Ogawa T, Ishikawa K, Harada K, Fukusaki E, Yoshimura K, Shigeoka S. Overexpression of an ADP-ribose pyrophosphatase, AtNUDX2, confers enhanced tolerance to oxidative stress in Arabidopsis plants. Plant J. 2009; 57 (2): 289-301.

Oka S, Kato J, Moss J. Identification and characterization of a mammalian 39-kDa poly(ADP-ribose) glycohydrolase. J Biol Chem. 2006; 281 (2): 705-13.

Okayama H, Edson CM, Fukushima M, Ueda K, Hayaishi O. Purification and properties of poly(adenosine diphosphate ribose) synthetase. J Biol Chem. 1977;

252 (20): 7000-5.

Okita N, Ohta R, Ashizawa D, Yamada Y, Abe H, Abe T, Tanuma S. Bacterial production of recombinant human poly(ADP-ribose) glycohydrolase. Protein Expr Purif. 2011; 75 (2): 230-5.

Oliver AW, Amé JC, Roe SM, Good V, de Murcia G, Pearl LH. Crystal structure of the catalytic fragment of murine poly(ADP-ribose) polymerase-2. Nucleic Acids Res. 2004; 32 (2): 456-64.

Ono T, Kasamatsu A, Oka S, Moss J. The 39-kDa poly(ADP-ribose) glycohydrolase ARH3 hydrolyzes O-acetyl-ADP-ribose, a product of the Sir2 family of acetyl-histone deacetylases. Proc Natl Acad Sci U S A. 2006; 103 (45): 16687-91.

Otto H, Reche PA, Bazan F, Dittmar K, Haag F, Koch-Nolte F. In silico characterization of the family of PARP-like poly(ADP-ribosyl)transferases (pARTs). BMC Genomics. 2005; 6: 139.

Paddock MN, Bauman AT, Higdon R, Kolker E, Takeda S, Scharenberg AM. Competition between PARP-1 and Ku70 control the decision between high-fidelity and mutagenic DNA repair. DNA Repair (Amst). 2011; 10 (3): 338-43.

Panda S, Poirier GG, Kay SA. tej defines a role for poly(ADP-ribosyl)ation in establishing period length of the arabidopsis circadian oscillator. Dev Cell. 2002; 3 (1): 51-61.

Park S, Rancour DM, Bednarek SY. In planta analysis of the cell cycle-dependent localization of AtCDC48A and its critical roles in cell division, expansion, and differentiation. Plant Physiol. 2008; 148 (1): 246-58.

Patel CN, Koh DW, Jacobson MK, Oliveira MA. Identification of three critical acidic residues of poly(ADP-ribose) glycohydrolase involved in catalysis: determining the PARG catalytic domain. Biochem J. 2005; 388 (2): 493-500.

Payne JF, Bal AK. Cytological detection of poly (ADP-ribose) polymerase. Exp Cell Res. 1976; 99 (2): 428-32.

Pellny TK, Locato V, Vivancos PD, Markovic J, De Gara L, Pallardó FV, Foyer CH. Pyridine nucleotide cycling and control of intracellular redox state in relation to

poly (ADP-ribose) polymerase activity and nuclear localization of glutathione during exponential growth of Arabidopsis cells in culture. Mol Plant. 2009; 2 (3): 442-56.

Pleschke JM, Kleczkowska HE, Strohm M, Althaus FR. Poly(ADP-ribose) binds to specific domains in DNA damage checkpoint proteins. J Biol Chem. 2000; 275 (52): 40974-80.

Poirier GG, de Murcia G, Jongstra-Bilen J, Niedergang C, Mandel P. Poly(ADP-ribosyl)ation of polynucleosomes causes relaxation of chromatin structure. Proc Natl Acad Sci U S A. 1982; 79 (11): 3423-7.

Poon IK, Jans DA. Regulation of nuclear transport: central role in development and transformation? Traffic. 2005; 6 (3): 173-86.

Puchta H, Swoboda P, Hohn B. Induction of homologous recombination in whole plants. Plant J. 1995; 7 (2): 203-10.

Rancour DM, Dickey CE, Park S, Bednarek SY. Characterization of AtCDC48 Evidence for multiple membrane fusion mechanisms at the plane of cell division in plants. Plant Physiol. 2002; 130 (3): 1241-53

Realini CA, Althaus FR. Histone shuttling by poly(ADP-ribosylation). J Biol Chem. 1992; 267 (26): 18858-65.

Ries G, Buchholz G, Frohnmeyer H, Hohn B. (b) UV-damage-mediated induction of homologous recombination in Arabidopsis is dependent on photosynthetically active radiation. Proc Natl Acad Sci U S A. 2000; 97 (24): 13425-9.

Ries G, Heller W, Puchta H, Sandermann H, Seidlitz HK, Hohn B. (a) Elevated UV-B radiation reduces genome stability in plants. Nature. 2000; 406 (6791): 98-101.

Riha K, Watson JM, Parkey J, Shippen DE. Telomere length deregulation and enhanced sensitivity to genotoxic stress in Arabidopsis mutants deficient in Ku70. EMBO J. 2002; 21 (11): 2819-26.

Rodriguez MC, Songyang Z. BRCT domains: phosphopeptide binding and signaling modules. Front Biosci. 2008; 13: 5905-15.

Rossi MN, Carbone M, Mostocotto C, Mancone C, Tripodi M, Maione R, Amati P.

Mitochondrial localization of PARP-1 requires interaction with mitofilin and is involved in the maintenance of mitochondrial DNA integrity. J Biol Chem. 2009; 284 (46): 31616-24.

Rozen S, Skaletsky H. Primer3 on the WWW for general users and for biologist programmers. Methods Mol Biol. 2000; 132: 365-86.

Ruf A, Rolli V, de Murcia G, Schulz GE. The mechanism of the elongation and branching reaction of poly(ADP-ribose) polymerase as derived from crystal structures and mutagenesis. J Mol Biol. 1998; 278 (1): 57-65.

Ruf A, Mennissier de Murcia J, de Murcia G, Schulz GE. Structure of the catalytic fragment of poly(AD-ribose) polymerase from chicken. Proc Natl Acad Sci U S A. 1996; 93 (15): 7481-5.

Ruscetti T, Lehnert BE, Halbrook J, Le Trong H, Hoekstra MF, Chen DJ, Peterson SR. Stimulation of the DNA-dependent protein kinase by poly(ADP-ribose) polymerase. J Biol Chem. 1998; 273 (23): 14461-7.

Saxena A, Saffery R, Wong LH, Kalitsis P, Choo KH. (a) Centromere proteins Cenpa, Cenpb, and Bub3 interact with poly(ADP-ribose) polymerase-1 protein and are poly(ADP-ribosyl)ated. J Biol Chem. 2002; 277 (30): 26921-6.

Saxena A, Wong LH, Kalitsis P, Earle E, Shaffer LG, Choo KH.(b) Poly(ADP-ribose) polymerase 2 localizes to mammalian active centromeres and interacts with PARP-1, Cenpa, Cenpb and Bub3, but not Cenpc. Hum Mol Genet. 2002; 11 (19): 2319-29.

Sbodio JI, Lodish HF, Chi NW. Tankyrase-2 oligomerizes with tankyrase-1 and binds to both TRF1 (telomere-repeat-binding factor 1) and IRAP (insulin-responsive aminopeptidase). Biochem J. 2002; 361 (3): 451-9.

Schreiber V, Amé JC, Dollé P, Schultz I, Rinaldi B, Fraulob V, Ménissier-de Murcia J, de Murcia G. Poly(ADP-ribose) polymerase-2 (PARP-2) is required for efficient base excision DNA repair in association with PARP-1 and XRCC1. J Biol Chem. 2002; 277 (25): 23028-36.

Schreiber V, Hunting D, Trucco C, Gowans B, Grunwald D, De Murcia G, De Murcia JM. A dominant-negative mutant of human poly(ADP-ribose) polymerase

affects cell recovery, apoptosis, and sister chromatid exchange following DNA damage. Proc Natl Acad Sci U S A. 1995; 92 (11): 4753-7.

Schreiber V, Dantzer F, Ame JC, de Murcia G. Poly(ADP-ribose): novel functions for an old molecule. Nat Rev Mol Cell Biol. 2006; 7 (7): 517-28.

Shah GM, Poirier D, Duchaine C, Brochu G, Desnoyers S, Lagueux J, Verreault A, Hoflack JC, Kirkland JB, Poirier GG. Methods for biochemical study of poly(ADP-ribose) metabolism in vitro and in vivo. Anal Biochem. 1995; 227 (1): 1-13.

Shieh WM, Amé JC, Wilson MV, Wang ZQ, Koh DW, Jacobson MK, Jacobson EL. Poly(ADP-ribose) polymerase null mouse cells synthesize ADP-ribose polymers. J Biol Chem. 1998; 273 (46): 30069-72.

Shiloh Y. The ATM-mediated DNA-damage response: taking shape. Trends Biochem Sci. 2006; 31 (7): 402-10.

Shimokawa T, Masutani M, Nagasawa S, Nozaki T, Ikota N, Aoki Y, Nakagama H, Sugimura T. Isolation and cloning of rat poly(ADP-ribose) glycohydrolase: presence of a potential nuclear export signal conserved in mammalian orthologs. J Biochem. 1999; 126 (4): 748-55.

Simonin F, Ménissier-de Murcia J, Poch O, Muller S, Gradwohl G, Molinete M, Penning C, Keith G, de Murcia G. Expression and site-directed mutagenesis of the catalytic domain of human poly(ADP-ribose)polymerase in Escherichia coli Lysine 893 is critical for activity. J Biol Chem. 1990; 265 (31): 19249-56.

Simonin F, Poch O, Delarue M, de Murcia G. Identification of potential active-site residues in the human poly(ADP-ribose) polymerase. J Biol Chem. 1993; 268 (12): 8529-35.

Skidmore CJ, Davies MI, Goodwin PM, Halldorsson H, Lewis PJ, Shall S, Zia'ee AA. The involvement of poly(ADP-ribose) polymerase in the degradation of NAD caused by gamma-radiation and N-methyl-N-nitrosourea. Eur J Biochem. 1979; 101 (1): 135-42.

Smith S, de Lange T. Tankyrase promotes telomere elongation in human cells. Curr Biol. 2000; 10 (20): 1299-302.

Smith S, Giriat I, Schmitt A, de Lange T. Tankyrase, a poly(ADP-ribose) polymerase at human telomeres. Science. 1998; 282 (5393): 1484-7.

Soldani C, Scovassi AI. Poly(ADP-ribose) polymerase-1 cleavage during apoptosis: an update. Apoptosis. 2002; 7 (4): 321-8.

Sparkes IA, Runions J, Kearns A, Hawes C. Rapid, transient expression of fluorescent fusion proteins in tobacco plants and generation of stably transformed plants. Nat Protoc. 2006; 1 (4): 2019-25.

St-Laurent JF, Gagnon SN, Dequen F, Hardy I, Desnoyers S. Altered DNA damage response in Caenorhabditis elegans with impaired poly(ADP-ribose) glycohydrolases genes expression. DNA Repair (Amst). 2007; 6 (3): 329-43.

Stellberger T, Häuser R, Baiker A, Pothineni VR, Haas J, Uetz P. Improving the yeast two-hybrid system with permutated fusions proteins: the Varicella Zoster Virus interactome. Proteome Sci. 2010; 8: 8.

Storozhenko S, Inzé D, Van Montagu M, Kushnir S. Arabidopsis coactivator ALY-like proteins, DIP1 and DIP2, interact physically with the DNA-binding domain of the Zn-finger poly(ADP-ribose) polymerase. J Exp Bot. 2001; 52 (359): 1375-80.

Stubbs M, Veech RL, Krebs HA. Control of the redox state of the nicotinamide-adenine dinucleotide couple in rat liver cytoplasm. Biochem J. 1972; 126 (1): 59-65.

Sugimura T, Fujimura S, Hasegawa S, Kawamura Y. Polymerization of the adenosine 5'-diphosphate ribose moiety of NAD by rat liver nuclear enzyme. Biochim Biophys Acta. 1967; 138 (2): 438-41.

Takeda S, Tadele Z, Hofmann I, Probst AV, Angelis KJ, Kaya H, Araki T, Mengiste T, Mittelsten Scheid O, Shibahara K, Scheel D, Paszkowski J. BRU1, a novel link between responses to DNA damage and epigenetic gene silencing in Arabidopsis. Genes Dev. 2004; 18 (7): 782-93.

Tarapore P, Horn HF, Tokuyama Y, Fukasawa K. Direct regulation of the centrosome duplication cycle by the p53-p21Waf1/Cip1 pathway. Oncogene. 2001; 20 (25): 3173-84.

Taylor RM, Thistlethwaite A, Caldecott KW. Central role for the XRCC1 BRCT I domain in mammalian DNA single-strand break repair. Mol Cell Biol. 2002; 22 (8): 2556-63.

Tischler ME, Friedrichs D, Coll K, Williamson JR. Pyridine nucleotide distributions and enzyme mass action ratios in hepatocytes from fed and starved rats. Arch Biochem Biophys. 1977; 184 (1): 222-36.

Tulin A, Chinenov Y, Spradling A. Regulation of chromatin structure and gene activity by poly(ADP-ribose) polymerases. Curr Top Dev Biol. 2003; 56: 55-83.

Tulin A, Spradling A. Chromatin loosening by poly(ADP)-ribose polymerase (PARP) at Drosophila puff loci. Science. 2003; 299 (5606): 560-2.

Tulin A, Stewart D, Spradling AC. The Drosophila heterochromatic gene encoding poly(ADP-ribose) polymerase (PARP) is required to modulate chromatin structure during development. Genes Dev. 2002; 16 (16): 2108-19.

Tulin A, Naumova NM, Menon AK, Spradling AC. Drosophila poly(ADP-ribose) glycohydrolase mediates chromatin structure and SIR2-dependent silencing. Genetics. 2006; 172 (1): 363-71.

Tuteja N, Ahmad P, Panda BB, Tuteja R. Genotoxic stress in plants: shedding light on DNA damage, repair and DNA repair helicases. Mutat Res. 2009; 681 (2-3): 134-49.

Uchida K, Hanai S, Ishikawa K, Ozawa Y, Uchida M, Sugimura T, Miwa M. Cloning of cDNA encoding Drosophila poly(ADP-ribose) polymerase: leucine zipper in the auto-modification domain. Proc Natl Acad Sci U S A. 1993; 90 (8): 3481-5.

Uchiyama Y, Suzuki Y, Sakaguchi K. Characterization of plant XRCC1 and its interaction with proliferating cell nuclear antigen. Planta. 2008; 227 (6): 1233-41.

Van Gool L, Meyer R, Tobiasch E, Cziepluch C, Jauniaux JC, Mincheva A, Lichter P, Poirier GG, Bürkle A, Küpper JH. Overexpression of human poly(ADP-ribose) polymerase in transfected hamster cells leads to increased poly(ADP-ribosyl)ation and cellular sensitization to gamma irradiation. Eur J Biochem. 1997; 244 (1): 15-20.

van Steensel B, de Lange T. Control of telomere length by the human telomeric protein TRF1. Nature. 1997; 385 (6618): 740-3.

Vanderauwera S, De Block M, Van de Steene N, van de Cotte B, Metzlaff M, Van Breusegem F. Silencing of poly(ADP-ribose) polymerase in plants alters abiotic stress signal transduction. Proc Natl Acad Sci U S A. 2007; 104 (38): 15150-5.

Veech RL, Eggleston LV, Krebs HA. The redox state of free nicotinamide-adenine dinucleotide phosphate in the cytoplasm of rat liver. Biochem J. 1969; 115 (4): 609-19.

Velculescu VE, Zhang L, Vogelstein B, Kinzler KW. Serial analysis of gene expression. Science. 1995; 270 (5235): 484-7.

Voinnet O, Rivas S, Mestre P, Baulcombe D. An enhanced transient expression system in plants based on suppression of gene silencing by the p19 protein of tomato bushy stunt virus. Plant J. 2003; 33 (5): 949-56.

Watts FZ, Brissett NC. Linking up and interacting with BRCT domains. DNA Repair (Amst). 2010; 9 (2): 103-8.

West CE, Waterworth WM, Story GW, Sunderland PA, Jiang Q, Bray CM. Disruption of the Arabidopsis AtKu80 gene demonstrates an essential role for AtKu80 protein in efficient repair of DNA double-strand breaks in vivo. Plant J. 2002; 31 (4): 517-28.

West CE, Waterworth WM, Sunderland PA, Bray CM. Arabidopsis DNA double-strand break repair pathways. Biochem Soc Trans. 2004; 32 (6): 964-6.

Whatcott CJ, Meyer-Ficca ML, Meyer RG, Jacobson MK. A specific isoform of poly(ADP-ribose) glycohydrolase is targeted to the mitochondrial matrix by a N-terminal mitochondrial targeting sequence. Exp Cell Res. 2009; 315 (20): 3477-85.

Whitby AJ, Stone PR, Whish WJ. Effect of polyamines and Mg++ on poly(ADP-ribose) synthesis and ADP-ribosylation of histones in wheat. Biochem Biophys Res Commun. 1979; 90 (4): 1295-304.

Whitby AJ, Whish WJ. Poly(adenoise diphosphate ribose) in wheat [proceedings].

Biochem Soc Trans. 1977; 5 (4): 948-9.

Wielckens K, George E, Pless T, Hilz H. Stimulation of poly(ADP-ribosyl)ation during Ehrlich ascites tumor cell "starvation" and suppression of concomitant DNA fragmentation by benzamide. J Biol Chem. 1983; 258 (7): 4098-104. PubMed

Wielopolska A, Townley H, Moore I, Waterhouse P, Helliwell C. A high-throughput inducible RNAi vector for plants. Plant Biotechnol J. 2005; 3 (6): 583-90.

Williamson DH, Lund P, Krebs HA. The redox state of free nicotinamide-adenine dinucleotide in the cytoplasm and mitochondria of rat liver. Biochem J. 1967; 103 (2): 514-27.

Willmitzer L. Demonstration of in vitro covalent modification of chromosomal proteins by poly(ADP) ribosylation in plant nuclei. FEBS Lett. 1979; 108 (1): 13-6.

Winstall E, Affar EB, Shah R, Bourassa S, Scovassi IA, Poirier GG. Preferential perinuclear localization of poly(ADP-ribose) glycohydrolase. Exp Cell Res. 1999; 251 (2): 372-8.

Woodman PG. p97, a protein coping with multiple identities. J Cell Sci. 2003; 116 (Pt 21): 4283-90.

Yamada M, Miwa M, Sugimura T. Studies on poly (adenosine diphosphate-ribose) X Properties of a partially purified poly (adenosine diphosphate-ribose) polymerase. Arch Biochem Biophys. 1971; 146 (2): 579-86.

Yamanaka H, Penning CA, Willis EH, Wasson DB, Carson DA. Characterization of human poly(ADP-ribose) polymerase with autoantibodies. J Biol Chem. 1988; 263 (8): 3879-83.

Yoshiyama K, Conklin PA, Huefner ND, Britt AB. Suppressor of gamma response 1 (SOG1) encodes a putative transcription factor governing multiple responses to DNA damage. Proc Natl Acad Sci U S A. 2009; 106 (31): 12843-8.

Yu SW, Andrabi SA, Wang H, Kim NS, Poirier GG, Dawson TM, Dawson VL. Apoptosis-inducing factor mediates poly(ADP-ribose) (PAR) polymer-induced cell death. Proc Natl Acad Sci U S A. 2006; 103 (48): 18314-9.

Yu SW, Wang H, Poitras MF, Coombs C, Bowers WJ, Federoff HJ, Poirier GG, Dawson TM, Dawson VL. Mediation of poly(ADP-ribose) polymerase-1-dependent cell death by apoptosis-inducing factor. Science. 2002; 297 (5579): 259-63.

Yélamos J, Schreiber V, Dantzer F. Toward specific functions of poly(ADP-ribose) polymerase-2. Trends Mol Med. 2008; 14 (4): 169-78.

Zahradka P, Ebisuzaki K. A shuttle mechanism for DNA-protein interactions The regulation of poly(ADP-ribose) polymerase. Eur J Biochem. 1982; 127 (3): 579-85.